Fault Location on Series Compensated Transmission Lines

A thesis submitted to the University of Manchester for the degree of

Doctor of Philosophy

In the Faculty of Engineering and Physical Sciences

2014

Shantanu Padmanabhan

School of Electrical and Electronic Engineering

Table of Contents

Word Count: 60,380

List of Figures

List of Tables

List of Abbreviations

ANN	Artificial Neural Network
ATP	Alternative Transients Program
CB	Circuit Breaker
CT	Current Transformer
DFT	Discrete Fourier Transform
DL	Double Line
DLG	Double Line to Ground
EHV	Extra High Voltage
EMTP	Electromagnetic transient Program
ENSG	Electricity Network Strategy Group
FACTS	Flexible AC transmission Systems
FLA	Fault Location Algorithm
FFNN	Feed Forward Neural Network
FFT	Fast Fourier Transform
FSC	Fixed Series Capacitor
GB	Great Britain
GCSC	Gate Controlled Series Compensator
GPS	Global Positioning System
KEPRI	Korean Electric Power Research Institute
MOV	Metal Oxide Varistor
OHTL	Overhead Transmission Line
PMU	Phasor Measurement Units
SCADA	Supervisory Control and Data Acquisition
SC	Series Capacitor
SC-MOV	Series Capacitor-Metal Oxide Varistor
SLG	Single Line to Ground
SMU	Synchronised Measurement Unit
SSSC	Static Synchronous Series Compensator
STATCOM	Static Synchronous Compensator
SVC	Static VAR compensator
TCR-FC	Thyristor Controlled Reactor-Fixed Capacitor
TCR-TSC	Thyristor Controlled Reactor-Thyristor Switched Capacitor
TPSC	Thyristor Protected Series Compensation
VSI	Voltage Source Inverter
VT	Voltage Transformer
WAPA	Western Area Power Administration

Abstract

Fault Location on Series Compensated Transmission Lines

Shantanu Padmanabhan, Doctor of Philosophy, The University of Manchester,
27 September 2014

Fault location for series compensated lines cannot be addressed sufficiently by conventional solutions developed for traditional uncompensated lines. Line-parameters vary with loading and weather conditions, and therefore settings used for fault location are often erroneous. Line-parameter free solutions for fault location are therefore more reliable and accurate than conventional solutions that require such settings. Hence, line-parameter free fault location algorithms for single-circuit and double-circuit series compensated transmission lines were developed during the research project. Single-circuit lines and double-circuit lines both present unique challenges for fault location. They also vary in the number of available measurements that can be used to arrive at a solution for distance to fault. A third algorithm is presented that allows the extension of existing short line algorithms to the case of long lines. This is done by providing a method for incorporating the line shunt admittance into these existing algorithms.The aforementioned three bodies of research work, form the focus of this thesis.

The algorithms are derived using two-terminal synchronised current and voltage sampled measurements. Of these, the algorithms for series compensated lines are also derived for asynchronous measurements. Phasors are obtained by carrying out a Fast Fourier Transform, and then appropriate calculations are performed for distance to fault. The thesis covers the mathematical derivations of the algorithms, involving the algebraic reduction of non-linear equations in numerous variables into a single expression for distance to fault. The results for a variety of simulation tests are shown subsequently and discussed. Various fault resistances, fault types, degrees of series compensation, line lengths, fault levels are considered in the tests carried out. The algorithms are largely found to be highly accurate under these various conditions, and where the algorithms perform to a lesser degree of accuracy are highlighted and discussed. Lastly, a detailed chapter discussing future work is also included in the thesis.

Declaration

No portion of the work referred to in the thesis has been submitted in support of an application for another degree or qualification of this or any other university or other institute of learning.

Copyright Statement

i. The author of this thesis (including any appendices and/or schedules to this thesis) owns certain copyright or related rights in it (the "Copyright") and he has given The University of Manchester certain rights to use such Copyright, including for administrative purposes.

ii. Copies of this thesis, either in full or in extracts and whether in hard or electronic copy, may be made only in accordance with the Copyright, Designs and Patents Act 1988 (as amended) and regulations issued under it or, where appropriate, in accordance with licensing agreements which the University has from time to time. This page must form part of any such copies made.

iii. The ownership of certain Copyright, patents, designs, trademarks and other intellectual property (the "Intellectual Property") and any reproductions of copyright works in the thesis, for example graphs and tables ("Reproductions"), which may be described in this thesis, may not be owned by the author and may be owned by third parties. Such Intellectual Property and Reproductions cannot and must not be made available for use without the prior written permission of the owner(s) of the relevant Intellectual Property and/or Reproductions.

iv. Further information on the conditions under which disclosure, publication and commercialisation of this thesis, the Copyright and any Intellectual Property and/or Reproductions described in it may take place is available in the University IP Policy. (see: http://documents.manchester.ac.uk/DocuInfo.aspx?DocID=487), in any relevant Thesis restriction declarations deposited in the University Library, The University Library's regulations (see: http://www.manchester.ac.uk/library/aboutus/regulations) and in The University's policy on presentation of Theses.

Acknowledgements

I would like to take this opportunity to thank National Grid, IET and PNRA for funding my Ph.D. project through the PNRA scheme and for their guidance during the course of the project. A special thanks to Andrew Taylor, who has been very helpful throughout the project duration, in providing necessary input and technical feedback.

I would like to graciously thank my supervisor Prof. Vladimir Terzija for his support, supervision, feedback, securing the funding of the project, and for his constant technical and moral support. Without you sir, this project could not have been accomplished and for this I would like to express my sincerest gratitude.

I would also like to thank all my dear friends at the University for making my journey in Manchester a rich and pleasurable experience, and for all the help you have given me. I would especially like to thank Ozgur, Jairo, Gary, Gustavo, Melios, Peter, Pawel, Yuhang, Adrien, Tee, Jonathan and Jiashen.

I am especially grateful and thankful to my parents for their constant perseverence in making my dream come true. You have helped me through thick and thin, to ensure I had nothing but the best of education even when times were hard. Your love and guidance means the world to me and has led me to where I am today. It is impossible for me to express in a matter of few words how grateful I feel for all the years of hard work you have put in getting me here nor can I express in words how much love and affection I have for you. To say that I love you would be an understatement.

Chapter 1. Introduction

1.1. Project Background

Transmission of electrical energy from generation to electrical substations is carried out through overhead transmission lines (OHTLs) and underground cables. In an ever-growing power network, transmission lines are increasingly required to be built to provide sufficient transmission capacity. Increasing the transmission capacity of a line by means of series compensation is an economically favourable option to building new transmission lines. Series compensated lines also have the advantages of reduced losses, increased power system stability and reduced space when considering the alternative. Long EHV transmission lines (>=230 kV) can especially benefit greatly from incorporating series compensation when considering the economic advantages. Series compensation may be in the form of Fixed Series Capacitors (FSCs) or or in the form of variable series compensation such as Thyristor Controlled Series Compensators (TCSCs). They are installed with overvoltage protection in the form of Metal Oxide Varistors (MOVs) and/or spark gaps in parallel with the capacitor. Series compensation may be installed at one or both ends of a transmission line, or in the middle of the transmission line.

Both uncompensated and series compensated lines are prone to electrical faults. This may be due to lightning, ageing of the line, trees falling onto or making temporary contact with the line etc. When a fault occurs on a line creating an electrical connection to ground or between phases, it leads to large currents flowing through the system. This current may be much higher in magnitude than the load current, and may significantly exceed the ratings of power system equipment, leading to damage and losses incurred in repair. Thus, transmission line protection is required to speedily detect and selectively isolate the faulted section of the network.

Faults on OHTLs can be generally classified into transient faults and permanent faults. Transient faults are temporary and clear after a short interval of time, e.g. lightning strike, branch of a tree contacting the line due to wind etc. In the event of such faults, although line protection operates and disconnects the line from the network, auto-reclosers re-

energise the line. However, if the fault is permanent, protection would re-operate and take the line out of service. In such cases, the fault does not self clear and service crews are required to remove the fault and repair the line. Utilities must quickly repair and re-energise the line in order to minimise losses. It is vital that outages and any disruption of supply be minimised resulting from such an event. For this purpose, fault locators are used to accurately and reliably locate the fault. The inclusion of series compensation within a transmission network alters its electrical composition on account of its capacitive nature. This affects the operation of distance protection and fault locators, and must hence be taken into account.

In a broad sense, this project is aimed at improving reliability of service and security of supply. The project aims to further the state of the art of fault location with a focus on series compensated transmission lines. This demands an in-depth understanding of series compensation, its interaction with power systems and most importantly, its electrical behaviour during the phenomenon of a fault. A comprehensive knowledge and understanding of all research work carried out in the field of fault location of series compensated lines is required so that shortcomings may be identified. The primary aim of the project is that innovative improved solutions be proposed by the author to address these shortcomings.

Fault location on series compensated lines is a challenging problem not sufficiently addressed by solutions used for traditional uncompensated lines. FLAs for uncompensated lines (when applied to series compensated lines) are prone to incorrect calculation of distance to fault due to the non-homogenous reactance across the length of such a line, and the varying impedance of the series compensation unit during fault due to the operation of its overvoltage protection. During fault, the overvoltage protection may bypass the capacitor entirely for the whole or segment of each power system cycle. The Metal Oxide Varistor (MOV) in parallel with the series capacitor has a nonlinear resistance which varies such that the higher the voltage across the series capacitor, the lower the resistance. While the MOV does not conduct any current during normal load conditions, during fault conditions the MOV significantly influences the effective impedance of the unit as a whole (this is discussed in more detail in Chapter 3 Section Metal Oxide Varistor3.5.3).

Design of FLAs for such lines must consider the operation of the overvoltage protection in parallel with the series capacitor and the location of the series capacitor on the line. Novel FLAs for series compensated lines thus form the key deliverables of the project. The algorithms discussed in this thesis are developed for lines compensated using Fixed Series Capacitors (FSCs). It is important to note that effective impedance of the unit as whole (the capacitor and its overvoltage protection) will still be variable during fault due to the MOV in parallel with the FSC (discussed in detail in Chapter 3). However, these algorithms may be extended for lines compensated using TCSC in future work. A literature review and discussion of research work carried out previously in this field is included in subsequent chapters of this thesis, highlighting the need and importance of these algorithms. It is hoped that the algorithms developed in this project can eventually be made available for implementation on real fault locators. These algorithms assume synchronisation of two-terminal measurements, although variations for the algorithms using asynchronous data are also discussed.

1.2. Research Objectives

The main objectives of the Ph.D. project detailed in this thesis are:

- To produce a comprehensive literature review of fault location techniques for single-circuit and double-circuit traditional uncompensated lines.

- To develop an in-depth understanding of the concept of series compensation of transmission lines and the body of research pertaining to fault location on such lines. Concepts pertaining to the electrical behaviour of series compensated lines are discussed in later chapters of this thesis and are demonstrated using simulations created in the ATP-EMTP software [1] (this simulation software is discussed briefly in Section 1.3).

- To create a model of a series compensated line in ATP-EMTP for the purpose of generating simulated measurement data to be used for validating FLAs developed for such lines.

- To derive, develop and program a novel FLA for single-circuit series compensated transmission lines. The most common type of series compensated lines i.e. lines compensated using FSCs are considered here. Two such installations for FSCs are planned for the Scottish Power Network at Gretna and Moffat substations on single-circuit lines Gretna-Harker and Moffat-Harker (expected 2015).

- To derive, develop and program a novel FLA for double-circuit series compensated transmission lines (Fixed Series Compensation). The most common type of series compensated lines i.e. lines compensated using FSCs are considered here. Two such installations for FSCs are planned for the Scottish Power Network at the Eccles substation on the two circuits Eccles-Stella West 1&2 (expected 2015).

- To derive, develop and program a novel algorithm for calculating shunt admittance parameters using only synchronised two-end current and voltage data for the purpose of improving the accuracies of existing two-terminal FLAs using synchronised measurements.

- To implement the algorithms using an appropriate programming language and to validate the accuracy of the algorithms using simulated measurement data. Such data was used due to the lack of availability of recorded fault data.

1.3. Research Methodologies

All research work in this Ph.D. project was carried out using software simulations and MATLAB processing on an Intel Core i3-2350M, 2.3 GHz processor. ATP-EMTP is a useful simulation tool used for electromagnetic transient studies, but is also highly useful in creating high-fidelity models of power networks and in accurately simulating measurement data. In this project, all input measurement data was generated using ATP-EMTP simulations of power networks. MATLAB is the most widely used programming language/interface in the field of electrical and mechanical engineering due to the large number of inbuilt toolboxes and its speed of processing and computation. MATLAB was used in the programming of all algorithms created in this project, and for the processing of

all measurement data. Data from ATP-EMTP was obtained in a *.pl4 format which was then required to be converted to *.mat format for it to be suitable for processing in MATLAB. This conversion was carried out using the PL42MAT software.

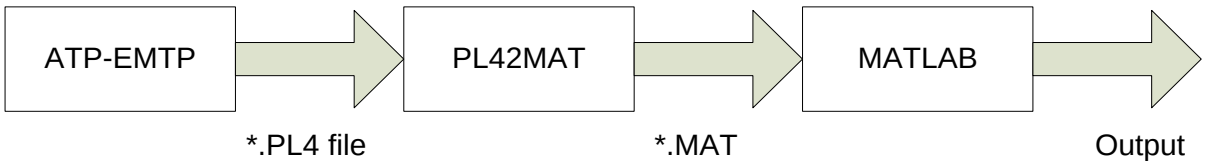

Figure 1.1: Block diagram – research methodologies

1.4. Thesis Overview

This section provides an overview of the content of the thesis. The original research contributions of the author are presented in Chapter 4, Chapter 5 and Chapter 7. The work carried out over the course of the PhD project, and the relevant background information is organised in this thesis into the following chapters:

Chapter 1- Introduction: This chapter provides an introduction to the thesis and a context to the work carried out over the course of the Ph.D. project. It lists and discusses the objectives of the project. It also discusses the methodology of research and provides an overview of the thesis.

Chapter 2- A Review of Fault Location Techniques: The chapter discusses the concept of fault location and its importance and relevance to power systems. It discusses the challenges of fault location and the methods and measurements used for fault location. It provides a literature review of past research pertaining to fault location on OHTLs and discusses the pros and cons of each method.

Chapter 3- Series Compensation of Transmission Lines: Background, Literature Review and Modelling: This chapter introduces the concept of series compensation, and the advantages of series compensated lines. It also specifically discusses the challenges of protection and fault location in the case of such lines. A detailed review of all fault location

techniques proposed for such lines is then provided, and each method is discussed. It also presents a simple but accurate model of an example series compensated line created in ATP-EMTP to test and thereby validate the novel FLAs developed by the author as a part of the project. A variety of simulation studies are shown to be carried out to show the applicability of this simulation framework for the purposes of this project.

Chapter 4- Novel Algorithm for Single-Circuit Series Compensated Transmission Lines: This chapter discusses a novel algorithm for fault location on series compensated single-circuit lines. It is an original accurate FLA for series compensated lines, which does not require the use of any line parameters. This is a significant advantage as line parameters vary greatly with varying loading and weather conditions. In recent years a number of line parameter free FLAs have been proposed but they do not accurately address series compensated lines.

The chapter includes the mathematical derivation of the algorithm, and the relevant assumptions made. It has been derived using the analysis of self and mutual phase network impedances of the line and the series capacitor reactance. These impedance terms are systematically eliminated, thus obtaining a line parameter free expression of distance to fault. The chapter also details the tests carried out to validate the algorithm and shows the results thus obtained. Measurement data from ATP-EMTP simulations of an example series compensated line is used for this purpose. The performance is quantified based on the errors in fault location i.e. the discrepancy in calculated and expected values of fault location expressed as a percentage of the total line length. The algorithm is later compared against an existing technique for single-circuit series compensated transmission lines in Chapter 6

Chapter 5- Novel Algorithm for Double-Circuit Series Compensated Transmission Lines: This chapter details the second FLA developed over the course of the Ph.D. project. The novel algorithm is aimed at locating faults on double-circuit series compensated lines without using any line parameters in its calculations. This is a significant advantage as previously mentioned owing to fact that use of line parameters for fault location is not reliable since such parameters vary significantly with varying loading and weather

conditions. The algorithm is shown to be thoroughly tested for a variety of fault types and for various types of series compensated double circuit lines. The performance is quantified based on the errors in fault location i.e. the discrepancy in calculated and expected values of fault location expressed as a percentage of the total line length. The algorithm is later compared against an existing technique for single-circuit series compensated transmission lines in Chapter 6.

Chapter 6- Comparison Study of Novel Algorithms and Existing Solutions: This chapter provides a comparison study by running the novel algorithms for a variety of fault types, fault distances and fault resistances, and subsequently carrying out this procedure for previously proposed existing solutions. The improvements brought about by the new algorithms are highlighted, and cases where these novel algorithms perform to a lesser degree of accuracy are also discussed.

Chapter 7- Novel Line parameter Free Algorithm to Account for Shunt Admittance: The algorithm described in this chapter is designed to calculate the self and mutual shunt admittances of single-circuit lines using online measurements during a fault, so that FLAs not require line parameter settings for this purpose. The derivation, simulation studies, tests and results are all discussed. The work presented in this chapter is also entirely the original contribution of the author.

Chapter 8- Conclusions and Future Work: A summary of the thesis and the Ph.D. project is provided in this chapter. Conclusions are presented for each of the individual original contributions of the project. Lastly, the chapter includes a discussion of potential future work pertaining to the area of research.

Chapter 2. A Review of Fault Location Techniques

A planned addition of 34 GW of wind energy generation detailed in Vision 2020 [139][1] demands transmission infrastructure reinforcements between the North of Scotland to England in the form of series compensation. As a result, FSCs are to be installed at Gretna, Moffat and Eccles substations. A TCSC is to be installed at the Hutton substation. Fault location on series compensated lines has thus gained significant research interest in recent years due to its increased relevance to the GB network. As highlighted in the introduction to this thesis, the primary aim of the project is the development of novel FLAs for series compensated lines, owing to unique challenges presented by such lines.

In order to innovate novel FLAs for series compensated lines, it is essential to develop a comprehensive understanding of both fault location techniques and the unique electrical aspects of locating faults on such lines. This chapter deals with the former. It provides a literature review of various fault location techniques proposed for traditional uncompensated lines with the aim of providing a background on fault location itself. FLAs for series compensated lines are then discussed in the next chapter. The review of fault location techniques covers a number of aspects of FLAs which are addressed by the algorithms proposed in this thesis. First the review is presented in itself. Later in Section 2.6 the novel algorithms are discussed in terms of the information presented in the review.

In the event of a permanent fault on a transmission line, it is essential to not only disconnect the faulted line from service, but also to precisely locate the fault thereby avoiding prolonged outages in order to minimise economic losses incurred by utilities. Service crews are required to repair faults as speedily as possible. For this purpose, a number of accurate Fault Location Algorithms (FLAs) have been proposed over the years. Protection of OHTLs greatly relies on these FLAs for the location and analysis of symmetrical and asymmetrical faults. The process of fault location may be defined in the context of power systems as the process of determining the distance to fault from a given line terminal with maximum accuracy and within the required operation time [2], [3].

Fault location is a functionality associated with microprocessor-based relays, fault analysis modules, stand-alone fault locators and fault recorders. FLAs are typically incorporated with little additional cost into relays and fault recorders. The ABB relays: REL 531, REL 501 [140], REL 511 [141] and REL 521 [142] (500 series) and the Siemens relays: SIPROTEC 7SA510 [143], SIPROTEC 7SA511 [144] and SIPROTEC 7SA513 [145] are some examples of relays with inbuilt fault location functionality. Conventionally, one-terminal current and voltage measurement data is used, and a variation of the Takagi algorithm [14] are used for this purpose of fault distance calculation. This algorithm is discussed in further detail in Section 2.1.1. More recently, relays employing travelling wave techniques for fault location have recently been proposed, owing to the advantage they offer in terms of higher levels of accuracy [146], [147]. This type of fault location is discussed further in Section 2.2. A fault locator is the auxiliary protection equipment, which performs fault location using FLAs. Stand-alone fault locators incur additional costs, but may use more sophisticated FLAs for their calculations **Error! Reference source not found.**[4]. The applicability of these algorithms may not be limited to only distance to fault calculations but also to carry out other types of fault analysis. FLAs may be used to verify the operation of distance relays, as well as calculate other fault data, such as fault voltage, arc resistance, to determine if the fault is transient or permanent etc.

Sensitivity, speed, selectivity and stability are the criteria used for assessing the performance and reliability of line protection [5]. FLAs must ensure sufficient speed and accuracy for various fault types, fault resistances, source impedances, etc. FLAs for protection relays and those for fault locators serve different purposes and hence are subject to different requirements. They differ in the following respects:

- Required level of accuracy: Protective relays are required to only identify a general area or zone where the fault is located. Fault locators on the other hand, are required to locate the fault to a higher degree of exactness to minimise inspection times required by service crews. Whilst distance relays identify the zone of protection and provide an indication of where the fault has occurred, the accuracy of such calculations is insufficient for the purpose of the speedy repair/re-

energisation of the line. A far more accurate calculation of distance to fault may be carried out by stand-alone fault locators for this purpose. [4]

- Required speed of calculation: Line protection demands that relays operate in real time, i.e. on-line calculations are required to be performed. High-speed and short fault clearing times are crucial requirements to avoid the spreading of the effects of the fault of a cascading nature. Protection must not only detect the fault, but also selectively isolate the faulted section whilst ensuring to avoid operation for faults external to the zone of the relay. This must be carried out typically within a few cycles (generally 2-5 cycles, 40-100 ms). In comparison, fault locators may be operated offline, and the time taken to calculate the distance to fault has no such stringent requirements, and may take seconds to a few minutes. [4]

- Required speed of communication between line-ends: Low speed data communication is sufficient for the purposes of fault locators, much different to the high speed communications required by protective relays (when essential) to ensure reliable fast operation whilst also ensuring sufficient accuracy despite any synchronisation errors. [4]

- Allowed complexity and processing capability: The offline operation of fault locators allows sufficient processing time to use far more complex calculations of distance to fault. Decaying DC component removal methods may be applied to achieve higher levels of accuracy for long transmission lines i.e. lines longer than 100 km. More accurate assumptions may be used with respect to the line model, fault model, Metal Oxide Varistor (MOV) operation etc. FLAs for protective relays require being simple so they may complete processing and calculations within the required operating times. [4]

- Available data-window of input measurements: Fault locators may use the last available data window (just prior to the disconnection of the faulted line) where harmonics and DC components are significantly damped to achieve the required levels of accuracies. On the other hand protective relays must calculate the

distance to fault in real time, and must use the earliest available data window(s) to ensure fast detection of fault. [4]

- Future FLAs must consider the impact of HVDC converters interfacing large infeed currents, where the high harmonic content in the terminal currents may have a significant negative influence on the accuracy of the algorithm [157].

FLAs may carry out analysis in the time domain or in the phasor domain. In the case of phasor domain algorithms, they may carry out analysis of phase network phasors or sequence network phasors. The time domain analysis requires inputs only as samples, while the phase and sequence network based approaches require a spectral transformation, typically using the Discrete Fourier Transform (DFT) in order to calculate the phasors corresponding to the sampled input measurements. Generally, these phasors for currents and voltages are calculated for the power system frequency component. Higher harmonics may be useful for fault analysis of arcs or for high frequency based FLAs. A limitation in using DFT is its ineffectiveness in accurately extracting the fundamental frequency component in presence of a high decaying DC component as seen in the current in the faulted phases. This may cause a significant error in the calculation of distance to fault. If distance to fault estimates are carried out from fault inception to a few cycles after, the errors are seen to diminish with the decay of the DC component and the solution appears to converge towards an accurate value. References [6], [7] propose some such examples of FLAs using DFT [8]. The algorithms for series compensated lines proposed in this thesis in Chapter 4 and Chapter 5, perform a DC component removal prior to carrying out an FFT.

FLAs using time-domain samples are derived from the relationships between terminal currents and voltages in terms of line parameters expressed in the form of differential equations [9]. The speed and accuracy of fault location depends on the model of the transmission line used in the mathematical assumptions of such algorithms. Simplifications allow for faster computation but compromise on the accuracy. Depending on whether the FLA is to operate in real time or offline, an appropriate model can be assumed. Although the analysis in time domain is more complex than the phasor domain or sequence network approaches, a significant advantage is that accuracies of such algorithms are not affected

by the presence of decaying DC components, or higher harmonics. Computation times for spectral domain approaches are significantly larger than time domain approaches due to the number of computations required to carry out the DFT. Real-time FLAs in time domain may require only the latest data samples, or may require a set of consecutive data samples, and may also require pre-fault data. Some such examples of FLAs directly using time domain samples of current and/or voltage are proposed in [10]-[11].

FLAs may or may not be sensitive to high fault resistances depending on the method used in the calculation of distance to fault. Single-ended algorithms are more likely to be affected by fault resistance than double-ended algorithms, as in the case of the latter, the fault resistance can effectively be eliminated from the calculations. High fault resistance may even affect the detection of the fault itself, if this is based on the magnitude of the fault current. Impedance-based calculations are considerably affected in accuracy if the simplifications made with respect to the fault resistance are not accurate in the case of high resistance faults. On the other hand, the influence of DC components may be lesser in the case of high resistance faults leading to slightly higher levels of accuracy in FLAs that consider the fault resistance but do not consider the influence of decaying DC components.

The methods used by FLAs in determining the fault location can be classified into the following types:

1. Impedance-based methods using the analysis of fundamental frequency currents and voltages
2. Time domain approaches based on differential equations describing the faulted network.
3. Methods using travelling-wave phenomenon
4. Methods using high frequency components of currents and voltages
5. Methods using knowledge-based approaches [4]

The accuracy of measurements used directly affects the accuracy of the FLA. The accuracy and availability of measurements are quite varied, as are the networks to which they are

applied. For this reason, a variety of FLAs have been proposed over the years. The chapter proceeds to provide a literature review. The emphasis of the review is on the general method, and the required input data (one terminal data, two terminal data etc).

2.1. Impedance-based Fault Location Algorithms

Such FLAs calculate the distance to fault generally using power system frequency phasors or time domain samples of currents and/or voltages. These methods are based on transmission line theory and impedance calculations. They may be classified based on whether they require current and/or voltage measurements from just one terminal or from both terminals of the line as follows.

2.1.1. Fault Location using One-End Measurement Data

The simplicity and the cost benefits of one-terminal FLAs are a major advantage over two-terminal FLAs and travelling wave based algorithms. Some FLAs require three-phase data for current or voltage alone while most FLAs require both. Line parameter settings are required per unit length of the line. Measurements carried out at the terminal using CTs and VTs are input to a microprocessor based relay which then carries out the distance to fault calculation accordingly. Supervisory Control and Data Acquisition (SCADA) or other communication equipment may send the estimates to the system operator [8], [3].

There are several factors that typically affect the accuracy and integrity of such algorithms [4]. High resistance faults may not be detected if magnitudes of fault currents are not significantly greater than those of pre-fault currents. High fault resistance is also known to negatively influence the accuracy of fault location. Incorrect fault classification can occur. Effect of the asymmetry of mutual coupling must be considered e.g. when using the transposed line assumption for untransposed lines. Mutual coupling effects due to parallel lines in the vicinity of each other will affect the calculations. Inaccuracy in zero sequence impedance settings can be a significant factor [12]. There are several other factors influencing fault location accuracy such as effect of shunt capacitance and line model

assumption, effects of CT saturation, noise in measurement, variations in impedance per unit length at different points on the line etc [3].

For real-time fault location one-terminal FLAs are preferred over two-terminal FLAs for two main reasons. Firstly, no communication infrastructure for the sending and receiving of data to a central location is required. Secondly, the computation times are much smaller due to the simplicity of the algorithms [4]. This is especially an advantage when considering autoreclosure. A wide variety of methods can be used for FLAs using only one-terminal data. The underlying principle in a majority of these methods is the calculation of reactances. It involves the use of voltages and currents to find the apparent impedance as seen at the given line terminal. This ratio of the apparent impedance to the total impedance of the line provides a useful basis for calculating the distance to fault or pinpointing the zone of a fault. If the impedance calculated by the relay is assumed to vary linearly with distance from the line- terminal, the ratio of the impedances is the ratio of the distance to fault to the entire line length. During the occurrence of a high resistance fault this assumption may lead to inaccuracies in fault distance calculation. Such errors can be minimised if only the reactances of the line are calculated instead of the full impedance. The calculations of imaginary components allow the elimination of fault resistance from equations used to derive the expressions of distance to fault. If only the currents at one terminal are measured, it may be required to assume that the fault current is in phase with the line-end current. It is also generally assumed there is no load current in the system prior to the fault. The accuracy of these methods depends on the extent of disparity of such assumptions in comparison with the actual faulted system. Errors due to the no load current assumption can be addressed by using instead, the difference in measured current caused by the occurrence of the fault [3], [13], [14], [15].

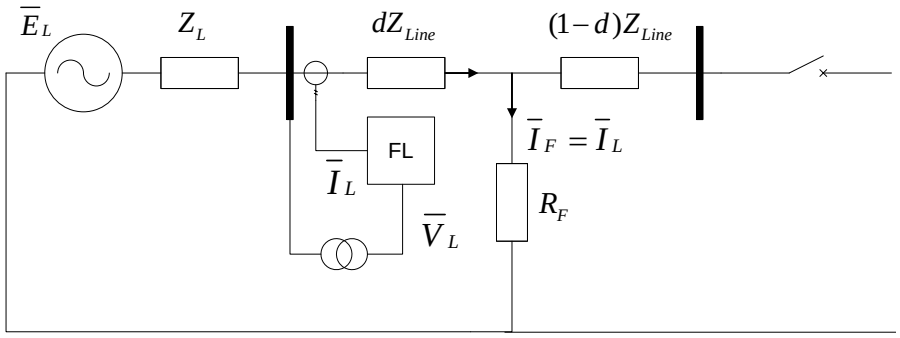

Figure 2.1: Single-phase line under fault (without remote-infeed current)

Shown in Figure 2.1 is a diagram of a single-phase faulted line where only the local line-end network contributes to the fault current. In such a system, it follows:

$$\overline{V}_L - (dZ_{Line} - R_F)\overline{I}_L \tag{2.1}$$

$$d = \frac{\left|\overline{V}_L / \overline{I}_L\right|}{\left|Z_{Line}\right|} \tag{2.2}$$

where, $\overline{V}_L$ is the local terminal voltage, $\overline{I}_L$ is the local terminal current, R_F is the fault resistance, Z_{Line} is the impedance of total length of the line and d is the fractional distance to fault. Thus, the distance to fault can be calculated simply using (2.2). This simple expression is limited in that it cannot be applied directly to faulted lines where there is a remote-infeed to the fault (except in the case of solid-earth faults) such as the system shown in Figure 2.2.

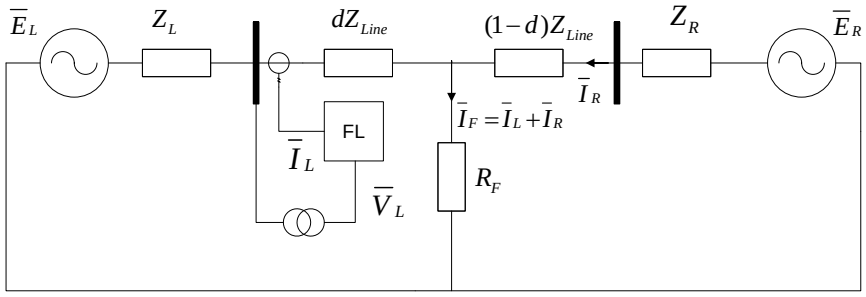

Figure 2.2: Single-phase line under fault (with remote-infeed current)

For single-terminal FLAs to take remote-infeed into consideration, simplifications are required to be made. This can be explained as follows. (2.1) may be modified for the faulted system in Figure 2.2 to (2.3) below by considering the total current:

$$\bar{V}_L - dZ_{Line}\bar{I}_L - R_F\bar{I}_F = 0 \tag{2.3}$$

where $\bar{I}_F$ is the total fault current. It follows that there are more unknowns than knowns (assuming voltages and currents from the local terminal are known). To address this, single-ended FLAs may use current distribution factors to account for the remote infeed current [15]. For example, [14] proposes an FLA (Takagi et. al) that considers the difference between the pre-fault current and fault current to calculate the distance to fault. It can be shown that this difference in current at the local terminal ($\Delta\bar{I}_L$) can be expressed as follows:

$$\Delta\bar{I}_L = \frac{(1-d)Z_{Line} + Z_R}{Z_L + Z_{Line} + Z_R}\bar{I}_F \tag{2.4}$$

where Z_L is the source impedance of the local line-end network and Z_R is the impedance of the remote line-end network. The current distribution factor (k_F) allows the computation of the total fault current (considering remote infeed) using the following expression:

$$\bar{I}_F = \frac{\Delta\bar{I}_L}{k_F} \tag{2.5}$$

Assuming k_F is available as a pre-determined setting, it follows from (2.4) and (2.5) that:

$$\bar{V}_L - dZ_{Line}\bar{I}_L - \frac{R_F\Delta\bar{I}_L}{k_F} = 0 \tag{2.6}$$

If $|k_F|$ is the magnitude of k_F and β is its phase angle such that:

$$k_F = |k_F| e^{j\beta} \tag{2.7}$$

Then, substituting for $\Delta\bar{I}_L$ from (2.4) and through algebraic manipulation of (2.6), the following expression of distance to fault in terms of known quantities as shown below is obtained:

$$d = \frac{\mathrm{Im}(\bar{V}_L \Delta\bar{I}_L^{\,*} e^{j\beta})}{\mathrm{Im}(Z_{Line} \bar{I}_L \Delta\bar{I}_L^{\,*} e^{j\beta})} \tag{2.8}$$

The method relies on the assumption that the fault current measured at the line terminal is in phase with the fault current at the fault point. The higher the fault resistance or sin(β), the higher the inaccuracies of the method. Here, β the current distribution factor angle varies depending on the fault location. It can be calculated only if the source impedance is known. The knowledge of source impedances allows the calculation of distance to fault accurately without the need for the aforementioned assumptions. The current distribution factor angle does not need to be taken into account and the reactance effect does not affect the accuracy of distance to fault. Errors in the source impedance settings will affect the accuracy of fault location [3]. Algorithms using the source impedance may be affected by mutual coupling effect between the phases of the transmission line [3], [8], [14].

One of the earliest numerical FLAs is proposed in [16]. The FLA requires current and voltage data from a single-terminal to calculate the distance to fault. The method does not require the need for source impedance settings. The major drawback with the FLA is that it does not consider the mutual coupling effects on the fault current due to healthy phases. Moreover, it neglects the shunt admittance of the line which introduces further inaccuracies in the algorithm. Several FLAs have since been proposed that take these factors into consideration. A statistical FLA was proposed in [17] to pinpoint the section of the line containing the fault. It uses a stochastic approach and is found to be reliably accurate for a wide variety of faults and fault resistances. The shortcoming of the algorithm

lies in that it only selects a section of the line and does not precisely calculate the exact distance to the fault.

In recent years the use of Artificial Neural Networks (ANNs) for the purpose of fault location using single terminal data has been proposed in a number of publications [18], [19]. One such fault locator proposed in [20]. The inputs to the ANN are currents and voltages measured at the terminal, the output being the distance to fault. The method in question was found to be reliably accurate for Single Line to Ground (SLG) faults but not for Double Line (DL), Double Line to Ground (DLG) or 3-phase faults. The other disadvantage of the fault locator lies in that ANNs require an extensive training data and can only be used to locate faults for which they are suitably trained. This is the reason that ANN based FLAs are not commonly implemented.

The FLA described in [36] uses high frequency transient data from a single terminal of the line. It is capable of very fast operation (to the order of 8ms). The drawback with the algorithm however is that it does not accurately consider the fault resistance and assumes that fault conditions will not be significantly different to the ones considered in the testing of the algorithm. Reference [37] describes an FLA that uses modal transformation in its analysis of single-terminal measurement data. As is the case with a number of such FLAs, its accuracy is significantly lowered when tested for high resistance faults.

Reference [21] discusses the applicability of FLAs using single-terminal measurement data. Such algorithms are often found to be very precise and reliable under certain conditions, but incapable of calculating the distance to fault for other conditions. The paper discusses the relative benefits and shortcomings of five categories of approaches used by one terminal FLAs namely: Iterative, Measurement Resistance, Quadratic Equation, Differential Equation, and High Impedance. The paper puts each method to the test under a variety of system operation modes, line lengths, source angle differences, fault inception angles, path resistances and source impedances. Additionally, it also considers the inaccuracies as a result of CT saturation and inaccuracy of line parameter settings. Of these methods, the measurement resistance method was found to operate best under a variety of

conditions. But more importantly the paper highlights the shortcomings of one-terminal FLAs due to the limited data available for the calculation of fault distance [21].

The accuracy and robustness of one-terminal FLAs is limited in this regard. Although the simplicity of these FLAs makes them more suited for real time fault location, far more accurate and robust FLAs can be developed with the availability of two terminal currents and voltages. Other one terminal FLAs have been cited in [22]-[25].

2.1.2. Fault Location using Two-End Measurement Data

The availability of current and voltage data from both terminals of a line, allows for far more accurate solutions for distance to fault. The fault current can be accurately accounted for without making any assumptions, given that it can be expressed as a sum of the terminal currents of the faulted phase. Two terminal FLAs can correctly determine the type of fault (SLG, DL, DLG, 3-phase) by comparison of incoming and outgoing currents of each phase. Analysis of phasors and impedances of the positive sequence network is simplified due to the availability of the additional data [3]. It is preferable to use positive sequence components as opposed to zero sequence components in fault location calculations [4]. The availability of the additional data in the case of two-terminal FLAs also allows for more complex fault analysis.

The general methods used for single terminal FLAs, apply to two-terminal algorithms as well. As is the case with one-terminal FLAs, the use of line impedance parameters in the development of such FLAs is common. Unlike one terminal FLAs, two terminal FLAs require communication of data to a central location where this data can then be processed. Two terminal FLAs require a higher number of computations due to their increased complexity leading to greater computation times. If two terminal FLAs are to be used for real-time fault location it would require a communication channel between the two terminals. This would affect the speed at which the algorithm arrives at a solution. For offline fault location however, the speed is not a major concern and algorithms may take up to a few minutes to perform their calculations. The level of accuracy required for offline fault location makes two terminal FLAs more suitable [3], [4].

Two terminal FLAs can be classified into algorithms that require measurements from the two terminals be time synchronised with one another i.e. synchronous data sampling [26]-[28] and algorithms that do not require any synchronisation of data i.e. asynchronous data sampling [6], [7]. FLAs using asynchronous data samples may not be as accurate as those using synchronous data, but they are simpler and more reliable. Thus, FLAs using asynchronous data sampling can still compute the distance to fault where data samples are synchronised and will not be affected by any synchronisation errors. In comparison, the synchronisation of samples from the two terminals allows for more accurate algorithms to be implemented. These algorithms are more complex and require a GPS or some other system of synchronisation, but the improvements in accuracy are significant.

2.1.2.1. Fault Location Using Asynchronous Data

Asynchronous data sampling FLAs perform sampling asynchronously before communicating the data to a common point via a communication channel. A common approach in FLAs requiring synchronised data but where only asynchronous data is available, is to apply a correction factor to voltages and currents phasors from one given terminal so that they are time-synchronised with phasors at the other terminal. For example, if δ is the synchronisation error, equal to the phase difference between the co-ordinate systems of the local line terminal phasors and remote line terminal phasors, this factor would equal $e^{j\delta}$. Multiplying each of the remote terminal phasors with this factor will allow the FLA to carry out analysis of the re-synchronised phasors. This synchronisation error can be determined comparing incoming and outgoing currents for healthy phases or pre-fault currents [4]. The FLA proposed in [29] uses asynchronous data and solves for the distance to fault taking into account a distributed line model. It calculates the synchronisation angle prior to determining the distance to fault. It first calculates an initial estimate for the distance to fault assuming a simplified model of the line and then uses a Newton-Rhapson procedure in the subsequent calculations for the distance to fault.

An example of an asynchronous two terminal FLA is proposed in [30]. The principle used in the algorithm is that the fault voltage as calculated in terms of the local line-end fault

loop and as expressed in terms of the remote line-end fault loop will have the same magnitude. This approach is useful when the data samples are not synchronised, since the amplitudes of the fault voltage phasors will be equal regardless of the instant in time that they are individually calculated. By expressing each term in the equation in terms of their real and imaginary components, a quadratic equation of the distance to fault from the local terminal is obtained. Only one of the two solutions lies within the appropriate range and also corresponds to one of the solutions obtained when this analysis is carried out for the zero-sequence circuit. The drawback of the FLA lies in that it is only be applicable to SLG faults.

Numerous other FLAs using asynchronous data have been proposed. Reference [31]-[34] are some important examples. One major disadvantage of FLAs using asynchronous data sampling is the additional complexities introduced typically either due to correction method the synchronisation error or the solution of complex nonlinear equations.

2.1.2.2. Fault Location Using Synchronous Data

Recent advances in the use of communication technology in power system protection have made the use of synchronised data for two-terminal algorithms feasible. The availability of synchronised data samples or phasors allows for the use of simpler and more effective methods to calculate the distance to fault. The method of time-synchronisation of data must be reliable, for the FLAs to produce accurate estimations. The use of a GPS system is one such reliable method of synchronisation. The mapping of data is accurate to 1 μs. The use of PMUs allows for such synchronisation of two-end data.

One major advantage of such FLAs is that they are not sensitive to factors outside the section of the line contained between the two such as source impedances or loading conditions. The fault voltage can effectively be eliminated in the analysis, and therefore the accuracy of these FLAs is not sensitive to fault resistance or remote-infeed. Synchronised sampling of voltages and currents at the terminals is carried out using Synchronised Measurement units (SMUs) and a GPS satellite synchronisation system. Data Concentrators then collect the synchronised phasor data. This is where the fault location is arrived at using the FLA along with other fault analysis. Clearly, a more complex

communication infrastructure is required for FLAs using synchronised two terminal data, than those using single terminal data or asynchronous data.

One such FLA using two terminal-synchronised data is proposed in [11]. It is an example of how two terminal synchronised data can be used to perform more complex analysis of fault data to arrive at more accurate solutions of distance to fault. The method not only calculates the distance to fault from the local terminal but also does so directly using time domain samples as opposed to performing a fast fourier transform to obtain phasors. The FLA is also shown to be tested using simulations of a real power system belonging to the Western Area Power Administration (WAPA). The drawbacks of the algorithm are the inaccuracies introduced by the presence of mutual coupling due to parallel lines and reflection of waves from points of transposition.

Fault currents are of a significantly larger magnitude than pre-fault load currents. The presence of high decaying DC components adds to high fault current measured by the CTs. At high fault currents, CTs may saturate distorting the current measurements. This has an impact on the accuracy of fault location. To solve this problem an FLA using only synchronised two terminal voltage data was proposed in [35]. The method requires settings for source impedances at the terminals. Only fault resistances of up to 60Ω have been considered in the testing of the algorithm. The impact of a higher fault resistance on the accuracy of distance of fault is not known. Given that the fault point voltage magnitudes are higher for higher fault resistances, the solutions may not be satisfactorily accurate.

References [66], [67] propose an FLA utilizing synchronised harmonic phasors from both ends of the line to perform fault detection/location. It is shown to be accurate for both arcing and permanent faults, and uses the distributed line model assumption. But the method is not without its drawbacks. The algorithm relies on synchronised data and cases where synchronisation is unreliable or unavailable have not been considered. Other important examples of FLAs using two terminal synchronised data have been listed in [27], [28], [68]-[71]. FLAs of this type require synchronised data making them sensitive to a loss of synchronisation. This makes them less robust in comparison to the FLAs using asynchronous data described previously.

2.2. Travelling-Wave Based Fault Location

The earliest travelling wave based method for fault location was proposed in the 1931 [42], [4]. Travelling wave based FLAs are generally found to be highly accurate at calculating the distance to fault [3]. Due to recent technological advances in communication, there has been growing research interest in this approach.

The principle behind these FLAs is that during a fault or switching, voltage and current transient waves travel from the fault to the line terminals and bounce backwards and forwards. These FLAs use the correlation between the forward and backward waves in their calculations of distance to fault. The current-voltage relationship of the waves can be expressed in terms of the characteristic impedance of the line. Given that the speed of propagation of these waves is equal to the speed of light, the time difference between the detection of forward and backward waves can be used to calculate the distance to the fault from the corresponding line terminal [3]. These FLAs also require a special sensor to detect the travelling transients when they reach the terminals. These techniques generally require that measurements at both terminals have synchronised with one another. A GPS synchronisation system is required for accurately time-stamping these detection events at each end. The synchronised data must be processed to a central point where the data is processed to carry out the fault location [8].

Unlike FLAs using fundamental frequency analysis, travelling wave based FLAs are not sensitive to loading levels, fault resistance or the presence of series compensation, making them favourable under certain conditions. However, a limitation of this method of fault location is that it cannot be applied to non-homogenous transmission corridors (mixed OHTL-cable). The accuracy of these algorithms largely depends on the accuracy of wave detection. The occurrence of multiple reflected transients is attributed as the cause of this error. For instance, in the case of lightning storms with multiple strikes, distinguishing between the two sets of transient waves may not be possible. Significant damping of voltage transients may occur at buses considerably making detection difficult. This has an impact on the accuracy of fault location. GPS errors may result in inaccurate timing of

waves resulting in further inaccuracy. It must be noted that the U.S. Department of defence purposefully introduces a level of uncertainty for security [3], [8].

The most economical and least complex type of travelling wave based FLAs are those that require wave detection at only one terminal. Unlike two terminal FLAs using travelling wave methods, they do not require any communication infrastructure. However, one terminal FLAs using this approach require the correlation of reflected waves to the forward wave. For faults close to the sensor, this procedure is found to be relatively inaccurate. For examples of such one terminal travelling wave based FLAs, see [38]-[40].

Travelling wave based FLAs using sensors at both terminals record the time instances when the original waves from the fault reach each of the line-ends. Based on the difference in timing of these events, accurate and reliable solutions of distance to fault can be obtained. This solution is calculated using the total line length and the speed of waves (assumed to be the speed of light - $3x10^{18}$ m/s). A GPS satellite system can be used to achieve precise time stamping. Unlike one-terminal travelling wave based FLAs, they do not require any correlation of forward and reflected waves. This is advantageous from the point of accuracy. The requirement of a communication infrastructure makes them more expensive and more complex to implement. From the point of reliability, travelling wave FLAs using two-terminal wave detection are less favourable to those using one-terminal data due to the use of the communication channel. Examples of such FLAs are [41]-[43].

A lattice diagram showing the forward and reflected transients as they move from the fault to the line-ends and back and forth between the two line-ends can be seen in Figure 2.3. The distance travelled by a wave from one terminal to another or one terminal to the fault point and back can be calculated using the time difference between the occurrence of the two corresponding events. A number of travelling wave based FLAs using the wavelet transform have been proposed in recent years. References [44], [45] are some important examples. Although such FLAs are useful and accurate for the purpose of fault location, they cannot be used to perform other fault analysis such as determining the nature and arc resistance of the fault.

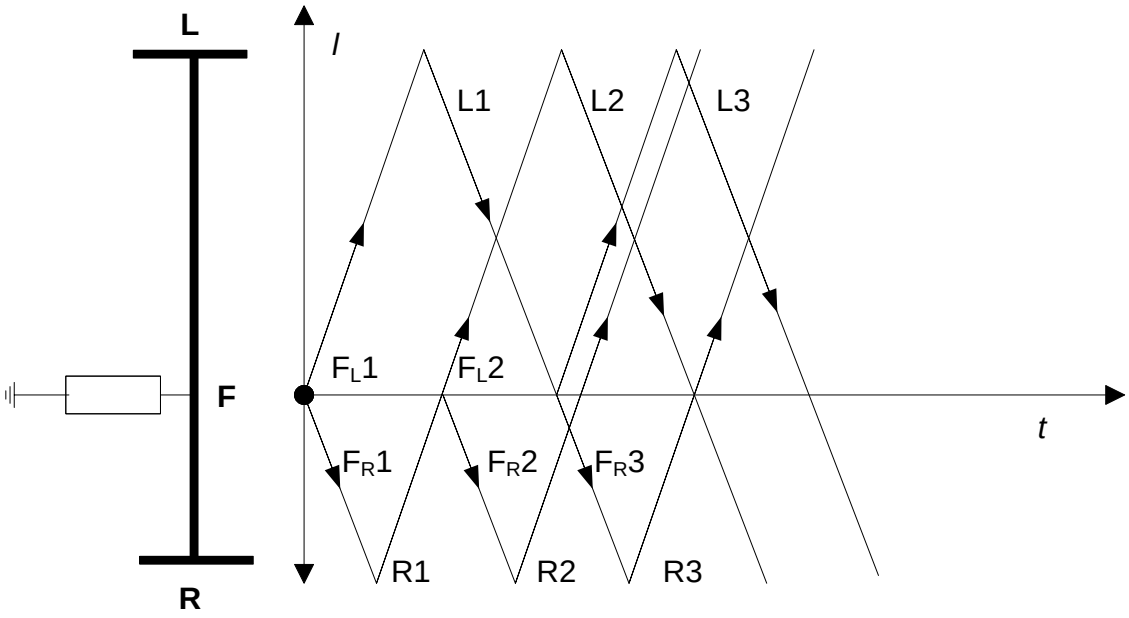

Figure 2.3: Lattice diagram - travelling waves generated and reflected during a fault

2.3. Considering the Effect of CT Saturation

CTs are rated to perform accurately under normal conditions. The currents measured using CTs during fault conditions may be inaccurate due to CT saturation under high fault currents. This introduces inaccuracies in FLAs using current measurements from one or more terminals. Given the point of inception on the fault voltage wave, high decaying DC currents will add to the fault currents adding to further inaccuracy in the estimation. Depending on how distorted the measured currents are in comparison to the actual currents and the method of the FLA, the estimate may be either inaccurate or the FLA may be completely inapplicable. This may cause malfunction of protective relays and grossly incorrect estimation of distance to fault in the case of fault locators.

The solutions proposed in the literature use one of the following approaches in dealing with the CT saturation:

1. They may use a hardware approach to avoid CT saturation [59].

2. They may use voltage measurements only in their calculations and reject current measurements [60], [61], [62]

3. They may use all voltage measurements, but use current measurements from only the CT that is not saturated. [63], [64].

4. Use currents from saturated CTs only during periods where this current is not high enough to cause saturation [65].

Rogowski coil CTs are an improvement over magnetic CTs in that they are free from magnetic saturation as the air-core of such CTs cannot saturate as does the iron-core in magnetic CTs. If Rogowski coil CTs are used, there is no requirement for any of the above procedures to arrive at an accurate calculation of distance to fault.

2.4. Use of Artificial Neural Networks in Fault Location

In recent years, the use of Artificial Intelligence based methods for fault location have gained significant research interest. These algorithms make use of either Artificial Neural Networks (ANNs) [46]-[48], Fuzzy logic [51]-[53] or genetic algorithms [49]-[50]. The literature review focuses on FLAs using ANNs since they are the most common of the Artificial Intelligence based methods. ANNs have been used to replicate the biological model of neural networks and thereby emulate the biological mechanisms for learning. They have been since used for a wide variety of applications including character recognition and stock market prediction. They have similarly been used to "learn" to reliably detect, classify and locate faults on power networks. This is based on the recognition of transient travelling waves corresponding to a certain fault type and location of a fault based on training data [46].

An ANN is capable of locating faults for systems it is trained for, given it has been trained extensively for all given fault types and a variety of fault locations. The reliability and accuracy of fault location thus depends on the extent to which it is trained. Insufficiently trained ANNs will not be able to correctly locate faults on the line or even identify the section of the line containing the fault. There are several different types of ANNs, but the

3-layer perceptron feed forward neural network (FFNN) is most commonly used in ANN based FLAs. Back propagation neural networks based FLAs have also been proposed [54].

ANN based FLAs have several advantages over FLAs using other approaches. They can correctly recognise and locate faults for a variety of source impedances and fault resistances. The disadvantage lies in that they must be trained using extensive training data. There always lies the possibility that the FLA cannot recognise a certain fault for which it is not trained, since it is practically impossible to train the ANN for every possibility. The use of ANNs for the purpose of fault location is found to be highly accurate in comparison to other methods due to their ability to learn and map non linear systems. But the need for extensive training data is a major drawback of these methods. This makes them less favourable over FLAs that locate faults by mathematically processing the measured data [46].

2.5. Fault Location for Parallel Lines

FLAs designed for use on parallel lines need to consider the influence of mutual coupling between lines in their calculations to ensure sufficient accuracy. The presence of phase currents in parallel healthy lines will cause an induced voltage drop on the faulted line due to mutual coupling. If the analysis is carried out in the sequence domain, the positive-sequence and negative-sequence mutual impedances are negligible, but the zero-sequence mutual impedance has a significant impact on the accuracy of fault location.

A single phase system comprising of parallel lines is shown in Figure 2.4. It can be seen that the current at the remote terminal in the faulted line is flowing opposite to that in the healthy line. This current will be reduced in magnitude in comparison with a fault at the same distance but without a parallel line in the vicinity. Parallel lines may not always be in the form of double circuit lines running n parallel from the local terminal to the remote terminal. There may be more than two lines entirely running parallel to one another or may be parallel for only sections of the entire distance. This introduces further complexities to be considered in the FLAs. See [55]-[58] for examples of FLAs for parallel lines.

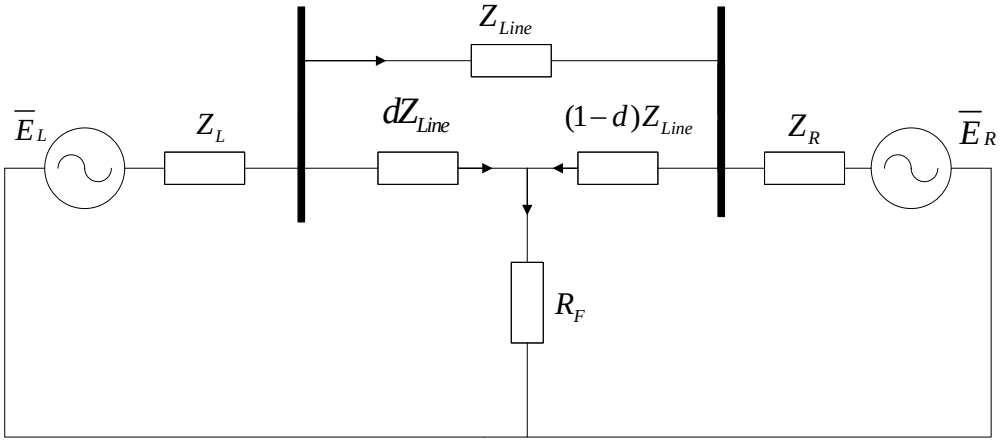

Figure 2.4: Faulted circuit in parallel with a healthy circuit (single line diagram)

2.6. Assessment of Proposed FLAs

The chapter thus far provided a literature review of various existing techniques for fault location. Each technique was criticised in terms of its advantages and shortcomings. This section provides a similar assessment of the proposed algorithms discussed in later chapters of this thesis. The aim of this assessment is to point out how a number of shortcomings have been discussed for existing solutions have been addressed for the proposed novel algorithms for series compensated lines. These are presented as follows in tabular form in Table 2.1.

Table 2.1: Assessment of proposed FLAs based on technique and measurements

Aspect of Fault Location	Novel FLA proposed for Single Circuit Series Compensates Transmission Lines	Novel FLA proposed for Double Circuit Series Compensates Transmission Lines
One-terminal measurements or two-terminal measurements?	Two-terminal measurements required	Two-terminal measurements from both circuits required
Complete measurements?	Current and Voltage at both terminals required	Current and Voltage at both terminals and for both circuits required
Relaying or fault locators?	Algorithm designed for the purpose of fault locators	Algorithm designed for the purpose of fault locators
Phasor domain or time	Phasor domain	Phasor domain

domain?	(Fundamental Frequency)	(Fundamental Frequency)
Phase networks or sequence networks?	Phase networks	Phase networks
Method of obtaining phasors?	FFT carried out after removal of DC components	FFT carried out after removal of DC components
Data Sampling used?	(64 samples per 50 Hz cycle)	(64 samples per 50 Hz cycle)
Accuracy based on requirement?	High accuracies under various fault conditions	High accuracies under various fault conditions
Speed based on requirement?	No stringent requirements for the speed of fault location. Not capable of real-time fault location.	No stringent requirements for the speed of fault location. Not capable of real-time fault location.
Complexity?	Algorithm is mathematically complex requiring large calculations, but not to the extent of being memory intensive	Algorithm is mathematically complex requiring large calculations, but not to the extent of being memory intensive
Applicability to fault types?	Applicable to all main fault types. Tested for SLG faults, DL faults, DLG faults, 3-phase faults	Applicable to all main fault types. Tested for SLG faults, DL faults, DLG faults, 3-phase faults. However, it is assumed that the fault occurs on only one of the two circuits
Sensitive to fault resistance?	Not sensitive to fault resistance	Not sensitive to fault resistance
Sensitive to accuracy of line-parameters?	Does not require the use of line parameters	Does not require the use of line parameters
Sensitive to CT saturation?	Use of Rogowski coil CTs assumed, otherwise sensitive to CT saturation	Use of Rogowski coil CTs assumed, otherwise sensitive to CT saturation
Sensitive to shunt admittance in the case of long lines?	Sensitive to shunt admittance in the case of long lines	Sensitive to shunt admittance in the case of long lines
Synchronous measurements or asynchronous measurements?	Applicable to both Synchronous measurements and asynchronous measurements	Applicable to both Synchronous measurements and asynchronous measurements
Any advantage over travelling wave or ANN based techniques?	Does not use line-parameters or expensive travelling wave filters.	Does not use line-parameters or expensive travelling wave filters.

	Proposed algorithm does not require extensive training as is the case for ANN-based techniques	Proposed algorithm does not require extensive training as is the case for ANN-based techniques

2.7. Chapter Summary

The significance of FLAs in the field of power system protection cannot be overstated. They enable line protection to locate and thereby selectively isolate the fault and they enable fault locators to precisely pinpoint the fault location so that utilities may repair and re-energise the line and thereby minimise any resulting financial losses. There are key differences between the requirements of FLAs developed for protective relaying and FLAs developed for fault locators. They differ in their required computation times, accuracy of fault location, communication infrastructure, complexity, and availability of data for calculation.

A number of factors influence the speed and accuracy of FLAs such as presence decaying DC components, higher harmonics, accuracy of spectral domain transformation and accuracy of mathematical assumptions used. There is often a trade-off between the speed of computation and the accuracy of the algorithm. That is to say the more accurate the algorithm, the higher the complexity of calculation, and therefore the higher the computation times.

A majority of fault location techniques fall under one of three main categories. These FLAs may use impedance-based methods, travelling-wave based methods or knowledge based methods. Each of these approaches offers its own advantages either in the simplicity and cost of implementation or the speed of calculation and the accuracy of fault location.

Travelling wave based methods are found to be highly accurate and may be applied to lines of various topologies. The disadvantage of such methods is that they require specialised filters for the extraction such signals incurring additional costs, whilst other approaches may directly make use of available CT and VT measurements. Knowledge based methods typically make use of Neural Networks, and whilst such methods are efficient and accurate, they require extensive training data.

Impedance based approaches may either use one-ended measurement data or two-ended measurement data and may or may not require that local and remote line-end measurements be synchronised. Fault location using fundamental frequency components or time domain samples of currents and voltages are conventionally used due to the aforementioned limitations of other approaches. The body of knowledge for such impedance based fault location is vast and can be applied in the development of newer, faster and more accurate algorithms.

In recent years, a number of FLAs have focused on the solution of two under-addressed factors contributing to the inaccuracies of fault location, namely; the effect of CT saturation and the influence of mutual coupling due to parallel lines. The saturation of CTs during the peak currents of high magnitudes leads to distortion of measured signals and inaccuracies in fault distance calculations. This problem is addressed either using hardware based approaches, use of only voltage signals, selective choice from available current signals, or the selective use of available current data samples from the saturated CT. A number of FLAs have been proposed that factor in the influence of mutual coupling between parallel lines.

The main focus of the Ph.D. project in the development of novel FLAs was to achieve high levels of accuracies demanded by fault locators for series compensated lines. Given the complexity of the electrical nature of such lines, efforts were focused on the use of two-terminal synchronised measurement data and in the development of an impedance-based approach. Given that a majority of series compensated transmission lines are either single circuit lines or double-circuit lines, the project was focused for such lines. This chapter only covers the background and literature review for uncompensated lines. Fault location on series compensated lines presents challenges over and above the challenges discussed in this chapter. These challenges and the literature view of existing solutions are discussed in the next chapter.

Chapter 3. Series Compensated Lines - Background, Literature Review and Modelling

In a growing power network, the need for higher transmission capability can be met by series compensation of transmission lines as a cost effective alternative to building new transmission lines. Series compensation also offers an array of other benefits such as increased voltage stability, minimised angular deviation and optimised power-sharing between circuits [73]. This chapter discusses these advantages with an aim to highlight the importance of the study carried out in this Ph.D. project. It aims to provide a background to the thesis and establishes the basic knowledge of the electrical behaviour of series compensated lines.

Chapter 3 also provides a literature review of various solutions for protection and fault location of series compensated lines proposed in literature and highlights the key drawback of existing solutions that is solved by solutions proposed in this Ph.D. project which are detailed in later chapters of this thesis. Lastly, it discusses the simulation framework used in the testing and validation of the novel algorithms discussed in this thesis.

Series compensated transmission lines offer a great many advantages to power systems. Mainly used to increase the power transfer capability of the line, they also have the advantages of increased power system stability, flexibility of power flow, voltage regulation and most importantly reduced cost and space considerations as an alternative to building new transmission lines [73]. Long EHV transmission lines (>=230 kV) can especially benefit greatly from incorporating series compensation when considering the economic advantages.

However, one of the shortcomings of compensating transmission lines using series capacitors is that standard algorithms for protection are no longer valid. The same problem applies to FLAs used for fault locators. Even the mere presence of the series capacitor in an otherwise inductive line presents some challenges to the operation of conventional

distance, differential and directional relays and in the accuracy of distance to fault estimation. Two major consequences are the over-reaching of distance relays, and the failure to operate for low current faults [74] (discussed in further detail in Section 3.7). Moreover, the impedance of the parallel combination of the capacitor, spark gap and MOV combination is not constant. Subharmonic frequency oscillations may also affect the operation of line protection [75], [76]. Directional protection may be affected by voltage inversion or current inversion in cases where the line compensated at the line-ends (discussed further in Section 3.7.1 and Section 3.7.2). Differential protection may also be affected by current inversion (discussed further in Section 3.8.4).

Line protection must ensure to protect the line despite this variability and with or without the capacitor in operation. As discussed in the previous chapter, fault locators require being highly accurate (to within a few kilometres [77]) since they determine how speedily a faulted line is brought back into service, thereby minimising outages and related costs. This is especially true since there often is no visual evidence for the fault, and thus accuracy within a few kilometres is essential in such cases to minimise inspection times required by repair crews [77]. Series compensation may be fixed or variable. Fixed series compensation is in the form of capacitor banks. Advanced variable series compensation allows the control of the reactive power compensation by means of solid state electronics using thyristors, gates, inverters etc. The most common of these is the TCSC which offers an array of advantages ranging from subsynchronous resonance mitigation to damping low-frequency inter-area oscillations (discussed further in Section 3.4).

3.1. Background

In an AC system (as shown in Figure 3.1, the reactive power is the sinusoidal component of the instantaneous power with a frequency which is twice the system frequency as shown in (3.1). Here, $P(t)$ is the instantaneous power, V and I are the magnitudes of the voltage drop and the current, ϕ is the phase difference between the current and the voltage, and ω is the system angular frequency. Reactive power represents the energy that oscillates between the source and reactive elements of the system, i.e. inductances and capacitances.

It is thus supplied and absorbed during the alternating halves of the cycle (quarter of the power system cycle). By means of reactive power compensation or VAR compensation, the magnitude of this reactive power can be decreased.

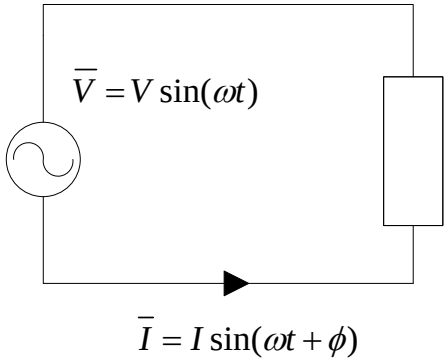

Figure 3.1: Simple AC network

$$P(t) = \frac{VI}{2}\cos(\phi) - \frac{VI}{2}\cos(2\omega t - \phi) \tag{3.1}$$

Reactive power compensation is a means to solve numerous power system issues relating to large interconnected networks. Power delivery and power quality issues in particular have a direct correlation to reactive power management of the network i.e. the additional supply or absorption of reactive power into or from the network. Reactive power compensation offers the following benefits:

- Improving the system power factor: It increases transmission capacity, transmission efficiency and reduces cost of power delivery.

- It provides voltage support and reduces voltage fluctuations due to fluctuations in the load. Its aids the maintenance of a flat voltage profile throughout the network.

- It enhances system stability, minimises current harmonic components, minimises the magnitude of overvoltages, and can thus avoid the occurrence of a blackout [78], [79], [80].

Traditionally, synchronous condensers were used to provide necessary VAR compensation. However, they are rarely used these days and compensators comprising of capacitors, reactors, and thyristors are increasingly becoming the preferred means of VAR compensation [81]. Newer controllable forms of compensation are important as they are integral to the growing technology of Flexible AC Transmission Systems (FACTS). Reactive power compensation can be broadly classified into shunt compensation and series compensation. Shunt compensation works by reducing the effective load impedance, whereas series compensation works by reducing the effective reactance of the transmission system. They are explained as follows:

Shunt Compensation: A line diagram of an uncompensated line is shown in Figure 3.2. The local line-end bus has been represented as a voltage source. An R-L model of the line is assumed for simplicity. The load is shown connected to the remote line-end, and is assumed to be a typical inductive load. As with any inductive load such as a motor, it draws real power, but also requires reactive power in order to maintain a magnetic field. In the case of the uncompensated line this reactive power is supplied by the source. Figure 3.3 shows the same line, but shunt compensated. The reactive power required by the inductive load is significantly contributed towards by the shunt compensator [82]. It follows that if the compensator is close to the load, the current flowing through the network is reduced, and the power factor is improved. Analysis can be simplified by viewing the shunt compensator as a voltage regulator, and in many cases, it is installed for this primary purpose.

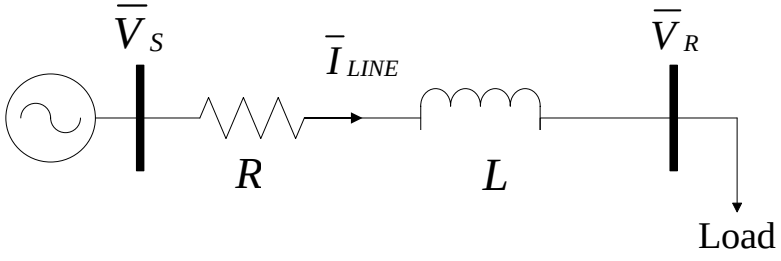

Figure 3.2: Single line diagram of an uncompensated line

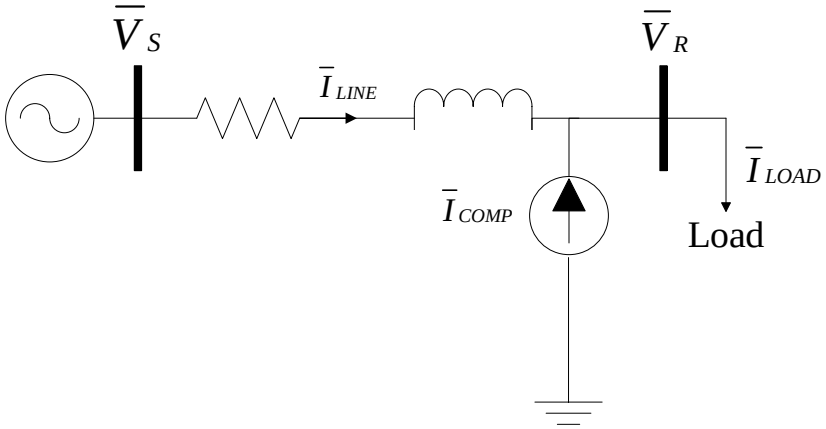

Figure 3.3: Single line diagram of a shunt compensated line

This is shown by means of phasor diagrams in Figure 3.4a and Figure 3.4b. All voltages, currents and reference directions are shown. For simplicity the shunt compensator in Figure 3.3 is shown as a current source, but it is typically a parallel combination of a capacitor and reactor or a voltage source. The use of thyristors or transistors provides flexibility and controllability, and can alter the electrical behaviour of the compensator to provide appropriate voltage regulation [82].

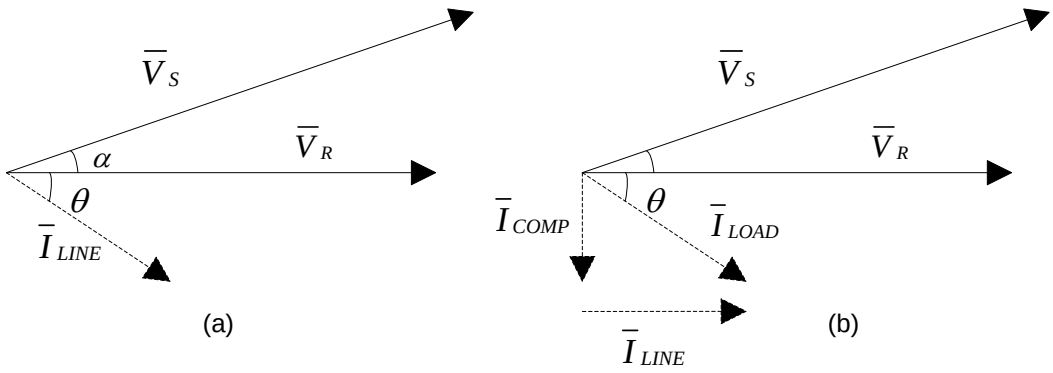

Figure 3.4: Phasor diagrams: a) Uncompensated line b) Shunt compensated line

The static VAR compensator is a type of shunt compensator comprising of a parallel combination of a capacitor branch, a reactor branch and harmonic filters. There may be additional branches in parallel consisting of mechanically switched capacitors or reactors.

Figure 3.5a shows an example of a Static VAR compensator (SVC). The primary purpose of an SVC is voltage regulation. Based on the thyristor switching of the reactor branch, the SVC can consume or supply reactive power. The very first solid state VAR compensator was installed by NOKIAN Capacitors in 1964. They fall under one of two broad types: TCR-FC (Thyristor Controlled Reactor-Fixed Capacitor) or TCR-TSC (Thyristor Controlled Reactor-Thyristor Switched Capacitor). SVCs have a significant advantage over VAR compensation using rotating synchronous machines in that they are faster, less expensive and do not comprise of any moving parts [83].

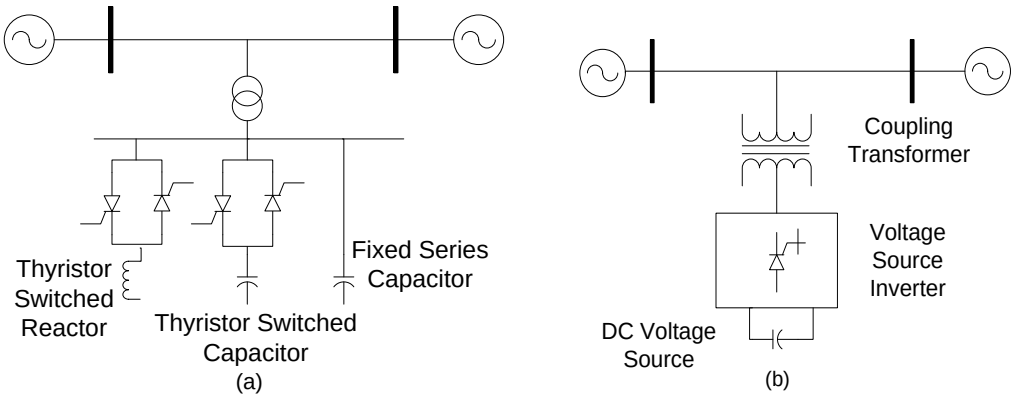

Figure 3.5: Types of shunt compensation a) SVC b) STATCOM

The second major type of shunt compensation is the Static Synchronous Compensator (STATCOM) shown in Figure 3.5b. Like the SVC it can vary the amount of VAR compensation. It consists of a Voltage Source Inverter (VSI) and a coupling transformer that connects onto the line. STATCOMs offer a number of advantages over SVCs such as faster response, improved flexibility of voltage regulation, increased efficiency etc. However they are also significantly more expensive. The first ever STATCOM was installed in 1991. Various types of STATCOMs have been proposed and implemented over the years. They vary primarily in the solid state technology used in the VSI [83].

Series Compensation: Reactive power required by the load can also be injected by means of series compensation. For simplicity, an ideal case of a series compensated line is considered. The line is compensated with a voltage source as shown in Figure 3.6a. The corresponding phasor diagram can be seen in Figure 3.6b. The aim once again in this ideal

case, is to supply reactive power required by the load entirely by means of VAR compensation. While in the case shown in Figure 3.3 this is achieved by injecting reactive power as a current source, here it is accomplished by introducing an appropriate voltage difference in series between the line and the load. It follows thus, that an appropriate voltage difference is required between points $\overline{V}_R$ and $\overline{V}_R'$ such that the line current is in phase with voltage at $\overline{V}_R'$. Given that the load is inductive, it can be seen that this voltage difference lags the line current. Thus, it follows that series compensation can be achieved by means of a series capacitor.

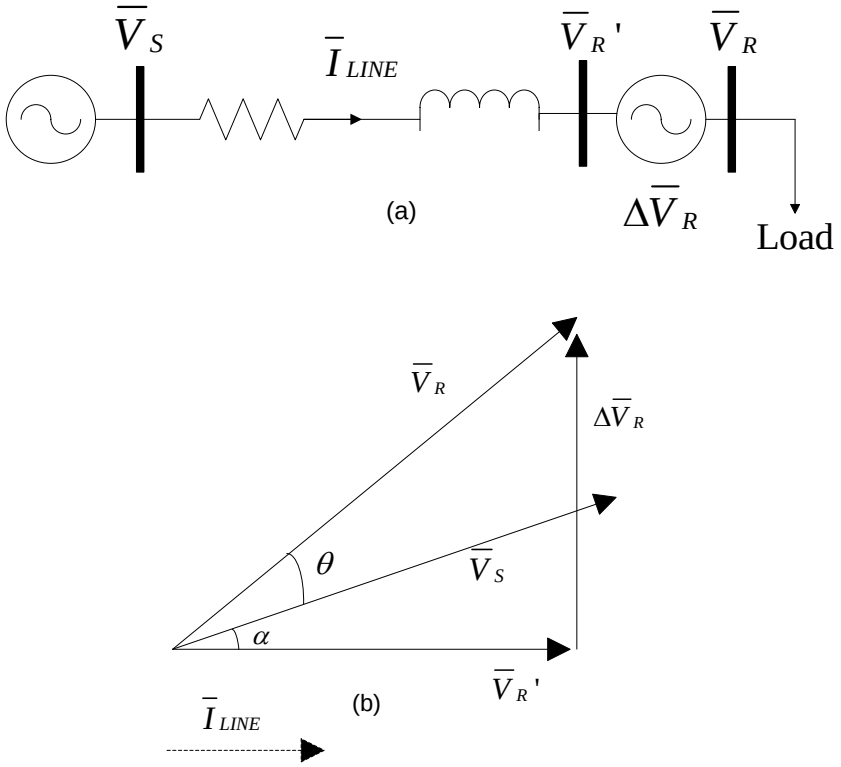

Figure 3.6: Series compensated line a) Single line diagram b) Phasor diagram

Series capacitors affect the voltage profile along a transmission line. Therefore they cannot simply be installed anywhere along the line. Typically, they are installed in the middle of the line, or at one of the line-ends, or both line-ends. These arrangements are shown in Figure 3.7. The degree of series compensation is defined as the ratio between the series capacitor reactance and the inductive reactance of the line expressed as a percentage as shown in (3.2) [85]. The location of series compensation has a very significant impact on

the directionality and distance estimation of protection. Several methods have been proposed for optimising the location and level of series compensation with respect to the primary purpose for which the series capacitor is installed in the line [85]. This thesis and the Ph.D. project focus on series compensated transmission lines and the problems associated with fault location on such lines.

$$rate\ of\ compensation\ (\%) = \frac{X_C}{X_L}.100 \tag{3.2}$$

where, X_C is the SC reactance and X_L is the inductive reactance of the line

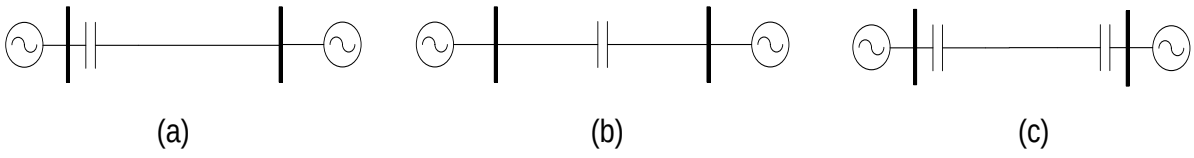

Figure 3.7: a) Line compensated at one line-end b) Line compensated in the middle c) Line compensated at both line-ends

3.2. Importance of Series Compensation for the GB network

According to targets laid out in Electricity Network Strategy Group's (ENSG) Vision for 2020 some 30% of all electrical energy and 15% of all energy are to be generated by renewable sources [139]. It is proposed that 34 GW of wind energy is to be generated as a part of this strategy, requiring capable transmission infrastructure to transmit this power from the North of Scotland to England.

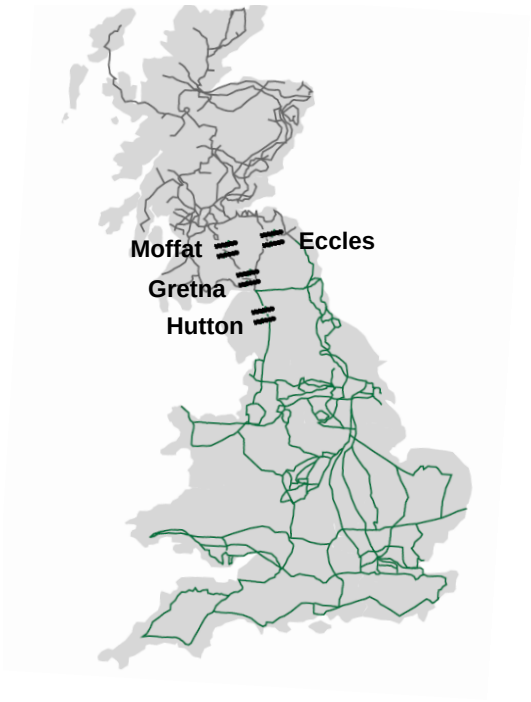

Figure 3.8: Planned installations of series compensation according to ENSG vision for 2020

In order to meet these targets, it is evident that onshore grid and offshore infrastructure reinforcements are needed. The Anglo-Scottish interconnection infrastructure is limited to 3300 MW to ensure angular stability. However, its thermal capacity is 4400 MW [86]. National Grid and Scottish Power are to include series compensation into the interconnection for this purpose. The expected locations of the new series capacitor installations are shown in Figure 3.8. To achieve the 4400 MW capability of the intertie, installations of series compensation have been planned at the following sites:

- Single-Circuit lines, FSC banks (introduced in Section 3.4) :

  -Gretna-Harker 400 kV circuit at Gretna.

  -Moffat-Harker 400 kV circuit at Moffat

- Double-Circuit line, Fixed Series Compensation:

  -Eccles-Stella West 1 & 2 400 kV circuit at Eccles

- Double Circuit line, TCSC: (introduced in Section 3.4)

  - Harker-Hutton 1 & 2 400kV circuit at Hutton

Thus, the study of series compensated lines is very important for the GB network. This is especially so, given the diverse range of advantages that series compensation offers to power systems.

3.3. Advantages of Series Compensation

Increasing transmission capacity: Space considerations in building new transmission lines are very important, especially given the cost benefits and the factor of public disapproval due to their lack of visual appeal. Series compensation of transmission lines offers the advantage of increased transmission capacity, minimising the need for building transmission lines by means of reduction of the effective line reactance. The expression for active power transfer is given in (3.3). Here, $\overrightarrow{V_S}$ and $\overrightarrow{V_R}$ are the sending and receiving end voltages, δ is the angular difference between them, and X is the effective line reactance. It follows that since the series capacitor reactance partially cancels that of the inductive line, there is an increased active power transfer. This increase in active power transfer is achieved without having to increase angular difference.

$$P = \frac{\left|\overrightarrow{V_S}\right| . \left|\overrightarrow{V_R}\right|}{X} \sin\delta = \frac{\left|\overrightarrow{V_S}\right| . \left|\overrightarrow{V_R}\right|}{X_L - X_C} \sin\delta \tag{3.3}$$

Enhancing dynamic stability: From (3.3) it can be seen that the converse is also true. Mathematically, that is to say that the angular difference can be decreased for the same active power transfer, by decreasing the effective reactance. This is an indicator of improved angular stability. The ability of a power system to maintain synchronism under transient disturbances is referred to as transient stability [87]. Rotor masses in synchronous machines oscillate during a disturbance, and thus the inertia of the power system governs its transient stability. The angular difference δ must not exceed limits as required to maintain system synchronism during disturbances and faults. In this regard, series

compensation assists the power system robustness and stability. The active power transfer-angle characteristic for a series compensated line and a traditional uncompensated line is shown in

Figure 3.9.

Equal area criterion is a well known concept in the academic field of power systems. Using the equal area criterion, the point of instability can be determined in terms of the available accelerating area and decelerating area on a graph showing power-angle curves for the system prior to, during, and after a disturbance. The difference between the accelerating area and available decelerating area determines the stability margin [88].

Figure 3.9a shows the power-angle curves and accelerating area (A1) and available decelerating area (A2) for a line without series compensation during a disturbance.

Figure 3.9b similarly shows these areas for the line with series compensation. It can be seen that series compensation improves the stability margin significantly.

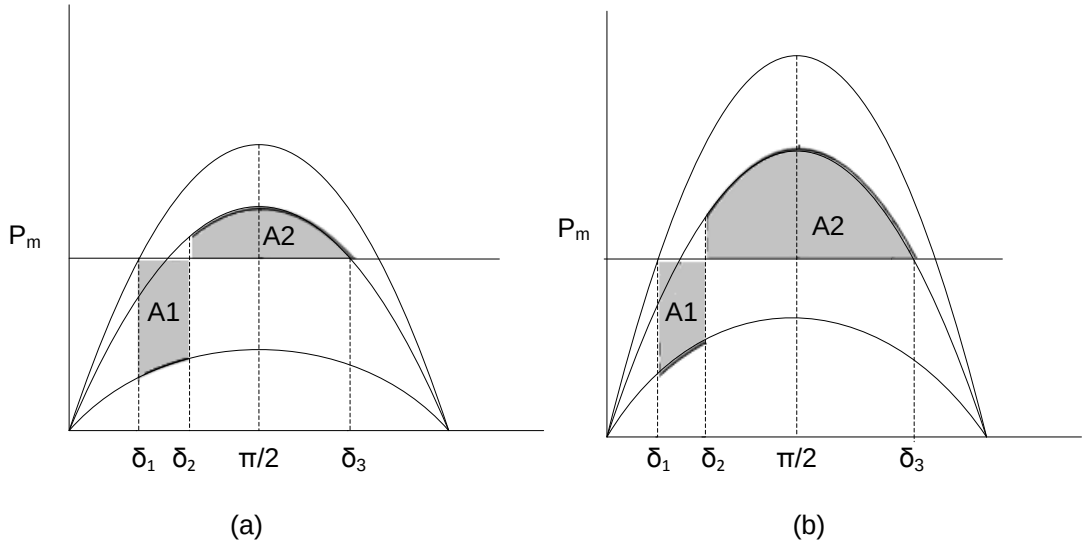

Figure 3.9: Equal Area Criterion a) Uncompensated line b) Series Compensated line

Enhancing voltage stability: Voltage stability in highly loaded lines requires to be taken into consideration. It is well known that bus voltages in a network are largely dependent on

the power flow through the network, and therefore so is voltage stability. The series capacitor supplies reactive power thereby enhancing the power balance. Moreover, with increasing current during a fault, this reactive power also increases. Thus, this reactive power contribution regulates itself in the event of a fault. Given that voltage instability can occur during faults and large disturbances, the presence of series capacitors enhances dynamic voltage stability [89], [90].

Variable series compensation such as by means of a TCSC allows for power flow control in the case of double-circuit lines. Thus the load can be shared unevenly between the two circuits. If one circuit is overloaded, power can be shifted to the lesser loaded circuit. Thus, there is further improvement in transmission capacity over and above the increase due to the lowered effective line reactance.

3.4. Types of Series Compensation

Fixed Series Compensation: This is the most fundamental and the oldest form of series compensation. It is also the most commonly installed. Figure 3.10 shows a line compensated using an FSC. It comprises of a series capacitor and its overvoltage protection. Series compensated lines offer great advantages over uncompensated lines as detailed previously. There are some drawbacks of series compensated lines, such as subharmonic-frequency oscillations, inaccuracy of fault location etc. FSCs have been studied since the 1920s, a number of protection solutions have been developed since. The simplicity, lower cost, and the availability of a number of protection and control solutions, are the key advantages of FSCs over other forms of series compensation.

The first FSC was installed in 1928 at the Ballston Spa substation, New York, USA. GE, ABB and Siemens are the main companies involved in series compensation as a power product, and also in its installation. The primary purpose for the installation of FSCs is increasing power capacity. The following are some examples:

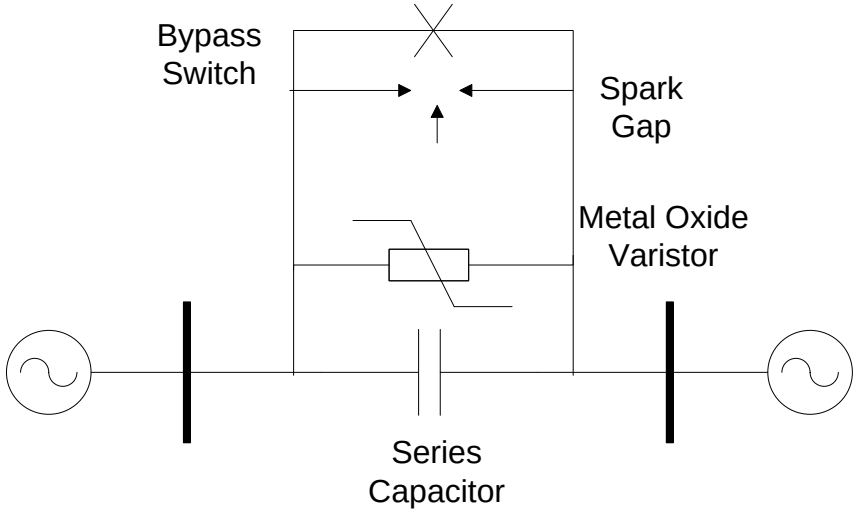

Figure 3.10: Line compensated by a FSC

- 70% compensation of a line is provided by FSC installed at Jacinto, Texas, USA

- FSC installed at Sambao substation, China provides 40% compensation of the line. FSC is also installed at Yangcheng substation in China to compensate a 744 km line by 40%.

- Installed at Vincent substation, California, USA, is the first Thyristor Protected Series Compensation (TPSC, a type of FSC), providing 35% compensation

Thyristor Controlled Series Compensation (TCSC): Figure 3.11 shows a line compensated using a TCSC. It comprises of the series capacitor, its overvoltage protection, a thyristor controlled reactor in parallel, and the firing mechanism for the thyristors. The thyristor controlled reactor branch allows the effective capacitive reactance of the compensator to be varied allowing great flexibility. It is also capable of operating in an inductive mode. Varying the reactance of the TCSC is achieved by means of controlling the firing angle of the thyristors. TCSCs are becoming increasingly popular due to their flexibility, but more importantly due to the feature of subsynchronous resonance mitigation.

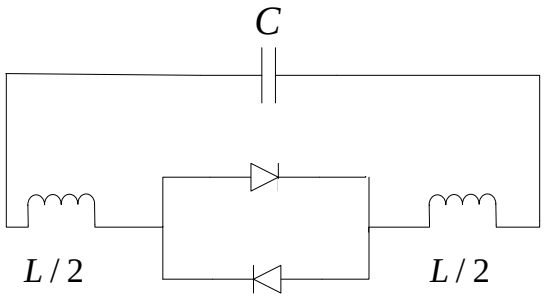

Figure 3.11: Block diagram of a TCSC

The first TCSC was installed in 1992 in Kayenta, Arizona, USA. Siemens, GE and ABB are the leaders in TCSCs and FACTS devices in general. TCSCs are ideal forms of series compensation as they have multiple advantages. In fact, the seven TCSCs in the world, installed before 2005 have each been installed for a different primary purpose. Some examples are listed below [91]:

- The first ever installed TCSC in Kayenta, is used along with two other series capacitor banks to compensate a 230 kV 320 km line. It was installed for increasing transmission capacity as with a FSC, but in a flexible fashion.

- GE installed six TCSC modules in Slatt, Oregon, USA for the purpose of controlling line power flow.

- At Stöde, Sweden, a TCSC was installed for the purpose of subsynchronous resonance mitigation. In fact, subsynchronous resonance mitigation, is increasingly becoming the most attractive advantage of TCSCs.

- At Sara de Misa in Brazil, to damp low-frequency inter-area oscillations

- TCSC at Pinguo substation, China was installed in 2002 primarily for enhancing stability

Static Synchronous Series Compensator (SSSC): A SSSC comprises of a voltage source inverter (VSI) and a solid state switching mechanism to control it, an example of which is shown in Figure 3.12. A number of papers using different types of VSIs have been proposed. An SSSC may use a gate turn-off inverter [92], a binary source voltage inverter [the thesis], a multipulse multilevel inverter [93] etc. The voltage across is in quadrature with the current and is variable. Thus, it is effective in controlling the power flow. It can operate in both inductive and capacitive modes. Another key advantage of the SSSC is that reactive power can be supplied to or absorbed from the line without the use of a series capacitor.

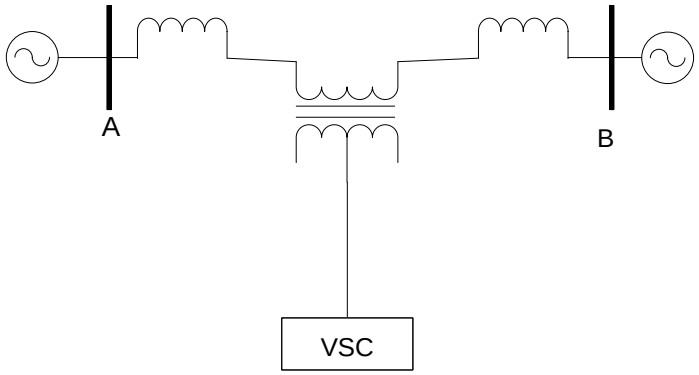

Figure 3.12: Line compensated by a SSSC

Gate Controlled Series Compensator (GCSC): This form of series compensation is recently proposed, and has attracted considerable research interest due to the advantages it offers. A GCSC is similar to a TCSC in that variable reactance is achieved by means of controlling the current through the capacitor by redirecting the current at certain firing angles, however here it is achieved using gates. It is different to a TCSC in that, it does not require a reactor branch. TCSCs may be capable of producing a parallel resonance (LC circuit) at fundamental frequency for certain angles. This is not true of the GCSC. The variability and range of reactance is also greater in the case of GCSCs.

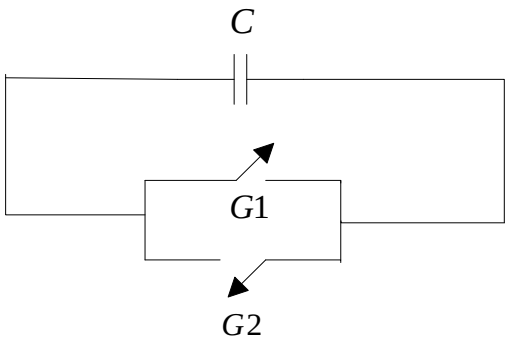

Figure 3.13: Block diagram of a GCSC

3.5. Series Capacitor Overvoltage Protection

Given that the capacitor is in series with the line, it must be capable of withstanding high voltages as a result of the line current during load conditions, but must also be able to withstand abnormally high voltages during overloading, and temporary overvoltage spikes. A capacitor of appropriate voltage ratings must be chosen. To protect the capacitor under fault conditions, it is equipped with overvoltage protection. It primarily comprises of a metal MOV, spark gap and bypass switch. They are explained below in more detail:

3.5.1. Bypass Switch

A bypass switch used in the overvoltage protection of the SC, is not very different to a circuit breaker (CB) in terms of its electrical constitution. But while a CB is used for the disconnection of a line or part of the network, a bypass switch is used to protect the capacitor from overvoltage in the event of a fault and also to bypass it manually when required. It is connected in parallel with the SC, MOV, and spark gap as shown in Figure 3.14. The typical duty cycle of a bypass switch is C-0.3s-OC [94]. The 'close' operation for a bypass switch is equivalent to the 'open' operation of a CB in terms of taking an element of the power system (SC/line) out of service. On the other hand, during normal load current, the bypass switch is in 'opened' status, to keep the SC in service and is thus equivalent to the 'closed' status for a CB. Considering the above it follows that the bypass switch must meets the following technical requirements:

1. The rated current of the bypass switch must be higher than the combined value of the high fault current and the additional current from the discharging of the capacitor in the event that the bypass switch must close due to an overvoltage. The maximum fault current and the protective level voltage of the SC must be used in the calculation of the switch rating.

2. The bypass switch must be capable of withstanding the resulting transient recovery voltage upon opening under normal-operation currents i.e. when bringing the capacitor back into service. Opening during fault currents is not a requirement.

3. It must also be able to withstand high voltages across the switch occurring due to high fault currents flowing through the capacitor [94].

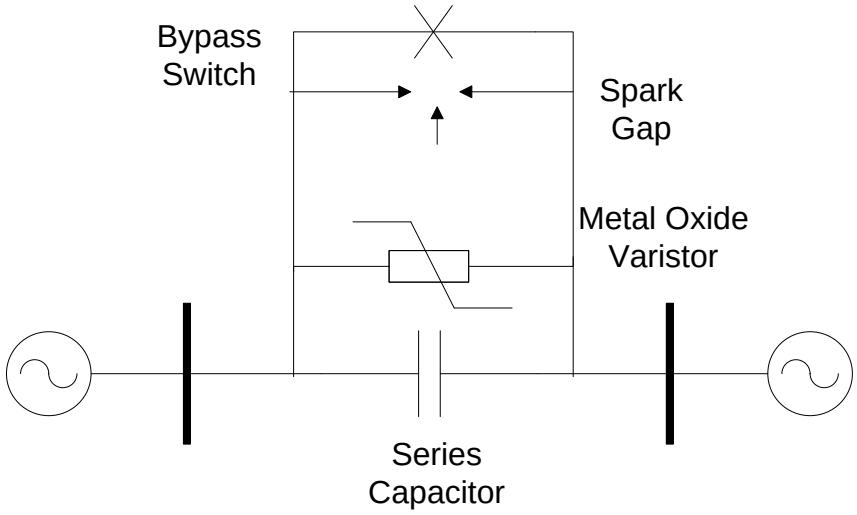

Figure 3.14: Series capacitor overvoltage protection

3.5.2. Spark Gap

During a fault on a series compensated line, fault currents can be very high. This can lead to an overload of the MOV. The spark gap is designed to protect the MOV under such circumstances, and is triggered by the MOV protection relay. It is designed to operate

typically within a millisecond, when the current through the MOV reaches a pre-defined high threshold. The installation of the spark gap is in the form of enclosures, containing the gap electrodes (graphite), and the trigger circuits (trigatrons) that fire individual air-gaps. Enclosures ensure that the air gaps do not flashover inadvertently during frost, snow or rain. [95]

The main gap must meet the following electrical requirements:

1. The gap must not fire during to normal operation of the bypass switch. Thus it follows that the main gap must withstand the combined value of the bypass-through fault current and the additional current from the discharging of the capacitor.

2. The delay time to fire the air-gap must not exceed the maximum delay required to protect the gap. This time delay is specified by the manufacturer and the details of the standard test can be found in [96].

3. The bypass switch must be capable of withstanding the resulting transient recovery voltage upon bringing the capacitor back into service.

4. The gap must not fire due to disturbances during normal or overload conditions. This is ensured by testing that the gap does not fire for voltage <1.5 x nominal voltage.

3.5.3. Metal Oxide Varistor

The MOV is the main element of the overvoltage protection of a series capacitor. The MOV is a surge protector fitted in parallel with the series capacitor and is used to limit the voltage across, by diverting some of the line current flowing into the combination. Zinc Oxide (ZnO) is the most commonly used type of MOV. The MOV has a non-linear resistance such that the higher the voltage across, the lower the resistance. Under load conditions, the voltage across is nominal, and the current passes entirely through the series capacitor. However, under high fault currents, the MOV allows a significant current through, preventing potentially damaging overvoltages from occurring across the capacitor. The general form of the current-voltage characteristic of an MOV is shown in (3.4).

$$I_{MOV} = p(\frac{v_x}{V_{REF}})^q \tag{3.4}$$

where p and q are constants, V_{REF} is the reference voltage, 'v_x' is the voltage across the combination and 'I_{MOV}' is the current flowing through the MOV. Figure 3.15 is an example characteristic of the MOV voltage against the MOV current shown on a linear scale. It can be seen that the MOV begins to operate just after the capacitor voltage exceeds the maximum overload voltage. It can also be seen that the current through the MOV increases (as the combination voltage increases) to ensure the capacitor voltage is always below the maximum to prevent any dangerous overvoltages.

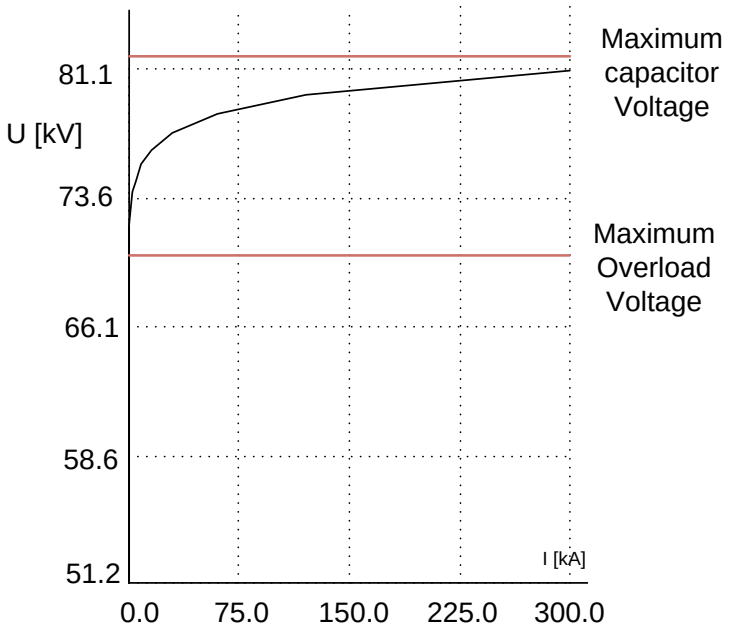

Figure 3.15: MOV voltage-current characteristic

Thus, these factors are important especially in the modelling of the MOV for simulation studies. An appropriate MOV is chosen to meet the following electrical requirements:

1) The MOV must be capable of withstanding the nominal voltage across the capacitor for any length of time. This is determined by the capacitor reactance and load current magnitude.

2) It must be capable of withstanding voltages as high as 1.35 pu [96] for short periods of time (half hour).

3) The voltage across the MOV during maximum fault current must not exceed its protective level voltage

4) The MOV must have sufficiently high energy dissipation capability. Depending on the fault current, duration of the fault and protective level voltage of the MOV, the MOV may be overloaded. Spark gaps are generally employed to prevent overloading and reduce maximum loading requirements of the MOV [96].

3.6. Series Compensated Lines under Fault Conditions

The typical voltage-current relationship of the MOV has been shown in (3.4) and it can be seen from Figure 3.14 that the MOV is installed in parallel with the series capacitor. Thus, it follows that impedance-based calculations must take the electrical behaviour of the MOV into account. Analysis can be largely simplified if the parallel combination can be reduced to a series combination of the effective resistance component and the effective reactance component. Based on the MOV characteristic it can be seen that this combination will be entirely capacitive during load currents and will effectively be a short circuit during abnormally large fault currents. The Goldsworthy model proposed in [97] mathematically reduces the parallel combination into the effective series resistance and reactance.

$$R_C = X_{C0}(0.0745 + 0.49e\wedge(-0.243i_{pu}) - 35e\wedge(-5i_{pu}) - 0.6e\wedge(-1.4i_{pu})) \tag{3.5}$$

$$X_C = X_{C0}(0.1010 + 0.005749i_{pu} + 2.088e\wedge(-0.8566i_{pu})) \tag{3.6}$$

Here, i_{pu} is the ratio of the phase current to the protective level current, X_{C0} is the series capacitor reactance, R_C is the effective resistance of the combination and X_C is the effective reactance. The Goldsworthy equivalent model is very useful for analysing a series compensated line in the phasor domain using phase currents. Fault analysis however, is

often carried out using sequence networks, as it simplifies the mutually coupled transmission line into three independent sequence circuits.

When, the three phases in the system are symmetrical both in terms of currents as well as phase impedances, only the analysis of the positive sequence network and positive sequence measurements is required. Such is the case for a healthy line under pre-fault conditions, and a line under symmetrical three-phase fault. However, in the case of asymmetry the analysis is a lot more complex due to the mutual coupling effect of transmission lines, and the presence of a return path to ground. This includes SLG, DL, and DLG faults. If phase network analysis is to be carried out, mutual and self impedances must all be considered. Equation (3.7) is the phase currents-phase voltages relationship in terms of the phase impedance matrix comprising of self and mutual impedances.

$$\begin{bmatrix} \Delta\bar{V}_a \\ \Delta\bar{V}_b \\ \Delta\bar{V}_c \end{bmatrix} = \begin{bmatrix} Z_a & Z_{ab} & Z_{ac} \\ Z_{ab} & Z_b & Z_{bc} \\ Z_{ac} & Z_{bc} & Z_c \end{bmatrix} \begin{bmatrix} \bar{I}_a \\ \bar{I}_b \\ \bar{I}_c \end{bmatrix} \tag{3.7}$$

Here, $\Delta\bar{V}_a$, $\Delta\bar{V}_b$ and $\Delta\bar{V}_c$ are the voltage drops across the three phases. $\bar{I}_a$, $\bar{I}_b$ and $\bar{I}_c$ are the phase currents. Z_a, Z_b and Z_c are the self-impedances, while Z_{ab}, Z_{ac} and Z_{bc} are the mutual-impedances. Sequence network analysis is often used in the case of traditional uncompensated lines, since it allows the system to be analysed as three independent circuits. In the case of transposed transmission lines, mutual coupling between the sequence components is negligible and thus the equivalent sequence impedance array is expressed below:

$$\begin{bmatrix} \Delta\bar{V}_0 \\ \Delta\bar{V}_1 \\ \Delta\bar{V}_2 \end{bmatrix} = \begin{bmatrix} Z_0 & Z_{01} & Z_{02} \\ Z_{01} & Z_1 & Z_{12} \\ Z_{02} & Z_{12} & Z_2 \end{bmatrix} \begin{bmatrix} \bar{I}_0 \\ \bar{I}_1 \\ \bar{I}_2 \end{bmatrix} \tag{3.8}$$

$$\begin{bmatrix} \Delta\bar{V}_0 \\ \Delta\bar{V}_1 \\ \Delta\bar{V}_2 \end{bmatrix} = \begin{bmatrix} Z_0 & 0 & 0 \\ 0 & Z_1 & 0 \\ 0 & 0 & Z_2 \end{bmatrix} \begin{bmatrix} \bar{I}_0 \\ \bar{I}_1 \\ \bar{I}_2 \end{bmatrix} \tag{3.9}$$

Here, $\Delta\bar{V}_0$, $\Delta\bar{V}_1$ and $\Delta\bar{V}_2$ are the sequence network voltage drops, $\bar{I}_0$, $\bar{I}_1$ and $\bar{I}_2$ are the sequence network currents, Z_0, Z_1 and Z_2 are the self impedances of the sequence networks, and Z_{01}, Z_{02} and Z_{12} are the mutual impedances between the sequence networks. The decoupling between sequence networks has been shown in (3.9). This decoupling however, is not the case for the series compensated lines. Unlike uncompensated transmission lines, SC-MOV phase impedances are not mutually coupled as there are no inductive elements and thus, the equivalent sequence impedances are not independent. Although the phase impedances may not be coupled, the sequence components may be coupled and this cannot be neglected. This is likely to happen during asymmetrical faults as the phase currents will be vastly different from each other and will accordingly change the phase impedances of each SC-MOV combination. The general equation for the phase quantities of the SC-MOV bank combination are as follows:

$$\begin{bmatrix} \Delta\bar{V}_a \\ \Delta\bar{V}_b \\ \Delta\bar{V}_c \end{bmatrix} = \begin{bmatrix} Z_a & 0 & 0 \\ 0 & Z_b & 0 \\ 0 & 0 & Z_c \end{bmatrix} \begin{bmatrix} \bar{I}_a \\ \bar{I}_b \\ \bar{I}_c \end{bmatrix} \tag{3.10}$$

when transformed into sequence domain:

$$\begin{bmatrix} \Delta\bar{V}_0 \\ \Delta\bar{V}_1 \\ \Delta\bar{V}_2 \end{bmatrix} = \frac{1}{3}\begin{bmatrix} 1 & 1 & 1 \\ 1 & a & a^2 \\ 1 & a^2 & a \end{bmatrix} \begin{bmatrix} Z_a & 0 & 0 \\ 0 & Z_b & 0 \\ 0 & 0 & Z_c \end{bmatrix} \begin{bmatrix} 1 & 1 & 1 \\ 1 & a^2 & a \\ 1 & a & a^2 \end{bmatrix} \begin{bmatrix} \bar{I}_0 \\ \bar{I}_1 \\ \bar{I}_2 \end{bmatrix} \tag{3.11}$$

$$\begin{bmatrix} \Delta\bar{V}_0 \\ \Delta\bar{V}_1 \\ \Delta\bar{V}_2 \end{bmatrix} = \frac{1}{3}\begin{bmatrix} Z_a+Z_b+Z_c & Z_a+a^2Z_b+aZ_c & Z_a+aZ_b+a^2Z_c \\ Z_a+aZ_b+a^2Z_c & Z_a+Z_b+Z_c & Z_a+a^2Z_b+aZ_c \\ Z_a+a^2Z_b+aZ_c & Z_a+aZ_b+a^2Z_c & Z_a+Z_b+Z_c \end{bmatrix}\begin{bmatrix} \bar{I}_0 \\ \bar{I}_1 \\ \bar{I}_2 \end{bmatrix} \quad (3.12)$$

Here, Z_a, Z_b and Z_c are individual phase impedances of the SC-MOV combination, the operator 'a' represents a shift in phasor angle by 2π/3 rad wheras 'a^2' represents a shift of 4π/3 rad. If Z_a, Z_b and Z_c are unequal, the non-diagonal elements of the above matrix would not be non-zero as a result of the asymmetry. In electrical terms, this implies that the sequence networks are mutually coupled. Different fault types are considered below and the sequence network impedances are shown. For simplicity, it is assumed that faulted phase currents are very high leading to MOV operation being equivalent to a closed switch, and magnitudes of the healthy phase currents are close to the nominal current magnitude.

During normal operation, the effective SC impedances of all three phases are the equal ($Z_a = Z_b = Z_c$). There is no asymmetry. As a result the sequence networks are decoupled. The sequence impedances (shown here as matrix Z_{012}) can be calculated to be:

$$Z_{012} = \begin{bmatrix} -jX_C & 0 & 0 \\ 0 & -jX_C & 0 \\ 0 & 0 & -jX_C \end{bmatrix} \quad (3.13)$$

It can be seen that during normal operation the sequence impedances are equal to the phase impedances all of which equal to the full capacitive reactance of the SC. Consider a SLG fault on phase-a. This would imply $Z_a = 0$, while $Z_b = Z_c = -jX_c$. The sequence components can be calculated as shown in (3.14). Thus, the self impedance for each of the sequence networks is 2/3rd of the full reactance of the SC while the mutual impedance between the sequence networks is -1/3rd of the full reactance of the SC. This means that

the positive sequence current will contribute a leading voltage to the negative sequence network voltage drop.

$$Z_{012} = \frac{1}{3}\begin{bmatrix} -j2X_c & jX_c & jX_c \\ jX_c & -j2X_c & jX_c \\ jX_c & jX_c & -j2X_c \end{bmatrix} \tag{3.14}$$

Consider a DL or DLG fault. This would imply $Z_a = Z_b = 0,\ Z_c = -jX_c$. The sequence components thus calculated are as follows:

$$Z_{012} = \frac{1}{3}\begin{bmatrix} -jX_c & -jX_c & -jX_c \\ -jX_c & -jX_c & -jX_c \\ -jX_c & -jX_c & -jX_c \end{bmatrix} \tag{3.15}$$

3.7. Challenges Associated with Series Compensated Transmission Lines

SCs are protected from overvoltages using MOVs and/or spark gaps. Spark gap operation is restricted to abnormally high currents (>0.98 p.u. using the protective level current of the MOV as base [97]). The impedance of the MOV depends on the voltage across the parallel combination of the series capacitor and MOV. This impedance is non-linear with respect to the voltage and allows it to clamp the voltage across this combination. The MOV may entirely short the series capacitor during very high voltages. Thus, the impedance of the capacitor, spark gap and MOV combination is not constant. Line protection must ensure to protect the line despite this variability and with or without the capacitor in the operation. As mentioned earlier, the subharmonic frequency component may also affect the operation of line protection. The main effects of series compensation on protective relays and fault locators have been discussed in more detail as follows:

3.7.1. Voltage Inversion

Due to the presence of the series capacitor in the circuit, the phase of the voltage may be inverted under certain conditions. In other words, a voltage phase angle change of π

radians may be experienced after the fault has occurred. This would clearly affect the distance and directional elements of protection relays. Due to voltage inversion, forward faults may be seen by the relay as a reverse fault and vice versa.

Figure 3.16 shows a scenario where a forward fault has occurred but is seen as a reverse fault by the relay at bus A (along with the corresponding voltage profile) [98].

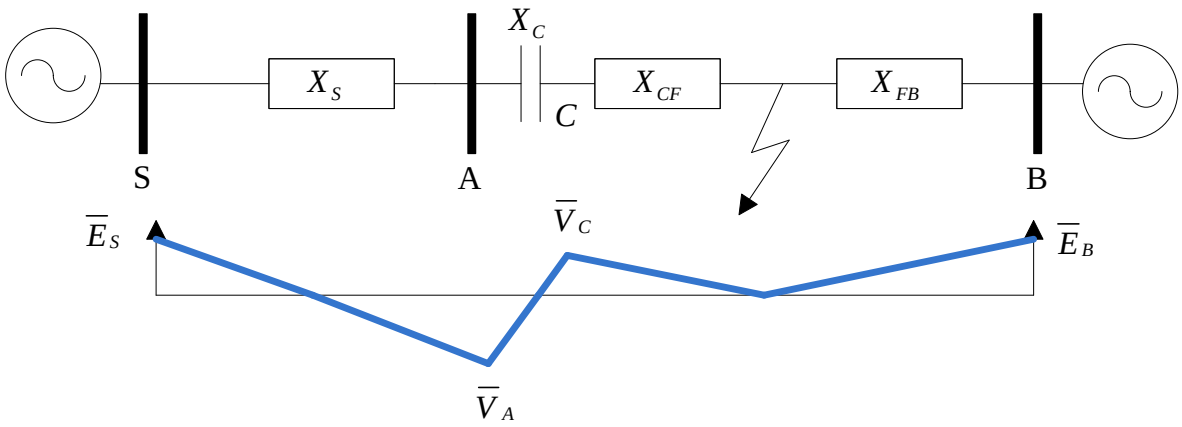

Figure 3.16: Voltage inversion on a series compensated line for a forward fault [75]

Consider the fault loop from the source to the fault. It comprises of three impedances i.e. the source impedance X_S, the series capacitor X_C and the line inductance up to the fault point X_{CF}. $\overline{E}_S$ and $\overline{E}_B$ are the source voltages at line-ends S and B. There are two conditions satisfying both of which would cause a voltage inversion to occur:

(1) The impedance from the relay to the fault is capacitive but the overall impedance of the fault loop is inductive. This requires the following mathematical conditions to be true:

$$\text{a)}\ X_C > X_{CF} \tag{3.16}$$

$$\text{b)}\ X_C < X_{CF} + X_S, \tag{3.17}$$

(2) If the fault is too close to the series capacitor, the spark gap may flash, causing the series capacitance to be entirely bypassed and thereby avoiding a voltage inversion. The magnitude of the voltage across the series capacitor would have to be low enough for the

spark gap to not flash and to cause a voltage inversion. If V_{MAX} is the maximum voltage across the capacitor before the spark gap flashes over, it can be shown that the following condition must also be satisfied for the voltage inversion to occur:

$$X_C \leq \left[\frac{|V_{MAX}|}{|V_{MAX}| + |E_S|} \right] * (X_{CF} + X_S) \tag{3.18}$$

If the MOV starts conducting without the spark gap flashing, the capacitance may be lowered to a value which does not cause voltage inversion. Voltage inversion can also be transient during the period prior to when the MOV starts conducting.

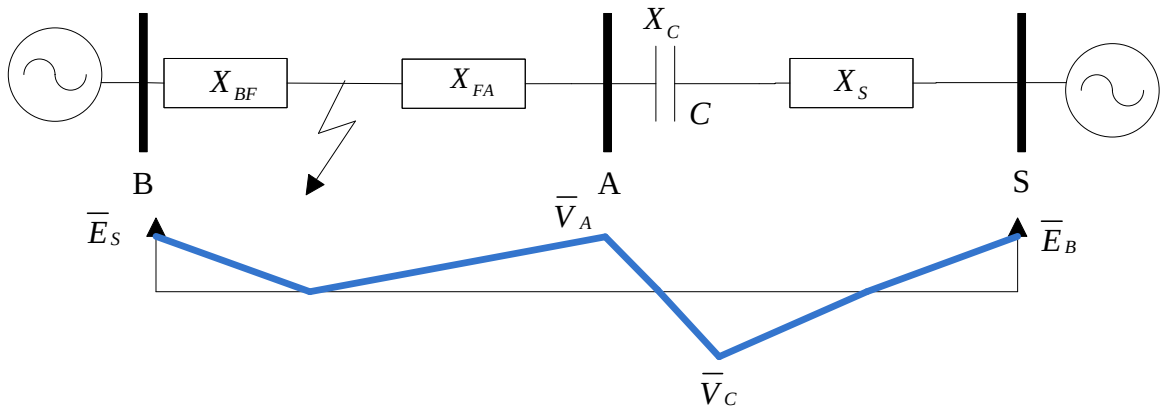

Figure 3.17: Voltage inversion on a series compensated line for a reverse fault [75]

(3) The voltage transformer (VT) is on the bus side of the series capacitor and the series capacitor lies between the fault and the relay. The above described problem does not occur if the voltage transformer is located at the line side of the series capacitor in the case of the line being compensated at the line-end. Figure 3.17 shows the opposite scenario where a reverse fault has occurred but is seen as a forward fault by the relay at the line side of the capacitor (along with a voltage profile) [98].

In this scenario the fault loop again comprises of three impedances. The first is the impedance of the forward line X_S (can be viewed as the source impedance behind the relay). The second is that of the series capacitor X_C and the third is line inductance from the relay to the fault point X_{FA}. Similar to the previous case, there are three conditions satisfying all of which would cause a voltage inversion to occur:

(1) The impedance from the relay point to the fault is capacitive but the overall impedance of the circuit is inductive.

$$\text{a)}\ X_C > X_{FA} \tag{3.19}$$

$$\text{b)}\ X_C < X_{FA} + X_S \tag{3.20}$$

(2) The spark gap must not flash to cause voltage inversion. This occurs when the following condition is satisfied:

$$X_C \leq \left[\frac{|V_{MAX}|}{|V_{MAX}| + |E_S|} \right] * (X_{FA} + X_S) \tag{3.21}$$

(3) The VT is on the line side of the series capacitor and the series capacitor lies between the fault and the VT.

In the case of relays that use sequence quantities, voltage inversion can still occur due to the presence of the series capacitor between the voltage transformer and the fault. Voltage polarised directional elements will be affected by the inversion of the negative sequence or zero sequence voltage. If the VT lies on the bus side of the capacitor, a forward fault may incorrectly be detected as a reverse fault. If the line side voltage is used to polarise the directional element, this problem is avoided. On the other hand, if the VT lies on the line side of the capacitor, a reverse fault may be detected as a forward fault and if the bus side voltage is used to polarise the directional element, this problem can be avoided.

3.7.2. Current Inversion

Current inversion occurs when the network from the source to the fault point is effectively capacitive. This is because while the fault current for uncompensated lines is always inductive, fault current in this case will be capacitive which corresponds to a phase shift of π radians. To understand this phenomenon, consider the following network where a current inversion has occurred:

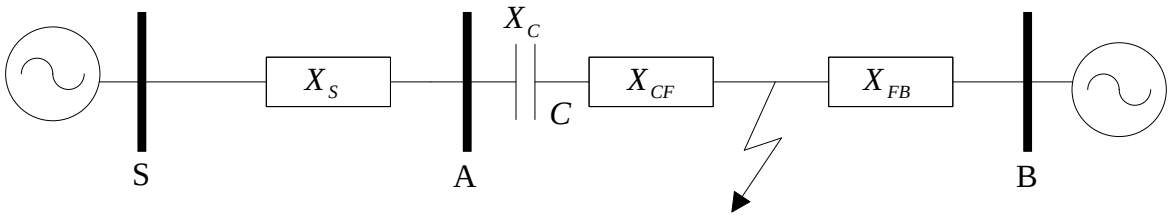

Figure 3.18: Current inversion on a series compensated line

The conditions causing a current inversion are as follows [99]:

(1) The capacitive reactance in the fault loop exceeds the inductive reactance, leading to a capacitive current. This occurs when the source impedance is small, and the fault occurs close the series capacitor:

$$X_C > X_{CF} + X_S \tag{3.22}$$

(2) The spark gap must not flash, allowing the capacitance in series with the line, without it being bypassed. It can similarly be shown that this occurs when the following criterion is met:

$$V_C = \frac{1}{1 - \frac{X_{CF} + X_S}{X_C}} E_S \leq V_{MAX} \tag{3.23}$$

If the MOV starts conducting without the spark gap flashing, the capacitance may be lowered to a value which does not cause current inversion. Current inversion can also be

transient in the period prior to when the MOV starts conducting. It may seem that both conditions stated above cannot be satisfied simultaneously since the magnitude of V_{MAX} is always less than that of E_S, and if condition 1 is true, the coefficient of E_S in (3.23) is greater than 1. But, that is because, the fault here is assumed to be solid earth for simplicity. Current inversion can occur if the fault resistance is high. A high fault resistance can prevent the MOV from conducting or the spark gap flashing, thereby allowing both conditions to be true and hence causing a current inversion. The modified equation for condition 2 in the case of high resistance faults is as shown below [98]:

$$V_C = \frac{1}{1-\frac{X_{CF}+R_F+X_S}{X_C}} V_S \leq V_{MAX} \tag{3.24}$$

However, if a current inversion does occur, the angle by which the current would lead the voltage would be small. When the magnitude of the reactance of the series capacitor X_C is equal to or nearly equal to the source reactance X_S, the relative contribution to the fault current from 'B' is almost zero. This introduces problems in fault type determination. As is the case with voltage inversion, current inversion too can occur in negative or zero sequence networks.

3.7.3. Incorrect Estimation of Distance to Fault

The distance to fault estimated by FLAs in distance protection and fault locators would be affected by the presence of the SC in the circuit. These FLAs assume the fault loop to have an entirely inductive and homogenous reactance. But the series capacitor modifies the effective impedance as seen by the relay or fault locator. Moreover, the problem is further complicated by other factors. Firstly, the primary capacitor overvoltage protection i.e. the spark gap and the MOV, make the effective capacitive reactance variable. Secondly, the operation of the capacitor protection largely depends on the magnitude of the fault current, and is not accounted for in FLAs designed for uncompensated lines. Thirdly, the series capacitor may or may not lie within the fault loop depending on the system in question and the location of the fault. Series compensation can be as high as 50-70%. This variable

electrical behaviour of the series capacitor protection means the overreach can also be as high as 50-70%. Consider a line with series compensation in the middle of a line as shown in Figure 3.19a. During a high current fault, the flashing of the spark gap would remove the capacitor from service, and the impedance of the line would be a direct indicator of the distance to fault. Conventionally for uncompensated lines, the characteristic of a zone 1 mho element is set to 90% of the line as shown in the dashed line characteristic in Figure 3.17b. This setting would provide correct zone 1 discrimination for high current faults in the case of series compensated lines [100].

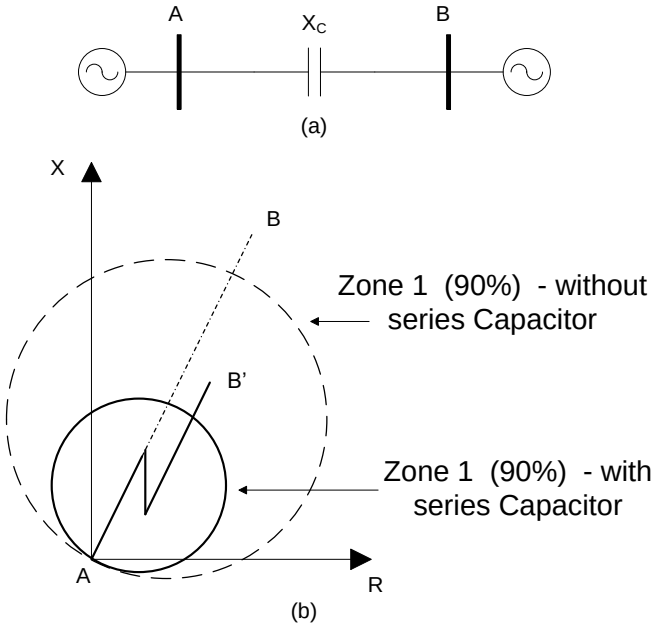

Figure 3.19: Mid-line compensated line: a) Single line diagram b) Zone 1 mho element characteristics [75]

On the other hand, for low current faults the spark gap will not flashover and the capacitive reactance would be included in the overall impedance measurement. For the conventional 90% setting, the mho element may overreach, since the estimated distance for out of zone faults will be inaccurate. The reach for zone 1 may be dropped to 50% to avoid overreach as shown in the solid line characteristic in Figure 3.19b. Line-end compensated lines affect distance estimation to a worse extent than mid-line compensated lines. These lines also affect directionality as explained in the previous sections, thus posing some serious

challenges for distance protection. Mid-line compensated lines will generally not affect the directionality unless the level of compensation is very high.

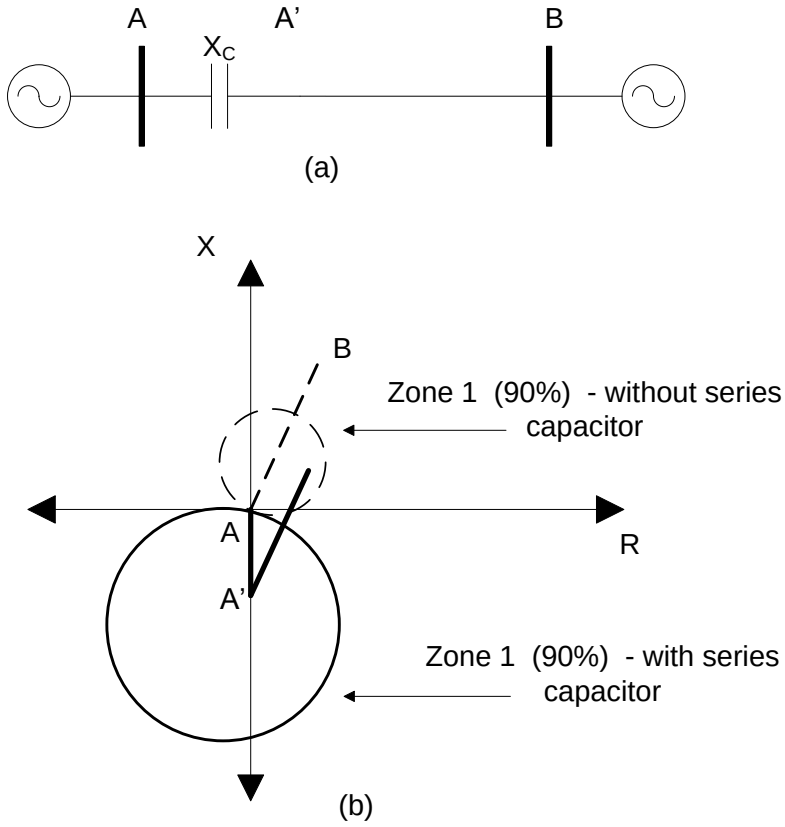

Figure 3.20: Line compensated at one line-end a) Single line diagram b) Zone 1 mho element characteristics [75]

Consider a line with series compensation at the line-ends as shown in Figure 3.20a. It also shows the zone 1 characteristic of compensated line (solid line) and the zone 1 characteristic of the adjacent line (dashed line). Both lines receive voltage measurements from the bus. As before, during high current faults, the capacitor is effectively removed from the fault loop due to the flashing of the spark gap, and both mho elements operate correctly. For low current faults on the other hand, the capacitor remains in circuit. If the fault occurs very close to the series capacitor, it is seen as a reverse fault by the compensated line relay. The impedance lies outside the zone 1 mho characteristic of the

compensated line and restrains. The adjacent line will see this as a forward fault and operate incorrectly [100].

As mentioned previously, subharmonic frequency oscillations cause the impedance calculations to vary with time. Figure 3.21 shows an example fault current where there is a significant subharmonic frequency component. It can be seen that the current is significantly distorted in comparison to a system-frequency sinusoidal current. Settings based on steady state impedances may under-reach. This may cause the impedance to oscillate on the mho-element characteristic and incorrect estimation of distance to fault. Zone 1 reach may be reduced to factor in the effect of such subharmonic oscillations.

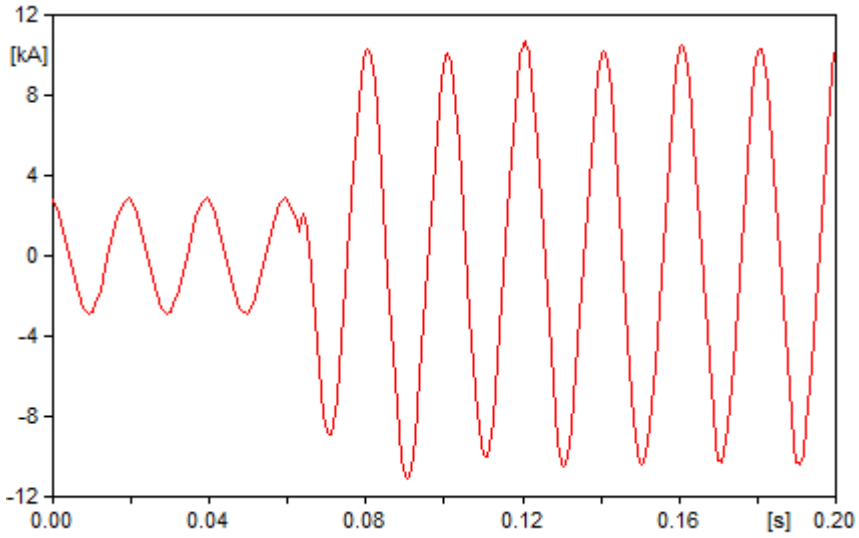

Figure 3.21: Example fault-current with high sub-harmonic frequency component

3.8. Solutions for Protection of Series Compensated Lines

The following solutions have been implemented in relays used to protect series compensated transmission lines:

3.8.1. Memory Polarisation

A mho element checks for whether the angle difference between the line-drop compensated voltage $\overrightarrow{\delta V}$ (3.25), and a pre-defined polarizing voltage $\vec{V}_P$ exceeds a given threshold. This line-drop compensated voltage is defined as follows:

$$\overrightarrow{\delta V} = m\overrightarrow{Z_R}.\vec{I} - \vec{V} \tag{3.25}$$

Here '*m*' is the per-unit reach in terms of the replica impedance and the fault point; $\overrightarrow{Z_R}$ is the replica line impedance (a relay setting); $\vec{I}$ is the current measured by the CT; $\vec{V}$ is the voltage measured at the VTs. The relationship between $\overrightarrow{\delta V}$ and the polarising voltage is seen in Figure 3.22. While the self-polarized mho element uses the present voltage $\vec{V}$, the memory polarised element uses the pre-fault voltage as the polarizing voltage [101].

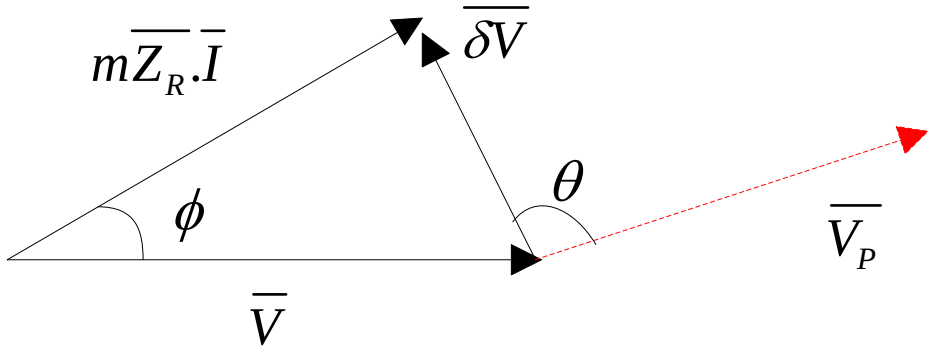

Figure 3.22: Phasor diagram – memory polarisation

Since self polarised elements are very much affected by voltage inversion, memory polarised elements are used instead for series compensated lines. They use a combination of the pre-fault voltage and measured voltage when its memory is active and once it is inactive it only uses the measured voltage. This memory is purposely time-limited to avoid operation due to transient system disturbances. However, this memory should be long enough to allow the mho elements to pick-up until the fault is cleared. Typically the worst

case scenario, i.e. the slowest fault clearing time is used to determine the length of the memory.

Thus, for a close in forward fault the self polarised mho element will use an out of phase bus voltage as the polarising voltage and restrain whereas the memory polarised mho element will use the in-phase voltage and thus operate correctly. For a close in reverse fault on the other hand, the self polarised mho element will operate incorrectly when using the line voltage while the memory polarised mho element will restrain. Polarised elements with memory will operate or restrain correctly irrespective of which side of the capacitor is used to measure the polarising voltage.

A major issue that requires consideration in protection of series compensated lines is the viability of directional comparison scheme logic. In some cases additional blocking elements may be required to prevent unwanted operation in the case of slow clearing faults. This however is not a problem in the case of memory polarised distance relays. They do not require any additional logic. Self polarised relays do require additional logic for secure operation during these faults.

3.8.2. Directional Elements Responding to Sequence Quantities

Certain directional elements namely the 32Q and 32V can correctly detect and differentiate between forward and reverse faults [102]. The 32Q uses negative sequence quantities while the 32V uses zero-sequence quantities. They use the calculated scalar quantities z_2 and z_0 respectively for this purpose. These are defined in (3.26) for 32Q and in (3.27) for 32V respectively:

$$z_2 = \frac{\mathrm{Re}[\overrightarrow{V_2}.(\overrightarrow{|I_2|}.1\angle Z1ANG)]}{\overrightarrow{|I_2|}^2} \tag{3.26}$$

$$z_0 = \frac{\mathrm{Re}[3\overrightarrow{V_0}.(3\overrightarrow{|I_0|}.1\angle Z0MTA)]}{\overrightarrow{3|I_2|}^2} \tag{3.27}$$

Here $\overrightarrow{V_2}$ is the negative sequence voltage and $\overrightarrow{I_2}$ is the negative sequence current. $Z1ANG$ and $Z0MTA$ are relay settings equal to the maximum torque angle. If z_2 is greater than a certain forward fault threshold, the fault is detected as a forward fault, and if it is greater than a second threshold defined for reverse fault, it is detected as a reverse fault. Consider the negative sequence network shown in Figure 3.23. z_{2S} and z_{2R} are the negative sequence source impedances at the two line-ends while z_{2L} is the negative sequence impedance of the line. The 32Q element calculates the scalar z_2 using the negative sequence voltage $\overrightarrow{V_2}$ and negative sequence current $\overrightarrow{I_2}$ at the relay location. The impedance calculated at the relay location is thus $\overrightarrow{V_2} / \overrightarrow{I_2}$. For a forward fault the scalar quantity z_2 should be equal to the impedance behind the line. Thus, for a forward fault $z_2 = |z_{2S}|$. For reverse faults on the other hand, $z_2 = |z_{2L} + z_{2R}|$. The settings for z_0 are calculated similarly using the zero sequence impedances.

For a purely inductive system, the maximum torque angle is 90^0 and the settings $Z1ANG$ and $Z0MTA$ are also 90^0. Figure 3.24 shows operating characteristics for the 32Q and the 32V elements. The z_2 and z_0 values have also been shown for all sets of forward and reverse faults. These settings can be recalculated correctly for series compensated lines to provide correct operation.

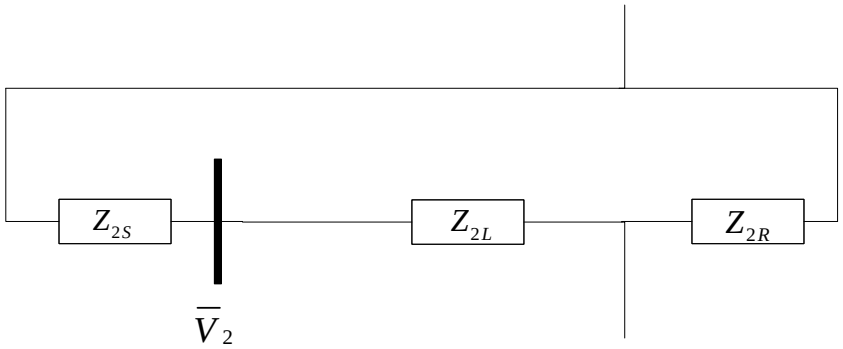

Figure 3.23: Negative Sequence Network

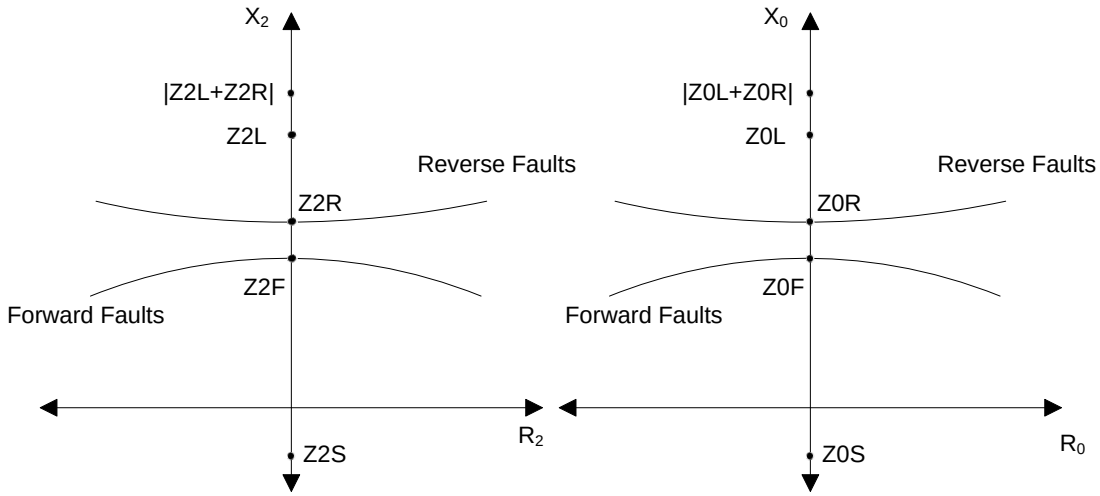

Figure 3.24: Characteristics for 32Q and 32V [75]

$$Z_2F = \frac{Z_{1L} - X_C}{2} \tag{3.28}$$

$$Z_2R = Z_2F + 0.1 \tag{3.29}$$

Since the scalar values will be opposite for forward and reverse faults (for both z_2 and z_0), there is a significant margin for setting the corresponding thresholds. This is true considering the worst case scenario where the remote and local sources are infinite busses, i.e. $Z_{2S} = 0$ and $Z_{2R} = 0$. This makes the forward fault threshold $z_2 = Z_{2S} = 0$ and the reverse fault threshold $z_2 = \left|Z_2R + Z_{2L}\right| = Z_{2L}$. In this case, the forward fault threshold can be set to $+Z_{2L}/2$ while the negative fault threshold can be set to $-Z_{2S}/2$.

Guidelines for directional element settings on series-compensated lines are provided in [103]. The settings for the thresholds largely depend on the whether the line is compensated at mid line or at line-ends. Proper time coordination is required between forward and reverse overcurrent elements.

1) Mid-line compensation: Figure 3.25 shows the system under consideration. Assuming the sources to be infinite, the negative sequence element will measure $z_2 = 0$ during a

forward fault. For a reverse fault $z_2 = |Z_{2L} - jX_C|$ assuming a purely inductive line, which can be approximated to $z_2 = |Z_{1L} - jX_C|$ since the positive and negative sequence impedances for a transmission line are approximately equal. Thus, the following settings can be applied:

$$Z_2F = \frac{Z_{1L} - X_C}{2} \tag{3.30}$$

$$Z_2R = Z_2F + 0.1 \tag{3.31}$$

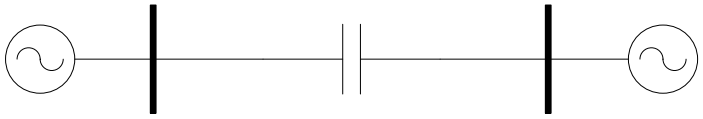

Figure 3.25: Mid-line compensated line

Given the assumptions, both local and remote line-end buses would have the same settings for forward and reverse fault thresholds.

2) Compensated at one line-end: If the voltage information is taken from the bus side, the relay settings are the same as for mid-line compensated lines. On the other hand, if the relay uses the line side potential as shown in Figure 3.26, the capacitive reactance is now effectively a part of the source impedance. Voltage inversion may occur if $X_C > X_S$. This may affect the directional integrity of the relay. The settings at the local and remote line-ends would be different for both thresholds. To avoid this, the forward fault threshold setting must be greater than X_C. The settings in this case would be:

$$Z_2F = \frac{Z_{1L} - X_C}{2} + X_C \tag{3.32}$$

$$Z_2R = Z_2F + 0.1 \tag{3.33}$$

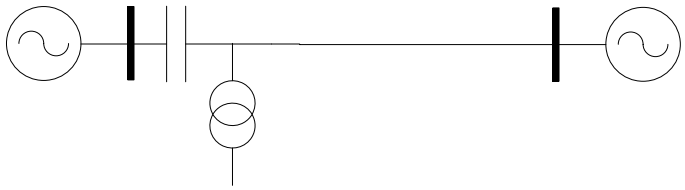

Figure 3.26: Line compensated at one line-end using line side voltage

3) Compensated at both line-ends: If the bus side voltage is used as shown in Figure 3.27, then settings will be determined in a similar way to the mid-line compensated case. Thus the settings would be:

$$Z_2F = \frac{Z_{1L} - (X_{CS} + X_{CR})}{2} \tag{3.34}$$

$$Z_2R = Z_2F + 0.1 \tag{3.35}$$

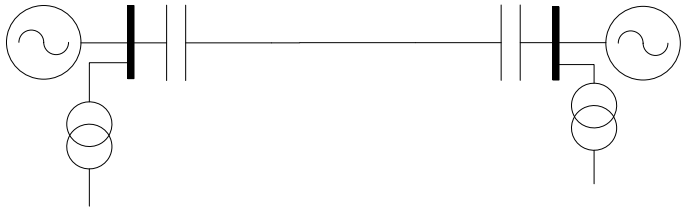

Figure 3.27: Line compensated at both line-ends using bus side voltage

On the other hand, if the line side potential is used as shown in Figure 3.28, then as before, the series capacitor reactance is to be considered as a part of the source impedance behind the relay. The reverse fault settings equations are the same as before. The forward fault settings for the relay close to bus S would be as follows:

$$Z_2F = \frac{Z_{1L} - (X_{CS} + X_{CR})}{2} + X_{CS} \tag{3.36}$$

Similarly for the relay close to bus R:

$$Z_2F = \frac{Z_{1L} - (X_{CS} + X_{CR})}{2} + X_{CR} \tag{3.37}$$

Figure 3.28: Line compensated at both line-ends using line side voltage

3.8.3. Avoiding Distance Element Overreach

This section discusses the method described in [104]. The zone 1 element is blocked until the series-compensation logic has determined which side of the series capacitor is the fault. The series compensation logic involves calculating a voltage $\overrightarrow{V_{CALC}}$ as shown below based on the current measurement (it is specially defined voltage required for the method, and its significance will be clarified shortly):

$$\overrightarrow{V_{CALC}} = \overrightarrow{Z_{1L}}(\overrightarrow{I_A} + k_0\overrightarrow{I_r}) + (-jX_C * \overrightarrow{I_A}) \tag{3.38}$$

Here $\overrightarrow{I_A}$ is the faulted phase current at the relay location. $\overrightarrow{I_r}$ is the residual current at the relay location. k_0 is the zero-sequence compensation factor. $\overrightarrow{Z_{1L}}$ is the positive-sequence line impedance. X_C is the series capacitor reactance. If the voltage measured at the bus is $\overrightarrow{V_{MEAS}}$, the ratio of $\left|\overrightarrow{V_{MEAS}}\right|$: $\left|\overrightarrow{V_{CALC}}\right|$ is used to determine which side of the series capacitor is the fault. This ratio is then compared against a certain threshold value. When the ratio is greater than the set threshold, zone 1 element operates. Consider a fault at bus R in Figure 3.29 below. It can be noticed from (3.38), that ignoring the fault resistance, the calculated value of $\left|\overrightarrow{V_{CALC}}\right|$ would equal the value of $\left|\overrightarrow{V_{MEAS}}\right|$ at bus R. Thus the ratio is approximately equal to 1 for faults occurring on the other side of the capacitor with respect to the relay.

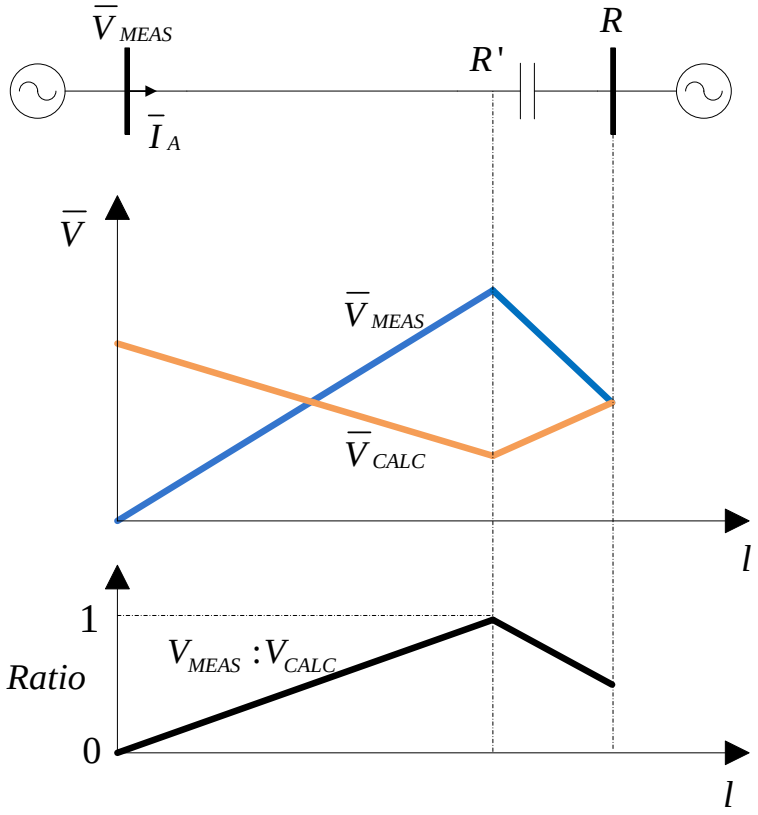

Figure 3.29: Method to avoid overreach

If the fault location is now altered from the bus R to the line side of the capacitor, the impedance in the fault loop would increase due to the exclusion of the capacitor (which contributes negative reactance in the overall impedance). Thus, as the fault location is moved away from the capacitor, getting closer to bus S, the fault current would be seen to increase, the measured voltage would be seen to decrease, while the calculated voltage would be seen to increase. Faults on the relay side of the capacitor, would have higher values for the ratio, since $\left|\overrightarrow{V_{MEAS}}\right|$ will not include the capacitor while $\left|\overrightarrow{V_{CALC}}\right|$ would be inclusive of the capacitor. The presence of the capacitor in the equation will lower the overall impedance calculated in $\left|\overrightarrow{V_{CALC}}\right|$, and thus be of a higher value than the measured $\left|\overrightarrow{V_{MEAS}}\right|$.

The ratio would be seen to increase very suddenly from a certain value (depending on the system) to 1, as the fault location is taken from the bus S side to the bus R side of the

capacitor. This allows some freedom in the setting of the threshold. The threshold is not set to 1, in order to consider the effect of the fault resistance.The above discussed method is capable of acoiding distance element overreach for lines that are compensated at one line-end, but this method is not suitable for series compensated lines that are compensated at the middle

3.8.4. Alpha-Plane Differential Protection

Current inversion occurring on series compensated lines, affects the operation of unit protection for such lines. Unit protection serves to provide clear discrimination between internal and external faults. The principle used in the standard differential protection of traditional uncompensated lines is the comparison of incoming current (local line-end) and outgoing current (remote line-end) in terms of magnitude and phase. This is accomplished as shown in Figure 3.30, where the difference in the incoming and outgoing current forms the operating current or the differential current (I_{Op}).

This operating current is compared against a restraining current (KI_{Res}) to determine if the fault is internal or otherwise.

$$I_{Op} > KI_{\mathrm{Res}} + I_P \tag{3.39}$$

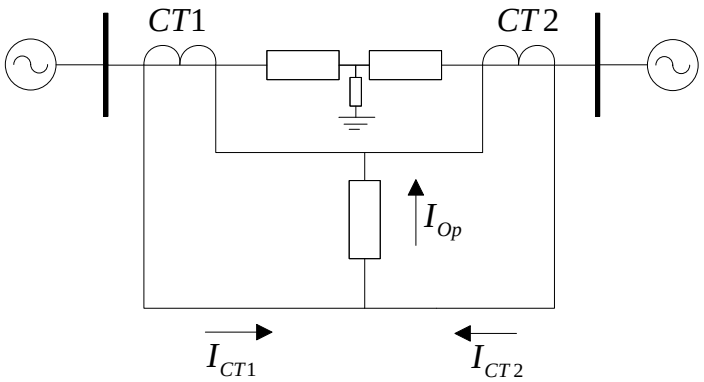

Figure 3.30: Operating current – differential protection principle

where, I_p is the relay pickup current. There is a considerable margin between the ranges of operating currents for internal faults and that for external faults. Hence, this principle provides clear discrimination between internal and external faults for uncompensated lines. For uncompensated lines, infeed is observed at both local and remote line-ends for internal faults, and outfeed is always observed at the remote end during external faults or on an unfaulted system. For series compensated lines however, current inversion may occur at the remote line-end, thereby leading to an outfeed for an internal fault. Therefore, clear selectivity between internal and external may not be achieved using the standard differential protection principle. Therefore, an alpha plane differential element may be used to provide unit protection for series compensated lines.

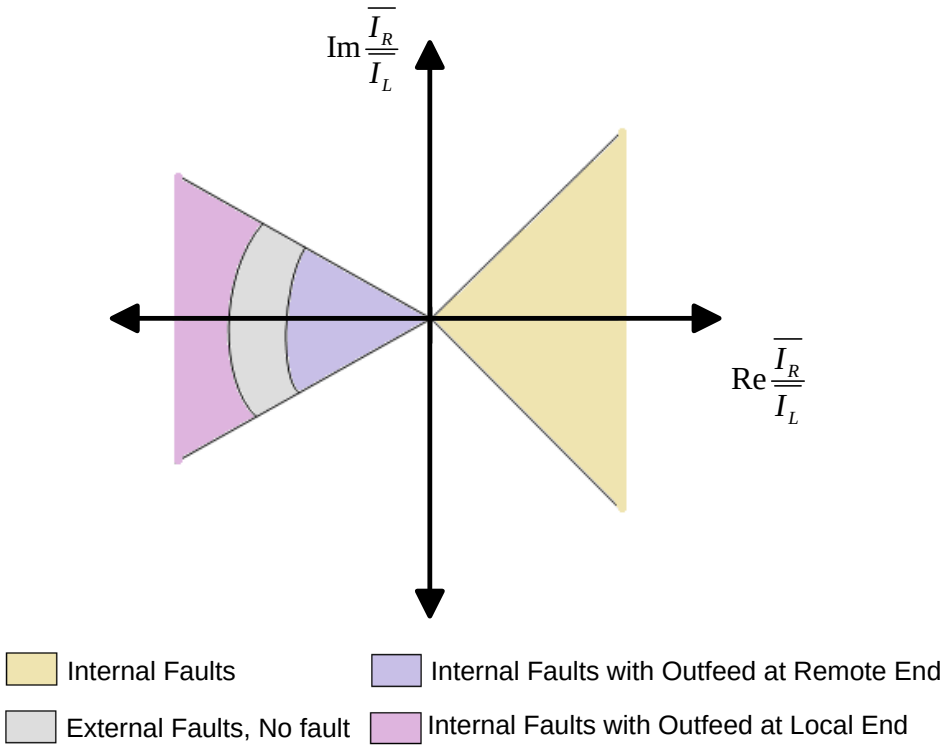

Figure 3.31: Alpha-plane regions for internal and external faults

It requires the calculation of $\bar{I}_R / \bar{I}_L$ where $\bar{I}_L$ is the outgoing local line-end current and $\bar{I}_R$ is the incoming current at the remote end. When this calculation is plotted on the alpha-plane line-differential characteristics shown in Figure 3.31, it may belong to one of the coloured regions shown. It can be seen that unless it lies within the blue arc the fault is internal. The alpha plane differential element is capable of discriminating between this region and outside regions on the plane. It achieves such selectivity by means of settings *87LANG* and *87LR*. The setting determines the outer radius (=*87LR*) and inner radius (=1/*87LR*) of the arc. *87LANG* determines the angular extent of the arc. These are shown below in Figure 3.32.

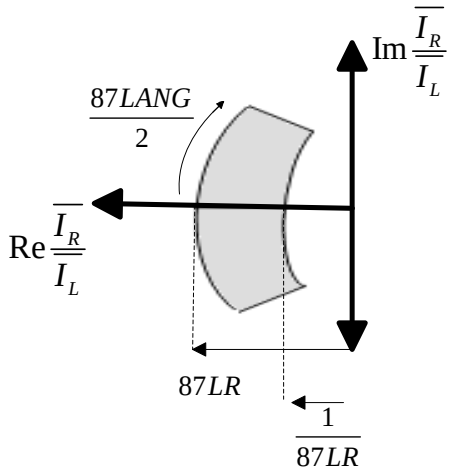

Figure 3.32: Alpha-plane differential element settings

3.8.5. Series Capacitor Voltage Compensation

It has been mentioned earlier that using the line side voltage provides better fault distance estimation, although it may still affect the directional integrity of the relays. If it is correctly determined that a fault is internal, determining the line side voltage is more useful in terms of accurately determining the zone of the fault. Several distance protection solutions have been proposed to deal with the problem of protecting series compensated lines. Accurately determining the voltage drop across the series capacitor would in effect allow the line side voltage to be determined. Two such methods have been described here.

The MOV was introduced previously in Section 3.5.3 and can be seen in Figure 3.14. The characteristic for the current I and voltage V of the Zinc-Oxide MOV can be approximated as follows:

$$I = (\frac{V}{\beta})^{\alpha} \tag{3.40}$$

where β = 137762.5 and α = 40. (3.5) and (3.6) together form the Goldsworthy model of the SC-MOV combination. However, the equations only apply after the MOV begins to operate, which happens after the peak current reaches 98% of the protective level current. In other words, the relay must use the entire series capacitor reactance X_{C0} of the capacitor to calculate the corresponding voltage drop when this condition is not satisfied. During a fault, either of these cases may be encountered. This algorithm calculates the voltage across the capacitor after determining whether the peak phase current is above or below the threshold. If the peak current is below 98% of the protective level current, then X_{CO} is used to calculate the voltage, else the Goldsworthy model equations are used to calculate the effective impedance, and this is then used to calculate the voltage across.

Figure 3.33 and Figure 3.34 show an example of the series capacitor current and series capacitor voltage respectively. These are shown using red solid lines. In Figure 3.33, the section of the waveform where the solid red line coincides with the green dashed line is the part of the waveform where the MOV does not conduct any current. All current flows through the capacitor in these sections, and the current is sinusoidal. The dashed green line is this section of the waveform extrapolated to full sinusoidal waveform. The black dashed line shows the peak value of this sinusoidal waveform (here 10kA).

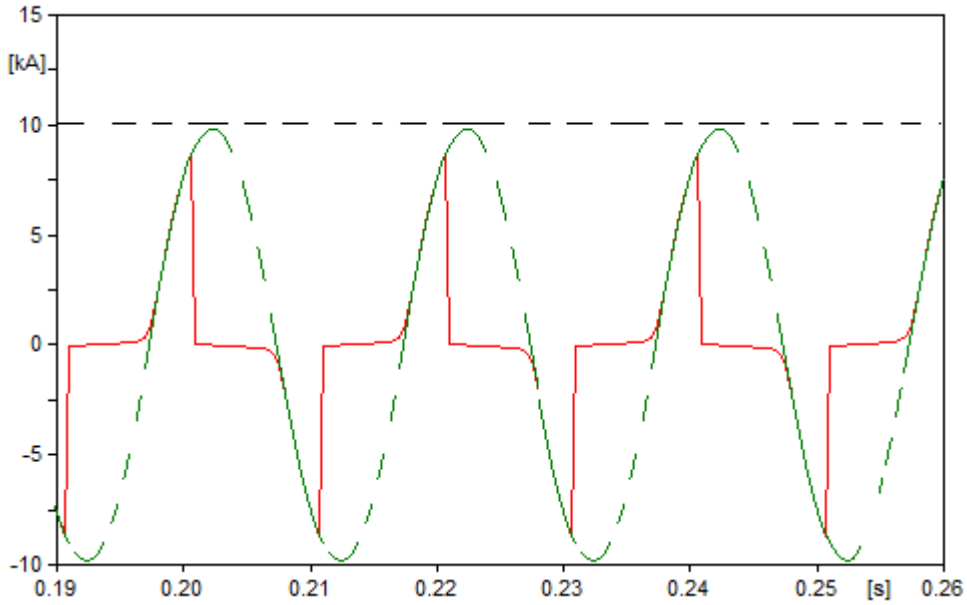

Figure 3.33: Series capacitor current

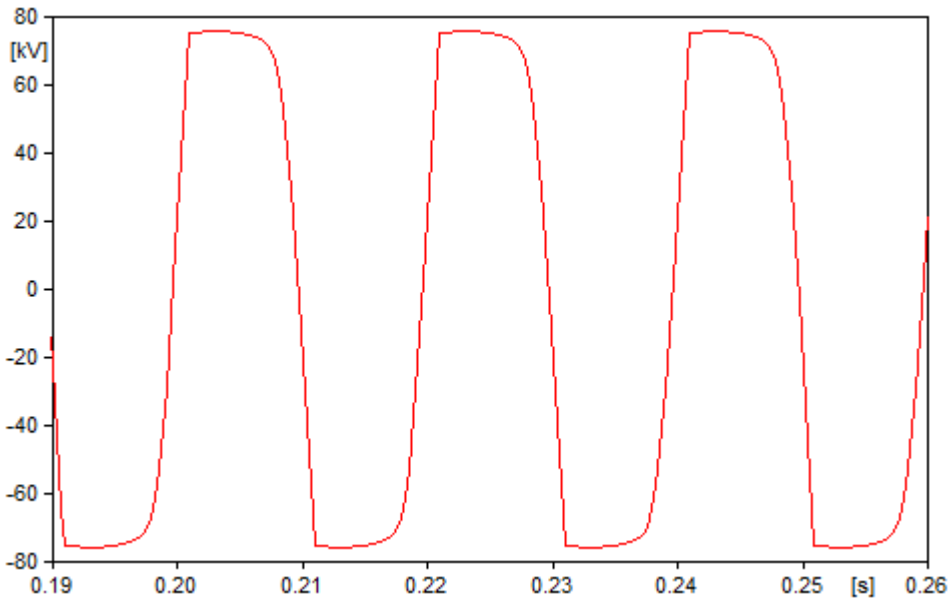

Figure 3.34: Series capacitor voltage

This value of the peak current is thus required for this determination and the subsequent calculations. Although there are many possible methods to determine the peak of a signal

in time domain applications from available measurement samples, the method used by the authors is as follows. The current $i(t)$ at times t_1 and t_2 are given by:

$$i(t_1) = I_{ph} \sin(\omega t_1) \tag{3.41}$$

$$i(t_2) = I_{ph} \sin(\omega t_2) \tag{3.42}$$

where ω = the supply angular frequency and I_{ph} is the peak current. If $t_2 = t_1 + T$, where T is the sampling period:

$$i(t_1 + T) = I_{ph} \sin(\omega(t_1 + T)) = I_{ph} \sin(\omega t_1)\cos(\omega T) + I_{ph} \sin(\omega T)\cos(\omega t_1) \tag{3.43}$$

Substituting for $i(t_1)$ gives:

$$i(t_1 + T) = i(t_1)\cos(\omega T) + I_{ph} \sin(\omega T)\cos(\omega t_1) \tag{3.44}$$

$$I_{ph} \cos(\omega t_1) = \frac{i(t_1 + T) - i(t_1)\cos(\omega T)}{\sin(\omega T)} = x \tag{3.45}$$

$$I_{ph} = \sqrt{(x^2 + i^2(t_1))} \tag{3.46}$$

Once the peak current is determined, if $I_{pu} = I_{ph} / I_{pr} > 0.98$, the following equation is used to calculate the voltage across the capacitor $v_C(t)$:

$$v_C(t) = v_C(t - T) + \frac{1}{C}\int_{t-T}^{t} i(\tau) d\tau \tag{3.47}$$

Otherwise the reactance and resistance values obtained from the linearised model calculations from (3.5) and (3.6) are used as follows:

$$V_C = Z'_C I = R'_C I - X'_C I \tag{3.48}$$

$$v_c(t) = \mathrm{Re}[V_C \exp(j\omega t)] \tag{3.49}$$

Thus, in effect the series capacitor is removed from the circuit. A mathematically different approach is used in [105] to calculate the series capacitor voltage drop. The total current entering the SC-MOV combination can be accounted for as follows:

$$C\frac{dv_x}{dt} + P(\frac{v_x}{V_{REF}})^q - i = 0 \tag{3.50}$$

Here, C is the capacitance of the series capacitor, the remaining terms have been defined previously in Section 3.5.3. This current is the measured fault current, which can hence be used to calculate the voltage drop across the capacitor, by solving the above differential equation. The authors use the discrete time form of the above equation using sampled information to arrive at a solution. Thus, the following continuous to discrete domain transformations are carried out:

$$i(t) \longrightarrow i_{(n)} \tag{3.51}$$

$$v_x(t) \longrightarrow v_{x(n)} \tag{3.52}$$

$$\frac{dv_x}{dt}(t) \longrightarrow D(3v_{x(n)} - 4v_{x(n-1)} + v_{x(n-2)}) \tag{3.53}$$

$$D = (2\pi f)/2\sqrt{(1-\cos(a))^4 + (2\sin(a) - 0.5\sin(2a))^2} \tag{3.54}$$

where f is the system frequency, T_S is the sampling period, $a = 2\pi f T_S$ and n is the discrete time index. Thus, the differential equation (3.53) now becomes:

$$F(x) = A_q x^q + A_1 x - A_0 = 0 \tag{3.55}$$

where,

$$x = \frac{v_{x(n)}}{V_{REF}} \tag{3.56}$$

$$A_q = P \tag{3.57}$$

$$A_1 = 3DCV_{REF} \tag{3.58}$$

$$A_0 = i_{(n)} + \frac{A_1}{3V_{REF}}(4v_{x(n-1)} - v_{x(n-2)}) \tag{3.59}$$

The constants A_q and A_1 can be determined through the MOV parameters. A_0 on the other hand, depends on the latest current samples, and two previous samples of voltage. Using the Newton Rhapson method, (3.55) is solved for the voltage and thus appropriately compensated for.

3.8.6. Other Important Solutions

The above mentioned solutions are the commonly implemented solutions. There have been several novel solutions proposed over the years to solve the problems of fault location on series compensated lines. They use a variety of methods and technologies and provide good accuracy of results.

In particular, a number of wavelet transform based novel methods have been proposed in the past. The method proposed in [106] uses the wavelet packet transform to decompose the fault current signal into several levels which are then grouped into frequency sub-bands. A phase selection signal is calculated, and its total harmonic distortion determines whether the phase is faulted. Similarly, another section identification signal is calculated and the same procedure is used to identify the faulted section. A wavelet transform based boundary method protection method is proposed in [107] which calculates the spectral energy in two frequency bands in the transient current signal to arrive at a decision whether the fault is internal or external. Reference [108] also uses high frequency voltage signals for the purpose of fault location. Reference [109] combines fuzzy logic and wavelet

transform for the fault classification of a series compensated transmission line. Other important wavelet based methods have been proposed in [110], [111], [112].

A number of methods applying neural networks have been proposed since the 90s. References [113] and [114] are two of the earliest papers to investigate the use of neural networks in this field. The authors of [115] have proposed a voltage compensation method for protecting series compensated lines using ANNs. Reference [116] uses high frequency voltage signals generated in series compensated lines for a single-ended protection scheme and makes use of trained ANNs. A phasor determination and fault identification technique using Multi-Input-Multi-Output Recurrent Neural Network (MIMO-RNN) has been proposed in [117]. Multi-layer-perceptron neural networks trained using the Levenberg-Marquardt (LM) training algorithm, have been used in [118]. However, a major disadvantage with these methods is that they require large sets of training data. A wide variety of other approaches have also been used in important novel algorithms. [119] describes a fast method using Support Vector Machines for fault classification, ground detection, and section identification for lines compensated with a TCSC. Although various FLAs that accurately locate faults on series compensated lines have been proposed, there are no existing solutions that are line parameter free and that use current and/or voltage measurement data. This is the single drawback in the existing methods that is addressed by the novel FLAs discussed in this thesis. This drawback is discussed in more detail Chapter 4 to highlight the need for line parameter free algorithms.

3.9. ATP-EMTP Modelling of a Series Compensated Line

ATP-EMTP is a highly useful tool for the study of transient processes, and can perform accurate simulations for a wide variety of power system studies such as overvoltage studies, switching transients, shaft torsional oscillations, ferroresonance etc. It contains a number of blocks to simulate power system elements such as various models of transmission lines, CTs, VTs, synchronous machines, etc. It is programmed to solve differential equations that govern the electrical behaviour of a simulated power system network. It also contains tools that plot analog and digital simulated signals, as well as

store output data in the form of *.LIS files that can be transferred to MATLAB for further analysis.

Throughout this project the ATP-EMTP software is used to simulate measurement data from series compensated single-circuit and double-circuit lines under steady-state and fault conditions. Shown in Figure 3.35 is an example system, modelled in ATP-EMTP containing a series compensated line. It contains sources at local and remote ends of the line, with source impedances modelled as R-L blocks. CTs and VTs can be seen at each end of the line. The line itself is modelled using the LCC line modelling block [1] in ATP-EMTP containing the functionality to model a J-Marti line [1], and is simulated as two separate segments to allow for the simulation of a fault. Splitters can be seen in the models of the fault and the series compensator. The splitter allows the modelling of each of the phases separately in a three-phase network. A fault is simulated using a fault resistance and a time controlled switch. The focus of the project is primarily on permanent faults.

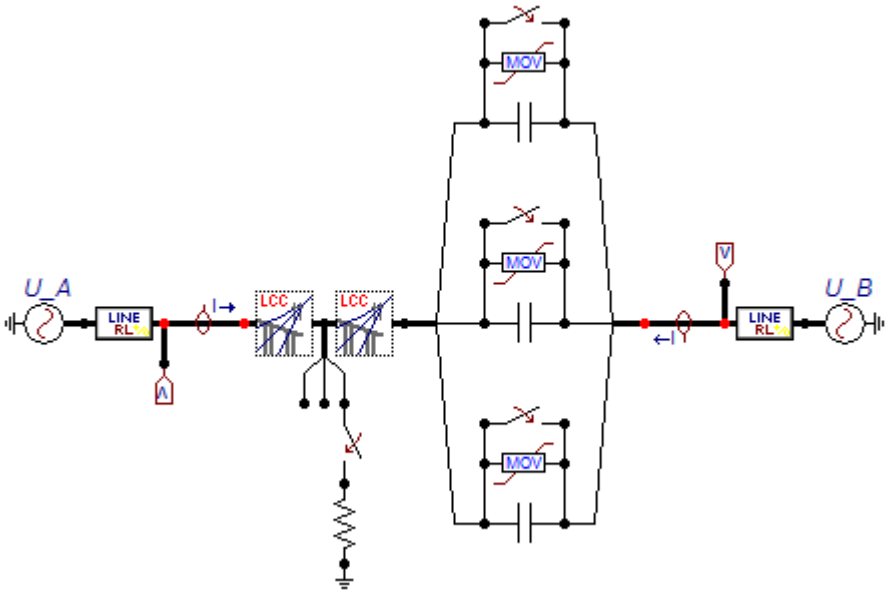

Figure 3.35: ATP-EMTP model of a series compensated line

The series capacitors are modelled using simple capacitor blocks available in ATP-EMTP. For the overvoltage protection a Zinc-Oxide MOV block is used. The MOV can be simulated accurately by setting the data parameters in the options menu as listed in Table 3.1. It shows an example set of entries for an MOV of a reference voltage of 63kV. The required parameters are the reference voltage (Vref), flashover voltage (Vflash), Initial voltage (Vzero), number of arrester columns (#COL), number of blocks (#SER) and fitting tolerance for the characteristic (ErrLim). The options menu also requires a set of points that define the characteristic of the MOV as can be seen in Table 3.2 and Figure 3.36 respectively. They are shown for an MOV of a reference voltage of 63kV.

Table 3.1: List of data parameters for ATP-EMTP modelling of MOV

Entry Title	Definition	Value Entered
Vref	Reference Voltage(V)	63000
Vflash	Flashover voltage (p.u.)	-1 (representing no gap)
Vzero	Initial Voltage (V)	0
#COL	Number of arrestor columns	1
#SER	Number of blocks in series in each branch	1
ErrLim	Fitting tolerance (p.u.)	0.01

Table 3.2: Example data points of the MOV-characteristic required for ATP-EMTP modelling of the MOV

Current (A)	Voltage (V)
3.00E-05	51154.39758
9.00E-05	52290.81366
0.0003	53565.23006
0.0015	55317.47836
0.03	58733.10684
3	64399.57104
30	67434.62931
375	70928.56522
750	71918.69109
1500	72922.63861
3000	73940.60071
4500	74542.64516
9000	75583.22171

15000	76359.37669
30000	77425.31386
60000	78506.13097
120000	79602.03571
300000	81074.25649

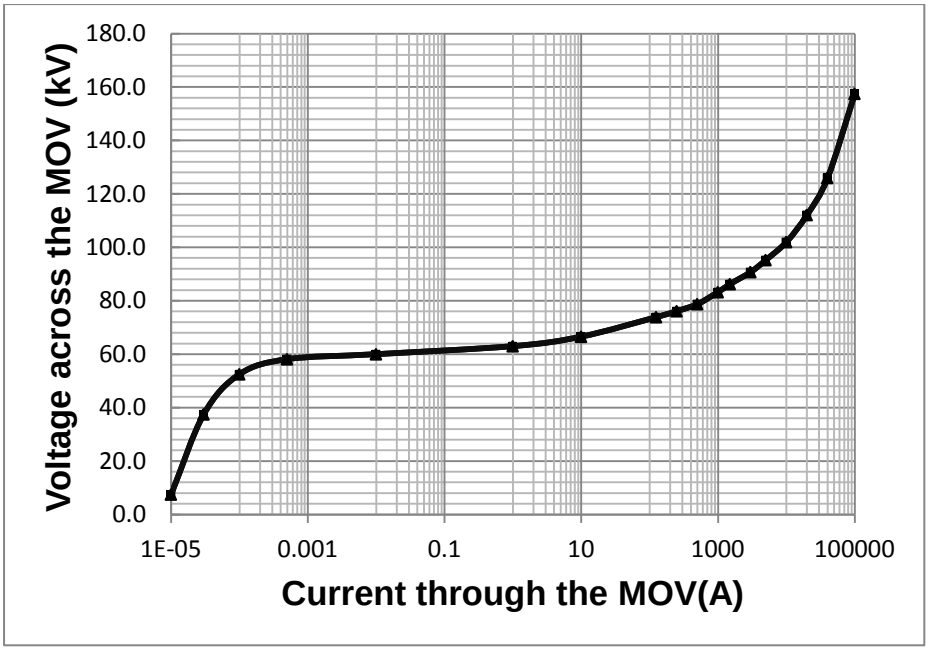

Figure 3.36: MOV V-I characteristic

3.10. Simulations

To illustrate the utility of ATP-EMTP for the purposes of the project, a number of simulations of the model used to generate measurement data have been included as follows. The currents and voltages measured at the line terminals will be used as input data for algorithms described in the later sections of this thesis.

3.10.1. Simulations for Steady-State Normal Operating Conditions

Single-circuit series compensated lines may be simulated using the model shown in Figure 3.37. It comprises of series compensation at both ends of the line, and each of the individual blocks is modelled as explained previously. For this system, the steady state line

terminal currents are shown in Figure 3.38 and the steady state voltages measured at the terminals are shown in Figure 3.39. The degree of series compensation is 50%. It can be seen that the currents for each phase at the local and remote line-ends are π^c out of phase with one another owing to the reference directions of the measurements of currents at the terminals being opposite to one another. It can be observed that the peak magnitudes of the three phase currents at any given terminal are not equal to each other since the line is untranposed.

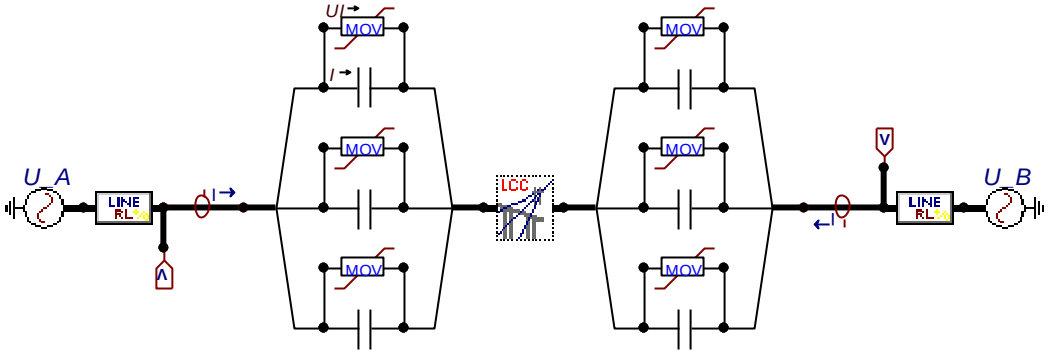

Figure 3.37: ATP-EMTP model of line compensated at both line-ends

Table 3.3: Network Parameters

Network Parameters	Local Network A	Remote Network B
Line to Line RMS Voltage (kV)	416	400
Phase Angle (^{o})	0	-20
+ve seq. Resistance (Ω)	1.019	0.637
+ve seq. Inductance (H)	0.051	0.031
$Z_1 = R_1+jX_1$	1.019+j16	0.637+j10
X_1/R_1	15.7	15.7
0 seq. Resistance (Ω)	2.037	1.273
0 seq. Inductance (H)	0.102	0.064
$Z_0 = R_0+jX_0$	2.037+j32	1.273+j20
X_0/R_0	15.7	15.7
Fault MVA	45MVA	70MVA

Table 3.4: Transmission Line Parameters

Transmission Line Parameters	Positive/Negative Sequence	Zero Sequence
resistance, Ω/km	0.065	0.195
inductance mH/km	0.955	2.864
Capacitance nF/km	10.5	5
R Ω /km	0.065	0.195
X Ω /km	0.3	0.9
B S/km	$0.329x10^{-5}$	$0.157x10^{-5}$
X/R	4.615	4.615

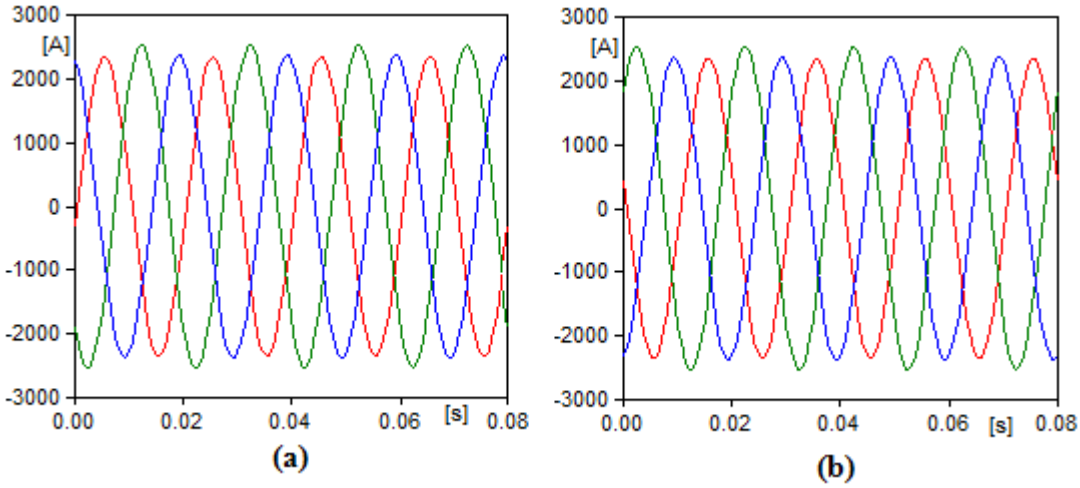

Figure 3.38: Phase currents – single circuit line a) Local line-end b) Remote line-end

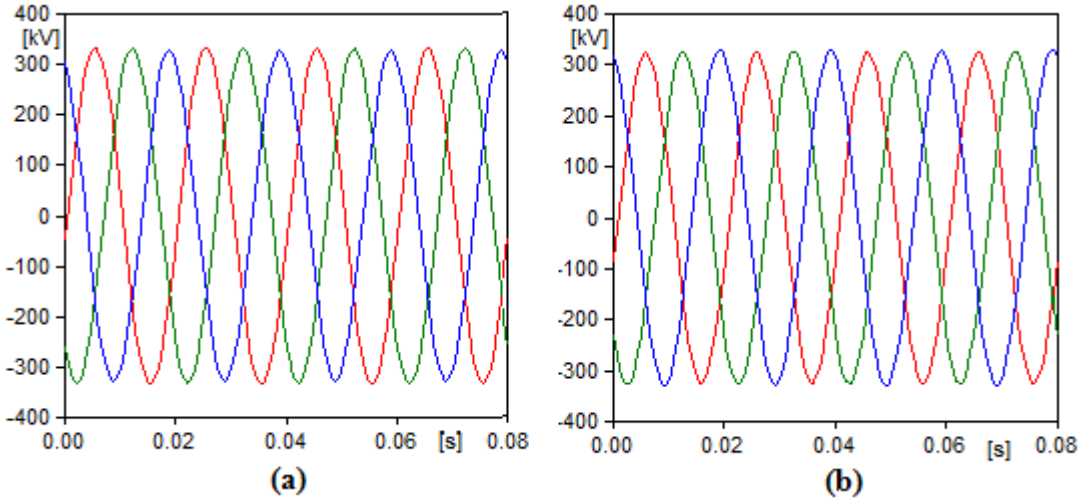

Figure 3.39: Phase voltages– single circuit line a) Local line-end b) Remote line-end

Double-circuit series compensated lines may be simulated using the model shown in Figure 3.40. Here as well, the line is compensated at both line-ends. A double-circuit J-Marti model is used instead. The LCC line-modelling block of the ATP-EMTP software is used for this purpose. The degree of series compensation is 50%. The corresponding steady state line terminal voltages are shown in Figure 3.41, and the currents flowing through circuits I and II are shown in Figure 3.42. The currents for each phase in circuit-I are seen to be identical in magnitude and phase to those in circuit-II. This is because the terminal voltages are equal for the two circuits, and the geometry and impedance of each circuit are also identical. Again, an imbalance between phase current magnitudes is observed due to this being an untransposed line.

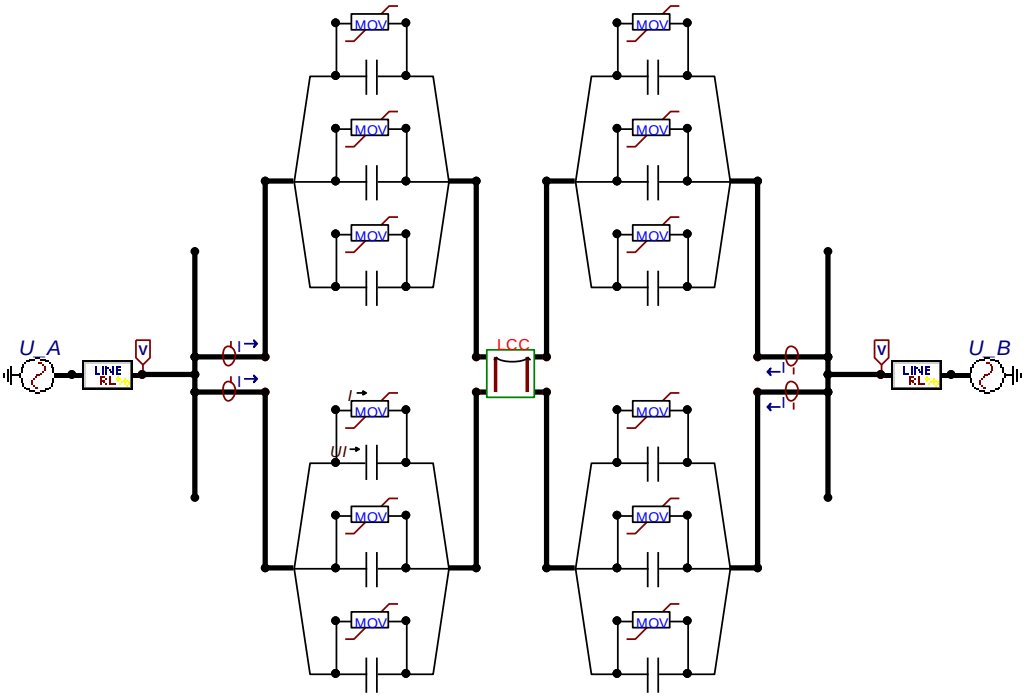

Figure 3.40: ATP-EMTP model of a double-circuit line

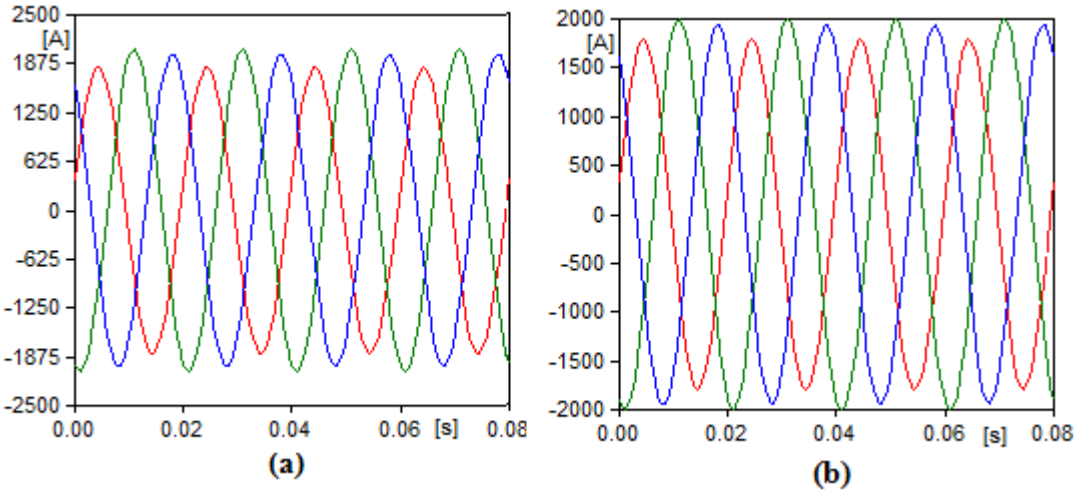

Figure 3.41: Phase currents – double-circuit line a) Local line-end b) Remote line-end

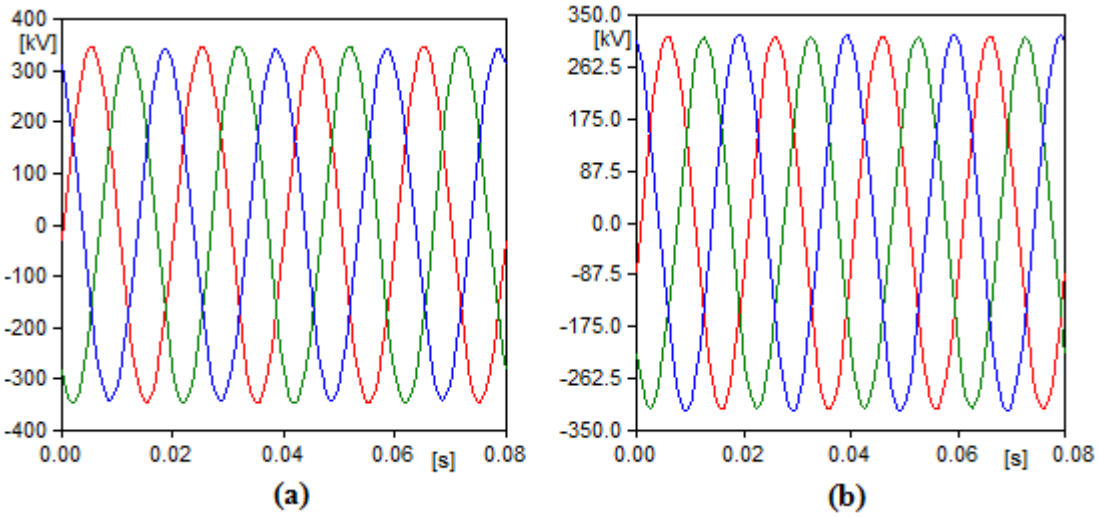

Figure 3.42: Phase voltages – double-circuit line a) Local line-end b) Remote line-end

3.10.2.Simulations for MOV Operation

This section discusses simulations for a single-circuit series compensated line under fault in order to show the electrical behaviour of the MOV during conditions of overvoltage across a series capacitor. The system has been shown in Figure 3.43. The degree of series compensation is 50%. The fault at 50 km on the 100 km line is simulated to occur at 13ms. The current through the MOV and the current through the series capacitor are shown in Figure 3.46. The voltage across the capacitor has also been shown in Figure 3.47. It can be seen the MOV limits the voltage across the capacitor around the peak region of the waveform. It can also be seen that both current waveforms are non-sinusoidal. The terminal currents and voltages are shown in Figure 3.44 and Figure 3.45. A combination of a decaying DC component and subharmonic oscillations can be observed in the faulted phase currents (the altering of peak magnitude every half cycle). Higher harmonics are observed in the voltage waveforms around the point of fault inception.

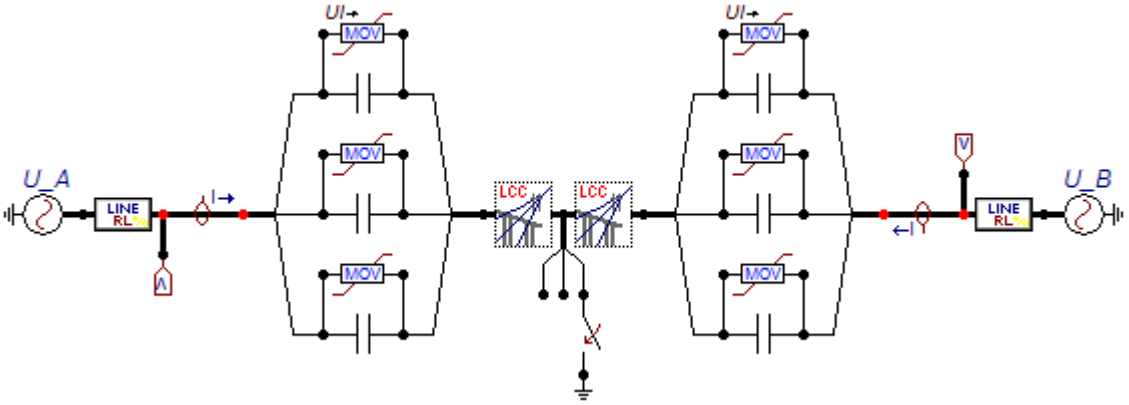

Figure 3.43: ATP-EMTP model of a line compensated at both line-ends under fault

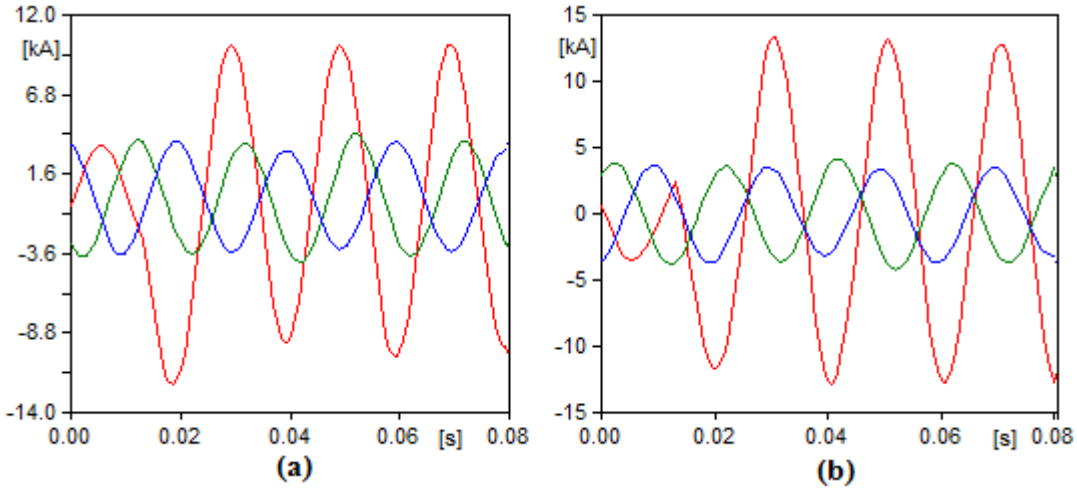

Figure 3.44: Phase currents – line under fault (compensated at both line-ends) a) Local line-end b) Remote line-end

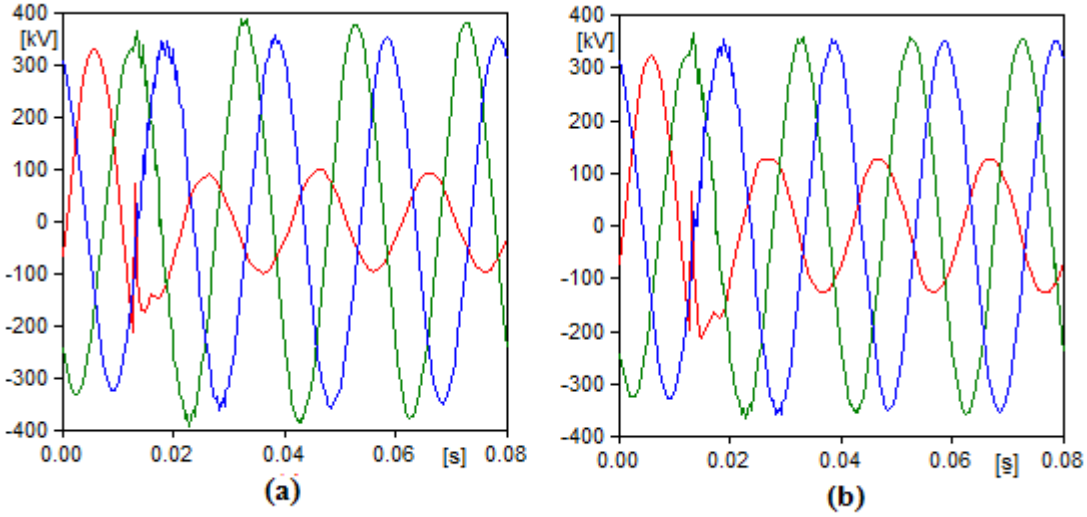

Figure 3.45: Phase voltages –line under fault (compensated at both line-ends) a) Local line-end b) Remote line-end

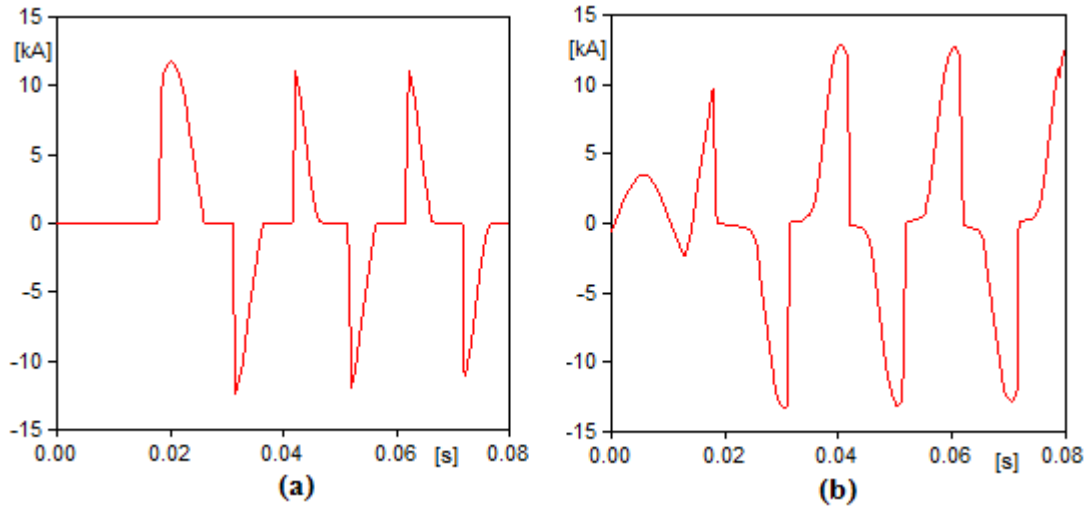

Figure 3.46: a) MOV current b) Capacitor current

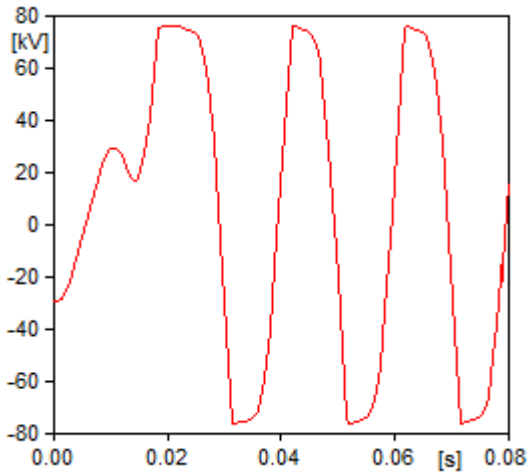

Figure 3.47: Series capacitor voltage

3.10.3.Simulations for Different Locations of Series Compensation

As mentioned previously, series compensation is commonly located either at only one line-end of the line, both ends of the line, or in the middle of the line. Simulations, so far, are shown for a line compensated at both line-ends. This section shows the corresponding current and voltage simulations for the other two cases. Simulations are shown for the line for a fault occurring at 13ms. First a line compensated at the local-end only is considered as shown in Figure 3.48. The degree of series compensation is 25%. Figure 3.49 and Figure 3.50 correspond to phase currents and phase voltages respectively. The faulted phase current waveforms show a significant decaying DC component. Higher harmonic transients are observed in the voltage waveforms.

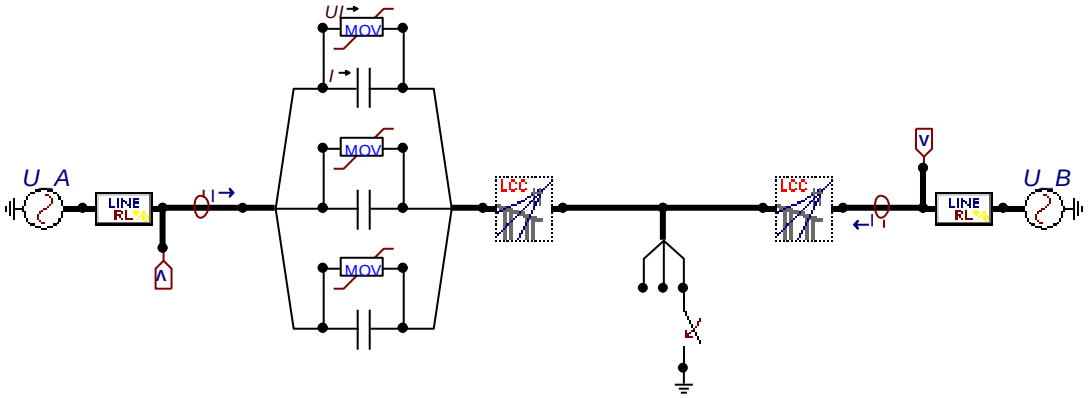

Figure 3.48: ATP-EMTP model of a line compensated at local line-end only

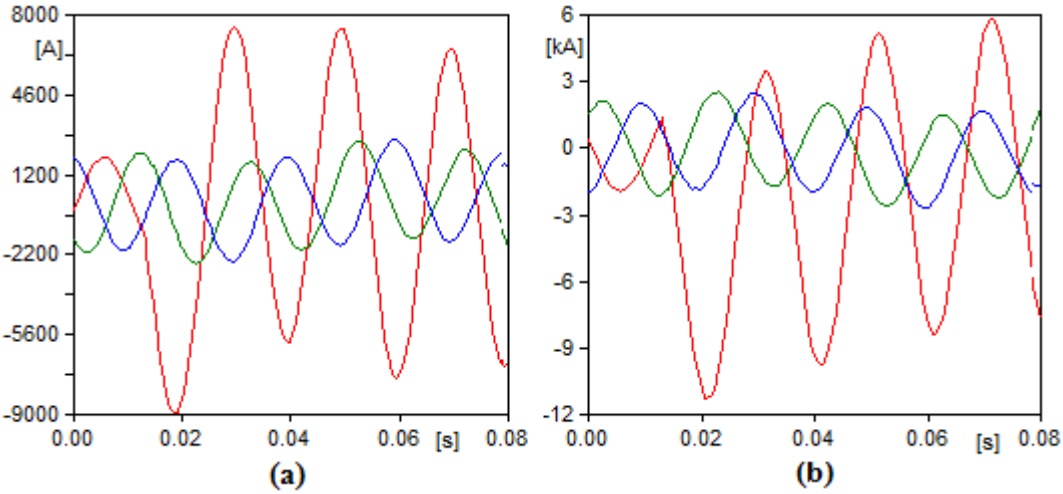

Figure 3.49: Phase currents – line under fault (compensated at local line-end only) a) Local line-end b) Remote line-end

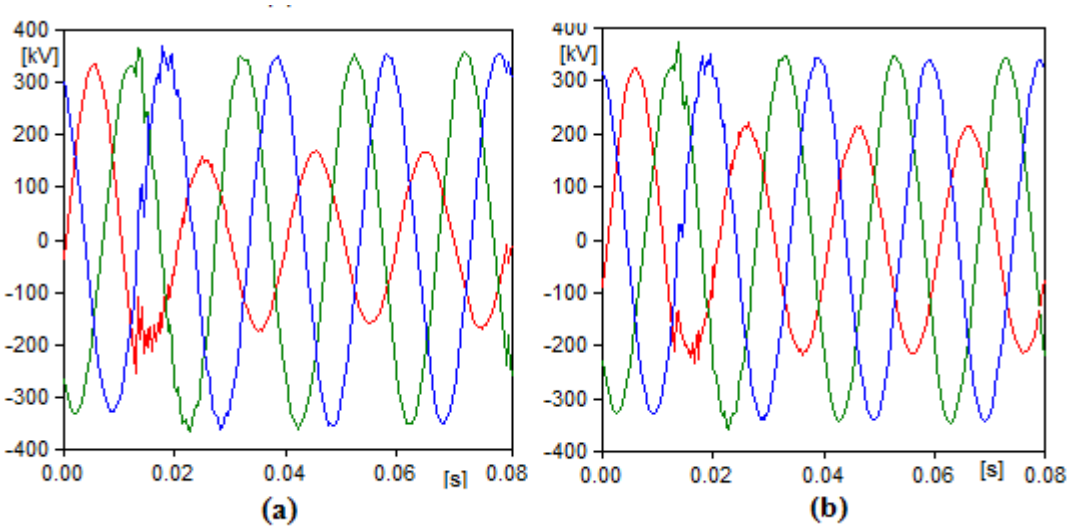

Figure 3.50: Phase voltages – line under fault (compensated at local line-end only) a) Local line-end b) Remote line-end

Similarly, the currents and voltages for a line compensated at the middle are shown in Figure 3.51 and Figure 3.52 respectively.

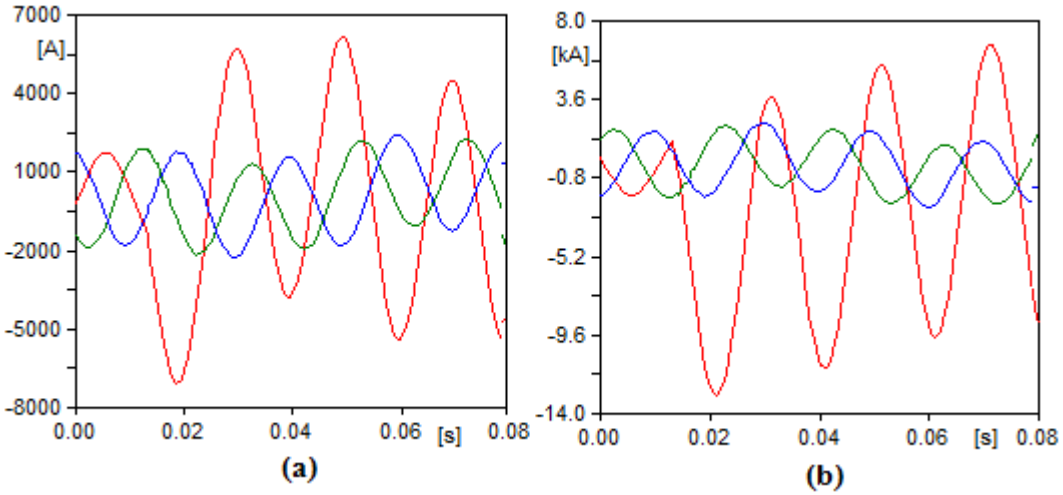

Figure 3.51: Phase currents – line under fault (compensated at the middle) a) local line-end b) remote line-end

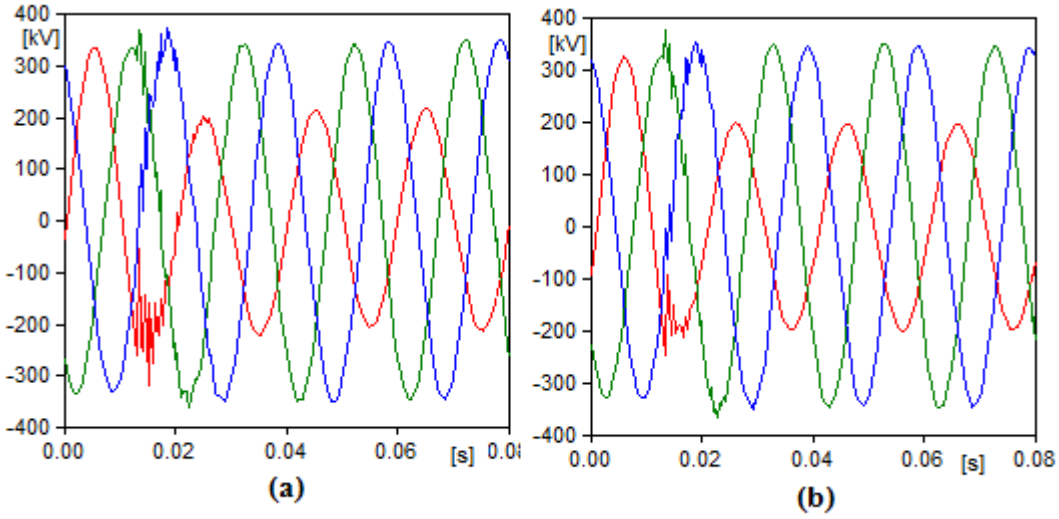

Figure 3.52: Phase voltages – line under fault (compensated at the middle) a) local line-end b) remote line-end

3.11. Chapter Summary

Series compensation of transmission lines is an economical means to achieve an increased transmission capacity by the lowering of its effective reactance. There are a multitude of advantages offered by series compensated lines when compared to traditional uncompensated lines. Series compensation reduces the losses in the line by increasing the power factor. It also offers increased voltage stability and increased angular stability. Series compensated lines have a higher dynamic stability margin when compared to the corresponding uncompensated lines.

A number of series capacitors have been installed across the world since as early as 1928. In the UK there are currently no series compensated lines. However, due to the planned increase in wind generation of 34 GW, there is a need to reinforce the transmission infrastructure between north of Scotland to England, and series compensation is one of the solutions to be implemented to achieve this. Furthermore, installations of fixed series capacitor banks at Gretna, Moffat and Eccles substations are planned to be completed by 2015. The UK's first TCSC is to be installed at Hutton substation by 2015. Thus, the importance and relevance of this study cannot be overstated.

This chapter details the ATP-EMTP modelling process of simulating the series compensated line, which will be used in subsequent chapters, to provide input measurement data for novel FLAs. The most common topologies of series compensation and the two main types of lines (single-circuit and double-circuit lines) found in the real world were shown to be modelled. It was demonstrated that the software and the model are capable of accurately simulating faulted and healthy lines including the simulation of transient phenomena such as the presence of decaying DC components and subharmonic frequency oscillations.

Protection and fault location of series compensated lines presents unique challenges owing to a number of important factors. FLAs designed for uncompensated lines incorrectly calculate the fault distance. Directional elements may incorrectly detect forward faults as reverse faults and vice-versa. Differential protection may be affected by remote-end outfeed. A number of solutions have been proposed to address these issues with respect to fault locators, directional elements, differential elements and distance protection relays. A key drawback of all existing solutions is the requirement of line parameters in their calculations leading to inaccuracies when implemented on a real power line. This is discussed in more detail in the next chapter, where this shortcoming is addressed in the form of a novel fault location algorithm developed for single-circuit series compensated lines.

Chapter 4. Novel Algorithm for Single-Circuit Series Compensated Transmission Lines

A significant common drawback that all existing solutions for fault location on series compensated lines have was identified, that they either require line parameter settings for their calculations or the use of extensive training data. This is significant, as the accuracy of line parameters is affected by weather and loading conditions.

Chapter 4 details the novel FLA for single-circuit series compensated lines developed by the author that addresses this problem. It does not require any line parameters for its calculations. The FLA is detailed in this chapter, the advantages of this aspect of the algorithm are discussed, the mathematical derivations are provided, simulation tests carried out are detailed, and the results are tabulated.

4.1. Introduction

In this chapter, a novel algorithm for fault location on series compensated transmission lines that does not require the use of line parameters is presented. This includes the resistance, inductance and capacitance of the line per unit length, which most FLAs typically use. Fault locators used for OHTLs estimate the distance to fault from a given line terminal. The importance of FLAs is significant in the case of fault locators as they determine how speedily the faulted line is repaired and restored back into service by repair crews, thus minimising outages and relevant costs. Thus, the need for fault location to be accurate and reliable cannot be overstated.

The resistance, inductance and capacitance per unit length are highly variable. They vary significantly for different weather and loading conditions [120], [121], [122], [123]. These factors introduce inaccuracies in the algorithm over and above their theoretical inaccuracies. Obtaining zero-sequence reactance per unit length parameters is difficult, and reliance on such parameters would affect the accuracy of fault location even more

significantly. Errors in fault distance estimation of FLAs based on simulations studies can be as low as <1%, whereas when implemented in real power systems the real accuracies may be significantly higher (this will be demonstrated in Chapter 6). This is because the simulation studies wholly satisfy assumptions that the FLAs are based on, which, may only be approximately true on real power systems, and lead to significant inaccuracies in fault location. Therefore, an algorithm such as the one presented in this chapter will be more accurate and reliable when locating faults on real power systems, simply from not relying on inaccurate and unreliable parameter-data.

Although it is well established that line parameters are often erroneous, very few studies have been carried out to numerically determine the extent of such errors, upon comparison of pre-determined settings to real-time calculated parameters. One reason for this is that the true values of such line parameters (that is to say, based on real-time measurements) will vary based on where the measurements are taken, the temperature of the line at the time of the year the measurements are taken, level of loading etc and therefore such an average numerical error value cannot be established unless a number of test cases are considered.

One study by Prado-Félix et al, finds errors in positive and negative sequence self impedance parameters to be as high as 6% and those in zero sequence self impedance parameters to be as high as 16% [120], [121]. Another report by Shweitzer Laboratories [122] shows calculations of zero-sequence parameters at two ends of 34.5 kV line between Centre and Jonestown, North Dakota, USA. It made use of field data to determine the sequence impedance parameters validated by distance protection algorithms. It finds an error of over 20% when comparing these values with the settings of zero-sequence impedance. The most relevant of such studies determining impedance-settings errors is that carried out by the Korea Electric Power Research Institute (KEPRI) [123]. In this study, positive sequence and zero sequence impedance measurements for 40 circuits are carried out and compared against impedances calculated using pre-determined line parameters. Maximum errors of up to 18.9% were found in the positive sequence impedances, and 5 of the 40 circuits showed errors of over 5% (standard deviation of 4.8%). Similarly for zero-sequence impedances, the errors were as high as 18.4%, but 23 out of the 40 circuits had errors greater than 5% (standard deviation of 7.6%).

Synchronised Measurement Technology is a relatively recent concept in power technology incorporating Phasor Measurement units (PMU), centralised Data Concentrators and a GPS-aided communication infrastructure and that offers great advantages for the purposes of transmission line protection and fault location. The algorithm discussed in this chapter makes use of two-terminal synchronised measurement data and can therefore benefit from (although it is not limited to) the use of this technology. The novel algorithm described in this chapter is developed in the spectral domain, and requires fundamental frequency phasors for phase currents and phase voltages from both ends of the line. The algorithm is shown to use synchronised data sampling. This means that data samples of these measurements are time-synchronised with one another. However, an additional algorithm that is capable of locating faults using asynchronous data samples is also presented in this chapter. This addresses the scenario where time-synchronisation is unavailable or unreliable. Some FLAs do not consider the fault resistance or the remote infeed current as is the case with transmission lines. This again, introduces inaccuracies over above those calculated using simulation studies. In this chapter, it is shown that the algorithm accuracy is not sensitive to the fault resistance. This is an additional advantage of the algorithm with respect to its reliability and accuracy.

In recent years, the importance of line parameter free fault location is increasingly becoming realised. A number of FLAs have been proposed in this field. In [124] a simple and accurate FLA is proposed that does not require the use of line parameters and the distance to fault is calculated in the sequence domain, but for uncompensated lines. A similar algorithm for uncompensated lines is proposed in [125] but in the phasor domain. A solution capable of locating faults on both transposed and untransposed lines is proposed in [126]. It requires an iterative process to calculate the distance to fault, and therefore requires sufficiently accurate initial values for parameter data. A closed form line parameter FLA is proposed in [127], which does not require time-synchronisation of two terminal data. However, it makes use of the transposed line assumption. Reference [128] proposes a line parameter free FLA for double circuit lines. However, none of the above described methods is suitably accurate when applied to series compensated lines. They each make mathematical assumptions about the transmission line that are not true for series compensated lines. [129] proposes a FLA that is line parameter free and for series

compensated lines. However, it assumes an uncompensated line, neglects the series capacitor reactance and is therefore not sufficiently accurate. Even so, it is only applicable to lines where the VT is on the line side of the series capacitor.

Chapter 3 discussed the various problems associated with fault location on series compensated lines such as voltage inversion, current inversion, etc. Fault location on series compensated lines is a complex problem due to the non-linear nature of the impedance of the overvoltage protection installed in parallel with the SC. Conventional impedance based algorithms for uncompensated lines would not be able to locate faults on series compensated lines accurately. The FLA discussed in this chapter takes all these aspects into account by using an accurate mathematical model of the faulted system, thereby giving an accurate estimate of distance to fault. Moreover, it does not require settings for series capacitor reactance, adding further reliability and applicability. It is assumed that Rogowski coil CTs are used in the measurement of currents at the two line-ends. Rogowski coil CTs are known for their high performance with respect to the requirements of fault location, linearity in measurement and no magnetic saturation.

The FFT is widely used in the field of fault location for the spectral domain analysis of sampled measurement data as it is fast, simple and easy to implement. However, it is also known for its sensitivity to DC components. However, several methods have been proposed over the years for the filtering-out of DC components. The method proposed in [131] was used in this FLA for this process. It is a simple method that efficiently eliminates DC components based on the determination of the magnitude and time constant of the dc component exponential characteristic. Upon diminishing the magnitude of DC components using the method, the FFT is carried out to obtain the fundamental frequency components of the required voltages and currents.

4.2. Derivation of the Novel Algorithm

This section details the derivation of the expressions for the fault distance used by the novel algorithm. The algorithm provides a different solution for each of the following categories of fault types, since the solution to any one will not be applicable to the others.

- SLG faults on transposed lines
- Symmetrical faults on transposed lines
- All other types of faults on transposed lines/all faults on untransposed lines

The derivation of the algorithm is carried out in a manner such that impedance variables are eliminated systematically from the mathematical model of the faulted series compensated line, thereby resulting in line parameter-free expressions for distance to fault. These expressions only contain voltage and current phasors from the line terminals, and certain MOV coefficients (discussed in Section 4.2.4). While this derivation is shown assuming that phasors are time-synchronised, Section 4.2.5 shows how the algorithm can also be applied for asynchronous measurements, i.e. the approach which does not rely on accurate time-synchronisation. The fault type here is assumed to be available from the microprocessor relay. Modern distance protection microprocessor relays are equipped with functionality for accurate fault type classification [140]-[145]. The fundamental concept of the algorithm derivation is the expression of the voltage drop across each of the phases as a sum of the voltage drops across the self, mutual and series compensation impedances. This is shown in Figure 4.1 and (4.1).

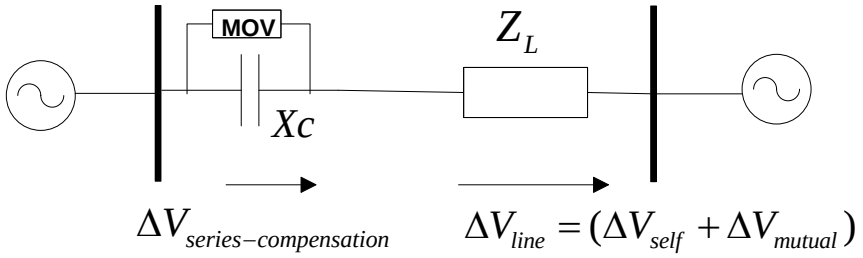

Figure 4.1: Single-line diagram of series compensated line

$$\begin{aligned} \Delta V_{phase} &= \Delta V_{line} + \Delta V_{series-compensation} \\ &= (\Delta V_{self} + \Delta V_{mutual}) + \Delta V_{series-compensation} \end{aligned} \tag{4.1}$$

Each of these voltage drops can be expressed in terms of certain impedance variables namely: the self impedance of the line, the mutual impedance of the line, and the series

capacitor reactance. Additionally, for simplicity of derivation, the positive sequence impedance of the line may also be considered as an intermediate variable in the analysis to be eliminated in the derivation. These quantities are all treated as variables in the derivation, and are systematically eliminated through algebraic manipulation. Each of these voltage drops is expressed in spectral domain, and the fundamental frequency phasors for all voltages and currents are obtained either using PMUs or by carrying out a FFT on time-domain measurement data samples. Both pre-fault and fault measurement data is used in the calculations. The distance to fault is also a variable in this analysis, expressed here as a fraction of the total line length as shown in (4.2). Thus, the impedances of faulted sections of the line can also be expressed in terms of the previously mentioned impedance variables and the per-unit length of the line-section. The expression for the self impedance of the faulted section of the line at the local line-end is shown in (4.3).

$$l = \frac{distance\ to\ \ fault}{total\ line\ length} \tag{4.2}$$

$$self\ impedance\ of\ local\ \ faulted\ seection\ of\ the\ line = l \cdot Z_S \tag{4.3}$$

Here, Z_S is the total self impedance of the line and l is the fractional distance to fault. All derivations have been carried out directly using currents and voltages from phases a, b, and c. Typically, FLAs are derived in time domain or in spectral domain but using sequence network phasors. The former type is used for real time application and the latter is used for simplicity of analysis. For transposed uncompensated lines, sequence networks are decoupled, that is to say there is negligible mutual coupling between the sequence networks. This simplifies analysis of the faulted network significantly, as the system is split into three independent networks, leading to simpler expressions for distance to fault. However, in the case of series compensated lines, the sequence networks are not decoupled. Secondly, mathematically determining the electrical behaviour of the series compensation unit is easier to carry out using analysis of the phase networks. It is thus important to accurately account for the mutual coupling effect between phases. During normal conditions (pre-fault) the following equation holds true:

$$\begin{bmatrix} \overline{V}_{La-pre} - \overline{V}_{Ra-pre} \\ \overline{V}_{Lb-pre} - \overline{V}_{Rb-pre} \\ \overline{V}_{Lc-pre} - \overline{V}_{Rc-pre} \end{bmatrix} = \begin{bmatrix} Z_S & Z_{Mab} & Z_{Mac} \\ Z_{Mab} & Z_S & Z_{Mbc} \\ Z_{Mac} & Z_{Mbc} & Z_S \end{bmatrix} \begin{bmatrix} \overline{I}_{a-pre} \\ \overline{I}_{b-pre} \\ \overline{I}_{c-pre} \end{bmatrix} - jX_C \begin{bmatrix} \overline{I}_{a-pre} \\ \overline{I}_{b-pre} \\ \overline{I}_{c-pre} \end{bmatrix} \quad (4.4)$$

where,

$\overline{V}_{La-pre}, \overline{V}_{Lb-pre}, \overline{V}_{Lc-pre}$ are the pre-fault local line-end voltages of phases a, b and c

$\overline{V}_{Ra-pre}, \overline{V}_{Rb-pre}, \overline{V}_{Rc-pre}$ are the pre-fault remote line-end voltages of phases a, b and c

$\overline{I}_{a-pre}, \overline{I}_{b-pre}, \overline{I}_{c-pre}$ are the pre-fault currents for phases a, b and c

Z_S is the self impedance of the line

Z_{Mab}, Z_{Mac} and Z_{Mbc} are the mutual impedances between the corresponding subscripted phases

X_C is the total reactance of series capacitor(s)

The above mentioned phasors are shown along with their reference directions in Figure 4.2. For transposed lines this can be simplified to:

$$\begin{bmatrix} \overline{V}_{La-pre} - \overline{V}_{Ra-pre} \\ \overline{V}_{Lb-pre} - \overline{V}_{Rb-pre} \\ \overline{V}_{Lc-pre} - \overline{V}_{Rc-pre} \end{bmatrix} = \begin{bmatrix} Z_S & Z_M & Z_M \\ Z_M & Z_S & Z_M \\ Z_M & Z_M & Z_S \end{bmatrix} \begin{bmatrix} \overline{I}_{a-pre} \\ \overline{I}_{b-pre} \\ \overline{I}_{c-pre} \end{bmatrix} - jX_C \begin{bmatrix} \overline{I}_{a-pre} \\ \overline{I}_{b-pre} \\ \overline{I}_{c-pre} \end{bmatrix} \quad (4.5)$$

where, Z_M is the mutual impedance between any two phases.

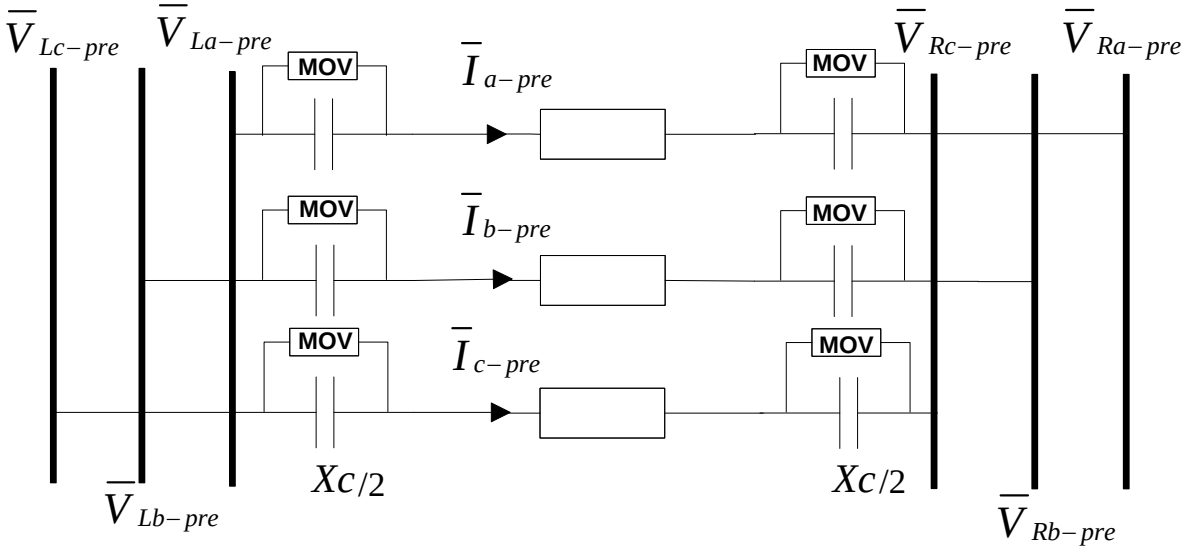

Figure 4.2: Series compensated line under pre-fault conditions

The positive sequence impedance of a transposed line (Z_1) is not an independent variable as it can be expressed in terms of the self and mutual impedances of the line as shown in (4.6) [130]. In the case of a series compensated line, the corresponding expression is shown in (4.7) and contains the series capacitor reactance (X_C).

$$Z_1 = Z_S - Z_M \tag{4.6}$$

$$Z_1 = Z_S - jX_C - Z_M \tag{4.7}$$

For simplicity, all derivations are carried out for a line compensated at both line-ends. Section 4.2.6 describes a method by which the derived expressions can be modified for other arrangements of series compensated lines. The equations for each arrangement are expressed as special cases of this arrangement.

4.2.1. Derivation of Distance to Fault - SLG Faults on Transposed Transmission Lines

Earlier in Section 4.2, the concept of using self and mutual impedances (phase network) to mathematically model the series compensated line was discussed. This section details the derivation of the expression for distance to fault for SLG faults on transposed lines using such a mathematical model. The derivation is divided into three major steps:

- Expression of effective positive sequence impedance
- Derivation of mutual impedance in terms of distance to fault
- Reduction of faulted phase equations into one equation of one variable - distance to fault

Each of these steps is discussed in detail as follows including the mathematical steps involved and their derivations:

A. Expression of the effective positive sequence impedance

The pre-fault line was shown in Figure 4.2. For transposed lines, the positive sequence impedance Z_1 can be calculated using the local and remote line-end voltages and the current through any given phase. This is shown in (4.8). It can be seen that it is calculated using known quantities, and thus Z_1 is not a variable but a calculated constant in this derivation.

$$Z_1 = Z_S - jX_C - Z_M = \frac{\overline{V}_{La-pre} - \overline{V}_{Ra-pre}}{\overline{I}_{a-pre}} \tag{4.8}$$

B. Derivation for Mutual Impedance in terms of 'l'

Figure 4.3 below shows the line under fault along with the reference directions of voltage and current phasors.

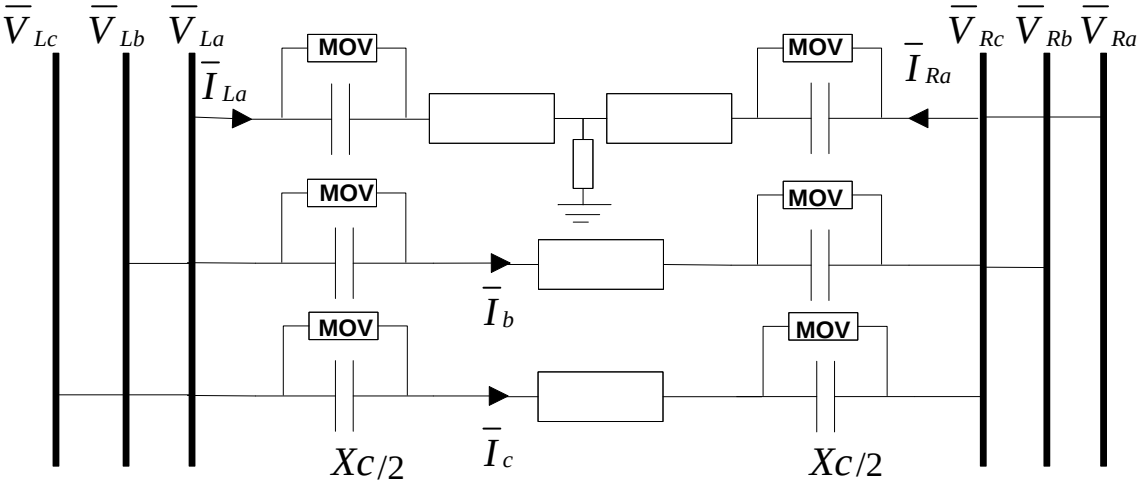

Figure 4.3: Series compensated line under SLG fault conditions

It is assumed here, that phase-a is faulted. In the event of a SLG fault on a single circuit line, it can be assumed that the magnitudes of the currents in the healthy phases are not sufficiently high to cause MOV conduction [149]. This is since the MOV is designed to have a considerably high margin above nominal load voltage level before it begins to operate. The voltage across the series capacitors of the healthy phases would therefore, also not exceed significantly. Thus, the MOVs for the healthy phases would not conduct any current, and the series compensation unit impedance for that phase would be purely constituted of the full reactance of the series capacitor. Thus, the equations for the healthy phases during fault are as follows:

$$\overline{V}_{Lb} - \overline{V}_{Rb} = (Z_S - jXc)\overline{I}_b + Z_M \overline{I}_c + Z_M (l(\overline{I}_{La} + \overline{I}_{Ra}) - \overline{I}_{Ra}) \tag{4.9}$$

$$\overline{V}_{Lc} - \overline{V}_{Rc} = (Z_S - jXc)\overline{I}_c + Z_M \overline{I}_b + Z_M (l(\overline{I}_{La} + \overline{I}_{Ra}) - \overline{I}_{Ra}) \tag{4.10}$$

where, $\overline{V}_{Lb}$ and $\overline{V}_{Lc}$ are the local line-end voltages of phases b and c respectively. $\overline{V}_{Rb}$ and $\overline{V}_{Rc}$ are the remote line-end voltages of phases b and c respectively. $\overline{I}_{La}$ and $\overline{I}_{Ra}$ are the local and remote line-end currents of phase a respectively. $\overline{I}_b$ and $\overline{I}_c$ are the currents flowing through phases b and c respectively. Adding (4.9) and (4.10) yields:

$$\bar{V}_{Lb} - \bar{V}_{Rb} + \bar{V}_{Lc} - \bar{V}_{Rc} = (Z_S - jXc - Z_M)(\bar{I}_b + \bar{I}_c) + 2Z_M(l(\bar{I}_{La} + \bar{I}_{Ra}) - \bar{I}_{Ra}) + 2Z_M(\bar{I}_b + \bar{I}_c) \quad (4.11)$$

Substituting for $Z_S - jX_C - Z_M$ from (4.8) and re-arranging the equation gives the following expression for Z_M in terms of l:

$$Z_M = \frac{(1/2)(\bar{V}_{Lb} - \bar{V}_{Rb} + \bar{V}_{Lc} - \bar{V}_{Rc} - (\frac{\bar{V}_{La-pre} - \bar{V}_{Ra-pre}}{\bar{I}_{La-pre}})(\bar{I}_b + \bar{I}_c))}{l(\bar{I}_{La} + \bar{I}_{Ra}) - \bar{I}_{Ra} + \bar{I}_b + \bar{I}_c} \quad (4.12)$$

Using the above expression, the imaginary and real components of the mutual impedance can be expressed as shown below:

$$\mathrm{Im}\, Z_M = \frac{l.m_{11} + m_{12}}{l^2.m_{15} + l.m_{16} + m_{17}} \quad (4.13)$$

$$\mathrm{Re}\, Z_M = \frac{l.m_{13} + m_{14}}{l^2.m_{15} + l.m_{16} + m_{17}} \quad (4.14)$$

The terms $m_{11}, m_{12}, m_{13}, m_{14}, m_{15}, m_{16}$ and m_{17} have been defined in Table 4.1 towards the end of this section.

C. Reduction of faulted phase equations

By considering the fault loops from each voltage source (local and remote line-ends of the faulted phase) to the ground through the fault resistance (*R*), the following equations for the faulted phase are obtained:

$$\bar{V}_{La} = lZ_S\bar{I}_{La} + Z_M l(\bar{I}_{Lb} + \bar{I}_{Lc}) + (Xc/2)SCa1 + R(\bar{I}_{La} + \bar{I}_{Ra}) \quad (4.15)$$

$$\bar{V}_{Ra} = (1-l)Z_S\bar{I}_{Ra} + Z_M(1-l)(\bar{I}_{Rb} + \bar{I}_{Rc}) + (Xc/2)SCa2 + R(\bar{I}_{La} + \bar{I}_{Ra}) \quad (4.16)$$

Since the MOV operation affects the effective impedance of the series compensator unit, this has been taken into account by the definition of coefficients $SCa1$ and $SCa2$ above. The derivation of these coefficients is explained in Section 4.2.4. Equations (4.15) and (4.16) can be re-arranged into a more reducible set of equations by substituting Z_S as $Z_p + jX_C + Z_M$, as shown below:

$$\bar{V}_{La} = Z_P l\bar{I}_{La} + Z_M l(\bar{I}_{Lb} + \bar{I}_{Lc} + \bar{I}_{La}) + (Xc/2)(SCa1 + j2l\bar{I}_{La}) + R(\bar{I}_{La} + \bar{I}_{Ra}) \quad (4.17)$$

$$\bar{V}_{Ra} = Z_P(1-l)\bar{I}_{Ra} + Z_M(1-l)(\bar{I}_{Rb} + \bar{I}_{Rc} + \bar{I}_{Ra}) + (Xc/2)(SCa2 + j2(1-l)\bar{I}_{Ra}) + R(\bar{I}_{La} + \bar{I}_{Ra}) \quad (4.18)$$

Since the fault resistance is a real value, it can be eliminated by the following algebraic manipulation:

$$\mathrm{Im}\frac{\bar{V}_{La}}{\bar{I}_{La} + \bar{I}_{Ra}} = l\,\mathrm{Im}\frac{Z_P\bar{I}_{La}}{\bar{I}_{La} + \bar{I}_{Ra}} + l\,\mathrm{Im}\frac{Z_M(\bar{I}_{Lb} + \bar{I}_{Lc} + \bar{I}_{La})}{\bar{I}_{La} + \bar{I}_{Ra}} + Xc(\mathrm{Im}\frac{SCa1}{\bar{I}_{La} + \bar{I}_{Ra}} + l\,\mathrm{Im}\frac{j\bar{I}_{La}}{\bar{I}_{La} + \bar{I}_{Ra}}) \quad (4.19)$$

$$\mathrm{Im}\frac{\bar{V}_{Ra}}{\bar{I}_{La} + \bar{I}_{Ra}} = (1-l)\,\mathrm{Im}\frac{Z_P\bar{I}_{Ra}}{\bar{I}_{La} + \bar{I}_{Ra}} + (1-l)\,\mathrm{Im}\frac{Z_M(\bar{I}_{Lb} + \bar{I}_{Lc} + \bar{I}_{La})}{\bar{I}_{La} + \bar{I}_{Ra}} + Xc(\mathrm{Im}\frac{SCa2}{\bar{I}_{La} + \bar{I}_{Ra}} + (1-l)\,\mathrm{Im}\frac{j\bar{I}_{La}}{\bar{I}_{La} + \bar{I}_{Ra}}) \quad (4.20)$$

Here 'Im' refers to the imaginary component. It can be seen that the above equations comprise of voltage phasors, current phasors, and the terms Z_P, Z_M, Xc and l. Z_M is eliminated by substituting for $\mathrm{Im}\,Z_M$ and $\mathrm{Re}\,Z_M$ from (4.13) and (4.14). This results in two equations of two variables (Xc and l). Upon eliminating Xc the following equation is obtained:

$$l^4A + l^3B + l^2C + lD + E = 0 \quad (4.21)$$

It is a quartic equation of one variable, and thus there are four potential solutions. However, only the correct solution will provide acceptable values for Z_M and Xc and must lie between 0 and 1 and will thus be chosen as such. This is discussed in Section

4.2.6. The terms *A, B, C, D,* and *E* have been defined in Table 4.2, along with definitions of terms contained within each of them.

Table 4.1: Definition of constants for Section 4.2.1 ($m_{20} - E$)

	Definition
m_1	$\bar{I}_{La} + \bar{I}_{Ra}$
m_2	$\mathrm{Im}(\bar{V}_{La} / m_1)$
m_3	$\mathrm{Im}(Z_P \bar{I}_{La} / m_1)$
m_4	$\mathrm{Im}(SCa1 / m_1)$
m_5	$\mathrm{Im}(j\bar{I}_{La} / m_1)$
m_6	$\mathrm{Im}((\bar{I}_{Lb} + \bar{I}_{Lc} + \bar{I}_{La}) / m_1)$
m_7	$0.5(\bar{V}_{Lb} - \bar{V}_{Rb} + \bar{V}_{Lc} - \bar{V}_{Rc} - (Z_S - jXc - Z_M)(\bar{I}_b + \bar{I}_c))$
m_8	$-\bar{I}_{Ra} + \bar{I}_b + \bar{I}_c$
m_9	m_1 / m_7
m_{10}	m_8 / m_7
m_{11}	$-\mathrm{Im}(m_9)$
m_{12}	$-\mathrm{Im}(m_{10})$
m_{13}	$\mathrm{Re}(m_9)$
m_{14}	$\mathrm{Re}(m_{10})$
m_{15}	$\lvert m_9 \rvert^2$
m_{16}	$2\,\mathrm{Re}(m_9 . m_{10}')$
m_{17}	$\lvert m_{10} \rvert^2$
m_{18}	$m_{11}.\mathrm{Re}(m_6) + m_{13}.\mathrm{Im}(m_6)$
m_{19}	$m_{12}.\mathrm{Re}(m_6) + m_{14}.\mathrm{Im}(m_6)$
m_{20}	$-m_3 m_{15}$

Table 4.2: Definition of constants for Section 4.2.1 ($m_{21} - E$)

	Definition
m_{21}	$-m_3 m_{16} + m_{15} m_2$
m_{22}	$-m_3 m_{17} + m_{16} m_2$
m_{23}	$m_{22} - m_{19}$
m_{24}	$m_{21} - m_{18}$
m_{25}	$m_{17} m_2$
m_{26}	$\mathrm{Im}(\bar{V}_{Ra} / m_1)$
m_{27}	$\mathrm{Im}(Z_P \bar{I}_{Ra} / m_1)$

m_{28}	$\mathrm{Im}(SCa2/m_1)$
m_{29}	$\mathrm{Im}(j\bar{I}_{Ra}/m_1)$
m_{30}	$\mathrm{Im}((\bar{I}_{Rb}+\bar{I}_{Rc}+\bar{I}_{Ra})/m_1)$
m_{34}	$m_{27}m_{16}+m_{15}(m_{26}-m_{27})$
m_{35}	$m_{27}m_{17}+m_{16}(m_{26}-m_{27})$
m_{36}	$m_{17}(m_{26}-m_{27})-m_{32}$
m_{38}	$m_{35}-(m_{31}-m_{32})$
A	$m_{27}m_{15}m_5+m_{20}m_{29}$
B	$(m_{34}+m_{31})m_5+m_{24}m_{29}+m_{27}m_{15}m_4-m_{20}(m_{28}+m_{29})$
C	$m_{38}m_5+m_{23}m_{29}+(m_{34}+m_{31})m_4-m_{24}(m_{28}+m_{29})$
D	$m_{36}m_5+m_{25}m_{29}+m_{38}m_4-m_{23}(m_{28}+m_{29})$
E	$m_{36}m_4+m_{25}m_{28}+m_{25}m_{29}$

4.2.2. Derivation of Distance to Fault - Symmetrical Faults on Transposed Transmission Lines

The algorithm for such faults is presented as follows. The effective positive sequence impedance (including the series compensation) of the circuit holds the following mathematical relationship to the positive sequence impedance of the transmission line (Z_{1-line}).

$$Z_1 = Z_{1-line} - jXc \tag{4.22}$$

Z_1 can be calculated directly using the pre-fault measurements as shown in (4.8). Given the fact that for a symmetrical fault on a transposed line, the fault is effectively a solid earth (this is since the total fault current through the fault resistance is equal to zero, meaning that there is no voltage drop between the fault point and the earth), the voltage drop across any section of any of the phases (here phase-a) can be expressed as a sum of the voltage drops across the line and the series capacitor as shown below.

$$\bar{V}_{La} = lZ_{1-line}\bar{I}_{La} + (Xc/2)SCa1 \tag{4.23}$$

$$\overline{V}_{Ra} = (1-l)Z_{1-line}\overline{I}_{Ra} + (Xc/2)SCa2 \tag{4.24}$$

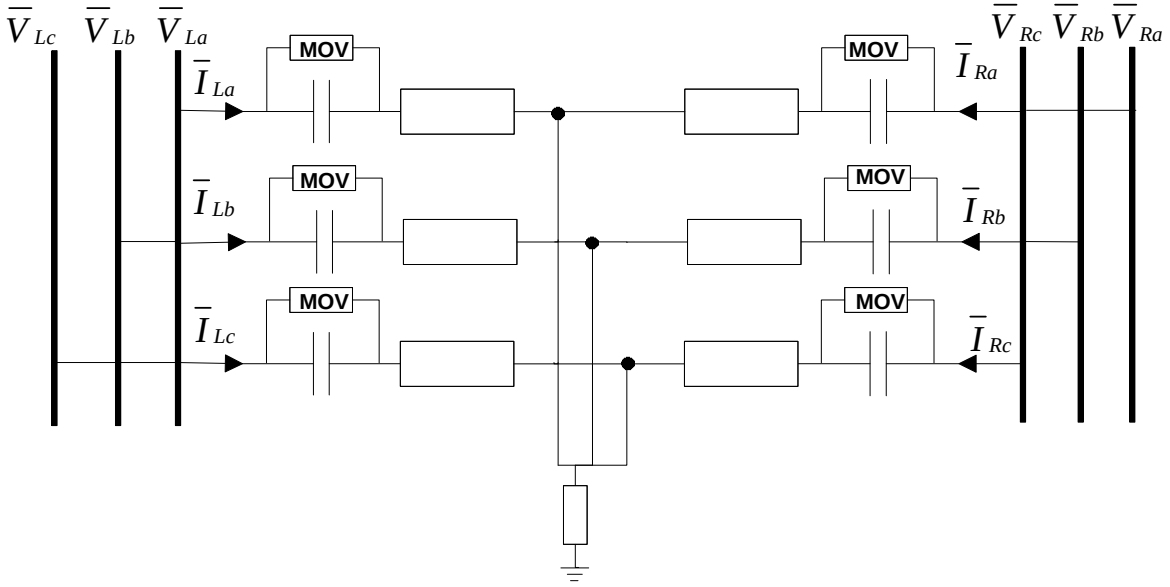

Figure 4.4: Series compensated line under symmetrical 3-phase fault

All currents, voltages and constants $SCa1$ and $SCa2$ have been introduced previously, and are also described in Section 4.2.4. These constants allow simpler derivations of distance to fault as well as adding to the ease of implementation. The constants are also useful as they allow for the derivation of a single expression for the distance to fault regardless of the location of the series capacitor on the line. Rearranging (4.23) and (4.24), the following equations are obtained:

$$\frac{\overline{V}_{La}}{\overline{I}_{La}} = lZ_{1-line} + \frac{(Xc/2)SCa1}{\overline{I}_{La}} \tag{4.25}$$

$$\frac{\overline{V}_{Ra}}{\overline{I}_{Ra}} = (1-l)Z_{1-line} + \frac{(Xc/2)SCa2}{\overline{I}_{Ra}} \tag{4.26}$$

$$\frac{\overline{V}_{La}}{\overline{I}_{La}} + \frac{\overline{V}_{Ra}}{\overline{I}_{Ra}} = Z_1 + jXc + (Xc/2)(\frac{SCa1}{\overline{I}_{La}} + \frac{SCa2}{\overline{I}_{Ra}}) \tag{4.27}$$

Thus, the series capacitor reactance, the positive sequence impedance of the line and the fault distance can be calculated as follows:

$$Xc = (\frac{\overline{V}_{La}}{\overline{I}_{La}} + \frac{\overline{V}_{Ra}}{\overline{I}_{Ra}} - Z_1) / (j + \frac{SCa1}{2\overline{I}_{La}} + \frac{SCa2}{2\overline{I}_{Ra}}) \tag{4.28}$$

$$Z_{1-line} = Z_1 + jXc \tag{4.29}$$

$$l = (\frac{\overline{V}_{La}}{\overline{I}_{La}} - \frac{(Xc/2)SCa1}{\overline{I}_{La}}) / Z_{1-line} \tag{4.30}$$

4.2.3. Derivation of Distance to Fault - All Other Fault Types

The method described in this section is applicable to all types of faults except symmetrical faults and SLG faults on transposed lines. That is to say this method covers all faults on untransposed lines, and it covers DL and DLG faults for transposed lines. It involves the solution of six nonlinear equations of six variables. The algorithm uses both pre-fault and fault measurement data.

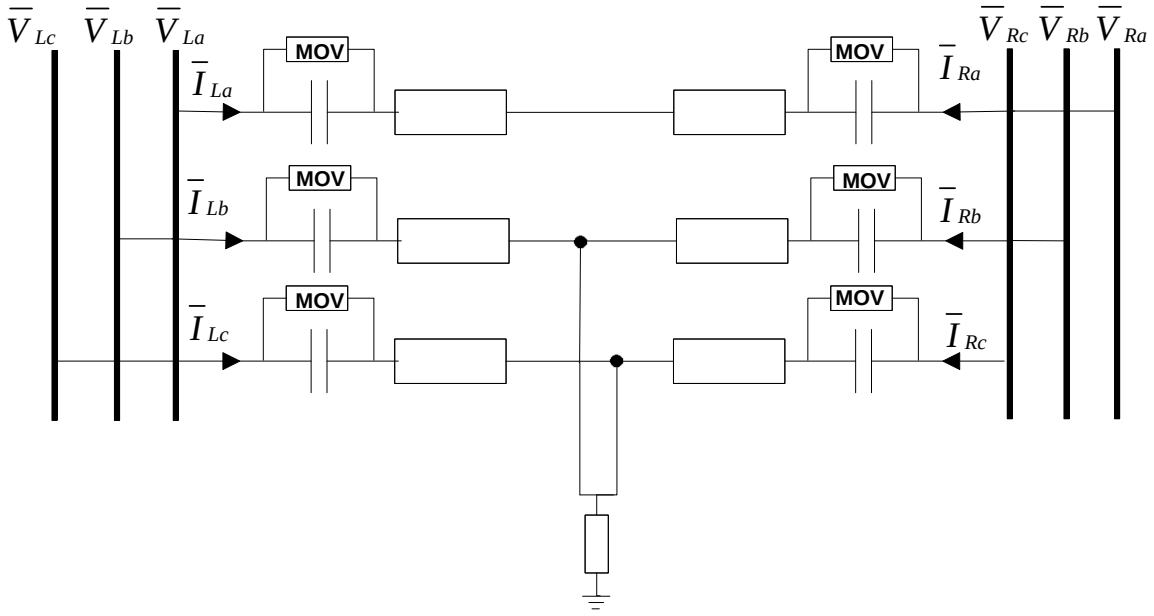

Figure 4.5: Series compensated line under a DLG fault

The equations express the total voltage difference between the terminals for each phase in terms of the phase currents. Figure 4.1 and Figure 4.5 show the pre-fault line and faulted line respectively for a line compensated at both ends of the line. The voltage and current phasors along with their conventional directions are also shown in the figures. Thus, the equations to be solved to calculate the distance to fault are as follows. Equations (4.31) - (4.33) apply to the pre-fault line while (4.34) - (4.36) apply to the faulted line. Z_{Mab}, Z_{Mac}, and Z_{Mbc} are the mutual impedances between pairs of phases a-b, a-c, and b-c respectively. Z_S is the self impedance of the line, X_C is the series capacitor reactance and l is the distance to fault expressed as a fraction of the total line length. Given that all voltage and current phasors are known quantities, the above mentioned variables constitute the six unknowns to be solved in order to calculate the distance to fault. The terms S_a, S_b and S_c are complex constants similar to *SCa*1 and *SCa*2 calculated using the method described in Section 4.2.4.

$$\bar{V}_{La-pre} - \bar{V}_{Ra-pre} = (Z_S - jX_C)\bar{I}_{pre-a} + Z_{Mab}\bar{I}_{pre-b} + Z_{Mac}\bar{I}_{pre-c} \quad (4.31)$$

$$\bar{V}_{Lb-pre} - \bar{V}_{Rb-pre} = (Z_S - jX_C)\bar{I}_{pre-b} + Z_{Mab}\bar{I}_{pre-a} + Z_{Mbc}\bar{I}_{pre-c} \quad (4.32)$$

$$\bar{V}_{Lc-pre} - \bar{V}_{Rc-pre} = (Z_S - jX_C)\bar{I}_{pre-c} + Z_{Mac}\bar{I}_{pre-a} + Z_{Mbc}\bar{I}_{pre-b} \quad (4.33)$$

$$\bar{V}_{La} - \bar{V}_{Ra} = Z_S(l\bar{I}_{La} - (1-l)\bar{I}_{Ra}) + X_C S_a + Z_{Mab}(l\bar{I}_{Lb} - (1-l)\bar{I}_{Rb}) + Z_{Mac}(l\bar{I}_{Lc} - (1-l)\bar{I}_{Rc}) \quad (4.34)$$

$$\bar{V}_{Lb} - \bar{V}_{Rb} = Z_S(l\bar{I}_{Lb} - (1-l)\bar{I}_{Rb}) + X_C S_b + Z_{Mab}(l\bar{I}_{La} - (1-l)\bar{I}_{Ra}) + Z_{Mbc}(l\bar{I}_{Lc} - (1-l)\bar{I}_{Rc}) \quad (4.35)$$

$$\bar{V}_{Lc} - \bar{V}_{Rc} = Z_S(l\bar{I}_{Lc} - (1-l)\bar{I}_{Rc}) + X_C S_c + Z_{Mbc}(l\bar{I}_{Lb} - (1-l)\bar{I}_{Rb}) + Z_{Mac}(l\bar{I}_{La} - (1-l)\bar{I}_{Ra}) \quad (4.36)$$

In order to calculate the distance to fault, the problem needs to be expressed in terms of a new variable set: [Z_{Mab} , Z_{Mac} , Z_{Mbc} , Z , X_C , l], where $Z = Z_S - jX_C$. In other words, Z_S is replaced with the new variable Z. Thus, (4.31)-(4.33) can be expressed as (4.37)-(4.39).

$$\bar{V}_{La-pre} - \bar{V}_{Ra-pre} = Z\bar{I}_{pre-a} + Z_{Mab}\bar{I}_{pre-b} + Z_{Mac}\bar{I}_{pre-c} \quad (4.37)$$

$$\bar{V}_{Lb-pre} - \bar{V}_{Rb-pre} = Z\bar{I}_{pre-b} + Z_{Mab}\bar{I}_{pre-a} + Z_{Mbc}\bar{I}_{pre-c} \quad (4.38)$$

$$\bar{V}_{Lc-pre} - \bar{V}_{Rc-pre} = Z\bar{I}_{pre-c} + Z_{Mac}\bar{I}_{pre-a} + Z_{Mbc}\bar{I}_{pre-b} \quad (4.39)$$

The above can be expressed in matrix form as shown below:

$$\begin{bmatrix} \bar{V}_{La-pre} - \bar{V}_{Ra-pre} - Z\bar{I}_{pre-a} \\ \bar{V}_{Lb-pre} - \bar{V}_{Rb-pre} - Z\bar{I}_{pre-b} \\ \bar{V}_{Lc-pre} - \bar{V}_{Rc-pre} - Z\bar{I}_{pre-c} \end{bmatrix} = W \begin{bmatrix} Z_{Mab} \\ Z_{Mac} \\ Z_{Mbc} \end{bmatrix} \quad (4.40)$$

where,

$$W = \begin{bmatrix} \bar{I}_{pre-b} & \bar{I}_{pre-c} & 0 \\ \bar{I}_{pre-a} & 0 & \bar{I}_{pre-c} \\ 0 & \bar{I}_{pre-a} & \bar{I}_{pre-b} \end{bmatrix} \tag{4.41}$$

Using the above equations the mutual impedance variables can be expressed in terms of Z as follows:

$$\begin{bmatrix} Z_{Mab} \\ Z_{Mac} \\ Z_{Mbc} \end{bmatrix} = \begin{bmatrix} p + qZ \\ r + sZ \\ t + uZ \end{bmatrix} \tag{4.42}$$

where,

$$\begin{bmatrix} p \\ r \\ t \end{bmatrix} = W^{-1} \begin{bmatrix} \bar{V}_{La-pre} - \bar{V}_{Ra-pre} \\ \bar{V}_{Lb-pre} - \bar{V}_{Rb-pre} \\ \bar{V}_{Lc-pre} - \bar{V}_{Rc-pre} \end{bmatrix} \tag{4.43}$$

$$\begin{bmatrix} q \\ s \\ u \end{bmatrix} = W^{-1} \begin{bmatrix} -\bar{I}_{pre-a} \\ -\bar{I}_{pre-b} \\ -\bar{I}_{pre-c} \end{bmatrix} \tag{4.44}$$

By substituting $Z_S = Z + jX_C$, and the expressions for Z_{Mab}, Z_{Mbc} and Z_{Mac} from (4.42) into (4.34)-(4.36), they are expressed together in matrix form as seen in (4.45). Carrying out a simple matrix inversion yields (4.46).

$$\begin{bmatrix} \bar{V}_{La}-\bar{V}_{Ra}+p\bar{I}_{Rb}+r\bar{I}_{Rc} \\ \bar{V}_{Lb}-\bar{V}_{Rb}+p\bar{I}_{Ra}+t\bar{I}_{Rc} \\ \bar{V}_{Lc}-\bar{V}_{Rc}+r\bar{I}_{Ra}+t\bar{I}_{Rb} \end{bmatrix} =$$

$$\begin{bmatrix} l\bar{I}_{La}-(1-l)\bar{I}_{Ra}+q(l\bar{I}_{Lb}-(1-l)\bar{I}_{Rb})+s(l\bar{I}_{Lc}-(1-l)\bar{I}_{Rc}) & S_a+j(l\bar{I}_{La}-(1-l)\bar{I}_{Ra}) & p(\bar{I}_{Lb}+\bar{I}_{Rb})+r(\bar{I}_{Lc}+\bar{I}_{Rc}) \\ l\bar{I}_{Lb}+(1-l)\bar{I}_{Rb}+q(l\bar{I}_{La}+(1-l)\bar{I}_{Ra})+u(l\bar{I}_{Lc}+(1-l)\bar{I}_{Rc}) & S_b+j(l\bar{I}_{Lb}+(1-l)\bar{I}_{Rb}) & p(\bar{I}_{La}+\bar{I}_{Ra})+t(\bar{I}_{Lc}+\bar{I}_{Rc}) \\ l\bar{I}_{Lc}+(1-l)\bar{I}_{Rc}+u(l\bar{I}_{Lb}+(1-l)\bar{I}_{Rb})+s(l\bar{I}_{La}+(1-l)\bar{I}_{Ra}) & S_c+j(l\bar{I}_{Lc}+(1-l)\bar{I}_{Rc}) & t(\bar{I}_{Lb}+\bar{I}_{Rb})+r(\bar{I}_{La}+\bar{I}_{Ra}) \end{bmatrix} \begin{bmatrix} Z \\ X_C \\ l \end{bmatrix} \quad (4.45)$$

$$\begin{bmatrix} Z \\ X_C \\ l \end{bmatrix} =$$

$$\begin{bmatrix} l\bar{I}_{La}-(1-l)\bar{I}_{Ra}+q(l\bar{I}_{Lb}-(1-l)\bar{I}_{Rb})+s(l\bar{I}_{Lc}-(1-l)\bar{I}_{Rc}) & S_a+j(l\bar{I}_{La}-(1-l)\bar{I}_{Ra}) & p(\bar{I}_{Lb}+\bar{I}_{Rb})+r(\bar{I}_{Lc}+\bar{I}_{Rc}) \\ l\bar{I}_{Lb}+(1-l)\bar{I}_{Rb}+q(l\bar{I}_{La}+(1-l)\bar{I}_{Ra})+u(l\bar{I}_{Lc}+(1-l)\bar{I}_{Rc}) & S_b+j(l\bar{I}_{Lb}+(1-l)\bar{I}_{Rb}) & p(\bar{I}_{La}+\bar{I}_{Ra})+t(\bar{I}_{Lc}+\bar{I}_{Rc}) \\ l\bar{I}_{Lc}+(1-l)\bar{I}_{Rc}+u(l\bar{I}_{Lb}+(1-l)\bar{I}_{Rb})+s(l\bar{I}_{La}+(1-l)\bar{I}_{Ra}) & S_c+j(l\bar{I}_{Lc}+(1-l)\bar{I}_{Rc}) & t(\bar{I}_{Lb}+\bar{I}_{Rb})+r(\bar{I}_{La}+\bar{I}_{Ra}) \end{bmatrix}^{-1} \quad (4.46)$$

$$\begin{bmatrix} \bar{V}_{La}-\bar{V}_{Ra}+p\bar{I}_{Rb}+r\bar{I}_{Rc} \\ \bar{V}_{Lb}-\bar{V}_{Rb}+p\bar{I}_{Ra}+t\bar{I}_{Rc} \\ \bar{V}_{Lc}-\bar{V}_{Rc}+r\bar{I}_{Ra}+t\bar{I}_{Rb} \end{bmatrix}$$

It can be noted that the left hand side comprises of three variables, Z, X_C and l, while the right hand side comprises of only one variable l. Expanding the matrix inverse seen in (4.46) and expanding the expression for l (last row of the matrix equation) gives a polynomial equation of order three. It is shown below in (4.47).

$$l^3 j_3 + l^2 j_2 + l j_1 + j_0 = 0 \quad (4.47)$$

The terms j_0, j_1, j_2 and j_3 have been defined in Table 4.3. Thus, there are three potential solutions for distance to fault, only one of which lies between 0-1 and yields reasonable estimates for the other variables Z_{Mab}, Z_{Mac}, Z_{Mbc}, Z and X_C and is thus chosen as the correct solution. This is discussed in Section 4.2.6.

Table 4.3: Definition of constants for Section 4.2.3

Term	Definition
k_1	$p(\bar{I}_{Lb}+\bar{I}_{Rb})+r(\bar{I}_{Lc}+\bar{I}_{Rc})$
k_2	$p(\bar{I}_{La}+\bar{I}_{Ra})+t(\bar{I}_{Lc}+\bar{I}_{Rc})$
k_3	$r(\bar{I}_{La}+\bar{I}_{Ra})+t(\bar{I}_{Lb}+\bar{I}_{Rb})$
k_7	$(\bar{I}_{La}+\bar{I}_{Ra})+q(\bar{I}_{Lb}+\bar{I}_{Rb})+s(\bar{I}_{Lc}+\bar{I}_{Rc})$
k_8	$q(\bar{I}_{La}+\bar{I}_{Ra})+(\bar{I}_{Lb}+\bar{I}_{Rb})+u(\bar{I}_{Lc}+\bar{I}_{Rc})$
k_9	$s(\bar{I}_{La}+\bar{I}_{Ra})+u(\bar{I}_{Lb}+\bar{I}_{Rb})+(\bar{I}_{Lc}+\bar{I}_{Rc})$
k_{10}	$-(\bar{I}_{Ra}+q\bar{I}_{Rb}+s\bar{I}_{Rc})$
k_{11}	$-(q\bar{I}_{Ra}+\bar{I}_{Rb}+u\bar{I}_{Rc})$
k_{12}	$-(s\bar{I}_{Ra}+u\bar{I}_{Rb}+\bar{I}_{Rc})$
k_{13}	$j(\bar{I}_{La}+\bar{I}_{Ra})$
k_{14}	$j(\bar{I}_{Lb}+\bar{I}_{Rb})$
k_{15}	$j(\bar{I}_{Lc}+\bar{I}_{Rc})$
k_{16}	$SCa-j\bar{I}_{La}$
k_{17}	$SCb-j\bar{I}_{Lb}$
k_{18}	$SCc-j\bar{I}_{Lc}$
k_{19}	$\bar{V}_{La}-\bar{V}_{Ra}+p\bar{I}_{Rb}+r\bar{I}_{Rc}$
k_{20}	$\bar{V}_{Lb}-\bar{V}_{Rb}+p\bar{I}_{Ra}+t\bar{I}_{Rc}$
k_{21}	$\bar{V}_{Lc}-\bar{V}_{Rc}+r\bar{I}_{Ra}+t\bar{I}_{Rb}$
k_{22}	$k_{10}(k_{14}k_3-k_{15}k_2)+k_7(k_{17}k_3-k_{18}k_2)-k_{16}(k_8k_3-k_9k_2)-k_{13}(k_{11}k_3-k_{12}k_2)+k_{11}k_1k_{15}+k_8k_1k_{18}-k_{17}k_1k_9-k_{14}k_1k_{12}$
k_{23}	$k_{10}(k_{17}k_3-k_{18}k_2)-k_{16}(k_{11}k_3-k_{12}k_2)+k_{11}k_1k_{18}-k_{17}k_1k_{12}$
k_{24}	$k_{19}(k_8k_{15}-k_{14}k_9)+k_{20}(k_{13}k_9-k_7k_{15})+k_{21}(k_7k_{14}-k_{13}k_8)$
k_{25}	$k_{19}(k_{11}k_{15}+k_8k_{18}-k_{17}k_9-k_{14}k_{12})+k_{20}(k_{16}k_9+k_{13}k_{12}-k_{10}k_{15}-k_7k_{18})+k_{21}(k_{10}k_{14}+k_7k_{17}-k_{16}k_8-k_{13}k_{11})$
j_0	$-k_{19}(k_{11}k_{18}-k_{17}k_{12})-k_{20}(k_{16}k_{12}-k_{10}k_{18})-k_{21}(k_{10}k_{17}-k_{16}k_{11})$
j_1	$k_{22}-k_{24}$
j_2	$k_{23}-k_{25}$
j_3	$k_7(k_{14}k_3-k_{15}k_2)-k_{13}(k_8k_3-k_9k_2)+(k_8k_1k_{15})-(k_{14}k_1k_9)$

4.2.4. Calculation of SC-MOV Coefficients

The coefficients $SCa1$ and $SCa2$ in Section 4.2.1 and Section 4.2.2 are calculated using the method described here. S_a introduced in Section 4.2.3, is then calculated using $SCa1$

and $SCa2$. S_b and S_c are calculated similarly. This is carried out as follows. The Goldsworthy linearised model reduction of an SC-MOV combination into a series resistance and series reactance was previously introduced in Chapter 3. Here, they are expressed for a line compensated at both line-ends. Two new functions $f(i_{pu})$ and $g(i_{pu})$ are also defined here.

$$R_C = X_{C0}(0.0745 + 0.49e\wedge(-0.243i_{pu}) - 35e\wedge(-5i_{pu}) - 0.6e\wedge(-1.4i_{pu})) \quad (4.48)$$

$$X_C = X_{C0}(0.1010 + 0.005749i_{pu} + 2.088e\wedge(-0.8566i_{pu})) \quad (4.49)$$

$$Z_{SC-MOV} = (X_C / 2)(f(i_{pu}) + jg(i_{pu})) \quad (4.50)$$

Expressions for $SCa1$ and $SCa2$ for each case are shown below.

1. If the line is compensated at both line-ends:

$$SCa1 = i_{La}(f(i_{pu-La}) + jg(i_{pu-La})) \quad (4.51)$$

$$SCa2 = i_{Ra}(f(i_{pu-Ra}) + jg(i_{pu-Ra})) \quad (4.52)$$

2. If the line is compensated at local line-end only:

$$SCa1 = 2i_{La}(f(i_{pu-La}) + jg(i_{pu-La})) \quad (4.53)$$

$$SCa2 = 0 \quad (4.54)$$

3. If the line is compensated at remote line-end only:

$$SCa1 = 0 \quad (4.55)$$

$$SCa2 = 2i_{Ra}(f(i_{pu-Ra}) + jg(i_{pu-Ra})) \quad (4.56)$$

4. If the line is compensated at the middle) calculations for the 'remote line-end only' case and the 'local line-end only' case are both carried out. This leads to eight potential solutions for distance to fault (four each). Only the correct one will provide acceptable values for Z_{Mab}, Z_{Mac}, Z_{Mbc}, Z and X_C and lie between 0 and 1. $SCb1$ and $SCb2$ for phase-b and $SCc1$ and $SCc2$ for phase-c can be calculated using the same equations but with their respective phase currents. S_a is calculated as shown in (4.57). S_b and S_c are calculated similarly.

$$S_a = (SCa1 - SCa2)/2 \tag{4.57}$$

$$S_b = (SCb1 - SCb2)/2 \tag{4.58}$$

$$S_c = (SCc1 - SCc2)/2 \tag{4.59}$$

In Figure 4.6, the flowchart of the presented algorithm is shown. It summarises the working of the algorithm from receiving input measurements to outputting the distance to fault.

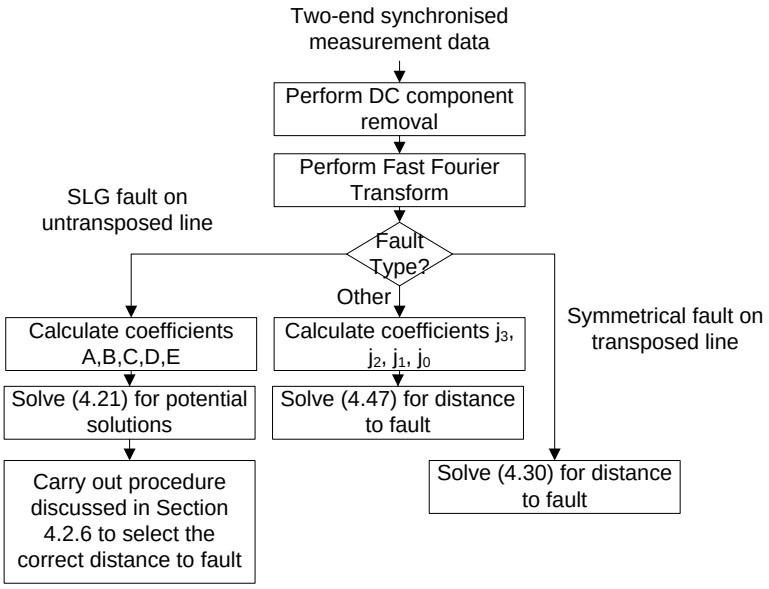

Figure 4.6: Algorithm flowchart

4.2.5. Algorithm using Unsynchronised Measurements

The algorithm presented so far assumes that the phasor measurements from both line-ends are time-synchronised. In the case where synchronisation is not available, the fault location can still be calculated using the mathematical expressions derived in the previous sections, after the synchronisation error has been detected and corrected for. For the case of symmetrical faults on transposed lines, the method in Section 4.2.2 is used without any requirement for correction of synchronization error. This can be explained as follows. If the local line-end measurements are used as reference for synchronization, (4.23) and (4.24) can be expressed as:

$$\overline{V}_{La} = lZ_{1-line}\overline{I}_{La} + (Xc/2)SCa1 \tag{4.60}$$

$$\overline{V}_{Ra}(e^{j\theta}) = (1-l)Z_{1-line}\overline{I}_{Ra}(e^{j\theta}) + (Xc/2)SCa2(e^{j\theta}) \tag{4.61}$$

where θ is the synchronisation error and $(e^{j\theta})$ is the correction factor for the remote line-end phasors. Dividing equation (4.61) by $(e^{j\theta})$ we obtain (4.62) which is identical to (4.24).

$$\overline{V}_{Ra} = (1-l)Z_{1-line}\overline{I}_{Ra} + (Xc/2)SCa2 \tag{4.62}$$

In other words, synchronisation error makes no difference to the starting equations of the derivations and hence, the equations that follow up to the derivation of distance to fault. Synchronisation error thus, has no effect on the distance to fault calculation for symmetrical faults. For asymmetrical faults, the healthy phases are used to detect and correct for the synchronization error. The assumption made here is that for the healthy phases, the sending end current is in phase with the receiving end current. While, this is not strictly true, and one can expect a phase difference between these currents due to the shunt admittance of the line, this phase difference is very small (<π/20). The effect of this method of synchronisation on the accuracy of the algorithm is discussed in Section 4.3.5.

4.2.6. Choice of Solution

The expression for distance to fault in the case of three phase symmetrical faults is a direct single solution equation. However, since (4.21) is a quartic (fourth-order) equation, there are 4 potential solutions in the case of SLG faults on transmission lines. Similarly, since (4.47) is a cubic equation, there are three potential solutions for other fault types. Thus, each of these potential solutions is required to be analysed until the correct solution is identified. The following conditions are used to filter out the correct solution from the list of potential solutions:

1. The distance to fault in this chapter is expressed as a fraction of the total line length. Thus the correct solution must lie between 0-1.

$$0 < \mathrm{Re}(l) < 1 \tag{4.63}$$

2. The subsequently calculated value of X_C corresponding to the correct solution for distance to fault must be very close to being purely a real value. Thus, the real component of X_C must be significantly greater than the imaginary component of X_C.

$$\mathrm{Re}(X_C) > \mathrm{Im}(X_C) \tag{4.64}$$

3. The effective pre-fault reactance between the two ends of the line is always inductive. In fact, the degree of series compensation is practically never over 80%, to avoid system instability (not covered in the scope of the project). Thus, the real component of X_C must also be lower than the imaginary component of the calculated value of Z_S. It is important to note that by definition X_C must be purely real as $(-jX_C)$ must be purely reactive but small errors in fault location lead to a negligible imaginary component of X_C.

$$0 < \mathrm{Re}(X_C) < \mathrm{Im}(Z_S) \tag{4.65}$$

4. Similarly, the imaginary components of the mutual impedances Z_{Mab}, Z_{Mac} and Z_{Mbc} are checked that they do not exceed the imaginary component of Z_S in the case of untransposed lines. The imaginary component of the mutual impedance Z_M must not exceed the imaginary component of Z_S. This condition can be shown to be true as being due to the fact that the positive sequence reactance of transmission lines ($= Z_S - Z_M$) is always inductive.

$$\mathrm{Im}(Z_{Mab}) < \mathrm{Im}(Z_S) \tag{4.66}$$

$$\mathrm{Im}(Z_{Mac}) < \mathrm{Im}(Z_S) \tag{4.67}$$

$$\mathrm{Im}(Z_{Mbc}) < \mathrm{Im}(Z_S) \tag{4.68}$$

$$\mathrm{Im}(Z_M) < \mathrm{Im}(Z_S) \tag{4.69}$$

4.2.7. Advantages of Novel FLA

Chapter 2 discussed the drawbacks of series compensated lines with respect to fault location and provided a literature review of implemented and previously proposed solutions. This section discusses the advantages of the novel solution proposed by the author in this chapter as discussed in previous sections. They are as follows:

- It is not affected by voltage inversion or current inversion: The FLA uses two-end voltage and current measurements. It is based on the mathematical relationship between the total voltage drop over the line length / fault loop and the phase currents. Thus, its accuracy is not affected by current inversion or voltage inversion at a given line terminal, as is the case with single-ended algorithms. This is because, despite a current inversion or a voltage inversion at one given line

terminal the voltage difference to phase currents mathematical relationships will still hold true and the FLA will accurately locate the fault.

- It makes accurate assumptions about the faulted line: The algorithm does not assume a purely inductive reactance across the length of the line as is the case with a number of other algorithms. It takes both the capacitive reactances and the inductive reactances into account, and does not assume a proportionally increasing net inductive reactance of the fault loop with increasing distance to fault. It accurately takes the MOV operation into account, and therefore the altered electrical behaviour of the series compensation unit as a whole. Thus, it does not incorrectly estimate the distance to fault as is the case with a number of other algorithms.

- It is not affected by fault resistance. For SLG faults, the fault resistance is taken into account to describe the system mathematically, and algebraically eliminated. For other fault types, the voltage difference between the two ends of the line is used and thus the fault resistance is effectively eliminated.

- Applicability of the algorithm: It is capable of locating various types of faults, for various different locations of SC installations on the line. It is capable of locating faults for lines of various degrees of series compensation, and is accurate even in the case of traditional uncompensated lines (this is validated in the results to be shown in sections to follow). In cases where the series compensation is at one or both ends of the line, the algorithm can be applied regardless of whether the VT is on the line side or the bus side of the series capacitor

- It does not require synchronisation of measurements: It is capable of locating faults with synchronous phasors as well as with asynchronous phasors.

- It is unaffected by source impedances: The algorithm is not affected by impedances outside the transmission system contained between the local and remote line-end busses. Thus, no settings for source impedances are required for the algorithm calculations.

- It is line parameter free: Such FLAs developed for uncompensated lines have been tested for series compensated lines in the past and found to not be sufficiently accurate as they do not take the electrical behaviour the series compensation unit under fault into account. The algorithm described in this chapter is an original line parameter free accurate FLA designed for series compensated lines. The FLA is an original contribution of the author.

4.3. Simulations and Algorithm Validation

Test results described in this section are based on measurement data obtained from ATP-EMTP simulations. Figure 4.7 shows an example of such a test circuit in ATP-EMTP used to validate the new FLA. It comprises of a 100km 400kV series compensated overhead transmission line. The LCC line modelling block of ATP-EMTP is used to model a J-Marti line. The line parameters and source impedance parameters are listed in Table 4.4. The transmission network used in [129] was made available by the authors for use of this project. The transmission parameters used here are therefore identical. The series capacitor reactance and MOV parameters can be adjusted to simulate a line compensated to a given degree of compensation. Sampled measurements of currents and voltages were obtained using these simulations. These were then converted to phasors in MATLAB using the Fast Fourier Transform (FFT), and subsequently processed to calculate the distance to fault.

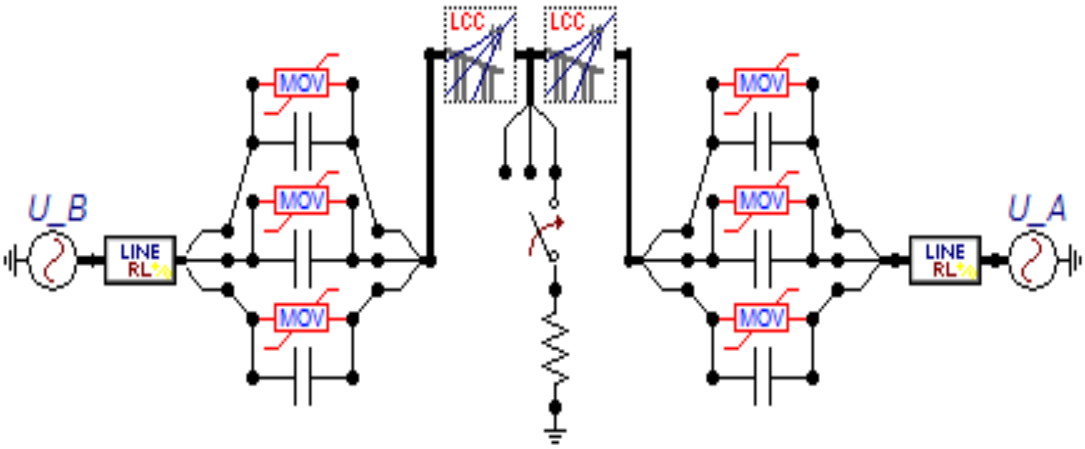

Figure 4.7: Test circuit for series compensated lines

The fault was simulated at 43 ms in each case. This was to allow for sufficient pre-fault and fault data required for the fault analysis. A sampling frequency of 6.4 kHz was used for the simulations, and the data was synchronously sampled. The data window size used for the FFT process to obtain the phasors was 20 ms. All errors presented in the results section are in accordance with IEEE standards [132] as shown below:

$$error(\%) = \frac{\text{calculated fault distance-actual fault distance}}{\text{total line length}} 100 = (l_{calculated} - l_{actual})100 \qquad (4.70)$$

Table 4.4: Network and Transmission Line Parameters

Network Parameters	Local Network A	Remote Network B
Line to Line RMS Voltage (kV)	416	400
Phase Angle (^{o})	0	-20
+ve seq. Resistance (Ω)	1.019	0.637
+ve seq. Inductance (H)	0.051	0.031
$Z_1 = R_1+jX_1$	1.019+j16	0.637+j10
X_1/R_1	15.7	15.7
0 seq. Resistance (Ω)	2.037	1.273
0 seq. Inductance (H)	0.102	0.064
$Z_0 = R_0+jX_0$	2.037+j32	1.273+j20
X_0/R_0	15.7	15.7
Fault MVA	45MVA	70MVA
Transmission Line Parameters	**Positive/Negative Sequence**	**Zero Sequence**
resistance, Ω/km	0.065	0.195
inductance mH/km	0.955	2.864
Capacitance nF/km	10.5	5
R Ω /km	0.065	0.195
X Ω /km	0.3	0.9
B S/km	$0.329x10^{-5}$	$0.157x10^{-5}$
X/R	4.615	4.615

4.3.1. Algorithm Accuracy for SLG Faults on Transposed Lines

An example simulation was carried out as follows. A SLG fault was simulated at 40 km from the local end of a line. A transposed J-Marti line was used with a total line length of 100 km. The line was compensated at both ends equally and at a degree of 30%. The fault resistance was chosen as 50 Ω. A high resistance fault was chosen as it is a common drawback of a number of FLAs that they are unable to accurately locate such faults (extensive tests for 0, 10 and 100Ω fault resistances have also been carried out and discussed later in this subsection). Waveforms for the local and remote line-end measurements are shown in Figure 4.8 and Figure 4.9 for currents and voltages respectively. They show the currents and voltages for both pre-fault and fault conditions used in the computation of the algorithm. The reference direction of current transformers both at local and remote ends is chosen such that a positive current is measured when it flows into the line (incoming). This explains the pre-fault phase currents at the local end being 180^{o} out of phase with the phase currents at the remote end.

The fault was simulated to occur at 0.043 sec, and the FFT data window size used was 20 ms. The calculation of distance to fault was carried out as per the method discussed in Section 4.2.1. The corresponding fault distance vs. time stamp plot is shown in Figure 4.10. The time stamp of the first sample used in the FFT of the measurements is plotted against the corresponding distance to fault calculated for those set of phasors. It can be seen that it only requires a short convergence period after which there is a steady distance to fault with minimal variation. An average of the values between 0.06s and 0.1s is used as the final distance to fault estimate. The calculated estimate of distance to fault was 0.3941 or 39.41 km. To thoroughly evaluate the accuracy of the algorithm, it is tested for a variety of fault resistances for both 50km and 100km transposed lines. The results have been tabulated in Table 4.5 for a 50 km line and in Table 4.6 for a 100 km line.

The high distortion in the voltage signal is owing to the travelling waves generated during the fault which introduces strong high frequencies into the voltage wave measured at the terminal [154]. The operation of the MOV also has a considerable impact on the travelling waves generated during fault. Although the high frequencies are considerably attenuated

by the resistance of the transmission line, fresh discontinuities are introduced for every time that the series capacitor is discharged [154]. Thus, such high frequencies are more persistent in a line containing capacitor banks [4], [155]. Lines of shorter length will experience greater high frequency content in the measured terminal voltage signals in comparison to lines of longer lengths [154]. However, given that the FLAs proposed in this thesis use an accurate FFT based method to extract the fundamental frequency signals, this does not have any significant impact on the accuracy of distance to fault calculation. Therefore, when considering the practical implementation of the algorithm, provided the sampling frequency for voltage measurement is as carried out in the tests discussed in this thesis (6.4 kHz), the higher frequencies in the voltage will not have any noticable impact on the accuracy of the FLA.

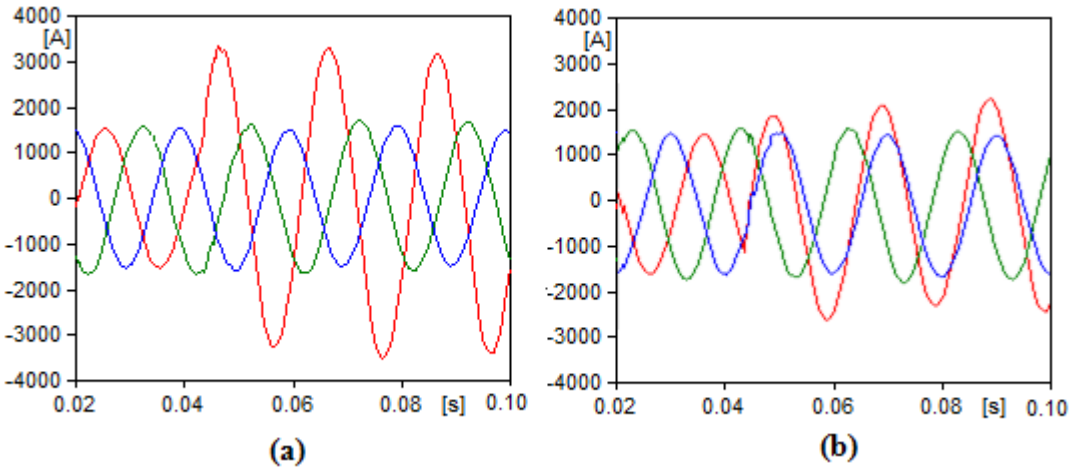

Figure 4.8: SLG fault on a transposed line: a) Local line-end currents b) Remote line-end currents

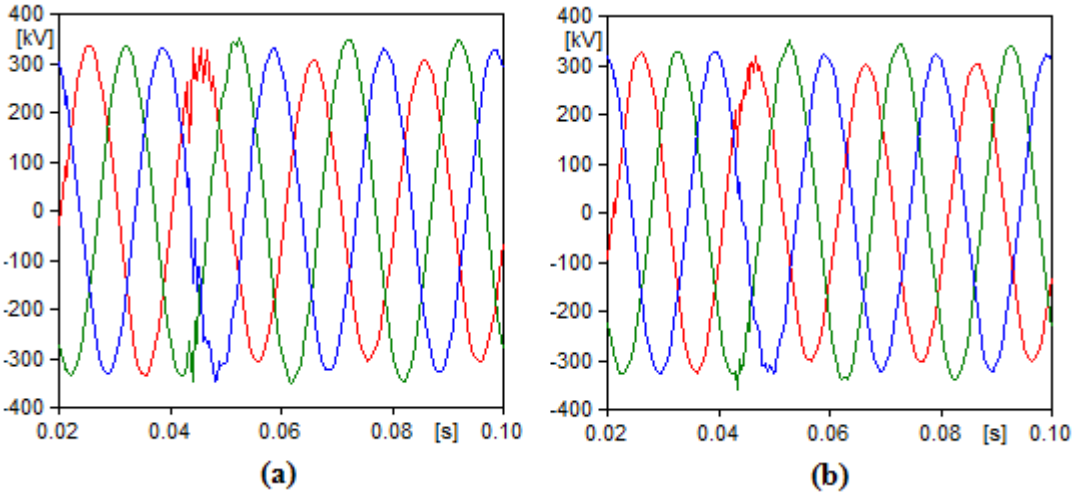

Figure 4.9: SLG fault on a transposed line: a) Local line-end voltages b) Remote line-end voltages

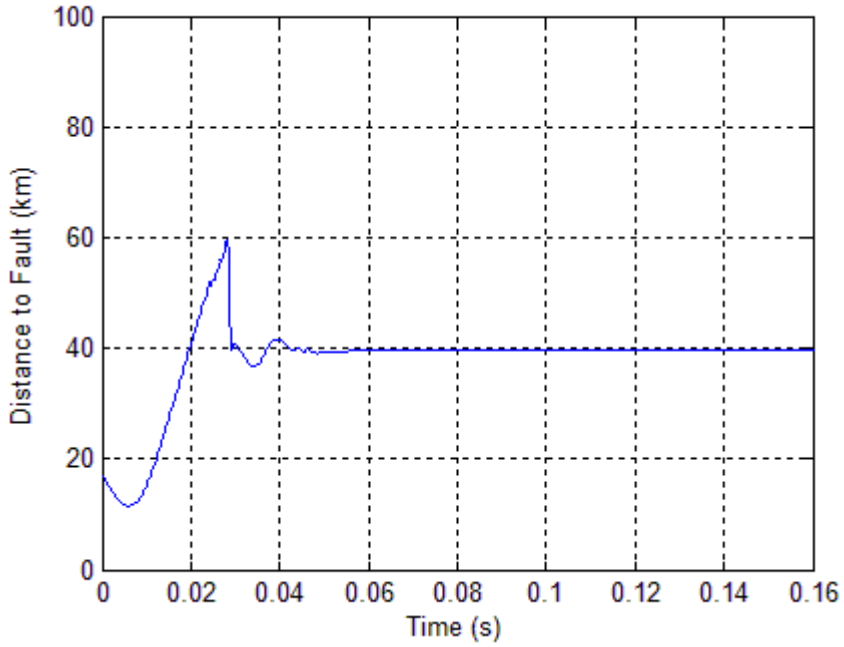

Figure 4.10: Fault Distance vs, Time Stamp for 'SLG fault on a transposed line'

Table 4.5: Sensitivity of algorithm for 'SLG faults on transposed lines' to fault resistance – 50 km line

Fault Type	Error of Estimated Fault Location(%)						
	Actual Fault Location (% of line length)						
	10	25	35	50	65	80	90
Line Length = 50km							
A-G $R_F = 0\Omega$	0.55	0.25	0.41	0.37	0.09	0.54	0.51
A-G $R_F = 1\Omega$	0.62	0.21	0.35	0.98	0.28	0.71	0.84
A-G $R_F = 10\Omega$	0.33	0.84	0.01	0.82	0.06	0.99	0.27
A-G $R_F = 100\Omega$	0.05	0.10	0.63	0.22	0.77	0.89	0.31

Table 4.6: Sensitivity of algorithm for 'SLG faults on transposed lines' to fault resistance – 100 km line

Fault Type	Error of Estimated Fault Location(%)						
	Actual Fault Location (% of line length)						
	10	25	35	50	65	80	90
Line Length = 100km							
A-G $R_F = 0\Omega$	0.23	0.18	0.33	0.09	0.21	0.16	0.13
A-G $R_F = 1\Omega$	0.81	0.72	0.69	0.41	0.25	0.47	0.32
A-G $R_F = 10\Omega$	0.31	0.12	0.28	0.11	0.37	0.21	0.08
A-G $R_F = 100\Omega$	0.17	0.03	0.13	0.62	0.86	0.44	0.15

4.3.2. Algorithm Accuracy for Symmetrical Faults on Transposed Lines

A solid earth three-phase symmetrical fault was simulated at 40 km from the local line-end of a 100km untransposed J-Marti line in ATP-EMTP. Once again, the line was

compensated at both ends equally at a degree of series compensation of 30%. The corresponding current and voltage waveforms over sufficient periods of pre-fault and fault conditions are shown in Figure 4.11 and Figure 4.12. It must be emphasised that the reference direction of current transformers both at local and remote ends is chosen such that a positive current is measured when it flows into the line (incoming). The fault inception time was set at 43 ms, and the FFT data window size used was 20 ms. The expression for distance to fault shown previously in (4.30) was used by the algorithm to determine the fault location. The calculated value of distance to fault was 0.4072 or 40.72 km. The fault distance vs. Time stamp plot is similarly shown in Figure 4.13.

This test was repeated for a variety of fault locations on a 50km line and a 100km line and for various fault resistances. The corresponding fault distance estimates have been tabulated in Table 4.7 for a 50 km line and in Table 4.8 for a 100 km line. The algorithm is found to be accurate in each case. It can be seen the fault location estimate does not change significantly on varying the fault resistance. This is explained as follows. In a symmetrical system, a three-phase to ground fault on a transposed line would lead to phase currents during fault being equal in magnitude and balanced, such that the total current is equal to zero. So although there is a contribution from each phase the vector sum is zero. Therefore, voltage drop across a 100Ω fault resistance and a 10Ω fault resistance for such a case is the same (this voltage magnitude = IR = 0). The errors presented are according to with (4.70). Although high resistance faults rarely occur on a power line, they are shown to demonstrate the accuracy of the algorithm for various possible fault conditions.

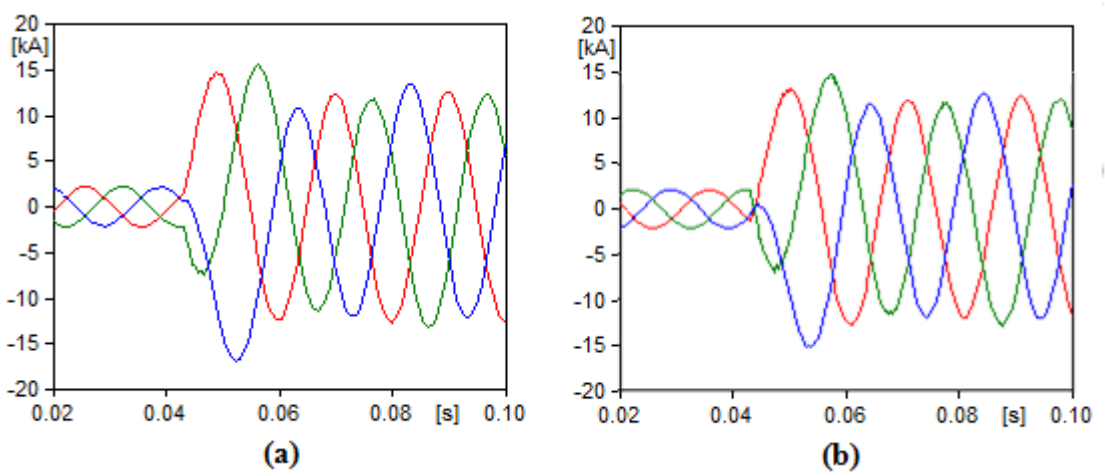

Figure 4.11: Symmetrical fault on a transposed line: a) Local line-end currents b) Remote line-end currents

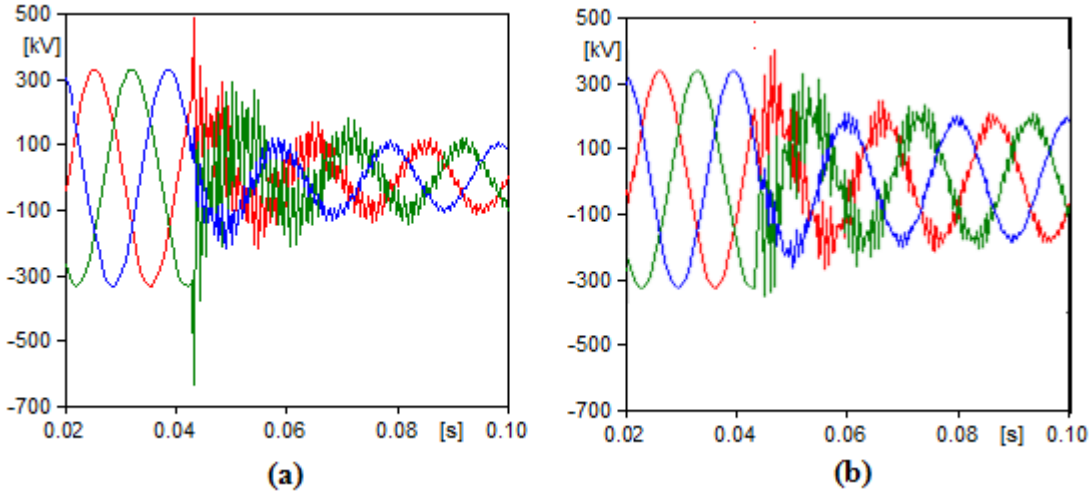

Figure 4.12: Symmetrical fault on a transposed line: a) Local line-end voltages b) Remote line-end voltages

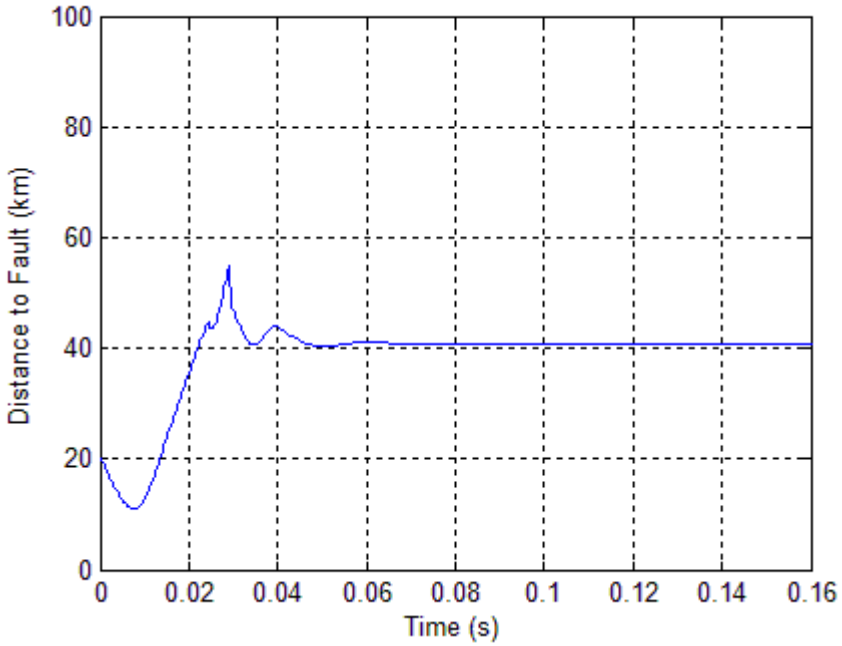

Figure 4.13: Fault distance vs. time stamp for 'symmetrical fault on a transposed line'

Table 4.7: Sensitivity of algorithm for 'symmetrical faults on transposed lines' to fault resistance

Fault Type	Error of Estimated Fault Location(%)						
	Actual Fault Location (% of line length)						
	10	25	35	50	65	80	90
	Line Length = 50km						
ABC-G $R_F = 0\Omega$	0.32	0.89	0.08	0.47	0.48	0.45	0.86
ABC-G $R_F = 1\Omega$	0.32	0.89	0.08	0.47	0.48	0.45	0.86
ABC-G $R_F = 10\Omega$	0.31	0.86	0.08	0.46	0.48	0.45	0.85
ABC-G $R_F = 100\Omega$	0.32	0.89	0.08	0.47	0.48	0.43	0.86

\

Table 4.8: Sensitivity of algorithm for 'symmetrical faults on transposed lines' to fault resistance

Fault Type	Error of Estimated Fault Location(%)						
	Actual Fault Location (% of line length)						
	10	25	35	50	65	80	90
	Line Length =100km						
ABC-G $R_F = 0\Omega$	0.51	0.05	0.48	0.82	0.37	0.80	0.16
ABC-G $R_F = 1\Omega$	0.51	0.05	0.48	0.82	0.37	0.80	0.16
ABC-G $R_F = 10\Omega$	0.51	0.05	0.48	0.82	0.37	0.80	0.16
ABC-G $R_F = 100\Omega$	0.51	0.05	0.48	0.82	0.37	0.80	0.16

4.3.3. Algorithm Accuracy for Other Fault Types

An example simulation was carried out for a DLG fault with a fault resistance of 50Ω on an untransposed line. The line length, fault location, fault inception time, data window size for the FFT, series compensation arrangement and degree of series compensation simulated were identical to the example simulations described in the previous sections. The corresponding current and voltage waveforms are shown in Figure 4.14 and Figure 4.15. The reference directions for the current transformers at the local and remote ends are as discussed in Section 4.3.1. The fault distance vs. time stamp plot is shown in Figure 4.16. The calculated average (between 0.06s to 0.1s) distance to fault was 0.391677 equal to of 39.17 km. The algorithm has been tested for a variety of fault resistance, fault types, for the 50 km line and the 100 km line and the results have been tabulated in Table 4.9 and Table 4.10 respectively.

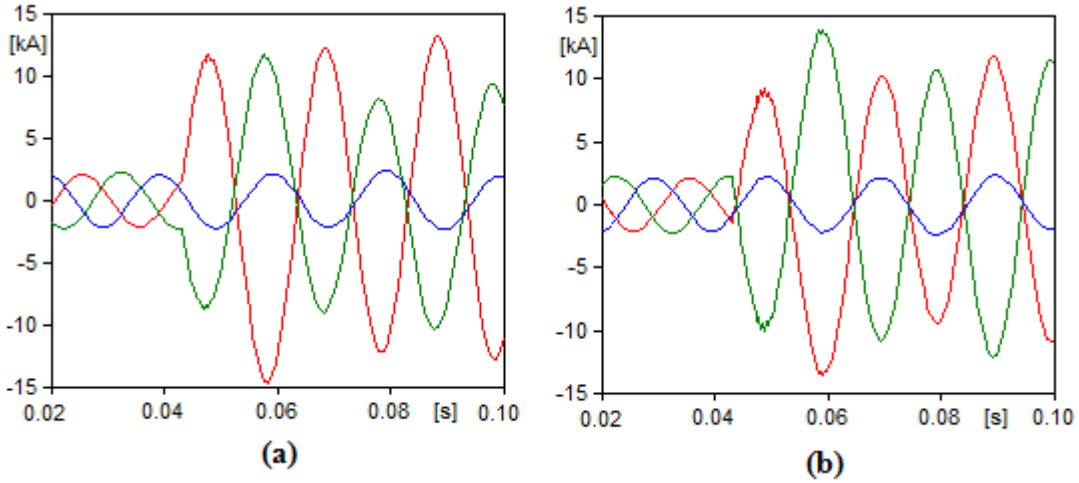

Figure 4.14: DLG fault: a) Local line-end currents b) Remote line-end currents

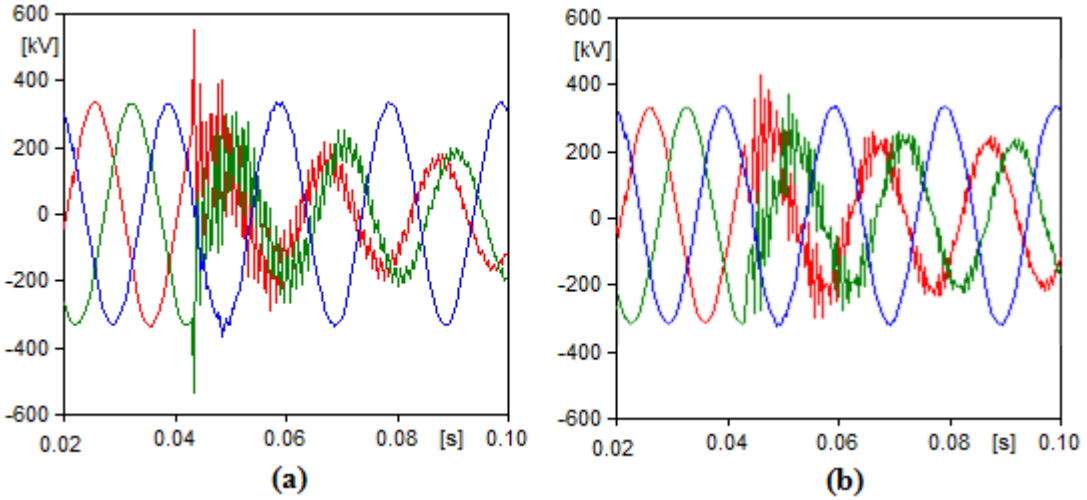

Figure 4.15: DLG fault: a) Local line-end voltages b) Remote line-end voltages

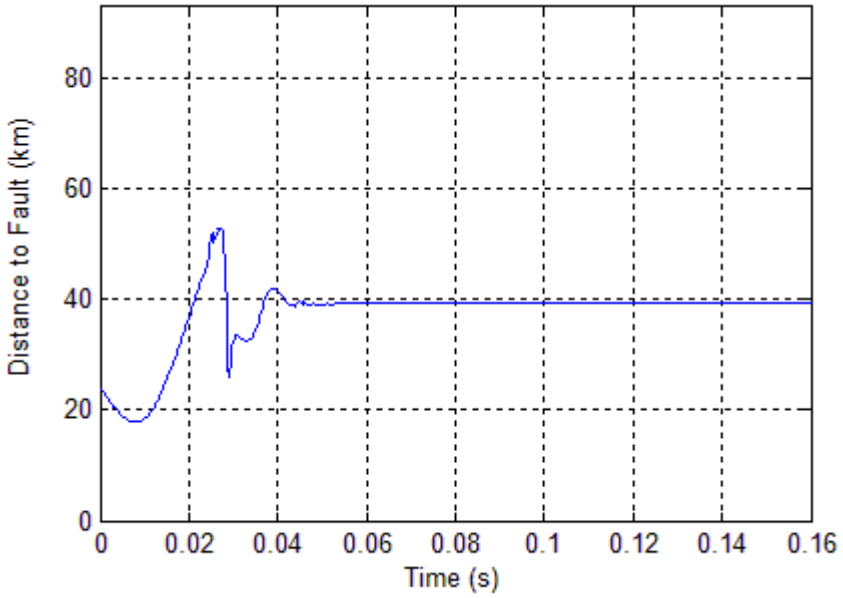

Figure 4.16: Fault distance vs. time stamp for 'other fault types'

Table 4.9: Sensitivity of algorithm for 'other fault types' to fault resistance -50km line

Fault Type	Error of Estimated Fault Location(%)						
	Actual Fault Location (% of line length)						
	10	25	35	50	65	80	90
	Line Length = 50km						
AB-G $R_F = 0\Omega$	0.74	0.38	0.99	0.63	0.09	0.28	0.30
AB-G $R_F = 1\Omega$	0.57	0.89	0.61	0.84	0.48	0.06	1.00
AB-G $R_F = 10\Omega$	0.41	0.61	0.66	0.03	0.45	0.88	0.51
AB-G $R_F = 100\Omega$	0.17	0.67	0.14	0.70	0.59	0.34	0.67
AB $R_F = 0\Omega$	0.13	0.01	0.49	0.59	0.26	0.34	0.63
AB $R_F = 1\Omega$	0.33	0.21	0.59	0.79	0.97	0.61	0.49
AB $R_F = 10\Omega$	0.17	0.78	0.32	0.20	0.73	0.36	0.31
AB $R_F = 100\Omega$	0.28	0.67	0.09	0.18	0.89	0.57	0.18

Table 4.10: Sensitivity of algorithm for 'other fault types' to fault resistance – 100 km line

Fault Type	Error of Estimated Fault Location(%)						
	Actual Fault Location (% of line length)						
	10	25	35	50	65	80	90
	Line Length =100km						
AB-G $R_F = 0\Omega$	0.07	0.02	0.45	0.41	0.38	0.13	0.03
AB-G $R_F = 1\Omega$	0.53	0.51	0.06	0.34	0.47	0.08	0.73
AB-G $R_F = 10\Omega$	0.41	0.37	0.36	0.21	0.03	0.637	0.13
AB-G $R_F = 100\Omega$	0.36	0.32	0.51	0.47	0.42	0.031	0.11
AB $R_F = 0\Omega$	0.78	0.4	0.53	0.073	0.35	0.66	0.34
AB $R_F = 1\Omega$	0.91	0.00	0.69	0.05	0.40	0.93	0.25
AB $R_F = 10\Omega$	0.18	0.59	0.19	0.36	0.27	0.55	0.29
AB $R_F = 100\Omega$	0.64	0.39	0.56	0.65	0.77	0.23	0.46

4.3.4. Algorithm Accuracy for Various Locations of Series Compensation

The use of general coefficients described in Section 4.2.5 allows the algorithm to locate faults for all main types of series compensated lines. Table 4.11 presents the errors in the fault distance estimates calculated upon varying the location of series compensation of the line. All the common cases have been considered i.e. series compensated at local line-end only, at remote line-end only, middle of the line and both ends of the line. In each case, various fault types (SLG, DLG, DL, 3-phase averaged) with fault resistances of 100Ω were simulated on a 100km line. The series compensation in each case was set to 30%. The fault distance was varied between 10% to 90% of the total line length. It can be seen that the algorithm performs accurately in each case.

Table 4.11: Sensitivity of algorithm to location of series compensation

Location of Ser.Comp.	Fault Resistance (Ω)	Actual Fault Location (% of line length)						
		Error of Estimated Fault Location(%)						
		10	25	35	50	65	80	90
Local Line-End Only	SLG	0.58	0.43	0.20	0.26	0.78	0.14	0.73
	DLG	0.19	0.80	0.29	0.79	0.11	0.23	0.85
	DL	0.23	0.74	0.07	0.54	0.38	0.16	0.24
	3-Phase	0.37	0.22	0.48	0.62	0.42	0.33	0.33
Remote Line-End Only	SLG	0.75	0.15	0.51	0.48	0.43	0.12	0.80
	DLG	0.07	0.55	0.74	0.50	0.24	0.23	0.14
	DL	0.28	0.58	0.47	0.53	0.03	0.66	0.34
	3-Phase	0.85	0.74	0.67	0.31	0.57	0.78	0.85
Middle of Line	SLG	0.55	0.29	0.17	0.32	0.59	0.39	0.08
	DLG	0.34	0.53	0.85	0.58	0.81	0.04	0.75
	DL	0.10	0.68	0.58	0.11	0.22	0.06	0.55
	3-Phase	0.83	0.74	0.28	0.64	0.44	0.74	0.27
Both Ends of Line	SLG	0.56	0.14	0.88	0.39	0.02	0.35	0.44
	DLG	0.07	0.09	0.81	0.01	0.63	0.43	0.16
	DL	0.37	0.14	0.63	0.35	0.24	0.78	0.87
	3-Phase	0.62	0.09	0.45	0.63	0.26	0.8	0.18

In the case where the line is compensated at one end, the VT may be on the line side or the bus side of the series capacitor as shown in Figure 4.17. If the VT is on the line side, the algorithm would treat the line as an uncompensated line as the voltage drops considered in the algorithm would not include the series capacitor. The results for this case are shown in Table 4.12.

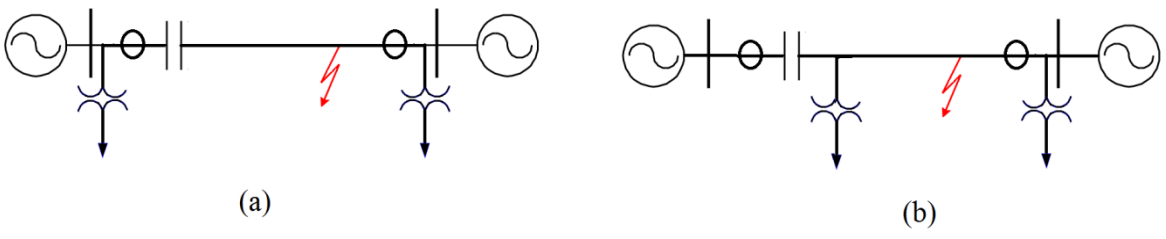

Figure 4.17: VT location a) bus side b) line side

Table 4.12: Sensitivity of algorithm to location of VT in relation to SC

Location of Ser.Comp.	Fault Type	Actual Fault Location (% of line length)						
		Error of Estimated Fault Location(%)						
		10	25	35	50	65	80	90
Local Line-End Only, VT on line side	SLG	0.21	0.68	0.06	0.86	0.86	0.80	0.49
	DLG	0.70	0.10	0.61	0.69	0.58	0.85	0.53
	DL	0.10	0.13	0.19	0.66	0.10	0.67	0.45
	3-Phase	0.69	0.17	0.15	0.13	0.07	0.87	0.58
Local Line-End Only, VT on bus side	SLG	0.58	0.43	0.20	0.26	0.78	0.14	0.73
	DLG	0.19	0.80	0.29	0.79	0.11	0.23	0.85
	DL	0.23	0.74	0.07	0.54	0.38	0.16	0.24
	3-Phase	0.37	0.22	0.48	0.62	0.42	0.33	0.33

4.3.5. Algorithm Accuracy for Asynchronous Measurements

All tests carried out so far assume that current and voltage phasors from the two terminals of the line are perfectly synchronised. While the algorithm is developed for systems where synchronised measurements are available, the method described in Section 4.2.5 can be used to synchronise asynchronous measurements to within a very small margin of synchronisation error. The algorithm for symmetrical faults does not require any synchronisation of measurements, and therefore it is not considered here. The algorithm for SLG faults, and the algorithm for other fault types were thoroughly tested for a variety of fault distances (10%-90%) and varying synchronisation errors (0-1000 μs). This was carried out by introducing a corresponding delay in the time stamp of the remote line-end phasors in MATLAB. In each case, a phase-phase fault with a fault resistance of 100 Ω was simulated. Series compensation is set at 40% and the line is compensated at both ends of the line. The algorithm was run for each case after the synchronisation error correction was carried out. The errors for each case have been tabulated in Table 4.13 and Table 4.14.

The expected estimates of fault location for each distance to fault shown in the row titled “without synchronisation error correction” are shown for the ideal case of where perfectly synchronised measurements are available. The rows titled “with synchronisation error

correction" tabulate the errors calculated after the correction procedure is carried out. It can be seen that the distance to fault errors are equal for each case despite an increase in synchronisation error. This is because regardless of the synchronisation error, the phase difference between the remote line-end phasors and local line-end phasors is always equal after the correction procedure, provided the procedure is carried out and the phasors are not assumed to be synchronised.

Table 4.13: Sensitivity of algorithm to synchronisation error (DLG faults)

Synchronisation Error (μs)	Actual Fault Location (% of line length)						
	Error of Estimated Fault Location(%)						
	10	25	35	50	65	80	90
Without synchronisation error correction							
0	0.57	0.44	0.03	0.15	0.60	0.20	0.08
With synchronisation error correction							
50	0.67	0.11	0.93	0.20	0.67	0.68	0.90
100	0.67	0.11	0.93	0.20	0.67	0.68	0.90
200	0.67	0.11	0.93	0.20	0.67	0.68	0.90
600	0.67	0.11	0.93	0.20	0.67	0.68	0.90
1000	0.67	0.11	0.93	0.20	0.67	0.68	0.90

Table 4.14: Sensitivity of algorithm to synchronisation error (SLG faults)

Synchronisation Error (μs)	Actual Fault Location (% of line length)						
	Error of Estimated Fault Location(%)						
	10	25	35	50	65	80	90
Without synchronisation error correction							
0	0.47	0.58	0.19	0.07	0.44	0.38	0.21
With synchronisation error correction							
50	0.30	0.18	0.43	0.79	0.72	0.27	0.57
100	0.30	0.18	0.43	0.79	0.72	0.27	0.57
200	0.30	0.18	0.43	0.79	0.72	0.27	0.57
600	0.30	0.18	0.43	0.79	0.72	0.27	0.57
1000	0.30	0.18	0.43	0.79	0.72	0.27	0.57

4.3.6. Algorithm Accuracy for Various Degrees of Series Compensation

Table 4.15 presents the errors in the fault distance estimates calculated upon varying the level of series compensation from 10% to 50%. The line is compensated at both ends of the line equally. In each case, a phase-phase fault with a fault resistance of 100 Ω was simulated. The fault distance was varied between 10% and 90% of the total line length. The algorithm has also been tested for traditional uncompensated lines, and was found to perform very accurately. This corresponds to the first entry in the table for (0% degree of compensation).

Table 4.15: Sensitivity of algorithm to degree of series compensation

Level of Series Compensation (%)	Actual Fault Location (% of line length)						
	Error of Estimated Fault Location(%)						
	10	25	35	50	65	80	90
0	0.43	0.28	0.87	0.65	0.75	0.25	0.29
10	0.84	0.11	0.54	0.76	0.42	0.02	0.24
20	0.22	0.43	0.61	0.73	0.76	0.56	0.39
30	0.64	0.39	0.56	0.65	0.77	0.23	0.46
40	0.58	0.49	0.39	0.55	0.89	0.29	0.22
50	0.86	0.61	0.46	0.05	0.29	0.84	0.72

4.3.7. Results for Transposed Lines

So far, the errors presented in the previous tables of results have been calculated for untransposed lines. This subsection investigates the effect of transposition of the line on the accuracy of the algorithm. In the case of transposed lines $Z_{Mab} = Z_{Mac} = Z_{Mbc}$. The distance to fault, the total line length, the FFT window size, fault inception time, level of series compensation simulated are identical to those in Section 4.3.3, but a transposed line is used instead. Table 4.16 shows the results. Once again, the fault distance, type and resistance were varied. It can be seen that the algorithm performs accurately for transposed lines.

Table 4.16: Sensitivity of algorithm to transposition of the line

Fault Type	Fault Resistance (Ω)	Actual Fault Location (% of line length)						
		Error of Estimated Fault Location(%)						
		10	25	35	50	65	80	90
ABG	0	0.28	0.14	0.52	0.57	0.22	0.10	0.46
	10	0.68	0.42	0.12	0.76	0.47	0.74	0.65
	100	0.55	0.04	0.08	0.77	0.69	0.13	0.82
AB	0	0.31	0.56	0.22	0.09	0.25	0.33	0.84
	10	0.82	0.48	0.52	0.06	0.22	0.35	0.65
	100	0.34	0.71	0.24	0.98	0.44	0.68	0.58

4.3.8. Results for Longer Lines

Shunt admittance is not accounted for in the equations used to derive the expressions for distance to fault. So far, the line lengths for which the tests have been carried out are for 50km and 100km lines. They are consistently found to be accurate. However, the shunt admittance currents are negligible for such lines. In this section, the algorithm is run for 300 km lines to validate the algorithm's accuracy for a system where the shunt admittance currents are significantly larger in magnitude. The tests carried out were repeated exactly as in the case of Section 4.3.6 in every respect with the exception of the system being a 300km long untransposed line.

It can be seen that the accuracy is worse than in the case of the 100km line. While the algorithm still performs to an acceptable level of accuracy, there is still considerable room for improvement. If shunt admittance is considered, the accuracy would be of a similar order to the 100km case. To do so without the use of line parameters, a more complex set of equations would have to be used. This is discussed further as potential future work in Chapter 8.

Table 4.17: Sensitivity of algorithm to increasing the length of the line (300km)

Location of Ser.Comp.	Fault Type	Actual Fault Location (% of line length)						
		Error of Estimated Fault Location(%)						
		10	25	35	50	65	80	90
Local Line-End Only	SLG	1.52	0.86	1.70	0.91	2.27	1.33	0.41
	DLG	1.35	0.71	0.88	1.16	1.52	0.77	0.91
	DL	1.00	0.65	1.46	1.12	1.34	0.32	1.65
	3-Phase	0.84	1.05	1.16	0.96	1.26	1.21	2.46
Remote Line-End Only	SLG	0.51	2.82	1.33	1.52	1.07	1.72	1.43
	DLG	1.02	1.00	1.02	1.69	1.84	1.75	1.12
	DL	1.09	1.41	0.94	1.28	0.80	2.27	1.92
	3-Phase	0.26	1.06	1.04	0.21	1.43	1.21	1.62
Middle of Line	SLG	1.02	1.49	1.92	1.29	0.97	1.29	1.21
	DLG	1.13	1.23	0.89	1.16	1.66	2.85	1.93
	DL	1.50	1.76	1.16	1.72	1.52	0.59	1.97
	3-Phase	0.78	0.67	0.87	1.49	1.17	1.41	1.72
Both Ends of Line	SLG	1.02	1.58	1.37	1.01	2.02	1.23	1.17
	DLG	1.25	1.32	1.91	0.69	1.60	1.34	0.13
	DL	0.91	1.00	1.86	1.79	1.67	1.79	1.23
	3-Phase	0.85	2.55	1.59	1.77	1.64	1.74	1.05

4.3.9. Results for Double-Circuit Lines

The algorithm considers mutual coupling between phases. However, it neglects the presence of any zero-sequence mutual coupling such as in the case of parallel lines. This subsection analyses the performance of the algorithm in the presence of a parallel circuit. Table 4.18 presents the errors in the fault distance estimates calculated upon running the algorithm using synchronised current and voltage measurements from both line ends of the faulted circuit. The range of distances to fault, levels of series compensation, fault resistances and fault types is as considered in Section 4.3.6. It can be seen that the inaccuracies are significantly high, and it can be said that the algorithm discussed in this chapter is not applicable to double-circuit lines. The results for 3-phase faults and DL

faults are found to be acceptable as the neglecting of the zero-sequence mutual coupling between circuits does not have any significant impact on the accuracy of the algorithms for such fault types. Zero-sequence mutual coupling effects become significant however, for the ground faults.

Table 4.18: Sensitivity of algorithm to the mutual coupling effect of a double circuit line

Location of Ser.Comp.	Fault Type	Actual Fault Location (% of line length)						
		Error of Estimated Fault Location(%)						
		10	25	35	50	65	80	90
Local End Only	SLG	7.45	5.67	14.64	2.83	1.07	6.59	11.42
	DLG	1.39	0.14	11.43	6.63	3.47	3.44	1.89
	DL	0.38	0.66	0.05	0.48	0.42	0.04	0.83
	3-Phase	0.59	0.15	0.70	0.80	0.55	0.33	0.87
Remote End Only	SLG	17.67	6.59	4.57	2.75	7.04	10.92	41.59
	DLG	33.60	15.69	4.37	11.84	1.86	6.35	2.01
	DL	0.70	0.54	0.00	0.62	0.73	0.58	0.91
	3-Phase	0.63	0.19	0.21	0.79	0.63	0.42	0.68
Middle of Line	SLG	21.24	16.35	0.90	11.95	73.45	1.67	10.85
	DLG	3.31	8.50	19.25	40.18	4.64	12.78	14.00
	DL	0.79	0.89	0.13	0.35	0.68	0.13	0.20
	3-Phase	0.15	0.30	0.30	0.34	0.23	0.02	0.64
Both Ends of Line	SLG	1.04	12.77	3.06	0.31	27.40	14.55	32.06
	DLG	1.77	23.23	11.44	1.46	2.50	1.75	11.20
	DL	0.37	0.78	0.13	0.45	0.70	0.67	0.88
	3-Phase	0.54	0.04	0.33	0.66	0.17	0.50	0.48

4.3.10. Algorithm Accuracy for Faults Close to Line Ends

A solid earth SLG fault was simulated at 1 km from the local line-end of the 100km untransposed J-Marti line in ATP-EMTP. The line was compensated at both ends equally at a degree of series compensation of 50%. The fault inception time was set at 43 ms, and the FFT data window size used was 20 ms. The corresponding current and voltage waveforms over sufficient periods are shown in Figure 4.18 and Figure 4.19 respectively.

It must be emphasised that the reference direction of current transformers both at local and remote ends is chosen such that a positive current is measured when it flows into the line (incoming). Unlike simulations for a fault distance closer to the middle of the line, it can be observed that the local line-end current for faulted phase-a is significantly larger than that for the remote end.

Another interesting observation is that the voltage measured at the terminal is now largely dominated by the voltage across the series capacitor parallel to which the MOV has operated during segments of the power system cycle. Thus the voltage waveform seen for local-end phase-a is non-sinusoidal. The expression for distance to fault shown previously in (4.47)(4.30) was used by the algorithm to determine the fault location. The error calculated for this case was found to be 1.46%. This test was repeated for a variety of fault locations on a 50km line and a 100km line and for various fault resistances and fault types. The corresponding fault distance estimates have been tabulated in (4.18)Table 4.19 for a 50 km line a 100 km line respectively. The algorithm is found to be largely inaccurate for faults at line-ends. The results and the impact of this level of inaccuracy are discussed towards the end of this section.

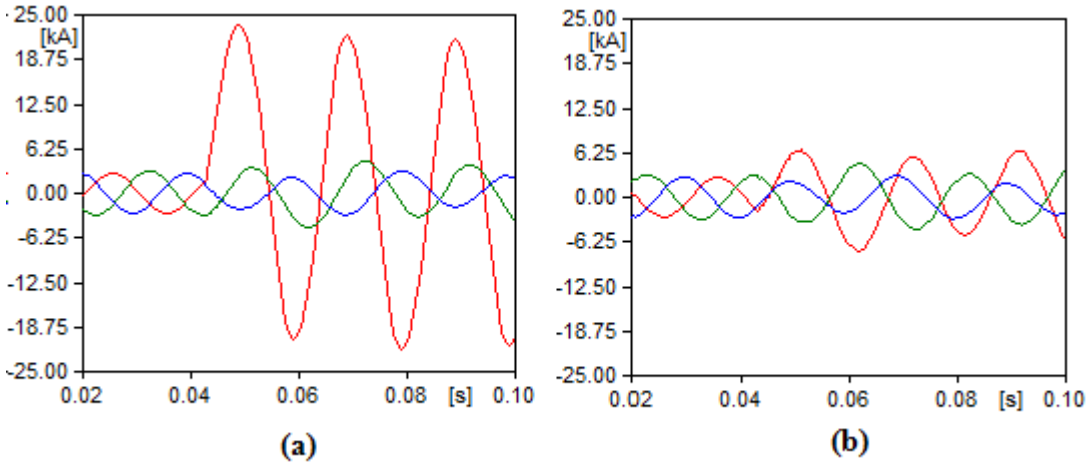

Figure 4.18: SLG fault at 1%: a) Local line-end currents b) Remote line-end currents

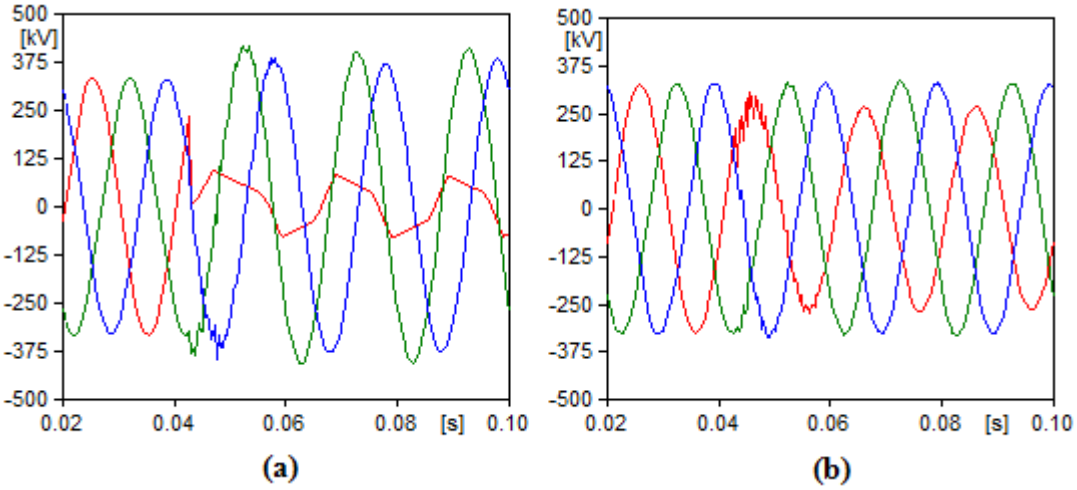

Figure 4.19: SLG fault at 1%: a) Local line-end voltages b) Remote line-end voltages

Table 4.19: Sensitivity of algorithm to the faults close to the line-ends (1% and 99%)

Fault Type	50 km line		100 km line	
	1%	99%	1%	99%
A-G RF = 0Ω	1.46	0.89	2.10	1.23
A-G RF = 100Ω	2.77	1.28	3.63	2.26
AB-G RF = 0Ω	1.09	1.67	2.84	2.43
AB-G RF = 100Ω	2.19	1.86	3.21	3.15
AB RF = 0Ω	2.56	2.91	3.32	2.64
AB RF = 100Ω	3.59	2.27	4.26	4.57
ABC-G RF = 0Ω	0.78	0.91	1.25	0.69
ABC-G RF = 100Ω	1.13	1.71	1.54	1.20

It can be observed that the errors in distance to fault are unacceptably for faults close to the line terminals. This is particularly the case for SLG, DL and DLG faults. The impact is less severe in terms of the accuracy for 3-phase faults. The errors overall are found to be higher for 100 km lines than 50 km lines. A key assumption used in the derivation of the algorithms is that the shunt admittance currents are negligible and that the measured line-terminal currents are equal to the series currents in the line. Whilst this assumption was found to be acceptable for fault distances simulated between 10% and 90%, for faults closer to the line-ends such as those presented in this section, the assumption is grossly violated.

This is the most significant drawback of this FLA. For this reason, as well as to improve the overall accuracy of the FLA including for faults closer to the line, methods to account for shunt admittance of the line in a line-parameter free manner are to be developed by the author as part of future work. Such a method is presented in Chapter 7 though it is currently limited to uncompensated lines. It is hoped that this work may be extended in future to include series compensated lines and thereby address the shortcoming highlighted in this section. Another contributing factor to the level of inaccuracy in such cases is that the presence of very high fault currents (for solid earth and low fault resistances) leads to the operation of the MOV aimed at protecting the capacitor from resulting overvoltages. An example simulation of this was shown earlier in this section.

4.3.11. Algorithm Accuracy –Varying Fault Levels

Thus far, the network parameters detailed in Table 4.4 were used in the simulations and in the results presented. This section investigates the influence of various the source fault levels as calculated at the local and remote ends of the line (where the measurements are taken). This is carried out by varying the positive and negative sequence source impedances. Two combinations of networks are used here. Combination-1 implements the source impedances of lower magnitudes than the case considered in previous sections (and therefore a higher fault level MVA). Combination-2 on the other hand implemented source impedances of larger magnitudes than the case considered in previous sections (and therefore a lower fault level MVA). The network parameters for these two new cases are

detailed in Table 4.20 and Table 4.21. A series of simulation tests are carried out using these new cases. The transmission line parameters used in the simulation of measurements previously are repeated here. Other aspects of the simulation are repeated as carried out in the previous section. The results for various fault types and fault resistances are presented in Table 4.22.

Table 4.20: Combination-1 (144 MVA, 89 MVA)

Network Parameters	Local Network A	Remote Network B
Line to Line RMS Voltage (kV)	416	400
Phase Angle (o)	0	-20
+ve seq. Resistance (Ω)	0.318	0.510
+ve seq. Inductance (H)	0.016	0.025
Z1 = R1+jX1	0.318+j5	0.510+j8
X1/R1	15.722	15.288
0 seq. Resistance (Ω)	0.637	1.018
0 seq. Inductance (H)	0.032	0.051
Z0 = R0+jX0	0.637+j10	1.018+j16
X0/R0	15.731	15.794
Fault MVA	143.912	88.927

Table 4.21: Combination-2 (36 MVA, 47 MVA)

Network Parameters	Local Network A	Remote Network B
Line to Line RMS Voltage (kV)	416	400
Phase Angle (^{o})	0	-20
+ve seq. Resistance (Ω)	1.274	0.956
+ve seq. Inductance (H)	0.064	0.047
$Z_1 = R_1+jX_1$	1.274+j20	0.956+j15
X_1/R_1	15.723	15.288
0 seq. Resistance (Ω)	2.546	1.910
0 seq. Inductance (H)	0.128	0.096
$Z_0 = R_0+jX_0$	2.546+j40	1.910+j30
X_0/R_0	15.731	15.794
Fault MVA	35.978	47.428

Table 4.22: Results for various fault levels

Fault Type	Fault Resistance (Ω)	Actual Fault Location (% of line length)					
		Combination-1			Combination-2		
		10	50	90	10	50	90
A-G	0	0.16	0.37	0.84	0.67	0.70	0.45
	100	0.72	0.66	0.24	0.52	0.01	0.69
AB	0	0.64	0.05	0.94	0.41	0.81	0.17
	100	0.83	0.60	0.11	0.49	0.55	0.70
AB-G	0	0.72	0.14	0.87	0.78	0.89	0.68
	100	0.34	0.15	0.76	0.83	0.53	0.84
ABC-G	0	0.86	0.11	0.88	0.51	0.03	0.59
	100	0.23	0.70	0.82	0.49	0.38	0.63

It can be seen that the FLA performs to a high level of accuracy for both network combinations used. The primary reason for this is that the FLA uses the equations describing the relationships between voltage differences between line-terminals and the phase currents. Unlike single-terminal algorithms that are limited to the use of only local-end measurements, two-terminal algorithms such as the FLA discussed in this chapter can be derived through complete descriptions of the voltage-current relationships without the need for gross simplifications regarding the fault resistance, remote infeed etc. Thus, the voltage difference becomes more significant here rather than the absolute voltages measured at the terminals. Combination-1 implemented source impedances of lower magnitudes of impedances than the case considered in previous sections (and therefore a higher fault level MVA). Combination-2 on the other hand implemented source impedances of larger magnitudes than the case considered in previous sections (and

therefore a lower fault level MVA). But for both cases, the accuracy is found to be sufficiently high. Moreover given that the range of source impedances/fault levels used here is broad (35MVA-143MVA) it may be concluded that the algorithm is not sensitive to the source fault level as calculated at the terminals (VTs) in the simulations. Another key advantage of the FLA being a two-terminal FLA can be seen here in that it is not sensitive to the remote-end infeed, despite varying the fault level at terminal-B (47MVA-89MVA).

4.3.12. Discussion of Results

The FLA was shown to be tested for a variety of conditions. This includes various fault distances, fault types, fault resistances, fault levels, locations and degrees of series compensation. The FLA was shown to also be tested for asynchronous measurements, transposed lines, double-circuit lines, longer line lengths, and for faults close to the line-ends. The general observation that can be made is that the algorithm is found to be highly accurate in a majority of cases. However, the FLA performs to a much lesser degree of accuracy for other cases. Therefore, this section aims to distinguish these to provide a clear analysis of the performance of the algorithm, highlighting both its advantages and drawbacks. The trends in the fault distance errors often do not seem to follow a repeatable or predictable pattern and experience "jumps". Where this is the case is discussed in subsequent explanations and the reasons for such a lack of predictability are also discussed:

- Observations for errors vs. simulated fault distances: The fault distance error variation with respect to simulated fault distance is often seen in the tables of results presented previously to not show a predictable or repeatable pattern. This is being due to the fact that the distance to fault is arrived at using complex equations involving numerous calculations in terminal voltages and phase currents. This is especially so for for "other faults" and "SLG faults on transposed lines" which require the solution of a complex cubic equation and a complex quartic equation respectively. The mathematical calculations were shown previously in Table 4.1 and Table 4.2 which show the complexity of the type of calculations required. So

although there is an underlying pattern in the errors it is not one that may be noticed through mere observation, and would require very complex analysis of the equations to derive.

Secondly, another aspect of the FLA that influences these trends is that where there are three or four potential solutions, the one that best fits the defined criteria, as discussed in Section 4.2.6, is chosen. There are instances where two potential solutions may be close to one another, as well as close to the actual distance to fault. In such instances, the solution that best fits these aforementioned criteria is chosen, although numerically the other solution may be closer to the actual distance to fault to a marginal degree. Where jumps are observed in the fault distance error it must be remembered that these are percentage errors with respect to the total line length. Therefore if for a SLG fault, the error jumps from 0.08% to 0.77%, it must be noted that these correspond to fractional distances to fault of 65.08/100 and 65.77/100 respectively. Thus, the "contrast bias" of viewing the numerical errors against one another must also be taken into consideration, that is to say, that the actual jumps with respect to the line length are not as significant as perceived when compared outside context.

- Trend observed for "Symmetrical Faults on Transposed Lines": It can be seen the fault location estimate does not change significantly on varying the fault resistance. In a symmetrical system, a three-phase to ground fault on a transposed line would lead to phase currents during fault being equal in magnitude and balanced, such that the total current through the fault resistance is equal to zero. So although there is a contribution from each phase the vector sum is zero. Therefore, voltage drop across a 100Ω fault resistance and a 10Ω fault resistance for such a case is the same (this voltage magnitude = IR = 0). Therefore, the errors are found not to vary with fault resistance.

- Trend observed for "Asynchronous Measurements": In Table 4.13 the rows titled "with synchronisation error correction" tabulate the errors calculated after the correction procedure is carried out. It can be seen that the distance to fault errors

are equal for each case despite an increase in synchronisation error. This is because regardless of the synchronisation error, the phase difference between the remote line-end phasors and local line-end phasors is always equal after the correction procedure, provided the procedure is carried out and the phasors are not assumed to be synchronised.

- Decline in accuracy observed for longer lines: Errors in fault distance are seen to be higher in the case of calculations carried out for lines of 300km length. The shunt admittance currents for such lines become a significant influence on the distance to fault calculations. The current derivations of the FLA do not consider the shunt admittance of the line due to the existing complexity of the equations used. This drawback is to be addressed as part of future work and is discussed briefly in Chapter 8.

- High inaccuracies observed for double-circuit lines: The FLA is seen to perform accurately for DL and 3-phase faults, but is found to be highly inaccurate for SLG and DLG faults, owing to the zero-sequence mutual coupling between the circuits of the double-circuit line not having been considered in the derivations. This drawback is addressed in the next Chapter by the proposal of a second FLA derived using similar principles, but with different expressions for distance to fault and requiring additional measurement data.

- Faults close to line-ends: It can be seen from results presented for faults at 1% and 99% that the FLA is very inaccurate at these points. This is a significant drawback of the algorithm.

- With the exception of the aforementioned categories where the FLA performs to a lesser degree of accuracy, it can be concluded that the FLA is accurate for various fault resistances, fault distances, degrees of series compensation, fault levels, transposed and untransposed lines and for both synchronous and asynchronous measurements provided the fault does not occur at the extremes of the transmission line.

4.4. Chapter Summary

This chapter discusses a novel, accurate, and reliable line parameter-free FLA designed to locate faults on series compensated OHTLs. The algorithm is shown to make use of synchronised two-end measurements, either as phasors or in the form of data samples that can then be converted to phasors using the FFT. It is intended primarily to serve the operation of fault locators in accurately locating the fault and thereby minimising outages, repair time and costs.

The novelty and the key advantage of the algorithm lies in that it does not require any line parameters in its calculations, and that it accurately calculates the distance to fault from the local line-terminal expressed as a fraction of the total line length. While traditionally line parameters are typically used in the calculations of impedance based FLAs, this introduces significant inaccuracies in the final estimation as such parameters are highly variable on a real power system. Thus, in recent years there has been a growing interest in the development of line parameter free solutions. Such FLAs are thus more accurate, reliable and robust in comparison. While a few such solutions have previously been designed for uncompensated lines, the FLA in this paper is designed for series compensated lines.

The mathematical descriptions of the system under fault are different for different fault types and thus they are analysed separately. It is found that a general expression can be used for nearly all types of faults with the exception of SLG faults and symmetrical 3-phase faults on transposed lines. Therefore, in this chapter, three expressions for distance to fault have been derived each corresponding to one of the aforementioned categories. These expressions have been subsequently implemented to locate faults on an accurately simulated power system containing a series compensated transmission line. They are found to be accurate in each case. Algorithms using line parameters typically use per-unit-length values of reactance and resistance. This allows the calculation of the distance to fault in units of distance. However, since the FLA described in this chapter uses a fractional distance, this may lead to inaccuracies during high temperatures due to line sag. This requires further analysis and is not in the scope of the project. Also the algorithm assumes that Rogowski coil CTs are used in the measurement of currents at the two line-ends. If

this is not the case, there may be distorted current measurements due to saturation of CTs at high fault currents, and may affect the accuracy of fault location.

Another limitation of the algorithm is that it requires high computation times when implemented on a desktop processor, typically in the order of 1-2 minutes. Thus, it cannot be implemented in real time, unless faster processing capability is available. This is however acceptable for the purposes of a fault locator. Also, its functionality is limited to locating faults and it is not capable of other kinds of fault analysis such as determining whether the fault is transient or permanent, calculating the arc resistance etc. Shunt admittance has not been considered in the equations used to derive the distance to fault. It is found to be accurate despite this assumption for 50km and 100 km lines. However, the algorithm accuracy could be improved further shunt admittance is taken into account, and is to be carried out in potential future work. The FLA performs poorly for faults close to the line-ends i.e. 1% and 99%. The influence of the shunt admittance currents is too significant to be neglected unlike the cases shown for faults between 10% and 90%. It is hoped that an algorithm to accurately account for the shunt admittance of the line will be developed as part of future work. Although the algorithm considers the mutual impedances between the phases of the line, it does not consider zero-sequence mutual coupling between circuits in a double circuit line. Thus, the FLA is only applicable to single-circuit lines. A novel line parameter free FLA for double circuit lines has also been developed as a part of this project and is discussed in Chapter 5.

Chapter 5. Novel Algorithm for Double-Circuit Series Compensated Transmission Lines

Chapter 3 discussed the planned installation of fixed series compensation at various locations on the GB network. The Eccles-Stella West 1 and 2 circuits which together form a double circuit line, and the installation is expected to be completed by 2015. The novel contribution of the author as described in this chapter is applicable only to fixed series compensated lines and would be applicable to this line. It is also hoped that this work may also be extended in future to transmission lines compensated using TCSCs. An example of such a line would be the Harker-Hutton double circuit line for which installation of TCSCs are planned and expected to be carried out also by 2015.

Fault location on double-circuit lines is not addressed accurately by FLAs designed for single-circuit lines. The mutual coupling between circuits affects the accuracy of distance to fault calculations if such FLAs are to be used. Therefore, Chapter 5 details a novel FLA derived and developed by the author that addresses this problem. The FLA does not require the use of line parameters, and is capable of locating faults on double-circuit lines. The mathematical derivations are shown in this chapter, simulation tests carried out to validate the algorithm are detailed, and results are tabulated. The advantages of the algorithm are also discussed.

5.1. Introduction

In this chapter, a novel algorithm for the fault distance calculation for series compensated double circuit lines is presented. The novelty lies in that it does not require the use of line parameters in its calculations. It is important to make the distinction that the novel FLA in Chapter 4 is only applicable to single-circuit lines and the FLA in this chapter is only applicable to double-circuit lines. A background of line parameter free solutions and their importance was discussed previously in detail. They are more accurate, reliable and robust.

This minimises outage times, and relevant repair costs. As mentioned previously, obtaining zero-sequence reactance per unit length parameters is difficult, and unreliable. This makes the line parameter free aspect of the algorithm a significant advantage for double-circuit lines as the effect of mutual-coupling between circuits can be taken into account in an accurate and reliable manner. The measurement inputs required for the algorithm are similar to the ones used for the FLA described in Chapter 4. The exception is that since the line is double-circuit, measurements from both circuits are used. Hence, 6 phase voltages (3 from each terminal) and 12 phase currents are required. Although synchronised measurements are assumed, a synchronisation error correction method is detailed in Section 5.3, which can be used in the case where synchronisation is not reliable.

Double-circuit parallel lines are far more common than single-circuit lines in real power systems. Fault analysis of double-circuit lines differs significantly from that of single-circuit lines due to the phenomenon of zero-sequence mutual coupling between the two circuits. But while the system under fault is more complex for such lines, due to the presence of an additional circuit, there is also more measurement data available for analysis to deal with this complexity. In the derivation of the algorithm for single-circuit lines, the unavailability of line parameters was dealt with by reducing equations containing various impedances as variables and measurement data as constants. This method of arriving at line parameter free expressions for distance to fault is repeated here, with the zero-sequence mutual impedance as an additional variable. Here too, it is assumed that Rogowski coil CTs are used in the measurement of currents at the two line-ends and therefore no CT saturation is considered. The decaying DC component removal and the FFT are carried out as before to obtain the fundamental frequency phasors for the measurements.

5.2. Algorithm Derivation

This section details the derivation of the expressions for the distance to fault used by the algorithm. Solutions for symmetrical faults on transposed lines, asymmetrical faults on transposed lines and faults on untransposed lines are discussed separately as each solution

can only be applied to that specific category of fault types. The fundamental principles used in the previous chapter are also used here.

The derivations are carried out so that impedance variables are eliminated systematically thereby resulting in line parameter-free expressions for distance to fault. They however, do require the fixed series capacitor reactance for their calculations. The final expressions only contain voltage and current phasors from the line terminals, the capacitor reactance and MOV coefficients similar to those introduced in the previous chapter (Section 4.2.4). For simplicity, the algorithm is derived assuming synchronised measurement data. The fault type is assumed to be available from the microprocessor relay. It may be recalled that voltage drops across a given phase can be expressed as a sum of the voltage drops across the self impedance, mutual impedances between phases and series compensation impedance. In the case of double circuit lines, an additional voltage drop due to zero-sequence mutual coupling between circuits is also included as shown in (5.1):

$$\Delta V_{phase} = \Delta V_{self} + \Delta V_{mutual(phases)} + \Delta V_{mutual(circuits)} + \Delta V_{series-compensation} \qquad (5.1)$$

In the derivations to follow, they are each expressed in terms of corresponding impedance variables which are then systematically eliminated through algebraic manipulation. Fractional distance to fault (see (4.2)) is calculated as before, and the total length of the line would be required to calculate the distance in kilometres.

The algorithm assumes the fault only affects phases of one of the two circuits, and the fault only occurs at one given location. Thus, it is not applicable to locating cross-country faults (faults to ground, occurring simultaneously at two different locations in one or several circuits). Again, analysis was carried out directly using phasors for phases a, b, and c without converting them into the sequence network phasors. While zero-sequence mutual impedance is used as a variable in the analysis, voltage drops are still always analysed for the phase networks. The pre-fault equation that describes the current voltage relationships for circuit-I is shown below:

$$\begin{bmatrix} \bar{V}_{La-pre} - \bar{V}_{Ra-pre} \\ \bar{V}_{Lb-pre} - \bar{V}_{Rb-pre} \\ \bar{V}_{Lc-pre} - \bar{V}_{Rc-pre} \end{bmatrix} = \begin{bmatrix} Z_S & Z_{Mab} & Z_{Mac} \\ Z_{Mab} & Z_S & Z_{Mbc} \\ Z_{Mac} & Z_{Mbc} & Z_S \end{bmatrix} \begin{bmatrix} \bar{I}_{aI-pre} \\ \bar{I}_{bI-pre} \\ \bar{I}_{cI-pre} \end{bmatrix} - jX_C \begin{bmatrix} \bar{I}_{aI-pre} \\ \bar{I}_{bI-pre} \\ \bar{I}_{cI-pre} \end{bmatrix} \quad (5.2)$$

where,

$\bar{V}_{La-pre}, \bar{V}_{Lb-pre}, \bar{V}_{Lc-pre}$ are the pre-fault local line-end voltages of phases a, b and c

$\bar{V}_{Ra-pre}, \bar{V}_{Rb-pre}, \bar{V}_{Rc-pre}$ are the pre-fault remote line-end voltages of phases a, b and c

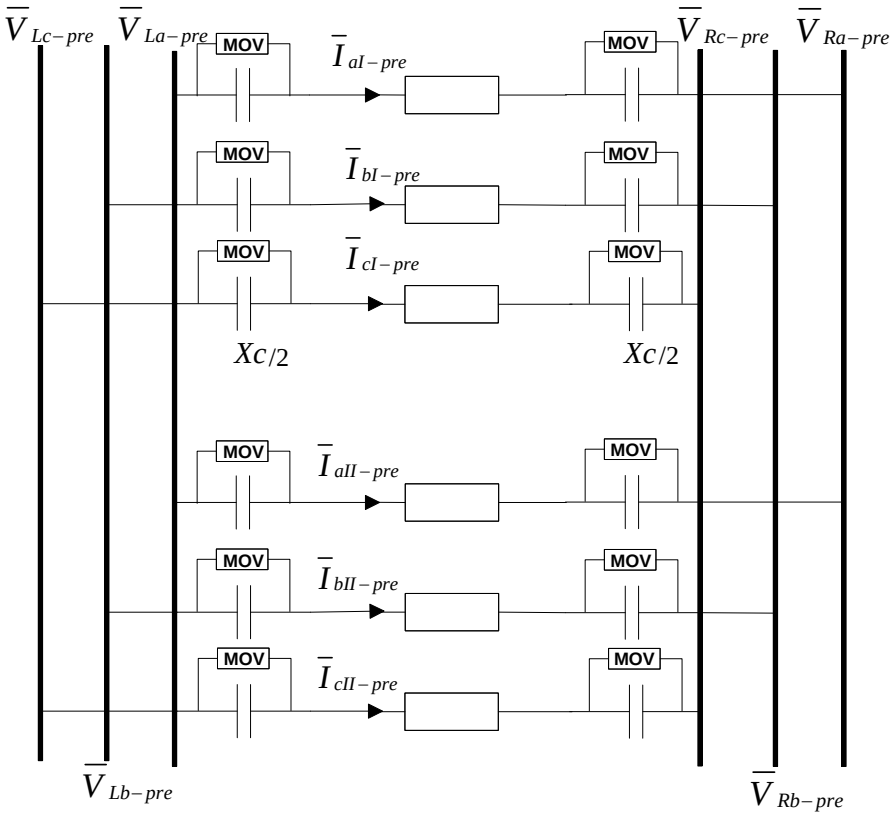

Figure 5.1: Double-circuit line under pre-fault conditions

It can be seen that there is no term in the equation for the mutual coupling effect between the two circuits. This is since the sum of the phase currents in circuit-II under pre-fault conditions is approximately zero, and would thus not induce a significant voltage on circuit-I. However, during fault conditions this voltage becomes significant and cannot be neglected. It is well known that positive sequence and negative sequence mutual coupling

between circuits is negligible and only zero-sequence mutual coupling is required to be considered in fault analysis to accurately calculate the distance to fault. This will not be required for DL and 3-phase faults. However, in considering a general solution covering all fault types, the mathematical formulation of the problem and the distance to fault must include the zero-sequence mutual impedance. In this chapter, since analysis is not carried out using sequence networks in this derivation, it is necessary to see how the zero-sequence mutual coupling translates in the phase network. This is explained as follows:

In the case of single-circuit uncompensated transmission lines, the mathematical relationship between the total voltage drops across the line in the phase network and total voltage drops in the sequence network is shown in (5.3). It can be expressed in terms of the sequence network impedances as shown in (5.4).

$$\begin{bmatrix} \Delta\bar{V}_a \\ \Delta\bar{V}_b \\ \Delta\bar{V}_c \end{bmatrix} = \begin{bmatrix} 1 & 1 & 1 \\ 1 & a^2 & a \\ 1 & a & a^2 \end{bmatrix} \begin{bmatrix} \Delta\bar{V}_0 \\ \Delta\bar{V}_1 \\ \Delta\bar{V}_2 \end{bmatrix} \tag{5.3}$$

$$\begin{bmatrix} \Delta\bar{V}_a \\ \Delta\bar{V}_b \\ \Delta\bar{V}_c \end{bmatrix} = \begin{bmatrix} 1 & 1 & 1 \\ 1 & a^2 & a \\ 1 & a & a^2 \end{bmatrix} \begin{bmatrix} \bar{I}_0 Z_0 \\ \bar{I}_1 Z_1 \\ \bar{I}_2 Z_2 \end{bmatrix} \tag{5.4}$$

where, $\Delta\bar{V}_a = \bar{V}_{La} - \bar{V}_{Ra}$ is the voltage drop across the inductive line for phase-a. $\Delta\bar{V}_b$ and $\Delta\bar{V}_c$ are the voltage drops across phases b and c calculated similarly. $\Delta\bar{V}_0, \Delta\bar{V}_1$ and $\Delta\bar{V}_2$ are the voltage drops across the three sequence networks. $\bar{I}_0, \bar{I}_1$ and $\bar{I}_2$ are sequence network currents. Z_0, Z_1 and Z_2 are the sequence network impedances. However, in the case of double-circuit lines, there is an additional term for the zero-sequence mutual impedance (shown here for circuit-II):

$$\begin{bmatrix} \Delta\bar{V}_{aII} \\ \Delta\bar{V}_{bII} \\ \Delta\bar{V}_{cII} \end{bmatrix} = \begin{bmatrix} 1 & 1 & 1 \\ 1 & a^2 & a \\ 1 & a & a^2 \end{bmatrix} \begin{bmatrix} \bar{I}_{0II}Z_0 + \bar{I}_{0I}Z_{0-M} \\ \bar{I}_{1II}Z_1 \\ \bar{I}_{2II}Z_2 \end{bmatrix} \tag{5.5}$$

where, $\Delta\bar{V}_{aII}, \Delta\bar{V}_{bII}$ and $\Delta\bar{V}_{cII}$ are the voltage drops across each of the three phases of circuit-II. $\bar{I}_{0II}, \bar{I}_{1II}$ and $\bar{I}_{2II}$ are the sequence network currents for circuit-II. Z_{0-M} is the zero sequence mutual impedance between circuit-I and circuit-II. Since $\bar{I}_{0I} = \bar{I}_{aI} + \bar{I}_{bI} + \bar{I}_{cI}$, (5.5) can be expressed as shown below:

$$\begin{bmatrix} \Delta\bar{V}_{aII} \\ \Delta\bar{V}_{bII} \\ \Delta\bar{V}_{cII} \end{bmatrix} = \begin{bmatrix} 1 & 1 & 1 \\ 1 & a^2 & a \\ 1 & a & a^2 \end{bmatrix} \left(\begin{bmatrix} \bar{I}_{0II}Z_0 \\ \bar{I}_{1II}Z_1 \\ \bar{I}_{2II}Z_2 \end{bmatrix} + \begin{bmatrix} (\bar{I}_{aI} + \bar{I}_{bI} + \bar{I}_{cI})Z_{0-M} \\ (\bar{I}_{aI} + \bar{I}_{bI} + \bar{I}_{cI})Z_{0-M} \\ (\bar{I}_{aI} + \bar{I}_{bI} + \bar{I}_{cI})Z_{0-M} \end{bmatrix} \right) \tag{5.6}$$

Thus, when analysing the zero-sequence mutual coupling in phase networks, the additional voltage drop due to mutual coupling between the circuits is equal for each phase, and is shown in (5.7):

$$\Delta\bar{V}_{aII-0M} = \Delta\bar{V}_{bII-0M} = \Delta\bar{V}_{cII-0M} = (\bar{I}_{aI} + \bar{I}_{bI} + \bar{I}_{cI})Z_{0-M} \tag{5.7}$$

For series compensated lines, this analysis can still be carried out by considering only the voltage drop across the inductive line. Thus, $\Delta\bar{V}_{aII}, \Delta\bar{V}_{bII}$ and $\Delta\bar{V}_{cII}$ are redefined here for series compensated lines:

$$\begin{bmatrix} \Delta\bar{V}_{aII} \\ \Delta\bar{V}_{bII} \\ \Delta\bar{V}_{cII} \end{bmatrix} = \begin{bmatrix} \bar{V}_{La} - \bar{V}_{Ra} - \bar{V}_{CaII} \\ \bar{V}_{La} - \bar{V}_{Ra} - \bar{V}_{CbII} \\ \bar{V}_{La} - \bar{V}_{Ra} - \bar{V}_{CcII} \end{bmatrix} \tag{5.8}$$

$$\begin{bmatrix} \Delta\overline{V}_{aI} \\ \Delta\overline{V}_{bI} \\ \Delta\overline{V}_{cI} \end{bmatrix} = \begin{bmatrix} \overline{V}_{La} - \overline{V}_{Ra} - \overline{V}_{CaI} \\ \overline{V}_{La} - \overline{V}_{Ra} - \overline{V}_{CbI} \\ \overline{V}_{La} - \overline{V}_{Ra} - \overline{V}_{CcI} \end{bmatrix} \tag{5.9}$$

where, $\overline{V}_{CaII}$, $\overline{V}_{CbII}$ and $\overline{V}_{CcII}$ are the total voltage drops across the series capacitors in phases a, b and c respectively for circuit-II. $\overline{V}_{CaI}$, $\overline{V}_{CbI}$ and $\overline{V}_{CcI}$ are defined similarly for circuit I. They are calculated in this algorithm using the setting of the total capacitor reactance X_C, and the measured currents flowing through the series capacitor(s). For e.g. in the case of a line compensated at both ends during pre-fault:

$$\overline{V}_{CaII} = X_C S_a \tag{5.10}$$

where, $\overline{I}_{LaII}$ and $\overline{I}_{RaII}$ are the local and remote line-end currents of phase a of circuit II. The voltage drops across the series capacitors for other types of series compensated lines and for other phases can be calculated similarly. All derivations are carried out for a line compensated at both ends and Section 4.2.4 details the modification of the MOV coefficients required to apply the FLA to other types of series compensated lines.

5.2.1. Derivation of Distance to Fault for Transposed Lines

Transposed lines are much simpler in nature and this allows for the derivation of simpler expressions for distance to fault. The expressions derived in this section are easy to compute and require very little computation time, and thus are also suited for real time applications.

5.2.1.1. Three phase faults on transposed lines

A three-phase symmetrical fault on a transposed line is shown in Figure 5.2. The derivation for the distance to fault for this category is similar to the method described in Chapter 4 in Section 4.2.2. This is because, the sum of the currents in the healthy circuit (circuit-I) would summate to zero, and the voltage due to zero sequence mutual coupling between the

circuits is negligible, and thus the faulted circuit can be treated effectively as being a single-circuit line. Analysis of the positive sequence impedance of the transmission line ($Z_{1\text{-}line}$) is used, although no pre-fault calculations are required for this. Given that, for a symmetrical fault on a transposed line, the fault is a solid earth (since total fault current=0), the voltage drop across any faulted section (here shown for phase-a) can be expressed purely in terms of the voltage drop across the positive sequence impedance of that faulted section.

$$\overline{V}_{La} - X_C SCa1 = lZ_{1-line}\overline{I}_{LaII} \tag{5.11}$$

$$\overline{V}_{Ra} - X_C SCa2 = (1-l)Z_{1-line}\overline{I}_{RaII} \tag{5.12}$$

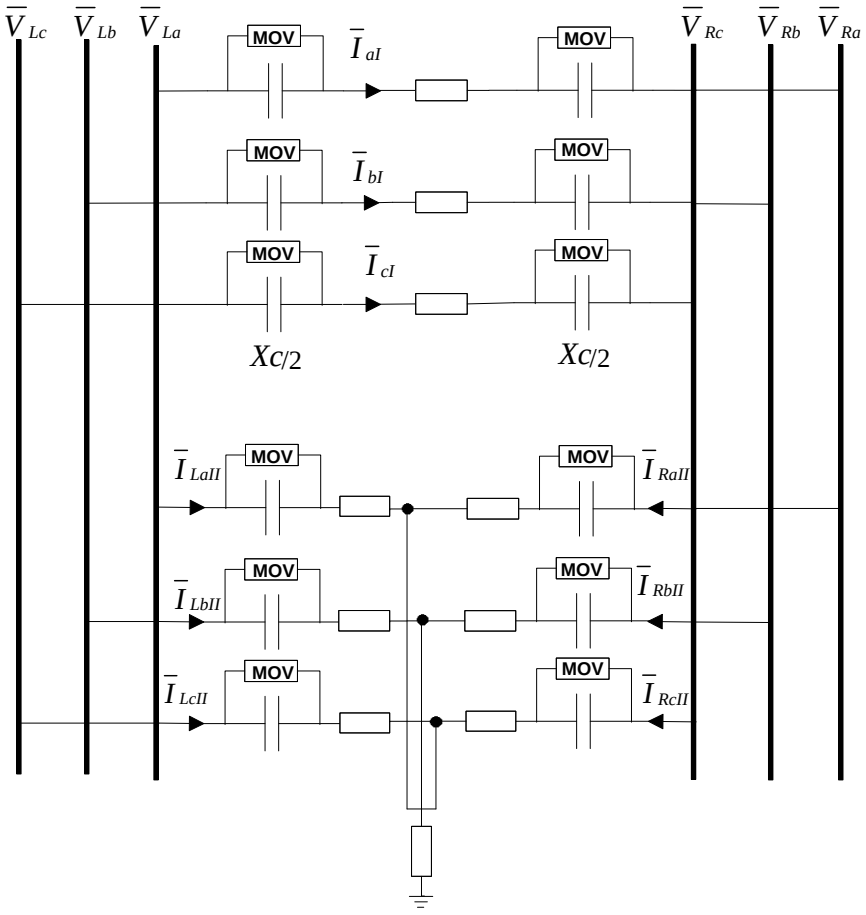

Figure 5.2: Double circuit line under 3-phase fault conditions

Here, $\overline{V}_{La}$ and $\overline{V}_{Ra}$ are the local and remote line-end voltages respectively for phase-a. $\overline{I}_{LaII}$ and $\overline{I}_{RaII}$ are the local and remote line-end currents respectively for phase-a. Terms $SCa1$ and $SCa2$ have been derived previously in Section 4.2.4. Thus, it follows:

$$\frac{\overline{V}_{La} - X_C SCa1}{\overline{V}_{Ra} - X_C SCa2} = \frac{l\overline{I}_{LaII}}{(1-l)\overline{I}_{RaII}} \tag{5.13}$$

$$l = \frac{\left|(\overline{V}_{La} - X_C SCa1)\overline{I}_{RaII}\right|}{\left|(\overline{V}_{Ra} - X_C SCa2)\overline{I}_{LaII}\right| + \left|(\overline{V}_{La} - X_C SCa1)\overline{I}_{RaII}\right|} \tag{5.14}$$

Thus, (5.14) is a line parameter free expression derived for locating three-phase faults on transposed double-circuit series compensated lines.

5.2.1.2. Other faults on transposed lines

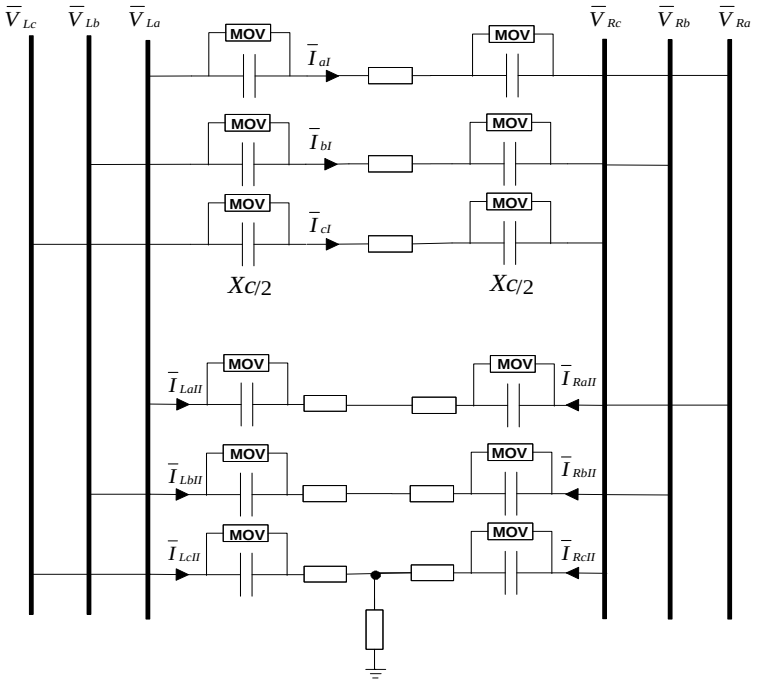

Figure 5.3: Double circuit line under SLG fault conditions

Figure 5.3 shows an example of a SLG fault on a transposed line. The principle described previously using (5.1) is used to describe the voltage drops across each phase. The fault condition equations for the three phases of the faulted circuit are as follows:

$$\begin{aligned}\Delta\bar{V}_{aII} = {} & lZ_S\bar{I}_{LaII} + (1-l)Z_S\bar{I}_{RaII} + lZ_M(\bar{I}_{LbII} + \bar{I}_{LcII}) + (1-l)Z_M(\bar{I}_{RbII} + \bar{I}_{RcII}) \\ & + lZ_{0-M}(\bar{I}_{LaI} + \bar{I}_{LbI} + \bar{I}_{LcI}) + (1-l)Z_{0-M}(\bar{I}_{RaI} + \bar{I}_{RbI} + \bar{I}_{RcI})\end{aligned} \tag{5.15}$$

$$\begin{aligned}\Delta\bar{V}_{bII} = {} & lZ_S\bar{I}_{LbII} + (1-l)Z_S\bar{I}_{RbII} + lZ_M(\bar{I}_{LaII} + \bar{I}_{LcII}) + (1-l)Z_M(\bar{I}_{RaII} + \bar{I}_{RcII}) \\ & + lZ_{0-M}(\bar{I}_{LaI} + \bar{I}_{LbI} + \bar{I}_{LcI}) + (1-l)Z_{0-M}(\bar{I}_{RaI} + \bar{I}_{RbI} + \bar{I}_{RcI})\end{aligned} \tag{5.16}$$

$$\begin{aligned}\Delta\bar{V}_{cII} = {} & lZ_S\bar{I}_{LcII} + (1-l)Z_S\bar{I}_{RcII} + lZ_M(\bar{I}_{LaII} + \bar{I}_{LbII}) + (1-l)Z_M(\bar{I}_{RaII} + \bar{I}_{RbII}) \\ & + lZ_{0-M}(\bar{I}_{LaI} + \bar{I}_{LbI} + \bar{I}_{LcI}) + (1-l)Z_{0-M}(\bar{I}_{RaI} + \bar{I}_{RbI} + \bar{I}_{RcI})\end{aligned} \tag{5.17}$$

Subtracting (5.16) from (5.15), and (5.17) from (5.15), (5.18) and (5.19) are obtained respectively:

$$\begin{aligned}\Delta\bar{V}_{aII} - \Delta\bar{V}_{bII} = {} & lZ_S(\bar{I}_{LaII} - \bar{I}_{LbII}) + (1-l)Z_S(\bar{I}_{RaII} - \bar{I}_{RbII}) - lZ_M(\bar{I}_{LaII} - \bar{I}_{LbII}) \\ & - (1-l)Z_M(\bar{I}_{RaII} - \bar{I}_{RbII})\end{aligned} \tag{5.18}$$

$$\begin{aligned}\Delta\bar{V}_{aII} - \Delta\bar{V}_{cII} = {} & lZ_S(\bar{I}_{LaII} - \bar{I}_{LcII}) + (1-l)Z_S(\bar{I}_{RaII} - \bar{I}_{RcII}) - lZ_M(\bar{I}_{LaII} - \bar{I}_{LcII}) \\ & - (1-l)Z_M(\bar{I}_{RaII} - \bar{I}_{RcII})\end{aligned} \tag{5.19}$$

The above equations can be simplified as follows by substituting for $Z_S - Z_M$ as Z_P

$$\Delta\bar{V}_{aII} - \Delta\bar{V}_{bII} = lZ_P(\bar{I}_{LaII} - \bar{I}_{LbII}) + (1-l)Z_P(\bar{I}_{RaII} - \bar{I}_{RbII}) \tag{5.20}$$

$$\Delta\bar{V}_{aII} - \Delta\bar{V}_{cII} = lZ_P(\bar{I}_{LaII} - \bar{I}_{LcII}) + (1-l)Z_P(\bar{I}_{RaII} - \bar{I}_{RcII}) \tag{5.21}$$

Dividing (5.20) by (5.21), an equation with one variable l is obtained. Re-arranging (5.22) a simple expression for distance to fault is derived as shown in (5.23).

$$\frac{\Delta\bar{V}_{aII}-\Delta\bar{V}_{bII}}{\Delta\bar{V}_{aII}-\Delta\bar{V}_{cII}}=\frac{l(\bar{I}_{LaII}-\bar{I}_{LbII}-\bar{I}_{RaII}+\bar{I}_{RbII})+(\bar{I}_{RaII}-\bar{I}_{RbII})}{l(\bar{I}_{LaII}-\bar{I}_{LcII}-\bar{I}_{RaII}+\bar{I}_{RcII})+(\bar{I}_{RaII}-\bar{I}_{RcII})} \tag{5.22}$$

$$l=\frac{(\Delta\bar{V}_{aII}-\Delta\bar{V}_{cII})(\bar{I}_{RaII}-\bar{I}_{RbII})-(\Delta\bar{V}_{aII}-\Delta\bar{V}_{bII})(\bar{I}_{RaII}-\bar{I}_{RcII})}{(\Delta\bar{V}_{aII}-\Delta\bar{V}_{bII})(\bar{I}_{LaII}-\bar{I}_{LcII}-\bar{I}_{RaII}+\bar{I}_{RcII})-(\Delta\bar{V}_{aII}-\Delta\bar{V}_{cII})(\bar{I}_{LaII}-\bar{I}_{LbII}-\bar{I}_{RaII}+\bar{I}_{RbII})} \tag{5.23}$$

Thus, (5.23) is a line parameter free expression derived for locating "other faults" (all except three-phase faults) on transposed double-circuit series compensated lines.

5.2.2. Derivation of Distance to Fault for Untransposed Lines

The derivation in this section is carried out by the reduction of equations for pre-fault and fault equations as done so in the previous chapter in Section 4.2.3. The system of equations to be solved is shown in (5.24) - (5.32). Here, (5.24) - (5.26) are the pre-fault equations for circuit-I, (5.27) - (5.29) are the equations for the healthy circuit (circuit-I) during fault conditions, and (5.30) - (5.32) are the equations for the faulted circuit (circuit-II). The voltage and current phasors used in the equations are as shown previously in Figure 5.3. Once again, the system of equations considered here is non-linear. It can be noted that when comparing the derivation in this section to that in Section 4.2.3 in Chapter 4, the number of equations has increased by three due to the presence of a second circuit available for analysis. The number of variables has increased by only one, allowing a relatively simpler expression for distance to fault.

$$\Delta\bar{V}_{aI-pre}=Z_S\bar{I}_{aI-pre}+Z_{Mab}\bar{I}_{bI-pre}+Z_{Mac}\bar{I}_{cI-pre}+lZ_{0-M}\sum\bar{I}_{II-pre}+(1-l)Z_{0-M}\sum\bar{I}_{II-pre} \tag{5.24}$$

$$\Delta\bar{V}_{bI-pre}=Z_S\bar{I}_{bI-pre}+Z_{Mab}\bar{I}_{aI-pre}+Z_{Mbc}\bar{I}_{cI-pre}+lZ_{0-M}\sum\bar{I}_{II-pre}+(1-l)Z_{0-M}\sum\bar{I}_{II-pre} \tag{5.25}$$

$$\Delta\bar{V}_{cI-pre}=Z_S\bar{I}_{cI-pre}+Z_{Mac}\bar{I}_{aI-pre}+Z_{Mbc}\bar{I}_{bI-pre}+lZ_{0-M}\sum\bar{I}_{II-pre}+(1-l)Z_{0-M}\sum\bar{I}_{II-pre} \tag{5.26}$$

$$\Delta\bar{V}_{aI}=Z_S\bar{I}_{aI}+Z_{Mab}\bar{I}_{bI}+Z_{Mac}\bar{I}_{cI}+lZ_{0-M}\sum\bar{I}_{LII}+(1-l)Z_{0-M}\sum\bar{I}_{RII} \tag{5.27}$$

$$\Delta\bar{V}_{bI} = Z_S\bar{I}_{bI} + Z_{Mab}\bar{I}_{aI} + Z_{Mbc}\bar{I}_{cI} + lZ_{0-M}\sum\bar{I}_{LII} + (1-l)Z_{0-M}\sum\bar{I}_{RII} \quad (5.28)$$

$$\Delta\bar{V}_{cI} = Z_S\bar{I}_{cI} + Z_{Mac}\bar{I}_{aI} + Z_{Mbc}\bar{I}_{bI} + lZ_{0-M}\sum\bar{I}_{LII} + (1-l)Z_{0-M}\sum\bar{I}_{RII} \quad (5.29)$$

$$\Delta\bar{V}_{aII} = l(Z_S\bar{I}_{LaII} + Z_{Mab}\bar{I}_{LbII} + Z_{Mac}\bar{I}_{LcII}) + (1-l)(Z_S\bar{I}_{RaII} + Z_{Mab}\bar{I}_{RbII} + Z_{Mac}\bar{I}_{RcII}) + Z_{0-M}\sum\bar{I}_{I} \quad (5.30)$$

$$\Delta\bar{V}_{bII} = l(Z_S\bar{I}_{LbII} + Z_{Mab}\bar{I}_{LaII} + Z_{Mbc}\bar{I}_{LcII}) + (1-l)(Z_S\bar{I}_{RbII} + Z_{Mab}\bar{I}_{RaII} + Z_{Mbc}\bar{I}_{RcII}) + Z_{0-M}\sum\bar{I}_{I} \quad (5.31)$$

$$\Delta\bar{V}_{cII} = l(Z_S\bar{I}_{LcII} + Z_{Mac}\bar{I}_{LaII} + Z_{Mbc}\bar{I}_{LbII}) + (1-l)(Z_S\bar{I}_{RcII} + Z_{Mac}\bar{I}_{RaII} + Z_{Mbc}\bar{I}_{RbII}) + Z_{0-M}\sum\bar{I}_{I} \quad (5.32)$$

where $\sum\bar{I}_{II-pre}$ is the sum of the pre-fault phase currents in circuit-II. $\sum\bar{I}_{I}$ is the sum of currents in circuit-I. $\sum\bar{I}_{LII}$ is the sum of the local line-end currents in circuit II and $\sum\bar{I}_{RII}$ is the sum of the remote line-end currents for circuit II. This derivation is detailed as follows. The first stage of the derivation is to express Z_{Mab}, Z_{Mac} and Z_{Mbc} in terms of Z_S. The second stage of the derivation is to substitute for these variables and through basic algebraic manipulation, to arrive at an equation purely in terms of distance to fault. The first stage is carried out as follows. Subtracting (5.25) from (5.24), (5.26) from (5.24), and (5.29) from (5.27) yields equations (5.33), (5.34) and (5.35) respectively.

$$\begin{aligned}&\Delta\bar{V}_{aI-pre} - \Delta\bar{V}_{cI-pre} - Z_S(\bar{I}_{aI-pre} - \bar{I}_{cI-pre})\\ &= Z_{Mac}(\bar{I}_{cI-pre} - \bar{I}_{aI-pre}) + Z_{Mab}\bar{I}_{bI-pre} - Z_{Mbc}\bar{I}_{bI-pre}\end{aligned} \quad (5.33)$$

$$\begin{aligned}&\Delta\bar{V}_{bI-pre} - \Delta\bar{V}_{cI-pre} - Z_S(\bar{I}_{bI-pre} - \bar{I}_{cI-pre})\\ &= Z_{Mbc}(\bar{I}_{cI-pre} - \bar{I}_{bI-pre}) + Z_{Mab}\bar{I}_{aI-pre} - Z_{Mac}\bar{I}_{aI-pre}\end{aligned} \quad (5.34)$$

$$\begin{aligned}&\Delta\bar{V}_{aI} - \Delta\bar{V}_{cI} - Z_S(\bar{I}_{aI} - \bar{I}_{cI})\\ &= Z_{Mac}(\bar{I}_{cI} - \bar{I}_{aI}) + Z_{Mab}\bar{I}_{bI} - Z_{Mbc}\bar{I}_{bI}\end{aligned} \quad (5.35)$$

The above can be expressed in matrix form as shown below:

$$\begin{bmatrix} \Delta\bar{V}_{aI-pre} - \Delta\bar{V}_{cI-pre} - Z_S(\bar{I}_{aI-pre} - \bar{I}_{cI-pre}) \\ \Delta\bar{V}_{bI-pre} - \Delta\bar{V}_{cI-pre} - Z_S(\bar{I}_{bI-pre} - \bar{I}_{cI-pre}) \\ \Delta\bar{V}_{aI} - \Delta\bar{V}_{cI} - Z_S(\bar{I}_{aI} - \bar{I}_{cI}) \end{bmatrix} = W \begin{bmatrix} Z_{Mab} \\ Z_{Mac} \\ Z_{Mbc} \end{bmatrix} \tag{5.36}$$

where,

$$W = \begin{bmatrix} \bar{I}_{bI-pre} & \bar{I}_{cI-pre} - \bar{I}_{aI-pre} & -\bar{I}_{bI-pre} \\ \bar{I}_{aI-pre} & -\bar{I}_{aI-pre} & \bar{I}_{cI-pre} - \bar{I}_{bI-pre} \\ \bar{I}_{bI} & \bar{I}_{cI} - \bar{I}_{aI} & -\bar{I}_{bI} \end{bmatrix} \tag{5.37}$$

Using the above equations, the mutual impedance variables can be expressed in terms of Z_S as shown in (5.38):

$$\begin{bmatrix} Z_{Mab} \\ Z_{Mac} \\ Z_{Mbc} \end{bmatrix} = \begin{bmatrix} k_1 + m_1 Z_S \\ k_2 + m_2 Z_S \\ k_3 + m_3 Z_S \end{bmatrix} \tag{5.38}$$

where,

$$\begin{bmatrix} k_1 \\ k_2 \\ k_3 \end{bmatrix} = W^{-1} \begin{bmatrix} \Delta\bar{V}_{aI-pre} - \Delta\bar{V}_{cI-pre} \\ \Delta\bar{V}_{bI-pre} - \Delta\bar{V}_{cI-pre} \\ \Delta\bar{V}_{aI} - \Delta\bar{V}_{cI} \end{bmatrix} \tag{5.39}$$

$$\begin{bmatrix} m_1 \\ m_2 \\ m_3 \end{bmatrix} = W^{-1} \begin{bmatrix} \bar{I}_{cI-pre} - \bar{I}_{aI-pre} \\ \bar{I}_{cI-pre} - \bar{I}_{bI-pre} \\ \bar{I}_{cI} - \bar{I}_{aI} \end{bmatrix} \tag{5.40}$$

Similarly, subtracting (5.31) from (5.30) and (5.32) from (5.30) yields (5.41) and (5.42) respectively.

$$\begin{aligned}\Delta\bar{V}_{aII}-\Delta\bar{V}_{bII} &= l(Z_S(\bar{I}_{LaII}-\bar{I}_{LbII})+Z_{Mab}(\bar{I}_{LbII}-\bar{I}_{LaII})+Z_{Mac}\bar{I}_{LcII}-Z_{Mbc}\bar{I}_{LcII})\\ &+(1-l)(Z_S(\bar{I}_{RaII}-\bar{I}_{RbII})+Z_{Mab}(\bar{I}_{RbII}-\bar{I}_{RaII})+Z_{Mac}\bar{I}_{RcII}-Z_{Mbc}\bar{I}_{RcII})\end{aligned} \quad (5.41)$$

$$\begin{aligned}\Delta\bar{V}_{aII}-\Delta\bar{V}_{cII} &= l(Z_S(\bar{I}_{LaII}-\bar{I}_{LcII})+Z_{Mab}\bar{I}_{LbII}+Z_{Mac}(\bar{I}_{LcII}-\bar{I}_{LaII})-Z_{Mbc}\bar{I}_{LbII})\\ &+(1-l)(Z_S(\bar{I}_{RaII}-\bar{I}_{RcII})+Z_{Mab}\bar{I}_{RbII}+Z_{Mac}(\bar{I}_{RcII}-\bar{I}_{RaII})-Z_{Mbc}\bar{I}_{RbII})\end{aligned} \quad (5.42)$$

The above equations are rearranged in terms of Z_S and the expressions for Z_{Mab}, Z_{Mac} and Z_{Mbc} from (5.38) are substituted in as shown in (5.43) and (5.44).

$$Z_S=\frac{\Delta\bar{V}_{aII}-\Delta\bar{V}_{bII}-k_1(\bar{I}_{RbII}-\bar{I}_{RaII})-(k_2-k_3)\bar{I}_{RcII}-l(k_1(\bar{I}_{LbII}-\bar{I}_{LaII}-\bar{I}_{RbII}+\bar{I}_{RaII})+(k_2-k_3)(\bar{I}_{LcII}-\bar{I}_{RcII}))}{(\bar{I}_{RaII}-\bar{I}_{RbII})+m_1(\bar{I}_{RbII}-\bar{I}_{RaII})+(m_2-m_3)\bar{I}_{RcII}+l(\bar{I}_{LaII}-\bar{I}_{LbII}-\bar{I}_{RaII}+\bar{I}_{RbII}+m_1(\bar{I}_{LbII}-\bar{I}_{LaII}-\bar{I}_{RbII}+\bar{I}_{RaII})+(m_2-m_3)(\bar{I}_{LcII}-\bar{I}_{RcII}))} \quad (5.43)$$

$$Z_S=\frac{\Delta\bar{V}_{aII}-\Delta\bar{V}_{cII}-k_2(\bar{I}_{RcII}-\bar{I}_{RaII})-(k_1-k_3)\bar{I}_{RbII}-l(k_2(\bar{I}_{LcII}-\bar{I}_{LaII}-\bar{I}_{RcII}+\bar{I}_{RaII})+(k_1-k_3)(\bar{I}_{LbII}-\bar{I}_{RbII}))}{(\bar{I}_{RaII}-\bar{I}_{RcII})+m_2(\bar{I}_{RcII}-\bar{I}_{RaII})+(m_1-m_3)\bar{I}_{RbII}+l(\bar{I}_{LaII}-\bar{I}_{LcII}-\bar{I}_{RaII}+\bar{I}_{RcII}+m_2(\bar{I}_{lcII}-\bar{I}_{LaII}-\bar{I}_{RcII}+\bar{I}_{RaII})+(m_1-m_3)(\bar{I}_{LbII}-\bar{I}_{RbII}))} \quad (5.44)$$

Equating the right hand side expressions of (5.43) and (5.44) and rearranging, results in (5.45):

$$l^2(TZ-VX)+l(SZ+TY-XU-VW)+SY-WU=0 \quad (5.45)$$

Thus, (5.45) is a line parameter free expression derived for locating faults on untransposed double-circuit series compensated lines. The terms *S, T, U, V, W, X, Y* and *Z* are constants and have been defined in Table 5.1. The final expression is a quadratic equation only in terms of l. Thus there are two potential solutions for distance to fault, only one of which lies between 0-1 and yields reasonable estimates for the other variables Z_{Mab}, Z_{Mac}, Z_{Mbc}, and Z_S and is thus chosen as the correct solution. The choice of solution is carried out

based on the criteria detailed previously Section 4.2.6. The flowchart shown in Figure 5.4 summarises the algorithm.

Table 5.1: List of constants in (5.45)

Term	Definition
S	$\Delta\bar{V}_{aII} - \Delta\bar{V}_{bII} - k_1(\bar{I}_{RbII} - \bar{I}_{RaII}) - (k_2 - k_3)\bar{I}_{RcII}$
T	$-(k_1(\bar{I}_{LbII} - \bar{I}_{LaII} - \bar{I}_{RbII} + \bar{I}_{RaII}) + (k_2 - k_3)(\bar{I}_{LcII} - \bar{I}_{RcII}))$
U	$(\bar{I}_{RaII} - \bar{I}_{RbII}) + m_1(\bar{I}_{RbII} - \bar{I}_{RaII}) + (m_2 - m_3)\bar{I}_{RcII}$
V	$(\bar{I}_{LaII} - \bar{I}_{LbII} - \bar{I}_{RaII} + \bar{I}_{RbII} + m_1(\bar{I}_{LbII} - \bar{I}_{LaII} - \bar{I}_{RbII} + \bar{I}_{RaII}) + (m_2 - m_3)(\bar{I}_{LcII} - \bar{I}_{RcII}))$
W	$\Delta\bar{V}_{aII} - \Delta\bar{V}_{cII} - k_2(\bar{I}_{RcII} - \bar{I}_{RaII}) - (k_1 - k_3)\bar{I}_{RbII}$
X	$-(k_2(\bar{I}_{LcII} - \bar{I}_{LaII} - \bar{I}_{RcII} + \bar{I}_{RaII}) + (k_1 - k_3)(\bar{I}_{LbII} - \bar{I}_{RbII}))$
Y	$(\bar{I}_{RaII} - \bar{I}_{RcII}) + m_2(\bar{I}_{RcII} - \bar{I}_{RaII}) + (m_1 - m_3)\bar{I}_{RbII}$
Z	$(\bar{I}_{LaII} - \bar{I}_{LcII} - \bar{I}_{RaII} + \bar{I}_{RcII} + m_2(\bar{I}_{LcII} - \bar{I}_{LaII} - \bar{I}_{RcII} + \bar{I}_{RaII}) + (m_1 - m_3)(\bar{I}_{LbII} - \bar{I}_{RbII}))$

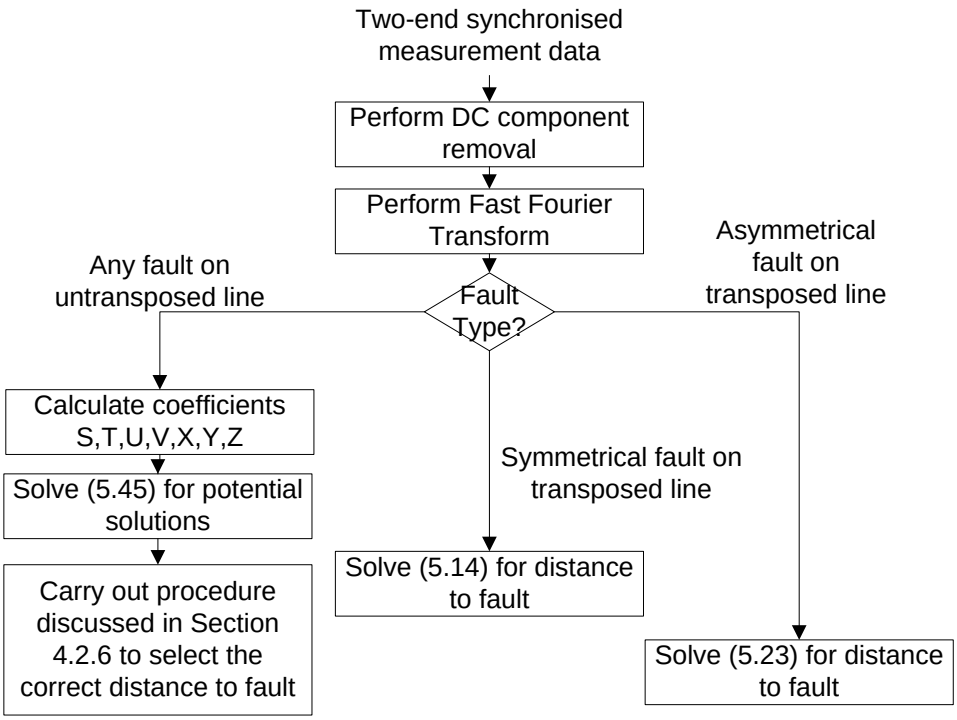

Figure 5.4: Algorithm flowchart

5.3. Algorithm using Unsynchronised Measurements

The necessity for synchronisation error correction and the method of such correction in the case when only asynchronous measurements are available are discussed below for each category of fault:

1. Three phase faults on transposed lines: No synchronisation is required. This can be explained as follows. Since, (5.46) and (5.47) are the initial equations used to derive the expressions, the final expression is determined by how these equations are affected by a synchronisation error. The modified equations are shown below:

$$\overline{V}_{La} - X_C SCa1 = lZ_{1-line}\overline{I}_{LaII} \tag{5.46}$$

$$\overline{V}_{Ra}(e^{j\theta}) - X_C SCa2(e^{j\theta}) = (1-l)Z_{1-line}\overline{I}_{RaII}(e^{j\theta}) \tag{5.47}$$

   Dividing (5.47) by $e^{j\theta}$ results in (5.12), and therefore the derivation thereafter follows exactly as before and it can be concluded that synchronisation error has no effect on the solution as calculated in (5.14).

2. All other faults on transposed lines: Method described for “all other fault types” in Section 4.2.5 of Chapter 4 is used.

3. Faults on untransposed lines: Method described for “all other fault types” in Section 4.2.5 of Chapter 4 is used.

5.4. Advantages of Novel FLA

This FLA shares nearly all the advantages mentioned for the FLA in Chapter 4. They are as follows:

- The FLA is not affected by current inversion or a voltage inversion at one given line terminal

- It takes the capacitor reactance and MOV operation into account accurately, and thereby correctly estimates the distance to fault.
- It's accuracy is not affected by fault resistance.
- It is capable of locating various types of faults, for various different locations of series capacitor installations on the line.
- It can locate faults even using asynchronous data.
- It is not affected by the source impedance.
- The algorithm is accurate regardless of whether the VT is on the line side or the bus side of the series capacitor
- It is an original line parameter free FLA for series compensated double-circuit lines.

5.5. Simulation and Algorithm Validation

ATP-EMTP is used to carry out simulations used to validate the algorithm. Sampled measurement data is generated here and processed in MATLAB. An example test circuit for a double-circuit lines is shown in Figure 5.5. It is a 100 km 400kV double-circuit transmission line. A J-Marti line model is used, and created using the LCC line modelling block of ATP-EMTP. The local and remote line-end network parameters and the line parameters are shown in Table 5.2 and Table 5.3 respectively. The networks at the line ends are the same as those discussed in Chapter 4, wheras the transmission line parameters were selected to closely simulate the positive, negative and zero sequence parameters used in [153]. Any degree of compensation can be obtained by adjusting the series capacitor reactance and the MOV parameters. The distance to fault is calculated using the algorithm described in this chapter, as programmed in MATLAB. The fault inception time in each case was 43 ms. This corresponds to two cycles of pre-fault data, sufficient for the calculations of the algorithm. A sampling frequency of 6.4 kHz was used for the

simulations, and all data was synchronously sampled. The data window size used for the FFT to obtain the phasors was 20 ms.

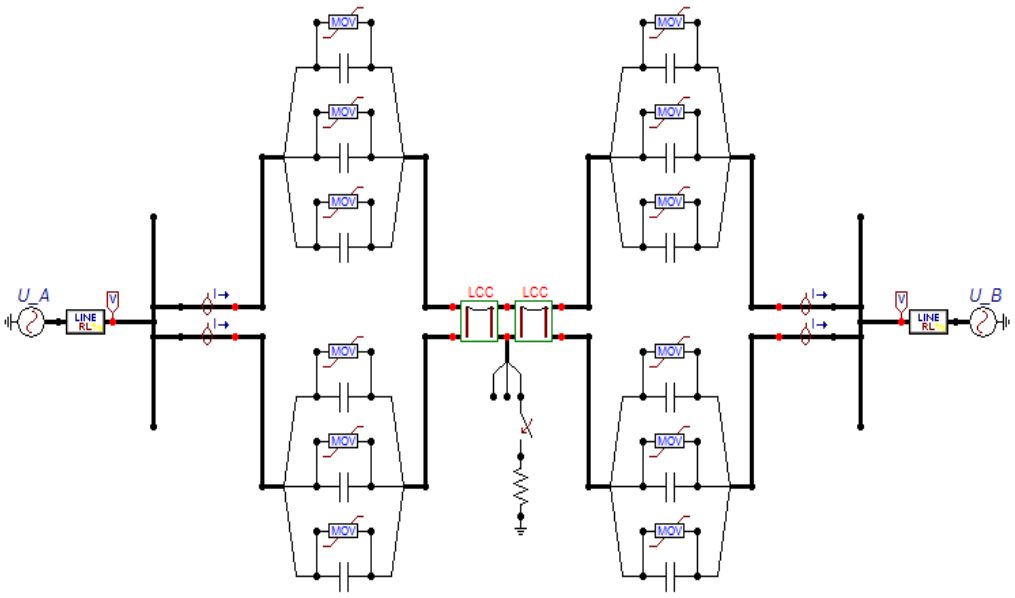

Figure 5.5: Test circuit for double circuit series compensated lines

As before, the method proposed in [131] was used in this FLA to remove the DC component of the current prior to the FFT. All errors presented in the results section are in accordance with IEEE standards [132] using (4.70).

Table 5.2: Network parameters

Network Parameters	Local Network A	Remote Network B
Line to Line RMS Voltage (kV)	416	400
Phase Angle (^{o})	0	-20
+ve seq. Resistance (Ω)	1.019	0.637
+ve seq. Inductance (H)	0.051	0.031
$Z_1 = R_1+jX_1$	1.019+j16	0.637+j10
X_1/R_1	15.7	15.7
0 seq. Resistance (Ω)	2.037	1.273
0 seq. Inductance (H)	0.102	0.064
$Z_0 = R_0+jX_0$	2.037+j32	1.273+j20
X_0/R_0	15.7	15.7
Fault MVA	45MVA	70MVA

Table 5.3: Transmission line parameters

Transmission Line Parameters	Positive/Negative Sequence	Zero Sequence
Resistance, Ω/km	0.0264	0.282
Inductance mH/km	1.014	3.271
Capacitance nF/km	12.5	9.2
R Ω /km	0.0264	0.282
X Ω /km	0.3187	1.027
B S/km	0.3926×10^{-5}	0.289×10^{-5}
X/R	12.07	3.641

5.5.1. Algorithm Accuracy for Symmetrical Faults on Transposed Lines

Section 5.2.1.1 discussed the derivation of the algorithm for three-phase symmetrical faults on transposed lines. An example simulation of a three-phase to earth fault was carried out in ATP-EMTP, at a distance of 40 km from the sending end of a 100 km J-Marti double circuit transposed line. The degree of compensation used was 40% and the line was compensated at both line-ends equally. A high resistance fault (50 Ω) was simulated as such faults are known to be problematic in fault distance calculations (as discussed in Chapter 2). Tests for ground faults and higher fault resistances are carried out later in this section. Waveforms for the local and remote line-end measurements are shown in Figure 5.6 and Figure 5.7. They show the current and voltage for both pre-fault and fault conditions used in the computation of the algorithm.

The fault was simulated to occur at 0.043 sec, and the FFT data window size used was 20 ms. The phasors thus obtained, are input to the expression for distance to fault in (5.14). Figure 5.8 shows the distance to fault vs. time stamp plot. It can be seen that after a short convergence period the fault distance shows a steady value. The time-stamp shown in the plot corresponds to the first time stamp of the FFT data window used in obtaining the phasors for the measurements corresponding to the fault distance estimate shown on the y-axis. An average was carried out for the estimates between 0.06s and 0.1s. The corresponding result for the distance to fault was 0.40117 or 40.12 km.

To thoroughly evaluate the accuracy of the algorithm, similar to the tests carried out in Chapter 4, 50 km and 100 km lines are used to test the algorithm for a variety of fault resistances. The results of each test are shown in Table 5.4 and Table 5.5. The algorithm performs accurately in each case. Once again, it can be noticed that the errors are approximately equal for a given fault location despite an increase in fault resistance. This is due to the fact that the sum of the phase currents through the fault resistance is equal to zero, thus the fault is not affected by the high the fault resistance as there is no current flowing through the resistance. In a symmetrical system, a three-phase to ground fault on a transposed line would lead to phase currents during fault being equal in magnitude and balanced, such that the total current is equal to zero. So although there is a contribution from each phase the vector sum is zero. Therefore, voltage drop across a 100Ω fault resistance and a 10Ω fault resistance for such a case is the same (this voltage magnitude = IR = 0).

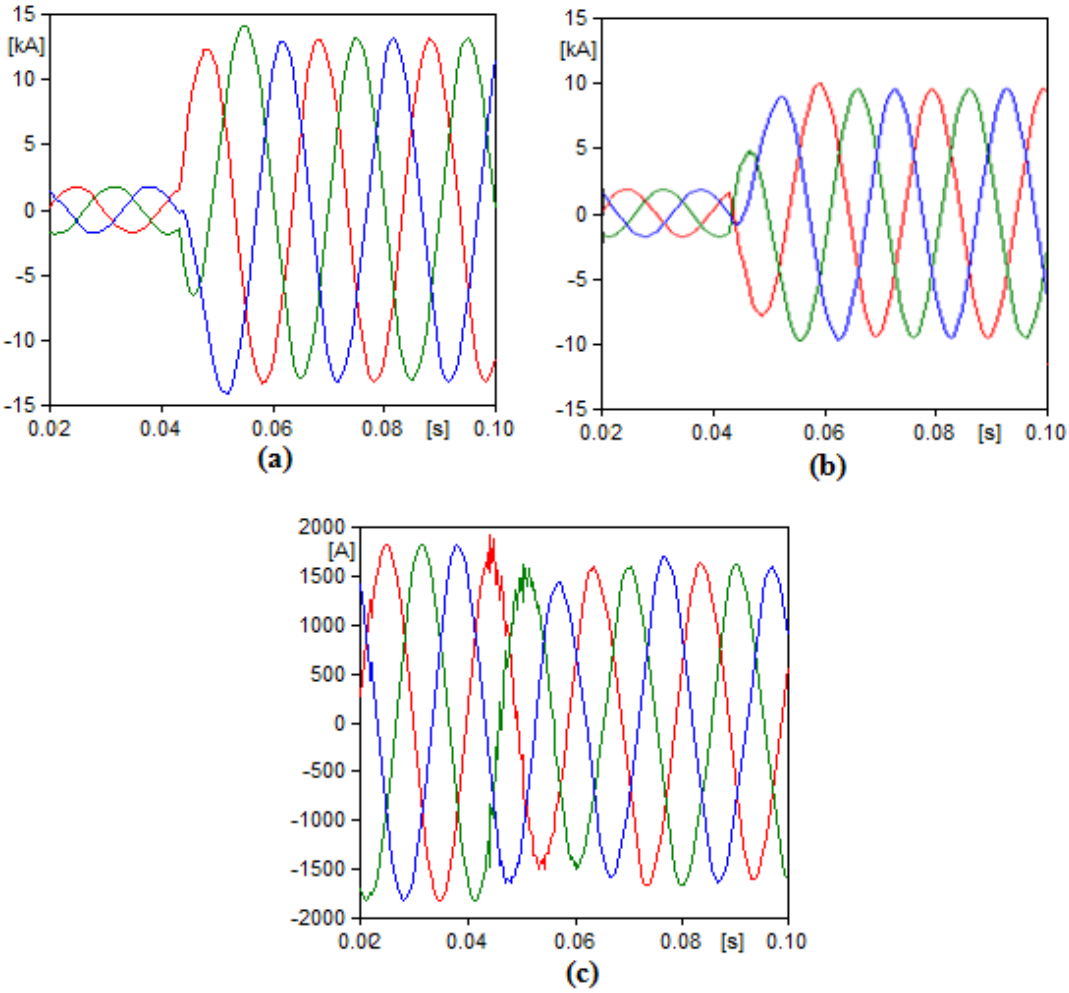

Figure 5.6: Symmetrical fault on a transposed line: a) Local line-end currents of faulted circuit b) Remote line-end currents of faulted circuit c) Currents through healthy circuit (neighbouring circuit on double circuit line)

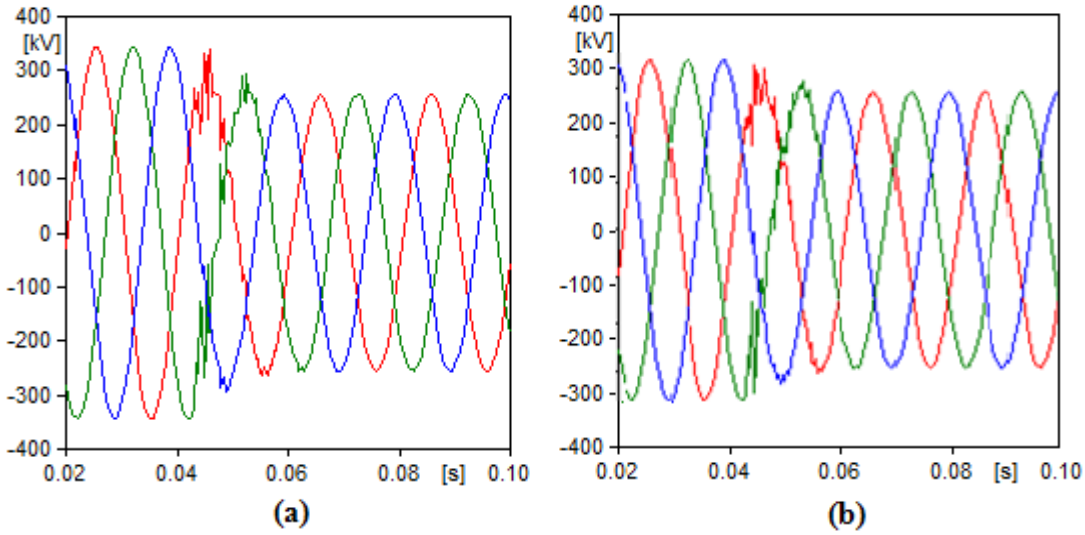

Figure 5.7: Symmetrical fault on a transposed line: a) Local line-end voltages b) Remote line-end voltages

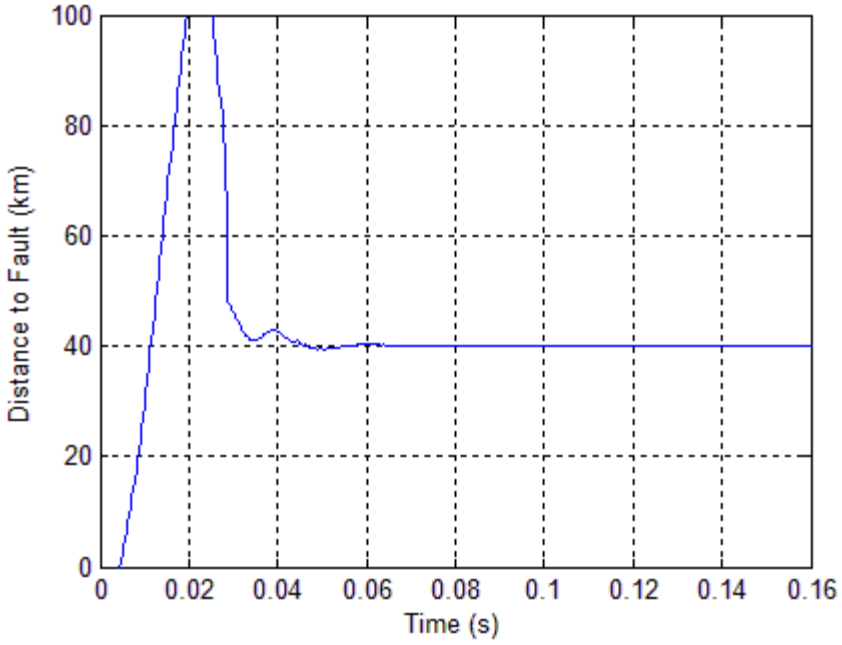

Figure 5.8: Distance to fault vs. time stamp for 'symmetrical faults on transposed lines'

Table 5.4: Sensitivity of algorithm for 'symmetrical faults on transposed lines' to fault resistance- 50 km line

Fault Type	Error of Estimated Fault Location(%)						
	Actual Fault Location (% of line length)						
	10	25	35	50	65	80	90
	Line Length = 50km						
ABC-G $R_F = 0\Omega$	0.66	0.06	0.81	0.11	0.09	0.88	0.31
ABC-G $R_F = 1\Omega$	0.66	0.08	0.81	0.11	0.09	0.87	0.31
ABC-G $R_F = 10\Omega$	0.67	0.08	0.79	0.11	0.10	0.87	0.31
ABC-G $R_F = 100\Omega$	0.67	0.08	0.79	0.11	0.10	0.87	0.31

Table 5.5: Sensitivity of algorithm for 'symmetrical faults on transposed lines' to fault resistance- 100 km line

Fault Type	Error of Estimated Fault Location(%)						
	Actual Fault Location (% of line length)						
	10	25	35	50	65	80	90
	Line Length =100km						
ABC-G $R_F = 0\Omega$	0.20	0.14	0.73	0.79	0.75	0.03	0.76
ABC-G $R_F = 1\Omega$	0.20	0.12	0.72	0.79	0.75	0.02	0.76
ABC-G $R_F = 10\Omega$	0.20	0.12	0.72	0.79	0.75	0.03	0.76
ABC-G $R_F = 100\Omega$	0.20	0.12	0.72	0.79	0.75	0.03	0.76

5.5.2. Algorithm Accuracy for Asymmetrical Faults on Transposed Lines

A DLG fault was simulated at a distance of 40 km from the one end of a two terminal 100 km untransposed J-Marti line. The degree of compensation was 40% for the line, compensated at both ends equally (20% at each end). The corresponding current and

voltage waveforms over sufficient periods of pre-fault and fault conditions are shown in Figure 5.9 and Figure 5.10. The fault was simulated to occur at 43 ms. The FFT window size and fault resistance simulated are equal to those used in the previous section. The method derived in Section 5.2.1.2. is specific for all asymmetrical faults occurring on double circuit transposed line, and was used to calculate the distance to fault. The distance to fault vs. time stamp plot is shown in Figure 5.11. The calculated average of distance to fault (between 0.06s and 0.1s) was 0.40381 or 40.38 km. This test was repeated for a variety of fault types, fault locations and for various fault resistances on a transposed 50 km and 100 km line. The corresponding results have been tabulated in Table 5.6 -Table 5.9. The algorithm is found to be accurate in each case. It can be seen the fault location estimate does not change significantly on varying the fault resistance. Although high resistance faults rarely occur on a power line, they are shown to demonstrate the accuracy of the algorithm for various possible fault conditions.

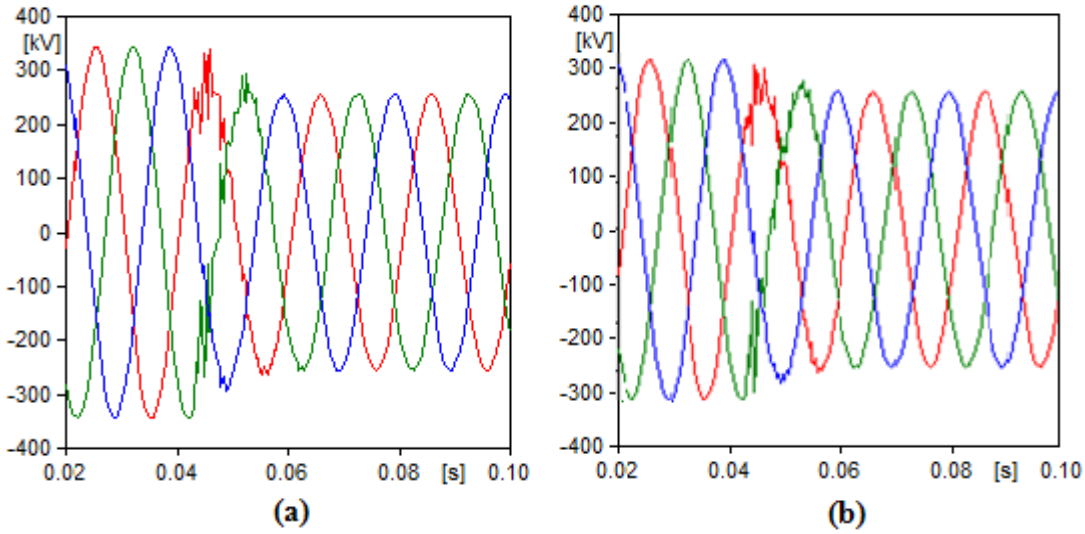

Figure 5.9: DLG Fault on a transposed line: a) Local line-end voltages b) Remote line-end voltages

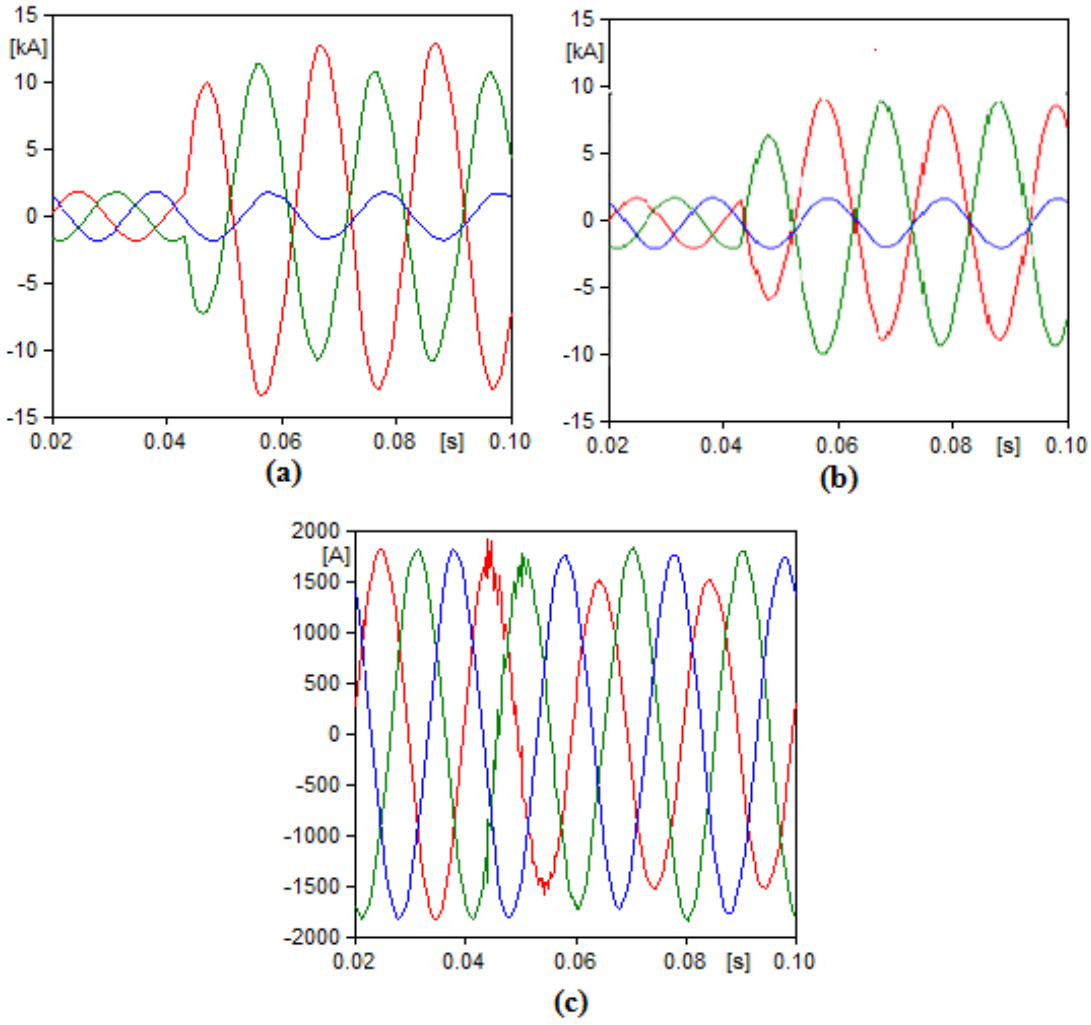

Figure 5.10: DLG fault on a transposed line: a) Local line-end currents of faulted circuit b) Remote line-end currents of faulted circuit c) Currents through healthy circuit (neighbouring circuit on double circuit line)

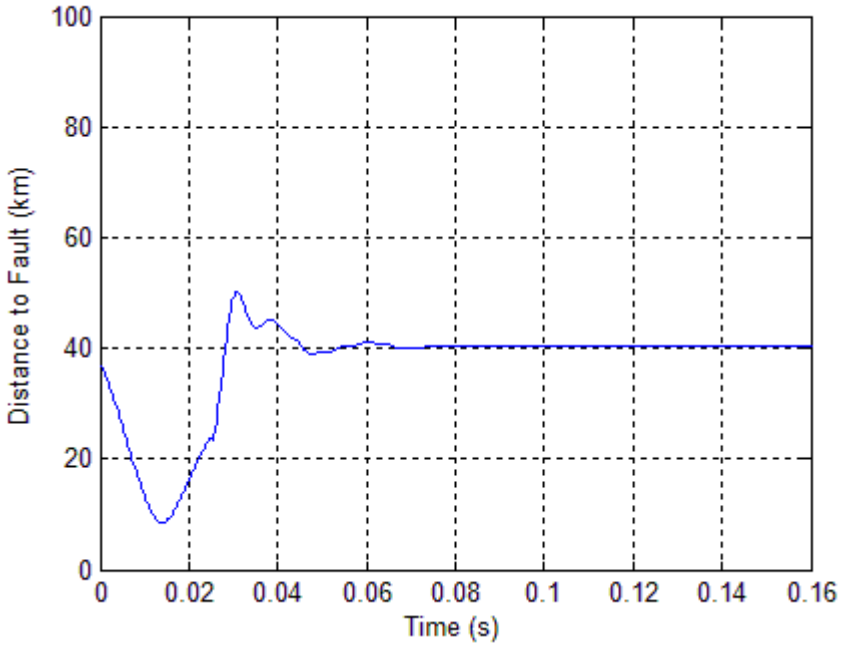

Figure 5.11: Distance to fault vs. time stamp

Table 5.6 Sensitivity of algorithm for 'SLG faults on transposed lines' to fault resistance-50km

Fault Type	Error of Estimated Fault Location(%)						
	Actual Fault Location (% of line length)						
	10	25	35	50	65	80	90
	Line Length = 50km						
A-G $R_F = 0\Omega$	0.15	0.31	0.25	0.43	0.27	0.55	0.37
A-G $R_F = 1\Omega$	0.65	0.41	0.35	0.59	0.36	0.68	0.41
A-G $R_F = 10\Omega$	0.82	0.64	0.39	0.61	0.41	0.71	0.46
A-G $R_F = 100\Omega$	0.91	0.55	0.37	0.61	0.47	0.71	0.53

Table 5.7 Sensitivity of algorithm for 'SLG faults on transposed lines' to fault resistance - 100km

Fault Type	Error of Estimated Fault Location(%)						
	Actual Fault Location (% of line length)						
	10	25	35	50	65	80	90
	Line Length =100km						
A-G $R_F = 0\Omega$	0.16	0.50	0.27	0.46	0.26	0.32	0.09
A-G $R_F = 1\Omega$	0.27	0.61	0.33	0.53	0.81	0.51	0.21
A-G $R_F = 10\Omega$	0.31	0.60	0.38	0.61	0.88	0.67	0.21
A-G $R_F = 100\Omega$	0.35	0.63	0.38	0.70	0.91	0.95	0.46

Table 5.8: Sensitivity of algorithm for 'DL and DLG faults on transposed lines' to fault resistance – 50 km

Fault Type	Error of Estimated Fault Location(%)						
	Actual Fault Location (% of line length)						
	10	25	35	50	65	80	90
	Line Length = 50km						
AB-G $R_F = 0\Omega$	0.29	0.48	0.15	0.08	0.19	0.61	0.42
AB-G $R_F = 100\Omega$	0.50	0.51	0.22	0.17	0.23	0.55	0.43
AB $R_F = 0\Omega$	0.50	0.55	0.27	0.22	0.76	0.91	0.49
AB $R_F = 100\Omega$	0.84	0.80	0.35	0.27	0.77	0.89	0.33

Table 5.9: Sensitivity of algorithm for 'DL and DLG faults on transposed lines' to fault resistance – 100km

Fault Type	Error of Estimated Fault Location(%)						
	Actual Fault Location (% of line length)						
	10	25	35	50	65	80	90
	Line Length =100km						
AB-G $R_F = 0\Omega$	0.10	0.23	0.09	0.29	0.19	0.02	0.19
AB-G $R_F = 100\Omega$	0.27	0.44	0.35	0.39	0.27	0.41	0.32
AB $R_F = 0\Omega$	0.33	0.47	0.40	0.45	0.36	0.22	0.63
AB RF = 100Ω	0.34	0.57	0.41	0.46	0.36	0.27	0.45

5.5.3. Algorithm Accuracy for Faults on Untransposed Lines

An example simulation was carried out as follows. A DLG fault was simulated at 40 km from the local line-end of a double-circuit line. An untransposed J-Marti line was used with a total line length of 100 km. The line was compensated at both line-ends equally and at a degree of 40%. The fault resistance was chosen as 50 Ω. As with previous simulations the fault was simulated to occur at 43 ms, and the data window used for FFT was 20ms. The corresponding current and voltage waveforms over sufficient periods of pre-fault and fault conditions are shown in Figure 5.12 and Figure 5.13. The expression for distance to fault in (5.45) was used. The distance to fault vs. time stamp plot has been shown in Figure 5.14. The calculated average result is 0.4071 or 40.71 km. The method in Section 0 is capable of locating faults for SLG, DLG, DL and symmetrical three-phase faults on untransposed double circuit lines. This test was repeated for each of these fault types for a variety of fault locations on a 50km line and a 100km line and for various fault resistances. The corresponding fault distance estimates have been tabulated in Table 5.10 - Table 5.15.

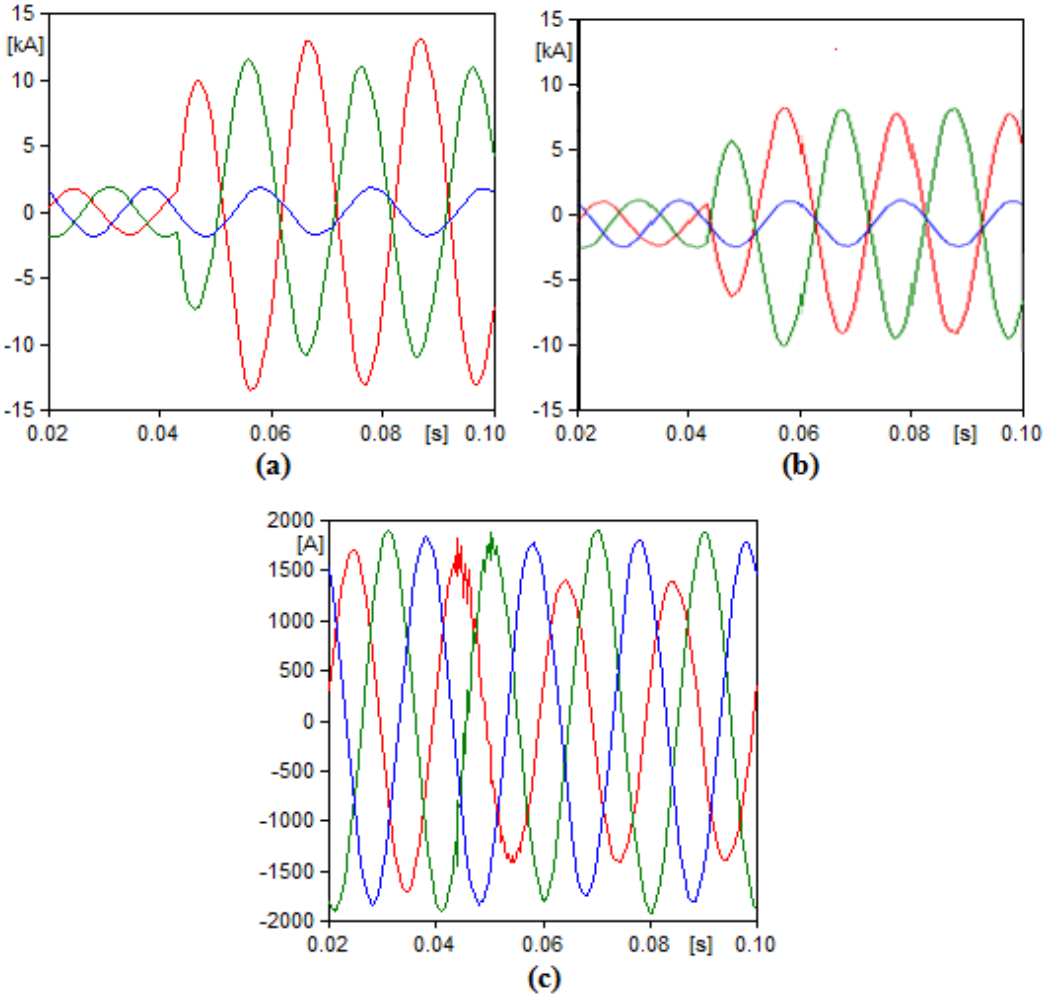

Figure 5.12: DLG fault on an untranposed line: a) Local line-end currents of faulted circuit b) Remote line-end currents of faulted circuit c) Currents through healthy circuit (neighbouring circuit on double circuit line)

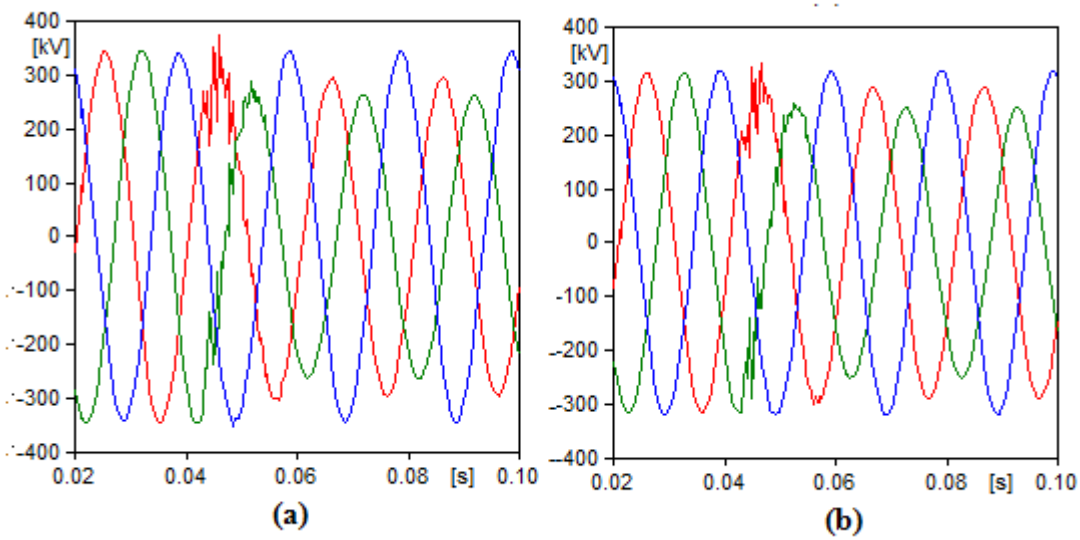

Figure 5.13: DLG fault on an untranposed line: a) Local line-end voltages b) Remote line-end voltages

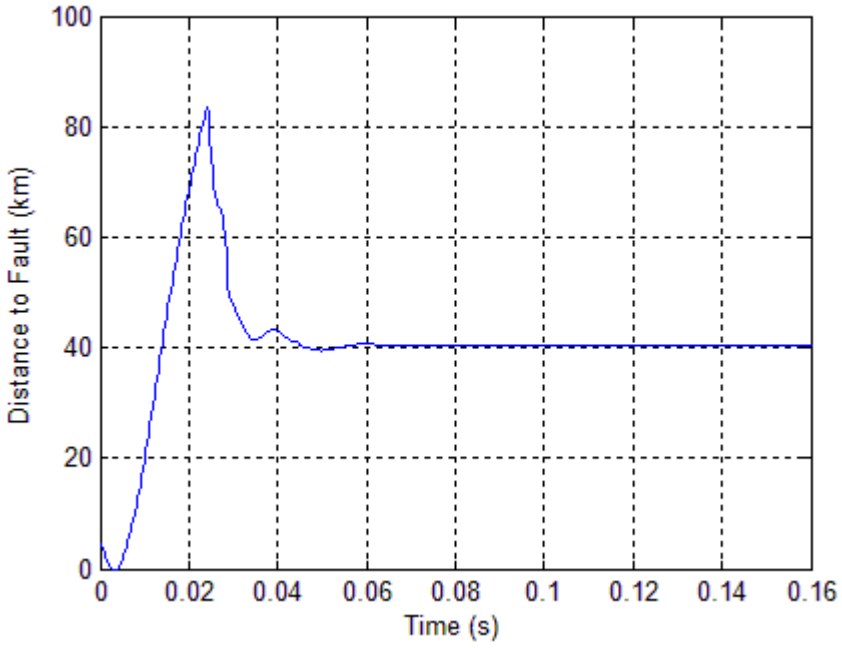

Figure 5.14: Fault distance vs. time stamp for 'DLG faults on untransposed lines'

Table 5.10: Sensitivity of algorithm for 'SLG faults on untransposed lines' to fault resistance – 50km

Fault Type	Error of Estimated Fault Location(%)						
	Actual Fault Location (% of line length)						
	10	25	35	50	65	80	90
	Line Length = 50km						
A-G $R_F = 0\Omega$	0.40	0.79	0.03	0.86	0.27	0.68	0.27
A-G $R_F = 1\Omega$	0.68	0.31	0.93	0.87	0.12	0.27	0.63
A-G $R_F = 10\Omega$	0.88	0.89	0.70	0.74	0.40	0.65	0.26
A-G $R_F = 100\Omega$	0.51	0.88	0.14	0.13	0.88	0.90	0.44

Table 5.11: Sensitivity of algorithm for 'SLG faults on untransposed lines' to fault resistance – 100km

Fault Type	Error of Estimated Fault Location(%)						
	Actual Fault Location (% of line length)						
	10	25	35	50	65	80	90
	Line Length =100km						
A-G $R_F = 0\Omega$	0.27	0.53	0.67	0.08	0.37	0.67	0.17
A-G $R_F = 1\Omega$	0.70	0.93	0.41	0.12	0.06	0.45	0.97
A-G $R_F = 10\Omega$	0.04	0.66	0.40	0.85	0.59	0.56	0.58
A-G $R_F = 100\Omega$	0.60	0.91	0.68	0.36	0.88	0.52	0.57

Table 5.12: Sensitivity of algorithm for 'DL and DLG faults on untransposed lines to fault resistance - 50km

Fault Type	Error of Estimated Fault Location(%)						
	Actual Fault Location (% of line length)						
	10	25	35	50	65	80	90
	Line Length = 50km						
AB-G $R_F = 0\Omega$	0.73	0.43	0.42	0.76	0.76	0.44	0.12
AB-G $R_F = 100\Omega$	0.12	0.57	0.91	0.96	0.30	0.44	0.09
AB $R_F = 0\Omega$	0.07	0.86	0.77	0.39	0.85	0.66	0.28
AB $R_F = 100\Omega$	0.67	0.33	0.50	0.79	0.86	0.02	0.74

Table 5.13: Sensitivity of algorithm for 'DL and DLG faults on untransposed lines to fault resistance -100km

Fault Type	Error of Estimated Fault Location(%)						
	Actual Fault Location (% of line length)						
	10	25	35	50	65	80	90
	Line Length =100km						
AB-G $R_F = 0\Omega$	0.99	0.74	0.71	0.21	0.62	0.89	0.34
AB-G $R_F = 100\Omega$	1.00	0.90	0.09	0.01	0.10	0.60	0.91
AB $R_F = 0\Omega$	0.16	0.30	0.17	0.61	0.79	0.66	0.85
AB $R_F = 100\Omega$	0.18	0.73	0.59	0.56	0.88	0.57	0.39

Table 5.14: Sensitivity of algorithm for '3-phase symmetrical faults on untransposed lines' to fault resistance – 50km

Fault Type	Error of Estimated Fault Location(%)						
	Actual Fault Location (% of line length)						
	10	25	35	50	65	80	90
	Line Length = 50km						
ABC-G $R_F = 0\Omega$	0.63	0.74	0.81	0.21	0.72	0.51	0.25
ABC-G $R_F = 1\Omega$	0.38	0.68	0.08	0.34	0.10	0.72	0.64
ABC-G $R_F = 10\Omega$	0.15	0.35	0.16	0.32	0.63	0.67	0.57
ABC-G $R_F = 100\Omega$	0.22	0.08	0.40	0.81	0.69	0.33	0.33

Table 5.15: Sensitivity of algorithm for '3-phase symmetrical faults on untransposed lines' to fault resistance -100km

Fault Type	Error of Estimated Fault Location(%)						
	Actual Fault Location (% of line length)						
	10	25	35	50	65	80	90
	Line Length =100km						
ABC-G $R_F = 0\Omega$	0.90	0.87	0.64	0.25	0.81	0.13	0.04
ABC-G $R_F = 1\Omega$	0.30	0.77	0.59	0.06	0.36	0.62	0.03
ABC-G $R_F = 10\Omega$	0.05	0.55	0.09	0.62	0.10	0.71	0.71
ABC-G $R_F = 100\Omega$	0.06	0.42	0.74	0.61	0.28	0.16	0.72

5.5.4. Algorithm Accuracy for Various Locations of Series Compensation

By the use of the appropriate SC coefficients, the expressions for distance to fault for each category of fault types can be modified based on the method described in Section 4.2.4, such that it can be applied for every common location of series compensation installation.

The results for various tests carried out with the aim of validating the algorithm for different series capacitor installation locations are tabulated in Table 5.16. All the common cases were been considered i.e. series compensated at local line-end only, at remote line-end only, middle of the line and both ends of the line. Different fault types (SLG, DLG, DL, 3-Phase averaged) were considered and in each case a fault resistance of 100 Ω was used in the simulations of a 100km untransposed line. The fault in each case was simulated to occur at 30km. A degree of series compensation of 40% based on the total reactance of the series capacitor/capacitors installed on the line was used in each case. The fault distance was varied between 10% to 90% of the total line length. It can be seen that the algorithm performs accurately in each case. The VT was always simulated at the bus for the results shown in Table 5.16. The results for a line compensated at the local line-end only with the VT on the line side in shown in Table 5.17.

Table 5.16: Sensitivity of algorithm to location of series compensation

Location of Ser.Comp.	Fault Resistance (Ω)	Actual Fault Location (% of line length)						
		Error of Estimated Fault Location(%)						
		10	25	35	50	65	80	90
Local Line-End Only	SLG	0.00	0.94	0.65	0.61	0.08	0.56	0.68
	DLG	0.73	0.74	0.94	0.61	0.91	0.89	0.28
	DL	0.04	0.63	0.68	0.56	0.02	0.60	0.02
	3-Phase	0.06	0.39	0.67	0.92	0.77	0.50	0.69
Remote Line-End Only	SLG	0.30	0.53	0.23	0.60	0.07	0.88	0.22
	DLG	0.33	0.84	0.05	0.65	0.43	0.00	0.32
	DL	0.35	0.27	0.49	0.55	0.10	0.21	0.16
	3-Phase	0.38	0.49	0.38	0.87	0.71	0.25	0.71
Middle of Line	SLG	0.28	0.01	0.92	0.52	0.12	1.00	0.18
	DLG	0.37	0.10	0.25	0.07	0.95	0.33	0.74
	DL	0.11	0.81	0.81	0.30	0.52	0.20	0.66
	3-Phase	0.52	0.56	0.35	0.94	0.30	0.16	0.03
Both Ends of Line	SLG	0.39	0.82	0.10	0.59	0.86	0.34	0.51
	DLG	0.40	0.23	0.82	0.50	0.88	0.63	0.95
	DL	0.36	0.87	0.48	0.77	0.75	0.25	0.59
	3-Phase	0.66	0.77	0.14	0.42	0.99	0.21	0.51

Table 5.17: Sensitivity of algorithm to location of VT in relation to SC

Location of Ser.Comp.	Fault Resistance (Ω)	Actual Fault Location (% of line length)						
		Error of Estimated Fault Location(%)						
		10	25	35	50	65	80	90
Local Line-End Only, VT on line side	SLG	0.64	0.50	0.60	0.05	0.16	0.27	0.03
	DLG	0.30	0.92	0.23	0.51	0.92	0.46	0.67
	DL	0.01	0.84	0.43	0.81	0.63	0.31	0.59
	3-Phase	0.49	0.52	0.42	0.30	0.74	0.67	0.94
Local Line-End Only, VT on bus side	SLG	0.00	0.94	0.65	0.61	0.08	0.56	0.68
	DLG	0.73	0.74	0.94	0.61	0.91	0.89	0.28
	DL	0.04	0.63	0.68	0.56	0.02	0.60	0.02
	3-Phase	0.06	0.39	0.67	0.92	0.77	0.50	0.69

5.5.5. Algorithm Accuracy for Synchronisation Error Correction

This section considers the effect of synchronising two-terminal phasors based on the method described in Section 5.3 on the accuracy of the algorithm where there may be a considerable synchronisation error. Whilst synchronisation was carried out with a reasonably good accuracy, there was still a small but negligible synchronisation error due to not considering shunt admittance currents. The algorithm for symmetrical faults on transposed lines does not require any synchronisation of measurements, and therefore it is not considered here. Algorithms for the other two categories of faults, i.e. for asymmetrical faults on transposed and untransposed lines were tested. The fault resistance, fault inception time, data window size used were identical to the previously described simulations.

SLG faults were simulated for transposed and untransposed 100 km lines, for a variety of fault distances (10%-90%) and varying synchronisation errors (0-1000 μs). This was carried out by introducing a corresponding delay in the time stamp of the remote line-end phasors in MATLAB. Series compensation was set at 40% at both ends of the line. The algorithm was run for each case after the synchronisation error correction was carried out. The errors for each case have been tabulated in Table 5.18 and Table 5.19. A similar pattern to Section 4.3.5 in Chapter 4 is observed in the tables of results due to the same

reason, i.e. that the final synchronisation error after the correction procedure is always equal, thus giving the exact results in each case.

Table 5.18: Sensitivity of algorithm to synchronisation error (SLG fault on transposed lines)

Synchronisation Error (μs)	Actual Fault Location (% of line length)						
	Error of Estimated Fault Location(%)						
	10	25	35	50	65	80	90
Without synchronisation error correction							
0	0.03	0.57	0.86	0.10	0.21	0.89	0.36
With synchronisation error correction							
50	0.41	0.08	0.39	0.63	0.77	0.35	0.07
100	0.41	0.08	0.39	0.63	0.77	0.35	0.07
200	0.41	0.08	0.39	0.63	0.77	0.35	0.07
600	0.41	0.08	0.39	0.63	0.77	0.35	0.07
1000	0.41	0.08	0.39	0.63	0.77	0.35	0.07

Table 5.19: Sensitivity of algorithm to synchronisation error (SLG fault on untransposed lines)

Synchronisation Error (μs)	Actual Fault Location (% of line length)						
	Error of Estimated Fault Location(%)						
	10	25	35	50	65	80	90
Without synchronisation error correction							
0	0.55	0.33	0.65	0.45	0.26	0.10	0.83
With synchronisation error correction							
50	0.80	0.34	0.83	0.58	0.30	0.51	0.04
100	0.80	0.34	0.83	0.58	0.30	0.51	0.04
200	0.80	0.34	0.83	0.58	0.30	0.51	0.04
600	0.80	0.34	0.83	0.58	0.30	0.51	0.04
1000	0.80	0.34	0.83	0.58	0.30	0.51	0.04

5.5.6. Algorithm Accuracy for Various Degrees of Series Compensation

The algorithm was tested for various degrees of series compensation, by inputting the appropriate value of series capacitor reactance in the algorithm as explained in Section 5.2. Uncompensated lines are also tested by inputting a zero series capacitor reactance. The range of degrees of series compensation considered here are (10%-50%). Each case is based on a simulation of a 100km line compensated at both line-ends, DLG fault, fault resistance of 100 Ω, fault inception time of 43 ms and data window size of 20ms. The algorithm is found to be accurate even for high degrees of series compensation.

Table 5.20: Sensitivity of algorithm to degree of series compensation

Level of Series Compensation (%)	Actual Fault Location (% of line length)						
	Error of Estimated Fault Location(%)						
	10	25	35	50	65	80	90
0	0.27	0.34	0.05	0.35	0.08	0.05	0.68
10	0.48	0.27	0.22	0.01	0.71	0.84	0.64
20	0.17	0.42	0.88	0.62	0.73	0.30	0.15
30	0.62	0.25	0.31	0.91	0.68	0.73	0.79
40	0.55	0.90	0.40	0.93	0.88	0.13	0.36
50	0.05	0.09	0.41	0.39	0.74	0.38	0.31

5.5.7. Algorithm Accuracy for Longer Lines

All tests so far have been carried out for 50km and 100km lines, and the accuracy is found to be high, as the shunt admittance currents do not have a significant influence on the accuracy at such line lengths. Tests are carried out in this section for a line length of 300km. The tests carried out were repeated exactly as in the case of Section 5.5.2 in every other respect. The errors tabulated in Table 5.21 are found to be significantly worse than those for 100km lines and 50 km lines. As was the case of the novel FLA for single- circuit lines, the accuracy is acceptable in most cases, but not to the order of the results seen in previous tests for shorter lines. This significant difference in accuracy is due to the

algorithm neglecting the shunt admittance of the line. Shunt admiitance has a considerable impact on fault location accuracy for lines longer than 200km.

Table 5.21: Sensitivity of algorithm to increasing the length of the line (300km)

Location of Ser.Comp.	Fault Resistance (Ω)	Actual Fault Location (% of line length)						
		Error of Estimated Fault Location(%)						
		10	25	35	50	65	80	90
Local Line-End Only	SLG	0.18	1.60	0.88	1.10	1.55	1.68	0.65
	DLG	1.12	1.42	0.52	0.01	0.77	1.37	1.38
	DL	1.96	0.76	1.26	1.56	0.30	1.31	1.58
	3-Phase	0.63	1.80	0.82	2.05	0.33	1.40	1.37
Remote Line-End Only	SLG	1.10	1.48	0.07	1.92	0.39	1.30	1.62
	DLG	0.57	1.55	1.99	0.12	0.38	2.12	0.27
	DL	0.52	1.14	1.24	1.16	0.13	0.32	0.91
	3-Phase	1.06	1.05	0.17	0.80	0.66	0.79	1.13
Middle of Line	SLG	0.87	1.07	1.29	1.08	0.96	0.64	0.29
	DLG	1.07	0.34	1.78	0.16	0.54	1.10	0.61
	DL	0.62	2.36	0.31	1.11	0.94	1.29	1.02
	3-Phase	1.05	1.47	1.48	1.85	1.81	1.38	1.55
Both Ends of Line	SLG	2.01	1.85	0.44	1.37	1.23	0.32	1.42
	DLG	0.13	2.68	0.99	0.89	0.44	1.46	0.92
	DL	0.85	0.96	1.72	1.17	1.08	1.56	0.61
	3-Phase	0.30	0.90	1.47	0.06	0.50	1.84	1.28

5.5.8. Algorithm Accuracy for Faults Close to Line Ends

For this section, the tests carried out thus far for various fault types on untransposed lines are repeated but for faults at 1% and 99% of the line. This test was carried out for a variety of fault locations on a 50km line and a 100km line and for various fault resistances and fault types. The corresponding fault distance estimates have been tabulated in Table 5.22. As is the case with the algorithm presented in Chapter 4, the FLA for double circuit lines is also found to be largely inaccurate for faults at line-ends. It can be observed that these errors in distance to fault are unacceptably high for faults close to the line terminals. Errors

for three-phase faults are slightly less severe in comparison to SLG, DL and DLG faults. An important assumption used in the derivation of the algorithms is that the shunt admittance currents are negligible and that the measured line-terminal currents are equal to the series currents in the line. Whilst this assumption was found to be acceptable for fault distances simulated between 10% and 90%, for faults closer to the line-ends such as those presented in this section, the assumption is grossly violated.

The inaccuracy for line-end faults is a significant drawback of this FLA. For this reason, as well as to improve the overall accuracy of the FLA including for faults closer to the line, methods to account for shunt admittance of the line in a line-parameter free manner are to be developed by the author as part of future work. Such a method is presented in Chapter 7 though it is currently limited to uncompensated single-circuit lines. It is hoped that this work may be extended in future using similar principles to include double-circuit series compensated lines and thereby address the shortcoming highlighted in this section. The operation of the MOV is another contributing factor to the level of inaccuracy in such cases is that the presence of very high fault currents (for solid earth and low fault resistances).

Table 5.22: Sensitivity of algorithm to increasing the length of the line (300km)

Fault Type	50 km line		100 km line	
	1%	99%	1%	99%
A-G RF = 0Ω	3.47	2.66	4.67	3.14
A-G RF = 100Ω	1.46	2.13	3.73	2.72
AB-G RF = 0Ω	2.57	1.50	3.96	1.10
AB-G RF = 100Ω	1.18	2.70	2.78	2.94
AB RF = 0Ω	3.40	2.03	1.13	2.42
AB RF = 100Ω	3.78	1.85	4.10	2.20
ABC-G RF = 0Ω	0.84	0.31	1.14	1.27

ABC-G RF = 100Ω	0.66	1.20	1.19	1.83

5.5.9. Algorithm Accuracy –Varying Fault Levels

Thus far the network parameters detailed in Table 5.2 were used in the simulations and in the results presented. This section investigates the influence of varying the source fault levels as calculated at the local and remote ends of the line (where the measurements are taken). Combination-1 and Combination-2 used in Chapter 4 are repeated here for this analysis and are presented in Table 5.23 and

Table **5.24**. Combination-1 implements the source impedances of lower magnitudes than the case considered in the previous sections (and therefore higher fault level MVAs). Combination-2 on the other hand implements source impedances of larger magnitudes than the case considered in the previous sections (and therefore lower fault level MVAs). The network parameters for these two new cases are detailed in Table 5.23 and

Table **5.24**. A set of simulation tests is carried out using these new fault levels. The line parameters used previously are repeated here. Other aspects of the simulation are repeated as carried out in the previous section. The results for various fault types and fault resistances are presented in Table 5.25.

Table 5.23: Combination-1 (144 MVA, 89 MVA)

Network Parameters	Local Network A	Remote Network B
Line to Line RMS Voltage (kV)	416	400
Phase Angle (^{o})	0	-20
+ve seq. Resistance (Ω)	0.318	0.510
+ve seq. Inductance (H)	0.016	0.025
$Z_1 = R_1+jX_1$	1.019+j5	0.637+j8
X_1/R_1	15.722	15.288
0 seq. Resistance (Ω)	0.637	1.018
0 seq. Inductance (H)	0.032	0.051
$Z_0 = R_0+jX_0$	0.635+j10	1.0184+j16
X_0/R_0	15.731	15.794

Fault MVA	143.912	88.927

Table 5.24: Combination-2 (36 MVA, 47 MVA)

Network Parameters	Local Network A	Remote Network B
Line to Line RMS Voltage (kV)	416	400
Phase Angle (^{o})	0	-20
+ve seq. Resistance (Ω)	1.274	0.956
+ve seq. Inductance (H)	0.064	0.047
$Z_1 = R_1+jX_1$	1.019+j20	0.637+j15
X_1/R_1	15.723	15.288
0 seq. Resistance (Ω)	2.546	1.910
0 seq. Inductance (H)	0.128	0.096
$Z_0 = R_0+jX_0$	2.546+j40	1.909+j30
X_0/R_0	15.731	15.794
Fault MVA	35.978	47.428

Table 5.25: Results for various fault levels

Fault Type	Fault Resistance (Ω)	Actual Fault Location (% of line length)					
		Combination-1			Combination-2		
		10	50	90	10	50	90
A-G	0	0.43	0.39	0.77	0.46	0.22	0.58
	100	0.58	0.37	0.23	0.59	0.83	0.30
AB	0	0.64	0.57	0.26	0.19	0.15	0.75
	100	0.22	0.16	0.90	0.41	0.62	0.48
AB-G	0	0.45	0.28	0.15	0.23	0.26	0.32
	100	0.26	0.55	0.64	0.49	0.36	0.55
ABC-G	0	0.59	0.80	0.55	0.63	0.78	0.31

	100	0.27	0.57	0.64	0.86	0.34	0.24

The results show that the FLA performs to a equally high level of accuracy for both network combinations used, as well as for the network parameters used in the previous sections. The main reason for this is that the FLA uses the equations describing the relationships between voltage differences across the phases and the phase currents. While one-terminal algorithms are limited in the use of only local-end measurements, two-terminal algorithms such as the FLA discussed in this chapter can be derived through complete descriptions of the voltage-current relationships without the need for gross simplifications. Thus, the voltage difference becomes significant here rather than the absolute voltages measured at the terminals.

Combination-1 implemented source impedances of lower magnitudes of impedances than the case considered in previous sections (and therefore higher fault level MVAs). Combination-2 on the other hand implemented source impedances of larger magnitudes than the case considered in previous sections (and therefore lower fault level MVAs). But for both cases, the accuracy is found to be sufficiently high. Moreover given that the range of source impedances/fault levels used here is broad (35MVA-143MVA) it may be concluded that the algorithm is not sensitive to the source fault level as calculated at the terminals (VTs) in the simulations. Another key advantage of the FLA being a two-terminal FLA can be seen here in that it is not sensitive to the remote-end infeed, despite varying the fault level at terminal-B (47MVA-89MVA).

5.5.10.Discussion of Results

The FLA for double circuit lines is derived on similar principles to those of the FLA for single-circuit lines discussed in Chapter 4. In the previous sections it was shown to be tested for a variety of conditions. The various conditions include various fault distances, fault types, fault resistances, fault levels, degrees and locations of series compensation. The FLA was shown to also be tested for asynchronous measurements, transposed lines, longer line lengths, and for faults close to the line-ends. Overall, the conclusion that can be made

is that the algorithm is found to be highly accurate in a majority of cases. However, the FLA performs to a much lesser degree of accuracy for other cases. An analysis of the performance of the algorithm is carried out here highlighting both its advantages and drawbacks. The trends in the fault distance errors often do not seem to follow a repeatable or predictable pattern. Where this is not the case is discussed in subsequent paragraphs and the reasons for such a lack of predictability are also discussed:

- Observations for errors vs. simulated fault distances: There seems to be a lack of predictability or repeatability in the pattern of errors with respect to increasing fault distances. The reasons are similar to those discussed in the previous chapter for the FLA for single-circuit lines. The FLA requires the solution of very complex non-linear equations in distance to fault involving numerous mathematical calculations in terminal voltages and phase currents. And again, although there is most likely an underlying mathematical pattern in the errors it is not one that may be noticed through mere observation, and would require very complex analysis of the equations to derive and is not in the scope of the thesis. Here too, the "contrast bias" of viewing the numerical errors against one another must also be taken into consideration, that is to say, that the actual jumps with respect to the line length are not as significant as perceived when compared outside context. Thus an error of 0.05 and an error of 0.51 for a 65km line correspond to a fractional distance to fault of 0.6505 and 0.6551.

- Trend observed for "Symmetrical Faults on Transposed Lines": The FLA for this category of faults is derived almost identically to the FLA for single-circuit lines for the same category. Thus again it may be observed that the fault location estimate does not change significantly on varying the fault resistance. To repeat the explanation for this, in a symmetrical system a three-phase to ground fault on a transposed line would lead to phase currents during fault being equal in magnitude and balanced, such that the total current through the fault resistance is equal to zero. So although there is a contribution from each phase the vector sum is zero. Therefore, voltage drop across a 100Ω fault resistance and a 10Ω fault resistance

for such a case is the same (this voltage magnitude = IR = 0). Therefore, the errors are found not to vary with fault resistance.

- Trend observed for "Asynchronous Measurements": The method for synchronisation of asynchronous phasors again is identical to that used in Chapter 4. Therefore, here too similar observations can be made for the rows titled "with synchronisation error correction" tabulate the errors calculated after the correction procedure is carried out. It can be seen that the distance to fault errors are equal for each case despite an increase in synchronisation error. This is because regardless of the synchronisation error, the phase difference between the remote line-end phasors and local line-end phasors is always equal after the correction procedure, provided the synchronisation procedure is carried out and the phasors are not assumed to already be synchronised.

- Decline in accuracy observed for longer lines: The errors in fault distance are seen to be higher in the case of calculations carried out for lines of 300km length. This is owing to the fact that the shunt admittance currents for such line lengths become a significant influence on the distance to fault calculations. The derivations of the FLA do not consider the shunt admittance of the line due to the existing complexity of the equations used. This drawback is to be addressed as part of future work and is discussed briefly in Chapter 8.

- Fault close to line-ends: The FLA performs poorly for faults close to the line-ends i.e. 1% and 99%. The influence of the shunt admittance currents is too significant to be neglected unlike the cases shown for faults between 10% and 90%. It is hoped that an algorithm to accurately account for the shunt admittance of the line will be developed as part of future work.

- With the exception of the aforementioned categories where the FLA performs to a lesser degree of accuracy, it can be concluded that the FLA is accurate for various fault resistances, fault distances, degrees of series compensation, transposed and untransposed lines and for both synchronous and asynchronous measurements.

5.6. Chapter Summary

Fixed series compensation is planned to be installed at a number of locations on the GB network. Of these transmission lines, some are single-circuit lines i.e. the Gretna-Harker 400 kV and the Moffat-Harker 400kV, whilst others are double-circuit lines i.e. Eccles-Stella West 1 and 2. Therefore, in addressing these developments from a fault location perspective, it is necessary to consider both types of lines in the innovation of novel algorithms. Therefore in this Ph.D. project two algorithms were developed, one for each type of line. The novel algorithm developed for single-circuit series compensated lines was discussed in Chapter 4, whilst Chapter 5 discussed the novel algorithm developed for double-circuit series compensated lines.

The FLA discussed in this chapter locates faults on double-circuit series compensated OHTLs in a reliable and accurate manner, without the use of any line parameters. The entirety of the content in this chapter is the original contribution of the author and was derived, designed, developed and tested prior to the proposal of any similar algorithms for such type of lines. The inputs required by the algorithm are the synchronised current and voltage phasors from the two terminals of the line, or synchronously sampled measurement data which can then be converted to phasors using FFT. The novelty of the algorithm lies in that it does not require any line parameters in its calculations and unlike the algorithm described in Chapter 4 it is designed for double-circuit series compensated lines. The advantages of line parameter free solutions such as the ones described in this chapter are that they are more accurate and reliable when considering the actual implementation of these algorithms on transmission lines as opposed to simulation studies with definitive parameters.

The algorithm uses one of three equations in its calculation of distance to fault each corresponding to a category of fault types. These expressions have been derived for transposed lines and untransposed lines. Symmetrical and asymmetrical faults on transposed lines are required to be considered separately. Accurate simulation studies have been used in the validation of these algorithms using a variety of test conditions, and the algorithm was found to be accurate in all cases. The algorithm was also shown to be

applicable to a number of different types of series compensated lines, and capable of locating faults using synchronous as well as asynchronous measurement data. The algorithm is thus, highly accurate, reliable and implementable. However, it is not without its limitations. It is limited in similar ways as the algorithm for single-circuit lines, i.e. slow computation times, sensitivity to shunt admittance currents, and potential inaccuracy due to line sag. The FLA performs poorly for faults close to the line-ends i.e. 1% and 99%. The influence of the shunt admittance currents is too significant to be neglected unlike the cases shown for faults between 10% and 90%. It is hoped that an algorithm to accurately account for the shunt admittance of the line will be developed as part of future work. It too assumes that Rogowski coil CTs are used in the measurements of line-end currents, and therefore no CT saturation is considered. The algorithm must be extended for it to applicable to instances where such CTs are not used and there is considerable distortion in current measurement due to magnetic saturation.

Chapter 6. Comparison Study of Novel Algorithms and Existing Solutions

Chapter 4 and Chapter 5 described the novel algorithms developed during the course of the Ph.D. project. They were each shown to be tested for a variety of fault types, fault distances, fault resistances etc. It was found that they perform to a high level of accuracy in a majority of test cases. Cases where such algorithms are unable to locate faults accurately were identified as shortcomings of the algorithm.

This chapter aims to highlight the significance of the key advantage of these algorithms, that they do not require line parameters. The performance of these algorithms is compared against that of existing solutions detailed in subsequent sections. This comparison is carried out for various fault resistances and fault types. It is to be found that the line parameter free aspect of the algorithms is significant when considering the disparity between pre-determined line parameter settings and the actual parameters on account of changing loading and weather conditions.

Line parameters used typically in the calculations of FLAs vary with weather and loading conditions. This is especially true of zero-sequence parameters. Whilst, positive and negative sequence parameters are calculated based on the geometry, spacing and the material of the conductors, zero sequence parameter calculations also depend on soil resistivity. Soil resistivity is difficult to accurately determine, and varies with weather conditions [133]. This is especially significant in the case of FLAs for double-circuit lines, where zero-sequence mutual impedance between the two circuits greatly affects the accuracy of calculation.

The impact of line parameters was discussed previously in the introduction of Chapter 4. The study carried out by the KEPRI [123] discussed previously is used as the basis for the comparison study carried out in this chapter. In this study, positive sequence and zero sequence impedance measurements for 40 circuits were carried out and compared against

impedances calculated using pre-determined line parameters. Maximum errors of up to 18.9% were found in the positive sequence impedances, and 5 of the 40 circuits showed errors of over 5% (standard deviation of 4.8%). Similarly for zero-sequence impedances, the errors were as high as 18.4%, but 23 out of the 40 circuits had errors greater than 5% (standard deviation of 7.6%). Based on this study, the following guidelines will be used in the comparison carried out in this chapter:

Table 6.1: No disparity, small disparity and high disparity in line parameters

	ΔR_1	ΔX_{L1}	ΔY_1	ΔR_0	ΔX_{L0}	ΔY_0
No Disparity	0%	0%	0%	0%	0%	0%
Small Disparity	20%	5%	15%	20%	8%	25%
High Disparity	30%	15%	25%	30%	18%	30%

The subsequent sections discuss the comparison study carried out for the novel algorithms discussed in this thesis. Section 6.1 details the comparison study for single-circuit series compensated lines, where the algorithm discussed in Chapter 4 is compared against an existing algorithm proposed by Yu et al [134]. Section 6.2 similarly discusses the comparison study for the algorithm discussed in Chapter 5 for double-circuit series compensated lines by comparing it against an existing algorithm proposed by Kang et al [135].

6.1. Comparison of Algorithms for Single-Circuit Series Compensated Lines

6.1.1. Background

The FLA to be used in the comparison for single-circuit lines was proposed by Yu et al [134]. This algorithm was chosen for the comparison firstly since it has similar measurement requirements as the algorithm discussed in Chapter 4. Secondly, it is a highly accurate algorithm applicable to various fault types and fault resistances. The method is not derived here, but the calculations used to arrive at the distance to fault are listed and the

principles behind each step are stated. The FLA uses two-end current and voltage measurements and is carried out in the phasor domain using sequence networks. Similar to the novel algorithm presented in Chapter 4, it is applicable to single-circuit lines and is capable of calculating the distance to fault using both synchronised as well as unsynchronised measurements. It requires the positive sequence and zero sequence line parameters (resistance, inductance and capacitance per unit length) for its calculations. It also takes the shunt admittance of the line into account to be applicable to long lines. The key advantage of the algorithm is that it does not require performing any estimations of the impedance of the SC-MOV combination using Goldsworthy's linearised model or otherwise. It is also found to be accurate regardless of fault resistance, fault type, fault distances or degree of series compensation. However, this is provided the line parameters are acceptably accurate. These line–parameters are used to calculate the characteristic impedances ($Z_c^{(i)}$) and the propagation constants ($\gamma^{(i)}$) which are then used in the distance to fault calculations.

$$Z_c^{(i)} = \sqrt{\frac{z^{(i)}}{y^{(i)}}} \tag{6.1}$$

$$\gamma^{(i)} = \sqrt{z^{(i)} y^{(i)}} \tag{6.2}$$

where $i = 0,1,2$ and is used to denote the sequence component. $z^{(i)}$ and $y^{(i)}$ represent the sequence series impedances and the sequence shunt admittances respectively. The derivation of the algorithm is not carried out in this thesis. However, the mathematical steps constituting the algorithm are stated for completeness sake. The corresponding circuit diagram is shown in Figure 6.1. The terms used in the equations to follow are all defined in Table 6.2. The mathematical steps comprising the algorithm required to arrive at the distance to fault are as follows:

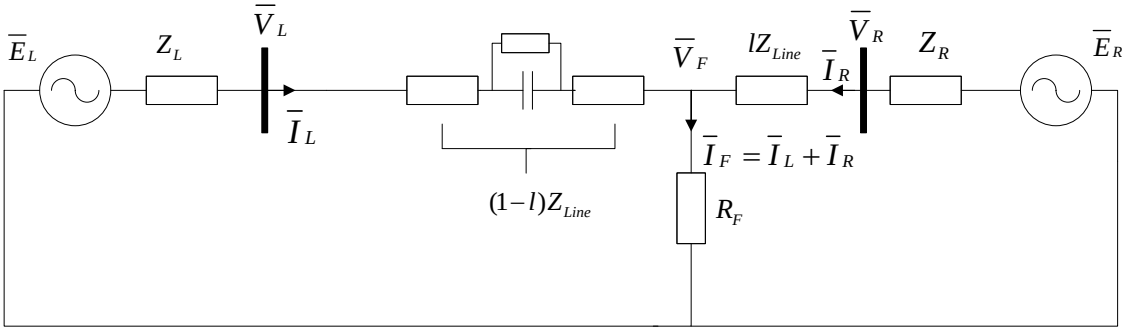

Figure 6.1: Series compensated line under fault

Table 6.2: Terms and definitions

Term	Definition
$\overline{V}_L$	Local line-end voltage
$\overline{V}_R$	Remote line-end voltage
$\overline{I}_L$	Local line-end current
$\overline{I}_R$	Remote line-end current
$\overline{V}_F$	Fault point voltage
$\overline{I}_F$	Fault current
l	Fractional distance to fault
L	Total line length

1. The sequence components of the fault point voltage $\overline{V}_F$ and fault current $\overline{I}_F$ shown in Figure 6.1 are first required to be expressed purely in terms of the distance to fault 'l'. These expressions for these phasors in terms of 'l' are as follows:

$$\overline{I}_F^{(i)} = [\frac{\overline{V}_R^{(i)} + \overline{I}_R^{(i)} Z_C^{(i)}}{2}\exp(\gamma lL) - \frac{\overline{V}_R^{(i)} - \overline{I}_R^{(i)} Z_C^{(i)}}{2}\exp(-\gamma lL)](Z_C^{(i)})^{-1} + [\frac{\overline{V}_L^{(i)} + \overline{I}_L^{(i)} Z_C^{(i)}}{2\exp(\gamma L)}\exp(\gamma lL) - \frac{\overline{V}_L^{(i)} - \overline{I}_L^{(i)} Z_C^{(i)}}{2\exp(\gamma L)}\exp(-\gamma lL)](Z_C^{(i)})^{-1} \quad (6.3)$$

$$\overline{V}_F^{(i)} = \frac{\overline{V}_R^{(i)} + \overline{I}_R^{(i)} Z_C^{(i)}}{2} \exp(\gamma l L) + \frac{\overline{V}_R^{(i)} - \overline{I}_R^{(i)} Z_C^{(i)}}{2} \exp(-\gamma l L) \quad (6.4)$$

2. The fault type is required to be identified (which is assumed to be available from the microprocessor relay), and (6.5) below is solved accordingly. The expanded form of (6.5) contains only one unknown i.e. the distance to fault, and can be derived based on the assumption that the fault resistance is a purely real value. The equations for phase-network phasors for $\overline{V}_F$ and $\overline{I}_F$ for each fault type are shown in (6.6)-(6.13):

$$\mathrm{Re}(\overline{V}_F)\mathrm{Im}(\overline{I}_F) = \mathrm{Re}(\overline{I}_F)\mathrm{Im}(\overline{V}_F) \quad (6.5)$$

- Single-Line to Ground faults:

$$\overline{V}_F = \overline{V}_F^{(0)} + \overline{V}_F^{(1)} + \overline{V}_F^{(2)} \quad (6.6)$$

$$\overline{I}_F = \overline{I}_F^{(0)} = \overline{I}_F^{(1)} = \overline{I}_F^{(2)} \quad (6.7)$$

- Double-Line faults:

$$\overline{V}_F = \overline{V}_F^{(1)} - \overline{V}_F^{(2)} \quad (6.8)$$

$$\overline{I}_F = \overline{I}_F^{(1)} \quad (6.9)$$

- Three-phase faults:

$$\overline{V}_F = \overline{V}_F^{(1)} \quad (6.10)$$

$$\overline{I}_F = \overline{I}_F^{(1)} \quad (6.11)$$

- Double-Line to Ground faults:

$$\overline{V}_F = \overline{V}_F^{(0)} - \overline{V}_F^{(1)} \tag{6.12}$$

$$\overline{I}_F = -\overline{I}_F^{(1)} - \overline{I}_F^{(2)} \tag{6.13}$$

3. So far it is assumed that the fault occurs on the remote side of the capacitor. Steps 1 and 2 are repeated for the following altered quantities in order to consider the case when the fault occurs on the local side of the series capacitor as shown in Figure 6.2:

$$\overline{V}_{L(altered)} = \overline{V}_R \tag{6.14}$$

$$\overline{V}_{R(altered)} = \overline{V}_L \tag{6.15}$$

$$\overline{I}_{L(altered)} = -\overline{I}_R \tag{6.16}$$

$$\overline{I}_{R(altered)} = -\overline{I}_L \tag{6.17}$$

Whilst the original algorithm uses a special subroutine selection procedure to determine which solution is the correct one, it may not choose the correct option when carried out on simulations with high disparity in line parameters. Therefore, for the purposes of this chapter, the solution which is the closest to the actual value of distance to fault is chosen. This way it is ensured that the resulting errors in distance to fault are due to the fault distance calculation itself rather than the incorrect selection of the subroutine.

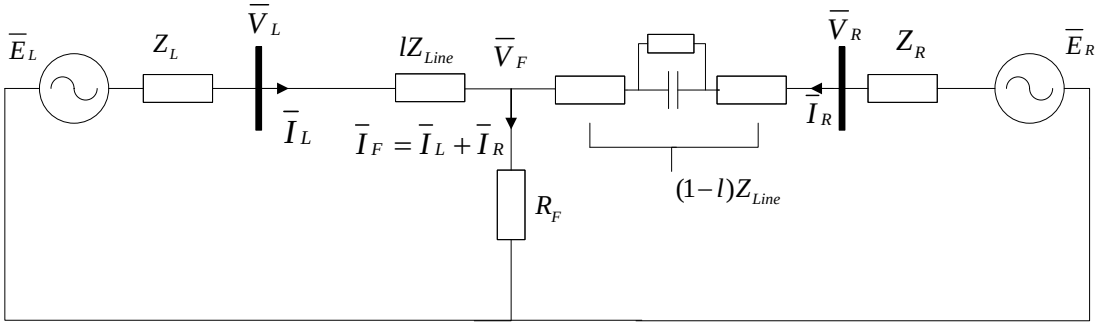

Figure 6.2: Fault on the local side of the series capacitor

6.1.2. Algorithm Testing

Section 4.3 previously discussed the ATP-EMTP test circuit used to validate the accuracy of the novel algorithm. The data obtained using these simulations, was then used as input to MATLAB where the algorithm was run and results were thus obtained. This procedure is repeated for the tests carried out in this chapter. The circuit modelled in ATP-EMTP is shown below in Figure 6.3. It comprises of a line compensated at the middle. All other aspects of the test-circuit are modelled identically to the circuit used in Chapter 4. The network parameters and line parameters are also as used before, as shown previously in Table 4.3 and Table 4.4. Line parameter settings used for the FLA discussed in Section 6.1.1 are varied depending on the tests carried out. The settings are modified based on the three categories shown previously in Table 6.1, each corresponding to different level of disparity between settings and actual line parameters. This list of settings to be used for the comparison is shown in Table 6.3. While the tests in Chapter 4 were carried out for four different locations of series compensation, here, tests are carried out only for the line compensated at the middle. This is since the FLA discussed in Section 6.1.1 is derived for such an arrangement.

Table 6.3: Modified parameters used for single-circuit line

	R_1 (Ω/km)	X_{L1} (Ω/km)	Y_1 (mho/km)	R_0 (Ω/km)	X_{L0} (Ω/km)	Y_0 (mho/km)
No disparity	0.065	0.300	3.298E-6	0.195	0.899	1.570E-6
Small disparity	0.078	0.315	3.792E-6	0.234	0.970	1.963E-6
High disparity	0.085	0.345	4.122E-6	0.253	1.061	2.041E-6

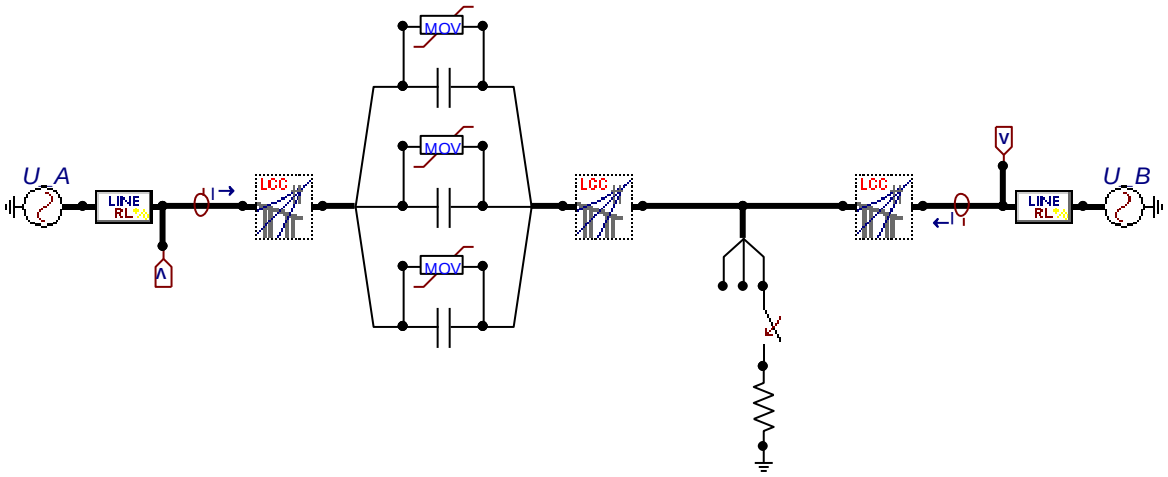

Figure 6.3: ATP-EMTP test-circuit used for the comparison of single-circuit algorithms

Since the line is compensated at the middle, it can be seen that it requires to be modelled as three segments (as opposed to two, when the line is compensated at both ends). This is since the line is split along its length at two points: at the series capacitor and at the fault point. The subsequent sections detail the results of the tests carried out and comparison of the fault location results obtained from the two algorithms. The fault was simulated to occur at 43 ms, and the data window size used for the FFT in each case was 20 ms. The decaying DC component removal method and the FFT used for the novel FLA discussed in Chapter 4 are carried out for both algorithms in the comparison.

6.1.3. Results of Comparison Study

For simplicity, in this section and subsequent sections, the novel algorithm for single-circuit lines will be referred to as algorithm-N1, and the algorithm discussed in Section 6.1.1 will be referred to as algorithm-E1. An example SLG fault simulation is carried out here similar to the one in Chapter 4 in Section 4.3.1 but for the test circuit shown in Figure 6.3. The fault distance calculations of the two algorithms are then carried out. For this example simulation, first, the parameters required for the calculations of algorithm-E1 used

were identical to those used in the simulations (no disparity). A fault resistance of 100Ω was used and the fault is simulated at 40km on a 100km untransposed line. The degree of compensation used is 30%. The voltage and current waveforms as seen at the local and remote ends of the line are shown in Figure 6.4 - Figure 6.7.

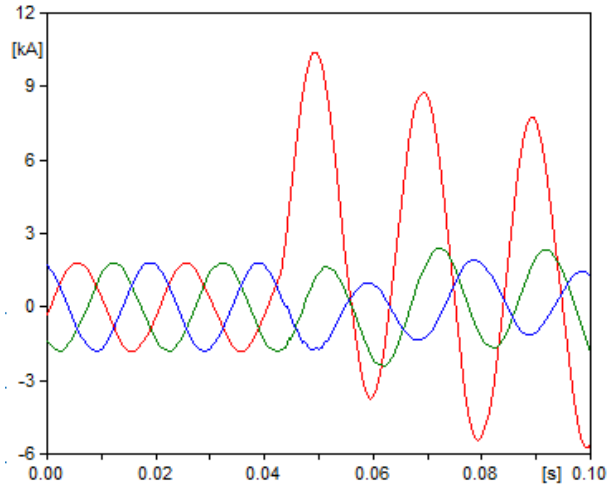

Figure 6.4: Local line-end phase currents – SLG fault on single-circuit series compensated line

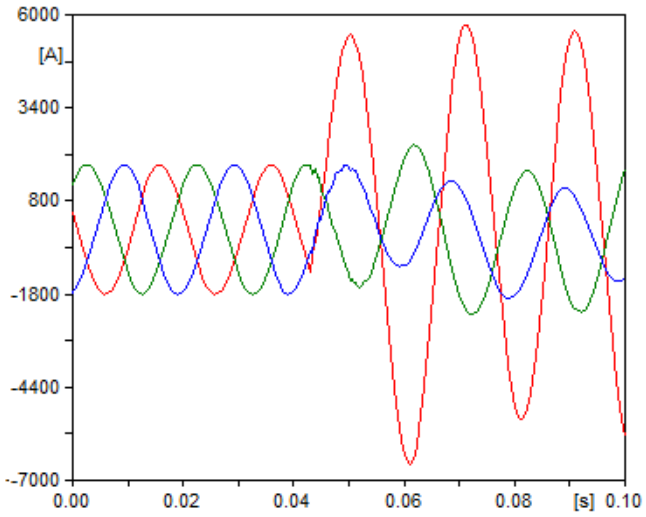

Figure 6.5: Remote line-end phase currents - SLG fault on single-circuit series compensated line

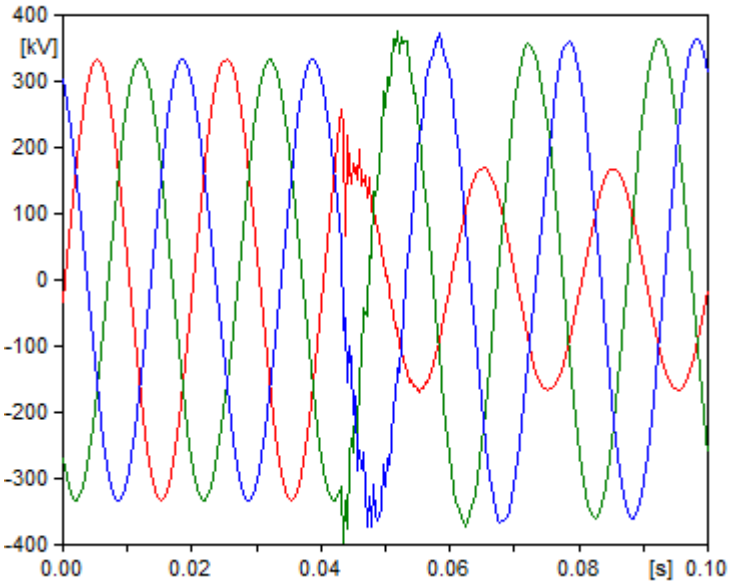

Figure 6.6: Local line-end phase voltages - SLG fault on single-circuit series compensated line

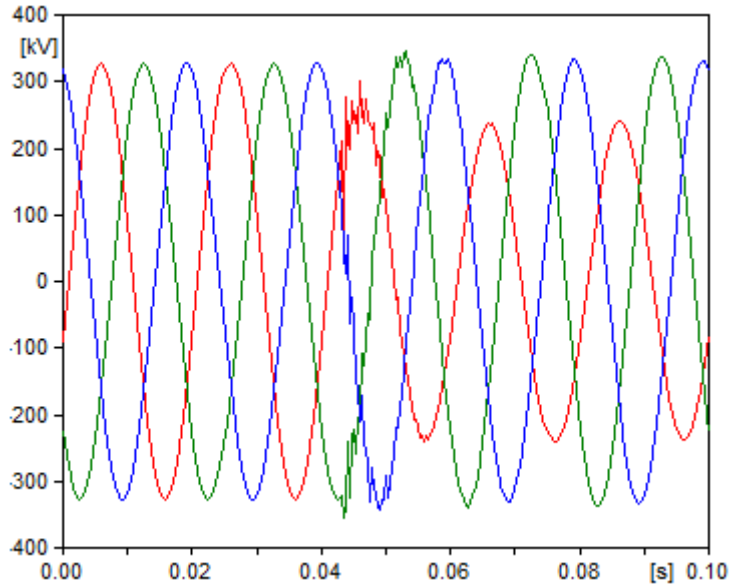

Figure 6.7: Remote line-end phase voltages - SLG fault on single-circuit series compensated line

The corresponding fault distance estimates from the two algorithms are shown in Figure 6.8. The averages of the estimates taken from 0.06s to 0.1s are calculated to be 40.374 and 39.948 for algorithm-N1 and algorithm-E1 respectively. It can be seen that they both perform very accurately, and the comparison indicates that in this case, algorithm-E1 performs more accurately than algorithm-N1. This comparison is now repeated after altering the line parameters of the simulation such that there is a small disparity in the parameters (see Table 6.3). The corresponding estimates are shown in Figure 6.9. The average estimate for algorithm-E1 is now 37.897. It can be seen in this case that algorithm-N1 performs more accurately than algorithm-E1, although the accuracy of algorithm-E1 is still acceptable (error<5%). Thirdly, a large disparity is introduced in the simulated line parameters, the comparison is repeated and the new average fault distance for algotihm-E1 is 32.864. Figure 6.10 comparing the resulting estimates, shows a significant difference in the fault distance error, and the estimates for algorithm-E1 are no longer within an acceptable range (error>5%).

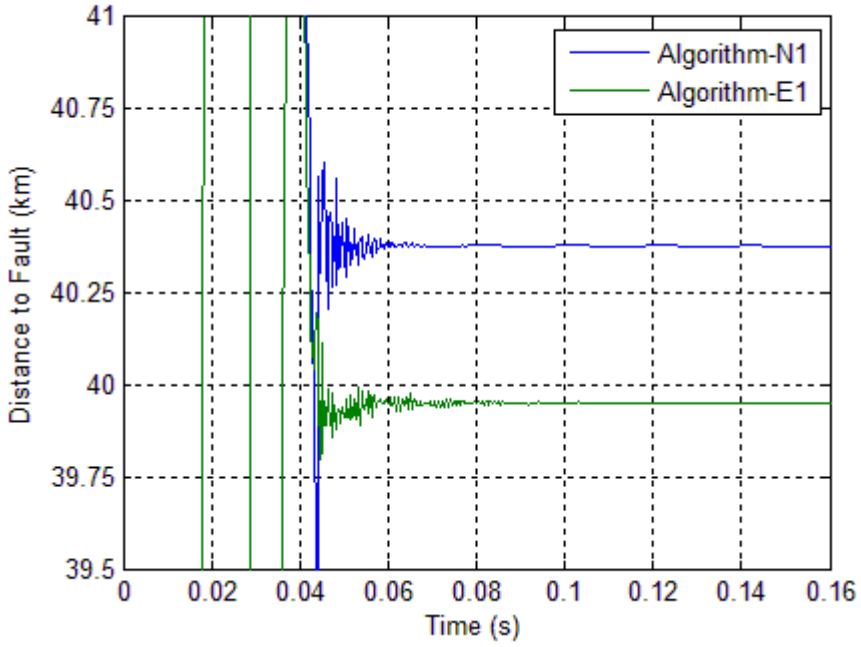

Figure 6.8: Fault distance estimates: SLG fault on single-circuit series compensated lines (no disparity)

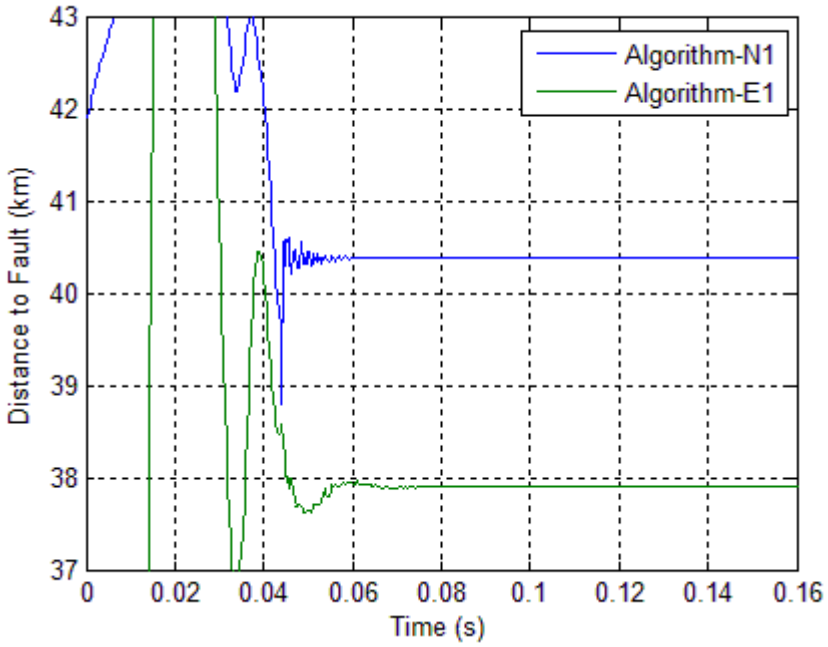

Figure 6.9: Fault distance estimates: SLG fault on single-circuit series compensated lines (small disparity)

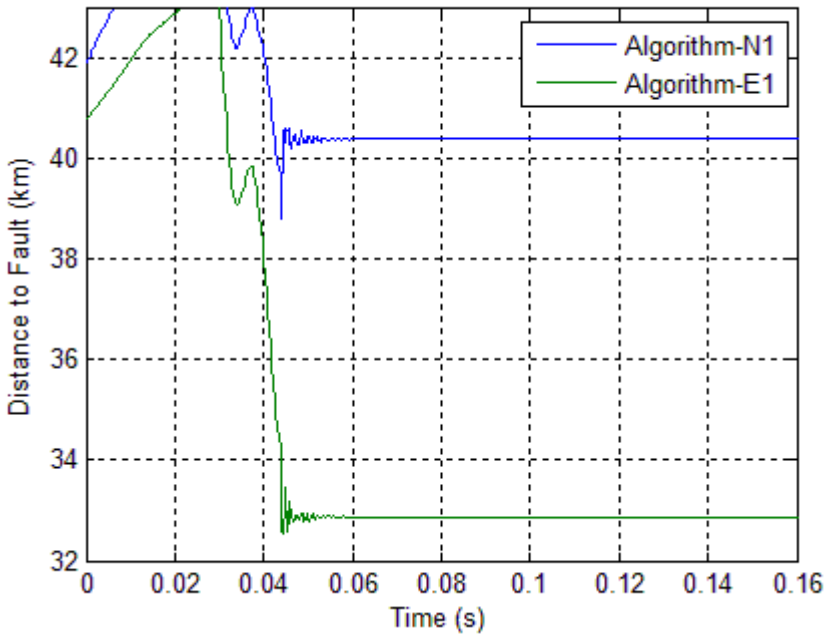

Figure 6.10: Fault distance estimates: SLG fault on single-circuit series compensated lines (large disparity)

This comparison is repeated for SLG faults for a variety of fault distances and fault resistances as shown in Table 6.4. The grey entries show the results for algorithm-N1 and the white entries show the results for algorithm-E1. It can be seen that sensitivity of algorithm-E1 to errors in line parameter settings follows the trend seen in the example simulation comparisons in Figure 6.8-Figure 6.10. In other words, when line parameter settings used are reasonably accurate, algorithm-E1 performs to a high degree of accuracy, but when the disparity between the settings and the actual line parameters increases, the accuracy of fault location suffers significantly. A similar set of results for DLG faults is shown in Table 6.5. The grey entries show the results for algorithm-N1 and the white entries show the results for algorithm-E1. The trend seen in the errors (for SLG faults) with respect to the disparity in settings is also observed for this fault type.

It can be said, that for the test cases considered for SLG faults and DLG faults, the novel algorithm-N1 is more reliably accurate than algorithm-E1. This is partially due to the simplification used in the derivation of algorithm-E1, in that it assumes that the sequence networks are decoupled, which leads to fault distance inaccuracies. Algorithm-N1, takes into account the untransposed nature of the line, without the need for such a simplification. However, the primary reason for the difference in accuracy is the reliance of algorithm-E1 on inaccurate line parameters. It can also be seen that an increased fault resistance introduces further inaccuracies in distance to fault calculation of algorithm-E1, and the significance of line parameters in such calculations becomes more prominent.

Results for 3-phase and DL fault types are shown in Table 6.6 and Table 6.7 respectively. The grey entries show the results for algorithm-N1 and the white entries show the results for algorithm-E1. The trend seen in accuracy vs. disparity in settings is similar to the SLG and DLG fault types, in that the accuracy worsens with increasing disparity. But unlike the previous cases, the impact of the disparity for these two fault types is found not to be as significant. In other words, even for a large disparity in settings, algorithm-E1 performs accurately to a sufficient degree. When the disparity is small, the increase in errors in fault distance is found to be marginal. This can be attributed to being due to the fact that disparity in zero sequence impedance settings has no impact for such fault types. Only the positive sequence impedance settings affect the accuracy of fault distance calculations.

Since the disparity for positive sequence impedance settings is relatively smaller than for zero sequence impedance settings, the resulting increase in fault distance errors is also small.

Table 6.4: Results of comparison for SLG faults - single-circuit series compensated line

Fault Type	Error of Estimated Fault Location(%)						
	Actual Fault Location (% of line length)						
	10	25	35	50	65	80	90
No Disparity in Line Parameters							
A-G $R_F = 0\Omega$	0.09	0.01	0.001	0.06	0.01	0.12	0.14
	0.28	0.15	0.41	0.09	0.55	0.74	0.25
A-G $R_F = 10\Omega$	0.15	0.10	0.04	0.07	0.11	0.16	0.21
	0.41	0.61	0.12	0.81	0.17	0.21	0.44
A-G $R_F = 100\Omega$	0.13	0.18	0.01	0.05	0.15	0.13	0.18
	0.77	0.94	0.54	0.64	0.01	0.63	0.73
Small Disparity in Line Parameters							
A-G $R_F = 0\Omega$	1.17	1.14	0.76	1.00	0.91	1.10	1.31
	0.28	0.15	0.41	0.09	0.55	0.74	0.25
A-G $R_F = 10\Omega$	2.67	1.16	1.81	0.17	2.74	1.61	1.42
	0.41	0.61	0.12	0.81	0.17	0.21	0.44
A-G $R_F = 100\Omega$	2.54	3.82	2.20	0.59	0.48	1.75	1.54
	0.77	0.94	0.54	0.64	0.01	0.63	0.73
Large Disparity in Line Parameters							
A-G $R_F = 0\Omega$	3.27	2.35	1.86	2.39	1.67	2.06	3.27
	0.28	0.15	0.41	0.09	0.55	0.74	0.25
A-G $R_F = 10\Omega$	3.60	4.93	2.78	7.69	9.35	7.64	8.60
	0.41	0.61	0.12	0.81	0.17	0.21	0.44
A-G $R_F = 100\Omega$	4.15	11.37	7.87	12.72	1.66	10.44	9.15
	0.77	0.94	0.54	0.64	0.01	0.63	0.73

Table 6.5: Results of comparison for DLG faults - single-circuit series compensated line

Fault Type	Error of Estimated Fault Location(%)						
	Actual Fault Location (% of line length)						
	10	25	35	50	65	80	90
No Disparity in Line Parameters							
AB-G $R_F = 0\Omega$	0.18	0.23	0.09	0.29	0.25	0.31	0.26
	0.35	0.22	0.59	0.94	0.79	0.52	0.31
AB-G $R_F = 10\Omega$	0.26	0.33	0.17	0.11	0.13	0.05	0.03
	0.36	0.69	0.33	0.86	0.25	0.93	0.96
AB-G $R_F = 100\Omega$	0.02	0.29	0.11	0.04	0.04	0.13	0.23
	0.51	0.75	0.89	0.01	0.47	0.49	0.85
Small Disparity in Line Parameters							
AB-G $R_F = 0\Omega$	4.07	3.91	5.58	2.77	1.33	1.19	1.06
	0.35	0.22	0.59	0.94	0.79	0.52	0.31
AB-G $R_F = 10\Omega$	2.93	6.69	2.52	3.13	8.63	4.54	5.06
	0.36	0.69	0.33	0.86	0.25	0.93	0.96
AB-G $R_F = 100\Omega$	2.78	1.27	4.74	5.70	4.56	2.03	0.17
	0.51	0.75	0.89	0.01	0.47	0.49	0.85
Large Disparity in Line Parameters							
AB-G $R_F = 0\Omega$	7.29	14.26	6.20	3.91	12.77	2.51	6.12
	0.35	0.22	0.59	0.94	0.79	0.52	0.31
AB-G $R_F = 10\Omega$	3.47	18.87	11.97	5.93	11.51	9.42	7.47
	0.36	0.69	0.33	0.86	0.25	0.93	0.96
AB-G $R_F = 100\Omega$	5.21	2.30	6.61	7.55	6.67	3.20	4.52
	0.51	0.75	0.89	0.07	0.47	0.49	0.85

Table 6.6: Results of comparison for 3-phase faults - single-circuit series compensated line

Fault Type	Error of Estimated Fault Location(%)						
	Actual Fault Location (% of line length)						
	10	25	35	50	65	80	90
No Disparity in Line Parameters							
AB $R_F = 0\Omega$	0.19	0.20	0.06	0.09	0.15	0.05	0.01
	0.19	0.65	0.47	0.49	0.66	0.72	0.12
AB $R_F = 10\Omega$	0.15	0.04	0.14	0.08	0.03	0.13	0.24
	0.29	0.48	0.08	0.79	0.09	0.39	0.89
AB $R_F = 100\Omega$	0.21	0.19	0.20	0.10	0.08	0.05	0.21
	0.19	0.45	0.06	0.17	0.59	0.35	0.82
Small Disparity in Line Parameters							
AB $R_F = 0\Omega$	0.44	0.74	0.92	0.17	0.31	0.86	0.24
	0.19	0.65	0.47	0.49	0.66	0.72	0.12
AB $R_F = 10\Omega$	0.33	0.79	0.88	0.10	0.55	1.03	1.27
	0.29	0.48	0.18	0.79	0.09	0.39	0.89
AB $R_F = 100\Omega$	0.31	0.29	0.45	0.36	0.11	1.27	1.64
	0.19	0.45	0.06	0.17	0.59	0.35	0.82
Large Disparity in Line Parameters							
AB $R_F = 0\Omega$	2.26	0.94	4.55	0.74	2.29	1.46	0.88
	0.19	0.65	0.47	0.49	0.66	0.72	0.12
AB $R_F = 10\Omega$	1.65	0.12	1.94	0.54	3.67	2.10	1.94
	0.29	0.48	0.08	0.79	0.09	0.39	0.89
AB $R_F = 100\Omega$	3.67	7.68	5.60	1.62	0.17	4.41	2.48
	0.19	0.45	0.06	0.17	0.59	0.35	0.82

Table 6.7: Results of comparison for DL faults - single-circuit series compensated line

Fault Type	Error of Estimated Fault Location(%)						
	Actual Fault Location (% of line length)						
	10	25	35	50	65	80	90
No Disparity in Line Parameters							
ABC $R_F = 0\Omega$	0.06	0.13	0.06	0.00	0.14	0.03	0.12
	0.72	0.27	0.88	0.35	0.13	0.06	0.55
ABC $R_F = 10\Omega$	0.08	0.12	0.04	0.12	0.15	0.03	0.08
	0.76	0.52	0.11	0.69	0.68	0.53	0.94
ABC $R_F = 100\Omega$	0.14	0.06	0.09	0.11	0.01	0.04	0.14
	0.25	0.42	0.09	0.03	0.97	0.44	0.20
Small Disparity in Line Parameters							
ABC $R_F = 0\Omega$	0.28	0.89	0.61	0.46	0.31	0.07	0.11
	0.72	0.27	0.88	0.35	0.13	0.06	0.55
ABC $R_F = 10\Omega$	0.63	0.76	0.09	0.62	0.44	0.74	0.15
	0.76	0.52	0.11	0.69	0.68	0.53	0.94
ABC $R_F = 100\Omega$	0.86	0.31	0.17	0.49	0.66	0.83	0.89
	0.25	0.42	0.09	0.03	0.97	0.44	0.20
Large Disparity in Line Parameters							
ABC $R_F = 0\Omega$	1.84	3.45	2.19	1.90	1.08	4.09	0.28
	0.72	0.27	0.88	0.35	0.13	0.06	0.55
ABC $R_F = 10\Omega$	3.93	0.56	2.74	1.99	4.41	2.84	2.67
	0.76	0.52	0.11	0.69	0.68	0.53	0.94
ABC $R_F = 100\Omega$	1.89	2.92	2.21	1.30	1.29	2.46	3.01
	0.25	0.42	0.09	0.03	0.97	0.44	0.20

6.2. Comparison of Algorithms for Double-Circuit Series Compensated Lines

6.2.1. Background

An FLA proposed by Kang et al [135] using double-end synchronised measurements is used in the comparison. The algorithm was chosen for the comparison firstly as it makes use of two-terminal voltage and current measurements. Secondly, it is a highly accurate algorithm which takes the mutual coupling between circuits into account in its calculations. It is applicable to only double-circuit lines. Unlike the algorithm presented in Chapter 5, It requires line parameters such as resistance, inductance and capacitance per unit length to arrive at the distance to fault. It is conceptually similar to the algorithm-E1, but it is developed for double-circuit series compensated lines. It is directly applicable to lines where the series capacitor is installed at the middle. It is capable of locating faults on long lines given that it takes shunt admittance into account. It uses a similar approach in its calculation of distance to fault as algorithm-E1 discussed in Section 6.1.1. The main advantage that the algorithm offers is that unlike a number of previously proposed algorithms for double-circuit lines, it does not require to calculate the effective impedance of the SC-MOV combination. The authors of the method have defined other terms Z_{cm1}, Z_{cm2}, γ_{m1} and γ_{m2} in order to take the zero-sequence mutual impedance into account (in addition to the sequence characteristic impedances and propagation constants defined for single-circuit lines):

$$Z_{cm1} = \sqrt{\frac{z^{(0)} - z_m{}^{(0)}}{y^{(0)} + 2y_m{}^{(0)}}} \tag{6.18}$$

$$Z_{cm2} = \sqrt{\frac{z^{(0)} + z_m{}^{(0)}}{y^{(0)}}} \tag{6.19}$$

$$\gamma_{m1} = \sqrt{(z^{(0)} - z_m{}^{(0)})(y^{(0)} + 2y_m{}^{(0)})} \tag{6.20}$$

$$\gamma_{m2} = \sqrt{(z^{(0)} + z_m{}^{(0)})y^{(0)}} \tag{6.21}$$

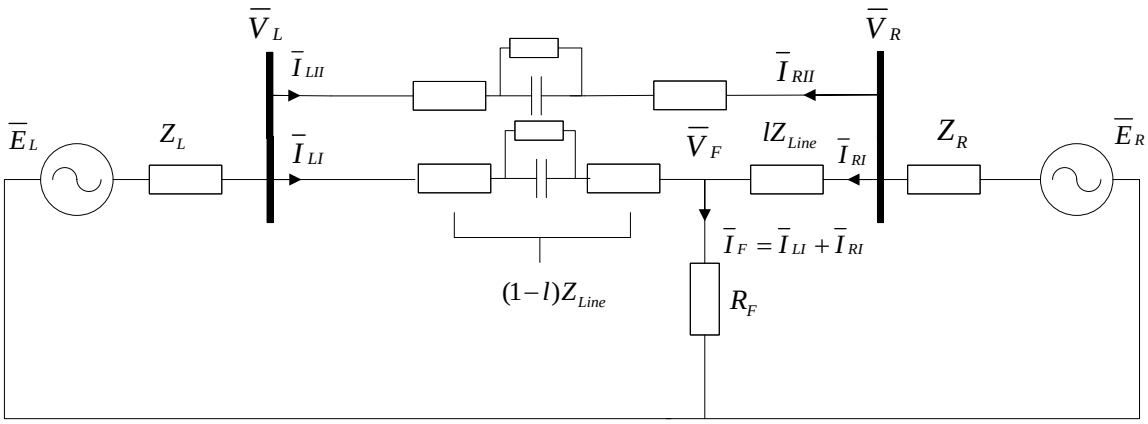

Figure 6.11: Double-circuit series compensated line – fault on the remote side of the capacitor

Table 6.8: Terms and definitions

Term	Definition
$\overline{V}_R$	Remote line-end voltage
$\overline{I}_{RI}$	Remote line-end current for circuit I
$\overline{I}_{RII}$	Remote line-end current for circuit II
$\overline{V}_L$	Local line-end voltage
$\overline{I}_{LI}$	Local line-end current for circuit I
$\overline{I}_{LII}$	Local line-end current for circuit II
$\overline{V}_F$	Fault point voltage
$\overline{I}_F$	Fault current
l	Fractional distance to fault
L	Total line length

The derivation of the algorithm is not carried out in this thesis. However, the mathematical steps constituting the algorithm are stated for completeness sake. The terms used in the equations are defined in Table 6.8. The steps of the algorithm are as follows:

1. The fault point voltage and fault current shown in Figure 6.11 are first required to be expressed purely in terms of the distance to fault 'l'. For the positive-sequence and negative sequence, these expressions are derived as follows:

$$\bar{I}_F^{(i)} = \frac{\bar{I}_{LI}^{(i)} \cosh(0.5\gamma^{(i)}) + \bar{I}_{LI}^{(i)} e^{j\delta} \cosh(0.5\gamma^{(i)}) - \frac{\bar{V}_L^{(i)}}{Z_c^{(i)}} \sinh(0.5\gamma^{(i)})}{\cosh[\gamma^{(i)}(0.5 - 0.5L)]} \tag{6.22}$$

$$\bar{V}_F^{(i)} = \bar{V}_L^{(i)} \cosh(\gamma^{(i)} lL) - \bar{I}_{LI}^{(i)} Z_c^{(i)} \sinh(\gamma^{(i)} lL) \tag{6.23}$$

where, $i = 1, 2$.

2. The zero sequence fault voltage is also required in subsequent calculations, and is expressed as follows using similar principles:

$$\begin{aligned} \bar{V}_F^{(0)} = \bar{V}_L^{(0)} \cosh(\gamma_{m2} lL) - \frac{\bar{I}_{LI}^{(0)}}{2}[Z_{cm2} \sinh(\gamma_{m2} lL) + Z_{cm1} \sinh(\gamma_{m1} lL)] \\ - \frac{\bar{I}_{LII}^{(0)}}{2}[Z_{cm2} \sinh(\gamma_{m2} lL) + Z_{cm1} \sinh(\gamma_{m1} lL)] \end{aligned} \tag{6.24}$$

3. Depending on the fault type one of the following equations is solved to determine the fault distance. They are each an expression of the fault resistance as being a purely real value:

   a) SLG faults:

$$\mathrm{Im}\left(\frac{\bar{V}_F^{(1)} + \bar{V}_F^{(2)} + \bar{V}_F^{(0)}}{\bar{I}_F^{(1)}}\right) = 0 \tag{6.25}$$

b) DL faults:

$$\mathrm{Im}\left(\frac{\overline{V}_F^{(1)} - \overline{V}_F^{(2)}}{\overline{I}_F^{(1)}}\right) = 0 \tag{6.26}$$

c) 3-phase faults:

$$\mathrm{Im}\left(\frac{\overline{V}_F^{(1)}}{\overline{I}_F^{(1)}}\right) = 0 \tag{6.27}$$

d) DLG Faults:

$$\mathrm{Im}\left(\frac{\overline{V}_F^{(0)} - \overline{V}_F^{(1)}}{-\overline{I}_F^{(1)} - \overline{I}_F^{(2)}}\right) = 0 \tag{6.28}$$

In each of the equations in step 3, the only variable is the distance to fault and is derived and solved as such.

4. Steps 1, 2 and 3 are repeated for the following altered variables in order to consider the case when the fault occurs on the local side of the series capacitor as shown in Figure 6.12:

$$\overline{V}_{L(altered)} = \overline{V}_R \tag{6.29}$$

$$\overline{V}_{R(altered)} = \overline{V}_L \tag{6.30}$$

$$\overline{I}_{RI(altered)} = -\overline{I}_{LI} \tag{6.31}$$

$$\overline{I}_{LI(altered)} = -\overline{I}_{RI} \tag{6.32}$$

$$\overline{I}_{RII(altered)} = -\overline{I}_{LII} \tag{6.33}$$

$$\bar{I}_{LII(altered)} = -\bar{I}_{RII} \tag{6.34}$$

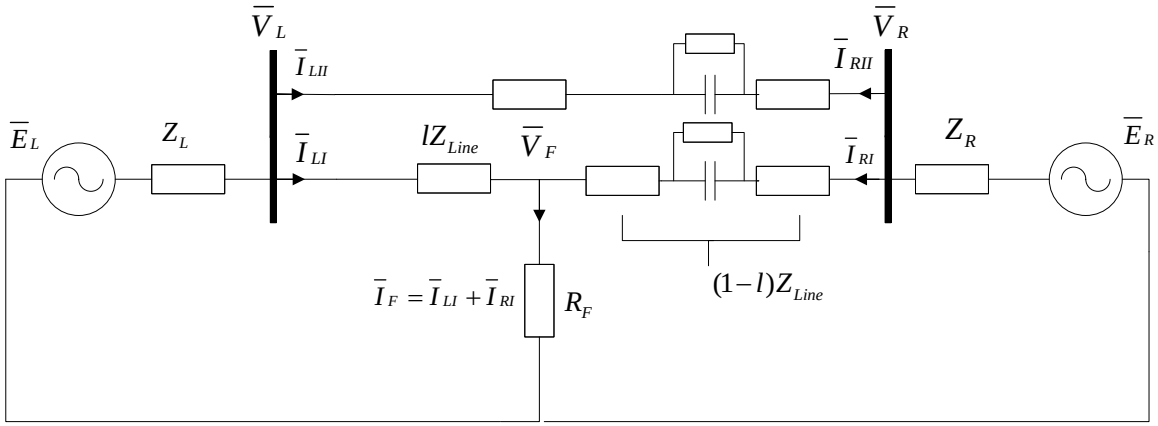

Figure 6.12: Double-circuit series compensated line – fault on the local side of the capacitor

Since, the aim of the comparison is to see the differences in accuracy of the two algorithms; the choice of subroutine is carried out here by selecting the one that is closest to the actual value. In this way, the incorrect selection of subroutine due to disparity in line parameters is avoided, and only the errors in distance to fault due to the algorithm itself are presented. In order to assess the true accuracy of the FLA, line parameter settings are adjusted so that they are not exactly equal to those in the simulations used in the comparison. These adjusted parameters for the different cases considered in this comparison are shown in Table 6.9.

Table 6.9: Modified Line-Parameters – double-circuit line

	R_1 (Ω/km)	X_{L1} (Ω/km)	Y_1 (mho/km)	R_0 (Ω/km)	X_{L0} (Ω/km)	Y_0 (mho/km)
No disparity	0.0264	1.215	3.926E-6	0.195	0.899	2.889E-6
Small disparity	0.0317	1.276	4.515E-6	0.234	0.971	3.612E-6
High disparity	0.0343	1.397	4.908E-6	0.254	1.061	3.756E-6

6.2.2. Algorithm Testing

Section 5.5 previously discussed the ATP-EMTP test circuit used to validate the accuracy of the novel algorithm for double circuit lines. A similar model of the line to be used for the comparison is shown in Figure 6.13. Unlike the test circuit shown in Figure 5.5 (in Chapter 5), the line here is compensated at the middle. All other aspects of the test-circuit model are as used in Chapter 5 (including the network parameters and line parameters). This list of the modified simulated line parameter settings is shown in Table 6.9. The DC component removal method and the FFT used for the novel FLA discussed in Chapter 5 are carried out for both algorithms in the comparison.

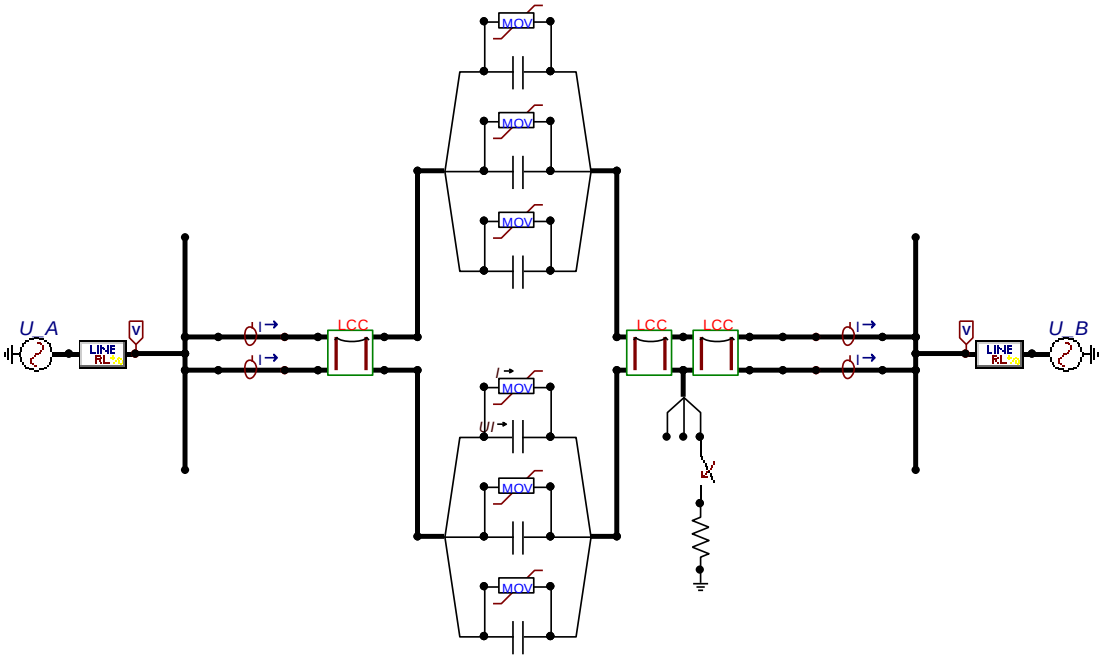

Figure 6.13: ATP-EMTP test circuit of a double-circuit series compensated line

A similar set of tests to those carried out in Section 6.1.3 is carried out here for the novel algorithm for double-circuit lines, and a discussion is provided for each fault type. For each test, the fault was always simulated at 83 ms, and the data window size used for the FFT in each case was 20 ms.

6.2.3. Results of Comparison Study

For the sections explaining the tests carried out for double-circuit lines, the novel algorithm for double-circuit lines will be referred to as algorithm-N2, and the algorithm discussed in Section 6.1.1 will be referred to as algorithm-E2. An example simulation of an SLG fault is simulated here and a comparison of the two algorithms is carried out whilst varying the settings required for algorithm-E2. First, the case of 'no disparity' is considered (in accordance with Table 6.9) and the fault distance calculations of the two algorithms are carried out. The corresponding current and voltage waveforms for the healthy and the faulted circuit of the line as seen at the two-ends are shown in Figure 6.14-Figure 6.18. The DC component removal method and the FFT as carried out for the single-circuit algorithms are also carried out here. The plot of the fault distance calculated against the time stamp (corresponding to the start point of data window for FFT) is shown in Figure 6.19. Both algorithms are seen to perform at a high level of accuracy; however, algorithm-E2 performs to slightly higher degree of accuracy than algorithm-N2. The averages of the estimates taken from 0.06s to 0.1s are calculated to be 39.431 and 40.226 for algorithm-N2 and algorithm-E2 respectively.

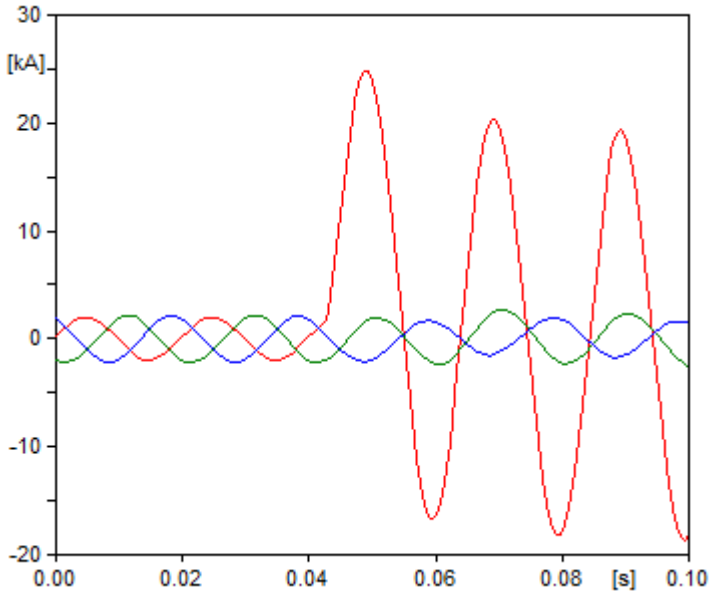

Figure 6.14: Local line-end phase currents (faulted circuit) - - SLG fault on double-circuit series compensated line

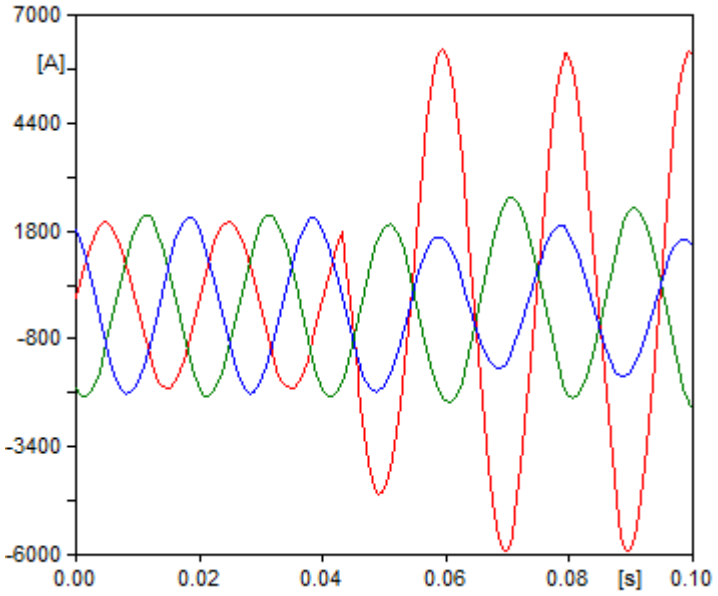

Figure 6.15: Remote line-end phase currents (faulted circuit)- - SLG fault on double-circuit series compensated line

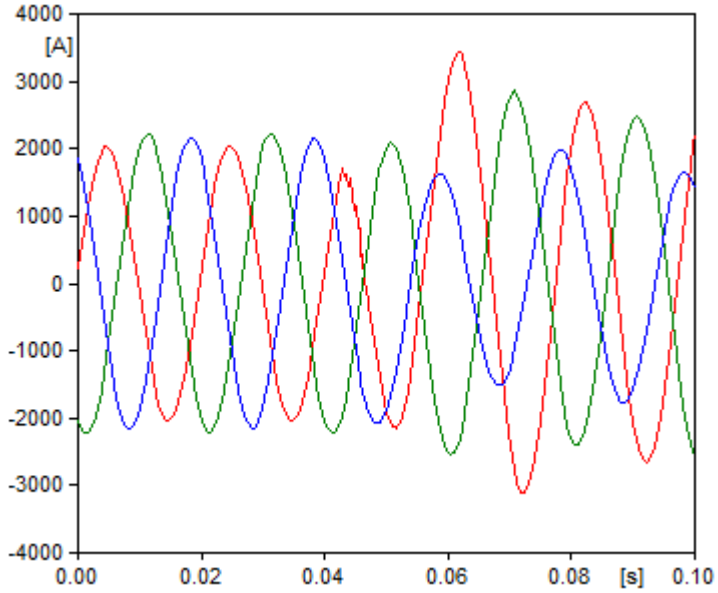

Figure 6.16: Healthy-circuit phase currents - SLG fault on double-circuit series compensated line

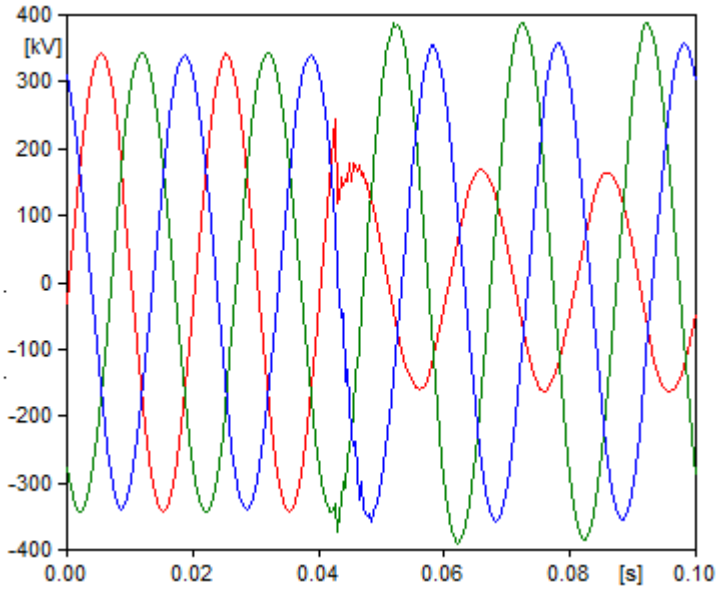

Figure 6.17: Local line-end phase voltages – - SLG fault on double-circuit series compensated line

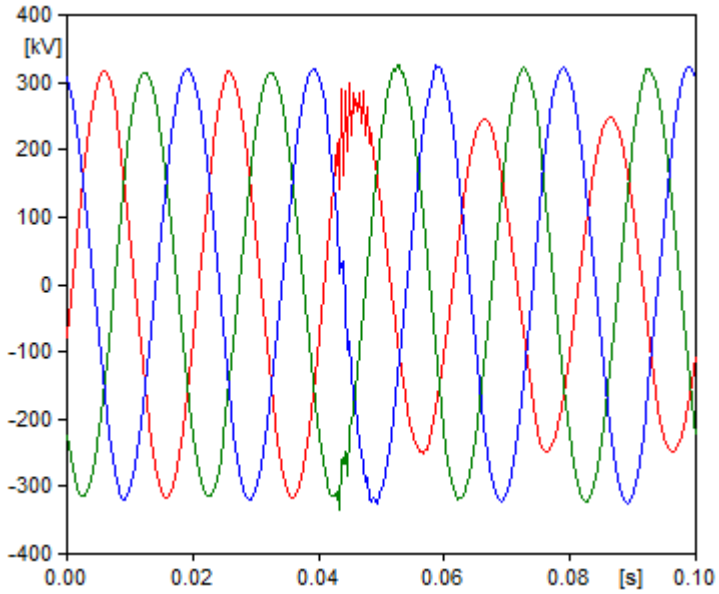

Figure 6.18: Remote line-end phase voltages double-circuit line - SLG fault on single-circuit series compensated line

Similar to the comparison carried out for the single-circuit lines, the above mentioned procedure is repeated for the same simulation, but with a small disparity in the settings of algorithm-E2 as defined in Table 6.9. The average estimate for algorithm-E2 is now 36.609. It can be seen that algorithm-N2 performs to a significantly higher degree of accuracy than algorithm-E2. Similarly, another comparison is carried for this very system, but with a large disparity in the settings of algorithm-E2 in accordance with Table 6.9. A similar trend can be observed, as algorithm-E2 is unable to locate the fault accurately and the error in fault distance is over 5%. The average fault distance for algorithm-E2 is now 32.879. Algorithm-N2 on the other hand performs accurately and does not rely on settings which may be inaccurate.

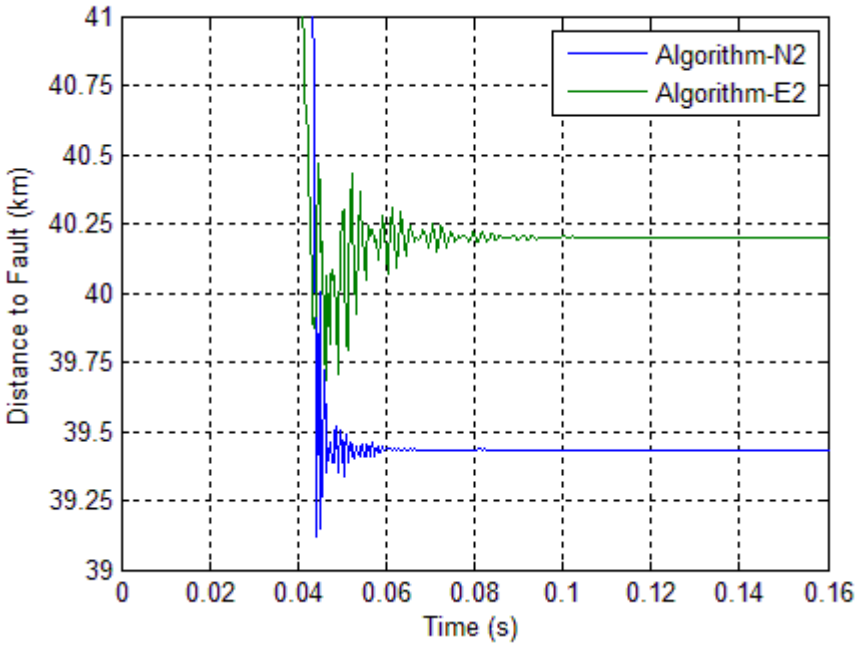

Figure 6.19: Fault distance estimates: SLG fault on double-circuit series compensated line (no disparity)

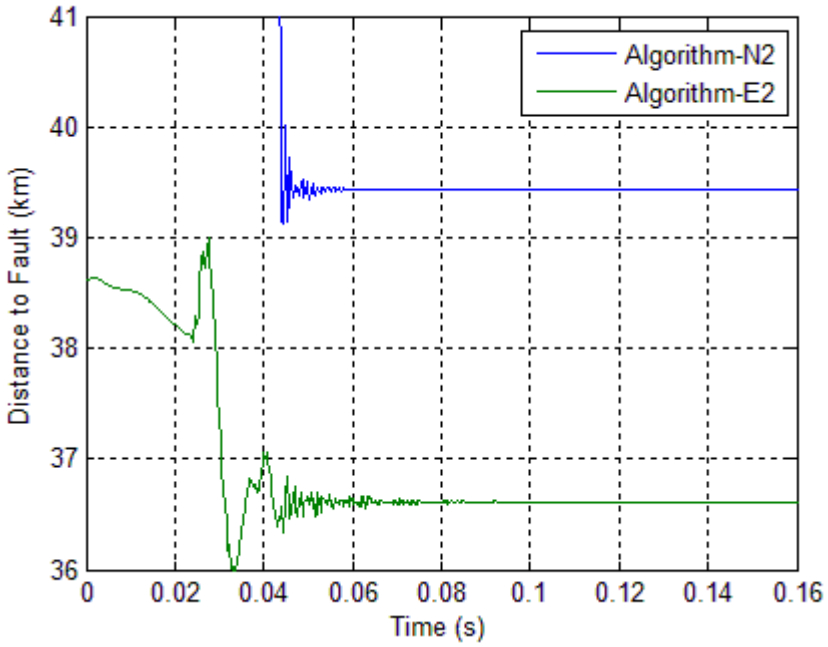

Figure 6.20: Fault distance estimates: SLG fault on double-circuit series compensated line (small disparity)

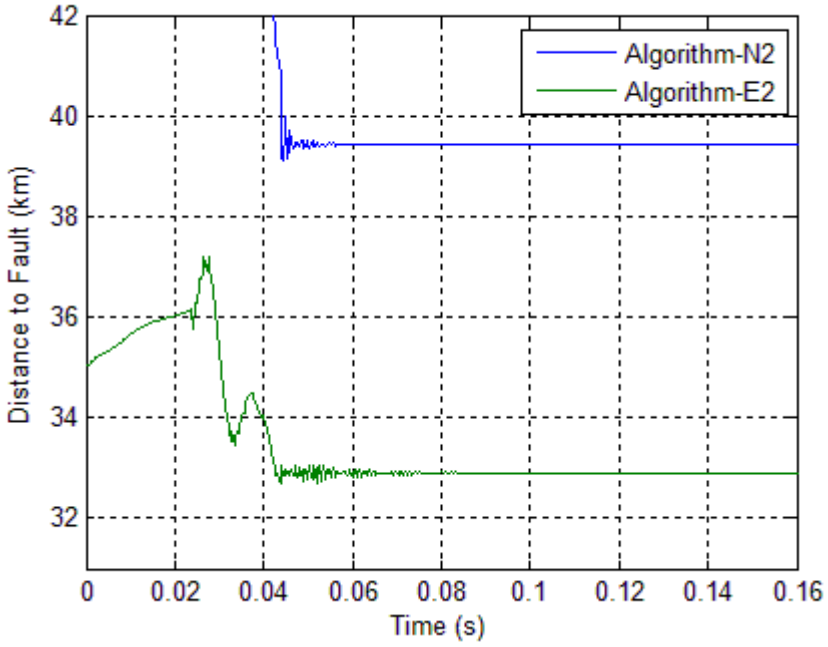

Figure 6.21: Fault distance estimates: SLG fault on double-circuit series compensated line (large disparity)

Much like the case with single-circuit series compensated lines, the results of comparison for double-circuit series compensated lines are found to vary depending on the fault type. Table 6.10 shows the results for various fault resistances and fault distances for SLG faults. The impact of the disparity in settings on the accuracy of algorithm-E2 is found to be similar to that seen in the example simulation. Table 6.11 similarly shows the results for DLG faults. For both these fault types, the algorithm-E2 is found to be more accurate than algorithm-N2 in a majority of test cases when there is 'no disparity' between settings and actual line parameters. The errors in fault distance are observed to increase as this disparity increases. When the disparity is large, the fault distance errors are often seen to be over 5%.

The line parameter free aspect of algorithm-N2 is found to be a significant advantage for such fault types as is the case with algorithm-N1. The high likelihood of errors in zero-sequence impedance parameter settings and the fact that over 90% of faults on transmission lines are SLG faults, imply that algorithm-N2 is favourable to algorithm-E2 based on the results presented thus far. The fault distance estimates for 3-phase and DL fault types are shown in Table 6.12 and Table 6.13 respectively. The comparison study finds that even in the case of double-circuit series compensated lines, the line parameter free aspect of the novel algorithm-N2 is not a significant advantage. This is since the disparity in settings and actual line parameters are found to have little impact on the errors in fault distance estimates. It can be seen that for both fault types, 3 phase and DL, the errors in fault distance estimates are smaller than those for algorithm-N2. For the 'small disparity' case, the increase in errors is marginal, and for the 'large disparity' case, the errors in most cases are still under 5%. Novel algorithms discussed in this thesis, i.e. algorithm-N1 and algorithm-N2 are based on similar principles and method of derivation. They vary in the measurements required, the equations used to derive for the distance to fault, and the variables to thus be solved for. Most importantly they both locate faults without requiring any line parameters. This is the key aspect that distinguishes these novel algorithms from existing solutions for series compensated transmission lines. This is also why the comparison study finds similar observations in terms of the usefulness of the novel algorithms in the two sets of comparison studies carried out.

Table 6.10: Results of comparison for SLG faults- double-circuit series compensated line

Fault Type	Error of Estimated Fault Location(%)						
	Actual Fault Location (% of line length)						
	10	25	35	50	65	80	90
No Disparity in Line Parameters							
A-G $R_F = 0\Omega$	0.09	0.01	0.11	0.02	0.15	0.17	0.10
	0.59	0.86	0.90	0.87	0.26	0.03	0.21
A-G $R_F = 10\Omega$	0.16	0.17	0.14	0.01	0.03	0.08	0.12
	0.30	0.51	0.10	0.57	0.37	0.19	0.77
A-G $R_F = 100\Omega$	0.11	0.19	0.15	0.14	0.08	0.18	0.12
	0.45	0.50	0.03	0.91	0.46	0.47	0.70
Small Disparity in Line Parameters							
A-G $R_F = 0\Omega$	3.33	0.59	1.83	4.21	2.94	2.39	1.03
	0.59	0.86	0.90	0.87	0.26	0.13	0.21
A-G $R_F = 10\Omega$	4.27	1.74	2.88	1.13	1.54	0.88	2.03
	0.30	0.51	0.10	0.57	0.37	0.09	0.77
A-G $R_F = 100\Omega$	3.40	0.23	1.91	2.93	2.52	3.76	2.44
	0.45	0.50	0.03	0.91	0.46	0.47	0.70
Large Disparity in Line Parameters							
A-G $R_F = 0\Omega$	7.64	3.41	8.50	1.24	6.43	2.06	3.16
	0.59	0.86	0.90	0.87	0.26	0.13	0.21
A-G $R_F = 10\Omega$	1.00	6.55	6.47	7.12	6.44	1.02	3.53
	0.30	0.51	0.10	0.57	0.37	0.09	0.77
A-G $R_F = 100\Omega$	8.08	6.99	1.57	6.35	8.35	3.28	0.98
	0.45	0.50	0.03	0.91	0.46	0.47	0.70

Table 6.11: Results of comparison for DLG faults- double-circuit series compensated line

Fault Type	Error of Estimated Fault Location(%)						
	Actual Fault Location (% of line length)						
	10	25	35	50	65	80	90
No Disparity in Line Parameters							
AB-G $R_F = 0\Omega$	0.02	0.05	0.03	0.12	0.09	0.13	0.11
	0.28	0.38	0.45	0.74	0.33	0.05	0.19
AB-G $R_F = 10\Omega$	0.19	0.10	0.03	0.01	0.17	0.05	0.12
	0.26	0.04	0.11	0.29	0.12	0.97	0.08
AB-G $R_F = 100\Omega$	0.14	0.11	0.09	0.01	0.06	0.17	0.21
	0.07	0.84	0.51	0.44	0.07	0.46	0.16
Small Disparity in Line Parameters							
AB-G $R_F = 0\Omega$	2.13	1.79	0.51	2.09	3.19	2.30	3.63
	0.28	0.38	0.45	0.74	0.33	0.05	0.19
AB-G $R_F = 10\Omega$	1.88	0.55	0.69	2.90	2.71	2.26	2.89
	0.26	0.04	0.11	0.29	0.12	0.97	0.08
AB-G $R_F = 100\Omega$	3.11	2.08	1.06	2.81	1.20	1.21	2.36
	0.07	0.84	0.51	0.44	0.07	0.46	0.16
Large Disparity in Line Parameters							
AB-G $R_F = 0\Omega$	3.06	8.81	3.71	3.46	9.09	5.42	2.51
	0.28	0.38	0.45	0.74	0.33	0.05	0.19
AB-G $R_F = 10\Omega$	9.66	4.12	3.26	7.34	8.58	1.47	0.56
	0.26	0.04	0.11	0.29	0.12	0.97	0.08
AB-G $R_F = 100\Omega$	3.22	7.33	7.07	4.55	8.88	2.06	5.74
	0.07	0.84	0.51	0.44	0.07	0.46	0.16

Table 6.12: Results of comparison for DL faults- double-circuit series compensated line

Fault Type	Error of Estimated Fault Location(%)						
	Actual Fault Location (% of line length)						
	10	25	35	50	65	80	90
No Disparity in Line Parameters							
AB $R_F = 0\Omega$	0.05	0.10	0.02	0.06	0.01	0.14	0.11
	0.67	0.56	0.13	0.47	0.84	0.59	0.64
AB $R_F = 10\Omega$	0.09	0.07	0.14	0.07	0.15	0.15	0.04
	0.52	0.95	0.80	1.08	0.40	0.41	0.74
AB $R_F = 100\Omega$	0.11	0.13	0.01	0.02	0.15	0.04	0.13
	0.04	0.46	0.34	0.93	0.21	0.05	0.72
Small Disparity in Line Parameters							
AB $R_F = 0\Omega$	0.47	0.76	0.71	0.49	0.72	1.55	0.63
	0.67	0.56	0.13	0.47	0.84	0.59	0.64
AB $R_F = 10\Omega$	0.05	0.44	0.56	1.01	0.31	0.50	0.71
	0.52	0.95	0.80	1.08	0.40	0.41	0.74
AB $R_F = 100\Omega$	0.40	1.09	0.55	0.31	0.11	0.12	0.46
	0.04	0.46	0.34	0.93	0.21	0.05	0.72
Large Disparity in Line-Parameters							
AB $R_F = 0\Omega$	0.98	2.18	5.44	3.59	1.86	2.19	2.51
	0.67	0.56	0.13	0.47	0.84	0.59	0.64
AB $R_F = 10\Omega$	0.83	0.33	2.72	1.12	2.97	5.95	0.59
	0.52	0.95	0.80	1.08	0.40	0.41	0.74
AB $R_F = 100\Omega$	2.77	2.05	6.34	3.69	1.80	3.87	2.46
	0.04	0.46	0.34	0.93	0.21	0.05	0.72

Table 6.13: Results of comparison for '3-phase faults'- double-circuit series compensated line

Fault Type	Error of Estimated Fault Location(%)						
	Actual Fault Location (% of line length)						
	10	25	35	50	65	80	90
No Disparity in Line Parameters							
ABC $R_F = 0\Omega$	0.08	0.19	0.18	0.12	0.00	0.04	0.01
	0.18	0.41	0.58	0.88	0.49	0.16	0.77
ABC $R_F = 10\Omega$	0.14	0.05	0.12	0.20	0.09	0.05	0.11
	0.15	0.18	0.11	0.40	1.54	0.92	0.08
ABC $R_F = 100\Omega$	0.20	0.15	0.11	0.09	0.10	0.03	0.18
	0.48	0.87	1.00	0.63	0.06	0.34	0.64
Small Disparity in Line Parameters							
ABC $R_F = 0\Omega$	0.63	1.17	0.97	1.25	1.30	0.74	1.10
	0.18	0.41	0.58	0.88	0.49	0.16	0.77
ABC $R_F = 10\Omega$	0.68	0.11	1.25	0.7	0.78	0.95	0.94
	0.15	0.18	0.11	0.40	1.54	0.92	0.08
ABC $R_F = 100\Omega$	0.06	1.44	1.15	0.89	1.09	0.71	0.73
	0.48	0.87	1.00	0.63	0.06	0.34	0.64
Large Disparity in Line Parameters							
ABC $R_F = 0\Omega$	3.48	1.14	4.01	4.07	0.47	1.82	2.26
	0.18	0.41	0.58	0.88	0.49	0.16	0.77
ABC $R_F = 10\Omega$	3.97	3.2	0.49	1.85	1.99	1.53	2.94
	0.15	0.18	0.11	0.40	1.54	0.92	0.08
ABC $R_F = 100\Omega$	3.35	1.55	3.93	2.05	1.21	3.32	0.44
	0.48	0.87	1.00	0.63	0.06	0.34	0.64

6.3. Chapter Summary

Novel algorithms discussed in Chapter 4 and Chapter 5 offer a similar advantage in fault location in that they are able to calculate the distance to fault without the need for any line parameter settings. The potential extension of the project with the industrial sponsor National Grid is currently under discussion. The work to be carried out as a part of the extended project is discussed in Chapter 8 as Future Work. The Whilst the FLA in Chapter 4 deals with single-circuit series compensated lines, the FLA in Chapter 5 deals with double-circuit series compensated lines. This line parameter free aspect of the novel FLAs is a significant advantage because line parameters are known to vary with weather and loading conditions. This chapter demonstrates the significance of this advantage by carrying out a comparison study with existing solutions that do require line parameters. An FLA proposed by Yu et al [134] is used in the comparison study for the single-circuit novel algorithm, and an FLA proposed by Kang et al [135] is used for the double-circuit novel algorithm. They are highly accurate, effective and simple algorithms, both using the analysis of characteristic impedances and propagation constants in their analysis.

Since both novel algorithms proposed in this thesis, are derived using similar principles, and offer the similar advantage of being line parameter free, the comparison yields similar conclusions for both algorithms regarding the significance of their novelty. They are validated in this chapter by testing the existing solutions upon introducing discrepancies in their settings (as listed in Table 6.3 and Table 6.9). The test circuits used in the analysis are the similar to those described in Chapter 4 and Chapter 5, and the same set of simulations are used for both algorithms (the existing and the novel) in each comparison. Example simulations of a SLG fault are carried out first with ideal settings, and a comparison each is made. The existing solutions are found to be more accurate in these conditions for both single-circuit lines as well as double-circuit lines. Upon increasing the disparity in settings, novel algorithms are found to be significantly more accurate.

Tables of results are presented containing comparisons for various simulations of different fault distances and fault resistances. The trends are observed to be similar to the example simulations. This was also found to be the case for DLG faults. However, when 3-phase

faults of DL faults are tested for and compared, the disparities in settings are found not significantly influence the accuracies of the existing solutions. This is understood as being due to small variance observed in positive-sequence impedance parameter settings as opposed to the large variance observed in negative-sequence impedance parameter settings.

Consequently, it may be concluded that both novel algorithms, algorithm-N1 and algorithm-N2 offer increased reliability and expected accuracy for fault types SLG and DLG, but not significantly for 3-phase faults and DL-faults. However, given that SLG faults constitute over 90% of faults on transmission lines, this makes the line parameter free aspect of the novel algorithms a significant advantage overall. The chapter also demonstrates how solutions often derived using line parameters are found to be very effective and accurate when using simulation studies using exact parameters (as the settings) to test the data. However, upon altering the settings, the accuracy of fault distance calculation is found to deteriorate. This is not the case for the novel algorithms since they don’t require any settings, and are thus more robust and reliable.

Chapter 7. Novel Line Parameter Free Algorithm to Account for Shunt Admittance

Shunt admittance of a transmission line affects the magnitude and phase of currents measured at the line-ends, and thus has a significant impact on the accuracy of fault locators. This becomes especially apparent for long transmission lines (>100km), for which fault locators are unable to locate faults with sufficient accuracy based on inductance and resistance parameters of the line alone. Although most lines on the GB transmission network are less than 100km [136], lines over 200 km in length are common in countries like USA, China, India and Brazil where the need for considering the shunt admittance of the line becomes apparent [137].

Chapter 7 details a novel algorithm, which allows fault locators using two-end synchronised current and voltage measurements, to account for the shunt admittance of the line. It does not require the use of any line parameters and only requires the synchronised phase currents and voltages from the two line-ends. Currently, the method is only limited to traditional uncompensated lines. It is hoped to develop this algorithm in future work for the purposes of improving fault location on series compensated lines. The method is derived in this chapter, simulation tests carried out are detailed and the corresponding results are tabulated.

FLAs using two-end synchronised measurements for phase voltages and currents can greatly benefit from the method described in this chapter. The method can be applied to any such FLA, regardless of the fault type. The method calculates the positive, negative and zero sequence values of the shunt admittance of the total length of the line using the synchronised input measurements alone. Thus, it does not require any settings for line parameters in its calculations. It is aimed at improving the overall accuracy of FLAs by accounting for currents in shunt admittances of the line, but without the need for any pre-determined line parameters. A number of FLAs either neglect the shunt admittance entirely or use line parameters.

There are two main disadvantages of using line parameters for shunt admittance. The first, as discussed previously is that line parameters are highly variable on account of weather and loading conditions. Secondly, accurate zero-sequence parameters are difficult to obtain. The method described here, in effect, calculates the shunt admittance parameters based on the synchronised measurements, and is capable of online calculations of these shunt admittance parameters. It is thus a more accurate and robust approach to fault location. The algorithm itself is detailed in Section 7.1, including the calculations to be carried out. The derivation of the equations used in the method are detailed in Section 7.2. Section 7.3 presents the dynamic simulation tests carried out to validate the algorithm and tabulates the corresponding results. The conclusions drawn from the study are provided in Section 7.4. It must be stated that the algorithm assumes that current measurements at line-ends are carried out using Rogowski coil CTs. The aim of the algorithm described in this chapter is to improve existing FLAs, by using an existing FLA in conjunction with the algorithm proposed in this paper. It is important to note that the novel algorithm is not a FLA, but an algorithm to improve the accuracy of existing FLAs.

7.1. Line Parameter Free Algorithm to Account for Shunt Admittance

The algorithm described in this chapter is capable of calculating the self and mutual components of the shunt admittance provided that voltage and currents at both ends of the line are available and are time-synchronised. It carries out this procedure without the need for any pre-defined line parameters. The central concept that forms the basis of the algorithm is that the difference in the local line-end current and remote line-end currents of any one of the phases under pre-fault conditions or of any of the healthy phases during fault must flow through the shunt admittance of the line.

For the sake of clarity of explanation, the algorithm to account for shunt admittance is discussed in two separate sections. The first of these sections (Section 7.1) only deals with the calculations used in the algorithm to arrive at the distance to fault. The derivations for each of these individual calculations are discussed in the subsequent section (Section 7.2). Therefore, Section 7.1 makes several references to Section 7.2. It is to be seen that the actual algorithm is simple in implementation (discussed throughout Section 7.1), even

though the derivation of the individual steps are complex (discussed throughout Section 7.2). It is also to be noted that the algorithm steps required in calculating the distance to fault for symmetrical faults and asymmetrical faults are discussed separately in this section as they require an entirely different set of calculations. It is important to emphasise that the algorithms steps are only stated here. The derivations for each of the individual equations are discussed in Section 7.2.

For lines less than 100 km shunt admittance and conductance may be neglected altogether. For lines longer than 100 km, shunt conductance can still be neglected but the shunt admittance must be taken into consideration to ensure sufficient accuracy [148]. The influence of the shunt admittance on the accuracy of fault location becomes significant for such lines. Commonly a pi-circuit line model is assumed and the shunt admittances are lumped at the ends of the line [148], [4]. The aim of the algorithm has thus far been described as to account for shunt admittance of the line. This is carried out by calculating the sequence network shunt admittances and recalculating the phase network series impedance currents by subtracting the currents lost in the shunt admittances.

Unlike the algorithms discussed in Chapter 5 and Chapter 6, the algorithm in this chapter does not require the analysis of any non-linear equations, and the solution is arrived by performing simple linear calculations. It is able to perform these calculations without the use of any line-parameters. In recent years a number of FLAs have been proposed that consider shunt admittance in the calculation of distance to fault. Reference [150] proposes an FLA which does not require the use of line parameters in its fault distance calculations and considers the shunt admittance of the line in its calculations. It performs these calculations through the analysis of positive sequence characteristic impedance and propogation constant. Another such FLA but for double-circuit lines in [32] considers the shunt admittance. It however does not explicitly calculate the shunt admittance currents, and arrives at the distance to fault directly. Reference [151] performs online calculations of line parameters using PMU measurement data. Reference [126] proposes a line-parameter FLA considering the shunt admittance in a two-step Newton Rhapson based process. In comparison, the algorithm discussed in this chapter explicitly calculates the shunt admittance currents and recalculates the series currents. This is so since it is aimed at

providing an addendum to existing FLAs using two-end current and voltage measurements which only consider series impedances of the line. The aim of the algorithm is unique and it is to improve the accuracy of such FLAs for long lines by means of simple additional calculations without the need for line parameters.

Asymmetrical faults and symmetrical faults require different set of calculations to arrive at the recalculated series-impedance phase currents. This is because symmetrical faults only require the analysis of the positive-sequence impedance and there are no healthy phases whereas asymmetrical faults require the analysis of zero sequence and positive sequence impedances and there are healthy phases available for analysis. The method of determining the fault type is identical to that described in Chapter 4, where each phase is analysed separately to determine if it is a healthy or faulted phase. The incoming current at the local end and the outgoing current at the remote end are compared, and also compared against the pre-fault current as carried out previously in Chapter 4 and Chapter 5. The two fault type categories are discussed as follows:

Algorithm for asymmetrical faults: Asymmetrical faults such as SLG, DL and DLG faults require the following procedure in order to arrive at the distance to fault. Although zero sequence impedance and admittance are calculated they are only required for the subsequent calculations of phase network impedances (i.e. the self and mutual impedances). Therefore, these calculations would apply even to DL faults, where even though there are no zero-sequence currents, the zero-sequence impedance is still required for subsequent calculations.

The steps involved in the algorithm are as follows:

1. Calculate an initial estimate for distance to fault *without* considering shunt admittance

2. Calculate the positive-sequence shunt admittance of the entire line length (Y_1) and the positive sequence series impedance (Z_1)

3. Calculate the self (Z_S) and mutual (Z_M) series impedances of the line

4. Calculate zero sequence shunt admittance (Y_0), phase-network self shunt-admittance (Y_S) and mutual shunt admittance (Y_M)

5. Recalculate the series currents (after subtracting the currents flowing through the shunt admittance)

6. Recalculate the distance to fault using the newly calculated series currents.

Each of these steps is explained as follows:

Step 1: *Calculate an initial estimate for fractional distance to fault ($l_{initial}$) using the FLA without considering shunt admittance*: There can be expected a small but considerable error in this initial estimate when applied for long lines. However, this initial estimate is sufficiently accurate to allow the calculations demanded of the subsequent steps in the algorithm. In this step, the existing FLA is carried out on its own, without the novel algorithm, to obtain the initial estimate.

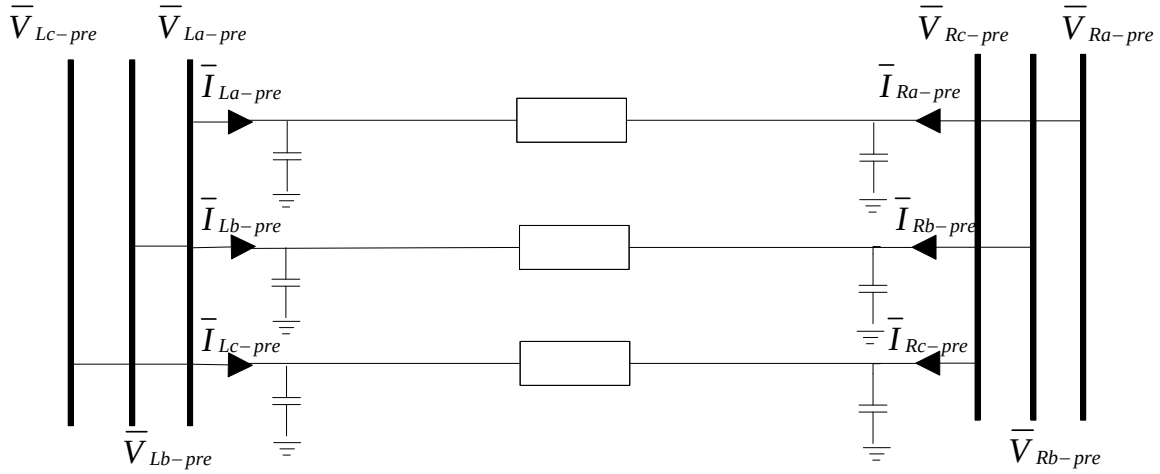

Figure 7.1: Uncompensated line under pre-fault conditions

Step 2: *Calculate the positive sequence shunt admittance of the entire line length (Y_1) and the positive sequence series impedance of the entire line length (Z_1):* They can be calculated using pre-fault currents and voltages as shown in (7.1) and (7.2). The negative

sequence series impedance and shunt admittance are assumed to be equal to the corresponding positive-sequence quantities the as is the case with transmission lines.

$$Y_1 = Y_2 = 2\frac{\bar{I}_{La-pre} + \bar{I}_{Ra-pre}}{\bar{V}_{La-pre} + \bar{V}_{Ra-pre}} \tag{7.1}$$

$$Z_1 = Z_2 = 2\frac{\bar{V}_{La-pre} - \bar{V}_{Ra-pre}}{\bar{I}_{La-pre} - \bar{I}_{Ra-pre}} \tag{7.2}$$

The derivation of these equations has been shown in Section 7.2.

Step 3: *Calculate the self and mutual series impedances of the line*: Once the positive-sequence series impedance has been calculated, this can then be used for the calculation of the self and mutual series impedances. These quantities allow the analysis of system and the recalculation of distance to fault using phase-networks rather than sequence-networks.

$$Z_M = \frac{\bar{V}_{Lc} - \bar{V}_{Rc} - Z_+ \bar{I}_{Lc}}{\bar{I}_{Lc} + l_{initial}\,(\bar{I}_{La} + \bar{I}_{Lb}) - (1 - l_{initial})\,(\bar{I}_{Ra} + \bar{I}_{Rb})} \tag{7.3}$$

$$Z_S = Z_1 + Z_M \tag{7.4}$$

The derivation of these equations has been shown in Section 7.2.

Step 4: *Calculate zero sequence shunt admittance (Y_0), self (Y_S) and mutual (Y_M) shunt admittance*s: Using the previously calculated voltages, the initial estimate of distance to fault and the positive sequence shunt admittance of the line, they are calculated using (7.5)-(7.7):

$$Y_0 = \frac{6(\bar{I}_{Lc} + \bar{I}_{Rc}) + Y_+(\bar{V}_{LFR-a} + \bar{V}_{LFR-b} - 2\bar{V}_{LFR-c})}{\bar{V}_{LFR-a} + \bar{V}_{LFR-b} + \bar{V}_{LFR-c}} \tag{7.5}$$

$$Y_M = \frac{Y_0 - Y_+}{3} \tag{7.6}$$

$$Y_S = \frac{Y_0 + 2Y_+}{3} \tag{7.7}$$

where,

$$\overline{V}_{Fa} = \overline{V}_{La} - l_1 Z_S \overline{I}_{La} - l_1 Z_M (\overline{I}_{Lb} + \overline{I}_{Lc}) \tag{7.8}$$

$$\overline{V}_{Fb} = \overline{V}_{Lb} - l_1 Z_S \overline{I}_{Lb} - l_1 Z_M (\overline{I}_{La} + \overline{I}_{Lc}) \tag{7.9}$$

$$\overline{V}_{Fc} = \overline{V}_{Lc} - l_1 Z_S \overline{I}_{Lc} - l_1 Z_M (\overline{I}_{La} + \overline{I}_{Lb}) \tag{7.10}$$

$$\overline{V}_{LFR-a} = l_{initial} \overline{V}_{La} + \overline{V}_{Fa} + (1 - l_{initial}) \overline{V}_{Ra} \tag{7.11}$$

$$\overline{V}_{LFR-b} = l_{initial} \overline{V}_{Lb} + \overline{V}_{Fb} + (1 - l_{initial}) \overline{V}_{Rb} \tag{7.12}$$

$$\overline{V}_{LFR-c} = l_{initial} \overline{V}_{Lc} + \overline{V}_{Fc} + (1 - l_{initial}) \overline{V}_{Rc} \tag{7.13}$$

The derivation of these equations has been shown in Section 7.2. Here, voltages $\overline{V}_{Fa}$, $\overline{V}_{Fb}$, and $\overline{V}_{Fc}$ are the phase voltages at the fault point, calculated by subtracting the voltage drop across the self and mutual impedances at each of the phases from the terminal voltage. Voltages $\overline{V}_{LFR-a}$, $\overline{V}_{LFR-b}$ and $\overline{V}_{LFR-c}$ in (7.8)-(7.10) are voltages that have been specially defined for the calculations to follow. The significance of these voltages becomes clear in the derivation of Y_0 discussed in Section 7.2.

Step 5: *Recalculate the series currents ($\overline{I}_{La}'$, $\overline{I}_{Lb}'$, $\overline{I}_{Lc}'$, $\overline{I}_{Ra}'$, $\overline{I}_{Rb}'$, $\overline{I}_{Rc}'$) by subtracting the shunt admittance currents assuming a pi-model line*: Figure 7.2 shows the recalculated series currents. FLAs are generally based on the relationships between series impedances of the faulted sections of the line and the currents flowing through these series impedances. In these FLAs, it is assumed that the shunt admittances are negligible and therefore, the

currents measured at the line-ends are assumed to be equal to the series currents. The validity of this assumption is affected by the magnitude of currents through the shunt admittances. For short lines, the resulting errors from this simplification are negligible. For longer lines however, the series currents must be recalculated as carried out in this step for the distance to fault to be accurate. The equations used in this recalculation are shown in (7.14)-(7.19). The derivation of these equations has been shown in Section 7.2.

$$\bar{I}_{La}' = \bar{I}_{La} - l_{initial}\frac{Y_S}{2}\bar{V}_{La} - l_{initial}\frac{Y_M}{2}(\bar{V}_{Lb} + \bar{V}_{Lc}) \tag{7.14}$$

$$\bar{I}_{Ra}' = \bar{I}_{Ra} - (1-l_{initial})\frac{Y_S}{2}\bar{V}_{Ra} - (1-l_{initial})\frac{Y_M}{2}(\bar{V}_{Rb} + \bar{V}_{Rc}) \tag{7.15}$$

$$\bar{I}_{Lb}' = \bar{I}_{Lb} - l_{initial}\frac{Y_S}{2}\bar{V}_{Lb} - l_{initial}\frac{Y_M}{2}(\bar{V}_{La} + \bar{V}_{Lc}) \tag{7.16}$$

$$\bar{I}_{Rb}' = \bar{I}_{Rb} - (1-l_{initial})\frac{Y_S}{2}\bar{V}_{Rb} - (1-l_{initial})\frac{Y_M}{2}(\bar{V}_{Ra} + \bar{V}_{Rc}) \tag{7.17}$$

$$\bar{I}_{Lc}' = \bar{I}_{Lc} - l_{initial}\frac{Y_S}{2}\bar{V}_{Lc} - l_{initial}\frac{Y_M}{2}(\bar{V}_{Lb} + \bar{V}_{La}) \tag{7.18}$$

$$\bar{I}_{Rc}' = \bar{I}_{Rc} - (1-l_{initial})\frac{Y_S}{2}\bar{V}_{Rc} - (1-l_{initial})\frac{Y_M}{2}(\bar{V}_{Rb} + \bar{V}_{Ra}) \tag{7.19}$$

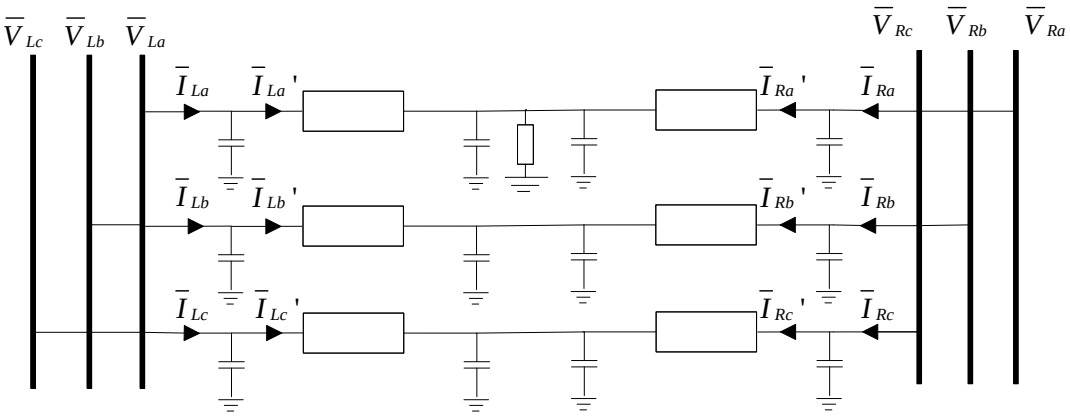

Figure 7.2: Uncompensated line under an asymmetrical fault

Step 6: *Recalculate the final estimate of distance to fault* l_{final} *using the new series currents thereby accounting for shunt admittance*: The recalculated series currents along with the terminal voltages are now used as the input for the FLA, and a more accurate estimate of distance to fault (l_{final}) is obtained.

Algorithm for symmetrical faults: All 3-phase symmetrical faults are covered in this subsection. Unlike for asymmetrical faults, analysis of only the positive sequence network is required for such faults. The algorithm for asymmetrical faults involved the calculation of self and mutual series impedances and shunt admittances. This analysis cannot be carried out here. Therefore, the algorithm for symmetrical faults is different to that for asymmetrical faults discussed previously. There are four steps involved in the algorithm. The algorithm is much simpler in comparison and only comprises of four steps:

Step 1: Calculate an initial estimate for fractional distance to fault ($l_{initial}$) using the FLA without considering shunt admittance.

Step 2: Calculate the positive sequence shunt admittance of the entire line length (Y_1) using (3.1) previously shown containing pre-fault currents and voltages. The derivation of these equations has been shown in Section 7.2.

Step 3: Recalculate the series currents by subtracting the shunt admittance currents as follows:

$$\bar{I}_{La}' = \bar{I}_{La} - l_{initial}\, Y_1 \bar{V}_{La} \tag{7.20}$$

$$\bar{I}_{Ra}' = \bar{I}_{Ra} - (1 - l_{initial})\, Y_1 \bar{V}_{Ra} \tag{7.21}$$

$$\bar{I}_{Lb}' = \bar{I}_{Lb} - l_{initial}\, Y_1 \bar{V}_{Lb} \tag{7.22}$$

$$\bar{I}_{Rb}' = \bar{I}_{Rb} - (1 - l_{initial})\, Y_1 \bar{V}_{Rb} \tag{7.23}$$

$$\bar{I}_{Lc}' = \bar{I}_{Lc} - l_{initial}\, Y_1 \bar{V}_{Lc} \tag{7.24}$$

$$\bar{I}_{Rc}' = \bar{I}_{Rc} - (1 - l_{initial}) Y_1 \bar{V}_{Rc} \tag{7.25}$$

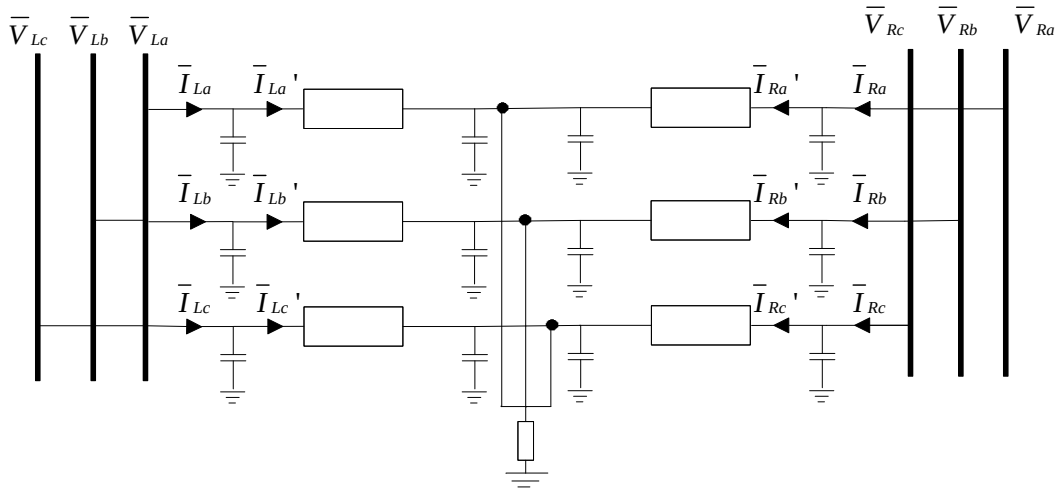

Figure 7.3: Uncompensated line under a symmetrical fault

Step 4: Recalculate the final estimate of distance to fault l_{final} using the new series currents to account for shunt admittance.

7.2. Algorithm Derivations

This section contains the derivations of equations used in Section 7.1, namely:

- The derivation of positive-sequence shunt admittance and positive sequence series impedance
- The derivation of self and mutual series impedances (phase-network)
- The derivation of self and mutual shunt admittances (phase-network)

They are each discussed as follows:

Derivation of Positive Sequence Quantities: The term Y_1 was calculated in (7.1) and represents the positive sequence shunt admittance of the line. It is calculated based on the difference between incoming and outgoing currents in any given phase. It is understood

that this difference in current flows through the shunt admittance. For instance, the incoming current through phase-a is $\bar{I}_{La}$ and the outgoing current from phase-a is $-\bar{I}_{Ra}$ (it is negative owing to the reference direction of the remote line-end currents as shown previously in Figure 7.1). Assuming a pi-model of the pre-fault line, its expression is derived as follows:

$$\bar{I}_{La-pre} + \bar{I}_{Ra-pre} = \bar{V}_{La-pre}\frac{Y_+}{2} + \bar{V}_{Ra-pre}\frac{Y_+}{2} \tag{7.26}$$

$$Y_1 = 2\frac{\bar{I}_{La-pre} + \bar{I}_{Ra-pre}}{\bar{V}_{La-pre} + \bar{V}_{Ra-pre}} \tag{7.27}$$

Note: The difference between incoming and outgoing currents appears as a sum due to the reference directions used for the current variables (see Figure 7.1). Given that during normal operating conditions, only the positive sequence network is active, Z_1 (the positive sequence series impedance) can be calculated as the voltage drop across any given phase divided by the series current flowing through that phase. The series current can be approximated as the average of the incoming and outgoing currents through that phase as shown below:

$$\bar{I}_{a-pre} = \frac{\bar{I}_{La-pre} + (-\bar{I}_{Ra-pre})}{2} \tag{7.28}$$

$$Z_1 = \frac{\bar{V}_{La-pre} - \bar{V}_{Ra-pre}}{\bar{I}_{a-pre}} = 2\frac{\bar{V}_{La-pre} - \bar{V}_{Ra-pre}}{\bar{I}_{La-pre} - \bar{I}_{Ra-pre}} \tag{7.29}$$

The sum of the incoming and outgoing currents appears as a difference once again, only due to the reference directions used for the remote line-end currents.

Derivation of Self and Mutual Series Impedances: The positive sequence series impedance calculated in (7.14) can be expressed in terms of the self and mutual series impedances [138]:

$$Z_1 = Z_S - Z_M \tag{7.30}$$

One of the healthy phases can be used to calculate the mutual impedance using the initial distance to fault estimate calculated in Step 1. The voltage drop across the healthy phase can be expressed in terms of the self and mutual series impedances. This is used below to derive expressions for both the self and mutual series impedances. If phase-c is healthy:

$$\overline{V}_{Lc} - \overline{V}_{Rc} = Z_S \overline{I}_{Lc} + Z_M (l_1 (\overline{I}_{La} + \overline{I}_{Lb}) - (1 - l_1)(\overline{I}_{Ra} + \overline{I}_{Rb})) \tag{7.31}$$

$$\overline{V}_{Lc} - \overline{V}_{Rc} = (Z_1 + Z_M)\overline{I}_{Lc} + Z_M (l_1 (\overline{I}_{La} + \overline{I}_{Lb}) - (1 - l_1)(\overline{I}_{Ra} + \overline{I}_{Rb})) \tag{7.32}$$

$$Z_M = \frac{\overline{V}_{Lc} - \overline{V}_{Rc} - Z_1 \overline{I}_{Lc}}{\overline{I}_{Lc} + l_1 (\overline{I}_{La} + \overline{I}_{Lb}) - (1 - l_1)(\overline{I}_{Ra} + \overline{I}_{Rb})} \tag{7.33}$$

$$Z_S = Z_1 + Z_M \tag{7.34}$$

Derivation of Zero-Sequence Line Admittance, self and mutual line admittance: Let $\mathbf{Y_{SEQ}}$ be a matrix containing the self and mutual admittances of the sequence network of line as shown below:

$$\mathbf{Y_{SEQ}} = \begin{bmatrix} Y_0 & 0 & 0 \\ 0 & Y_1 & 0 \\ 0 & 0 & Y_2 \end{bmatrix} = \begin{bmatrix} Y_0 & 0 & 0 \\ 0 & Y_1 & 0 \\ 0 & 0 & Y_1 \end{bmatrix} \tag{7.35}$$

The diagonal elements contain the self sequence impedances, and the non-diagonal elements contain the mutual sequence impedances. Assuming each faulted section as a pi-model line in itself, each phase contains four shunt admittances as shown in Figure 7.4Figure 7.3. Let $\overline{\mathbf{I}}_{\mathbf{Y-PHASE}}$ be a vector containing the sum of the phase currents flowing through the four shunt admittances for each phase. Let $\overline{\mathbf{I}}_{\mathbf{Y-SEQ}}$ be the $\overline{\mathbf{I}}_{\mathbf{Y-PHASE}}$ vector expressed in the sequence domain.

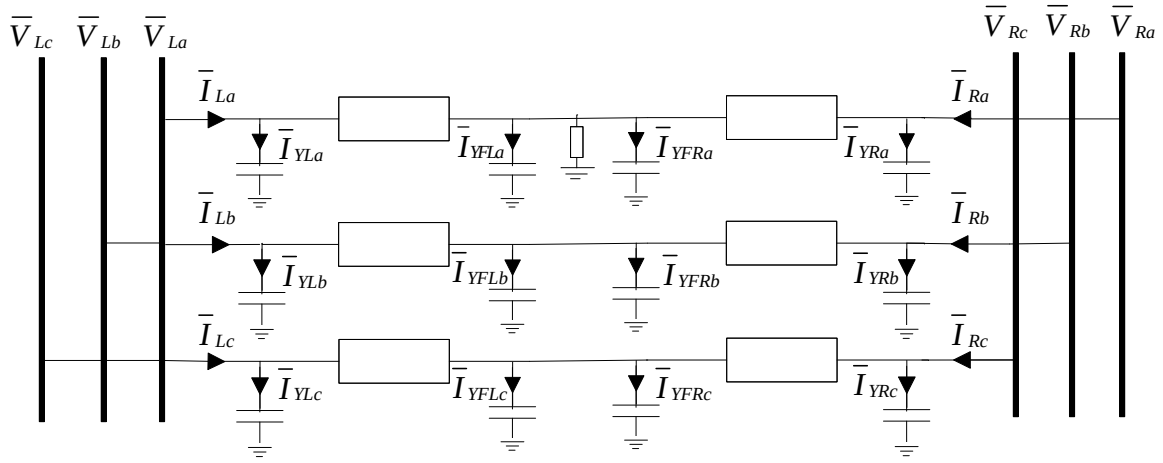

Figure 7.4: Shunt admittance currents

$$\bar{\mathbf{I}}_{\mathbf{Y-PHASE}} = \begin{bmatrix} \bar{I}_{Ya} \\ \bar{I}_{Yb} \\ \bar{I}_{Yc} \end{bmatrix} = \begin{bmatrix} \bar{I}_{YLa} \\ \bar{I}_{YLb} \\ \bar{I}_{YLc} \end{bmatrix} + \begin{bmatrix} \bar{I}_{YFLa} \\ \bar{I}_{YFLb} \\ \bar{I}_{YFLc} \end{bmatrix} + \begin{bmatrix} \bar{I}_{YFRa} \\ \bar{I}_{YFRb} \\ \bar{I}_{YFRc} \end{bmatrix} + \begin{bmatrix} \bar{I}_{YRa} \\ \bar{I}_{YRb} \\ \bar{I}_{YRc} \end{bmatrix} \tag{7.36}$$

$$\bar{\mathbf{I}}_{\mathbf{Y-SEQ}} = \begin{bmatrix} \bar{I}_{Y0} \\ \bar{I}_{Y1} \\ \bar{I}_{Y2} \end{bmatrix} = \frac{1}{3} \begin{bmatrix} 1 & 1 & 1 \\ 1 & a & a^2 \\ 1 & a^2 & a \end{bmatrix} \bar{\mathbf{I}}_{\mathbf{Y-PHASE}} \tag{7.37}$$

This vector can be expressed as the sum each of the four currents constituting $\bar{\mathbf{I}}_{\mathbf{Y-PHASE}}$ each expressed in the sequence domain.

$$\bar{\mathbf{I}}_{\mathbf{Y-SEQ}} = l_1 \frac{\mathbf{Y_{SEQ}}}{2}\begin{bmatrix}\overline{V}_{L0}\\ \overline{V}_{L1}\\ \overline{V}_{L2}\end{bmatrix} + l_1 \frac{\mathbf{Y_{SEQ}}}{2}\begin{bmatrix}\overline{V}_{F0}\\ \overline{V}_{F1}\\ \overline{V}_{F2}\end{bmatrix} + (1-l_1)\frac{\mathbf{Y_{SEQ}}}{2}\begin{bmatrix}\overline{V}_{F0}\\ \overline{V}_{F1}\\ \overline{V}_{F2}\end{bmatrix} + (1-l_1)\frac{\mathbf{Y_{SEQ}}}{2}\begin{bmatrix}\overline{V}_{R0}\\ \overline{V}_{R1}\\ \overline{V}_{R2}\end{bmatrix}$$
$$= \frac{\mathbf{Y_{SEQ}}}{2}\begin{bmatrix} l_1\cdot\overline{V}_{L0} + \overline{V}_{F0} + (1-l_1)\cdot\overline{V}_{R0}\\ l_1\cdot\overline{V}_{L1} + \overline{V}_{F1} + (1-l_1)\cdot\overline{V}_{R1}\\ l_1\cdot\overline{V}_{L2} + \overline{V}_{F2} + (1-l_1)\cdot\overline{V}_{R2}\end{bmatrix} = \frac{\mathbf{Y_{SEQ}}}{2}\frac{1}{3}\begin{bmatrix}1 & 1 & 1\\ 1 & a & a^2\\ 1 & a^2 & a\end{bmatrix}\begin{bmatrix}\overline{V}_{LFR-a}\\ \overline{V}_{LFR-b}\\ \overline{V}_{LFR-c}\end{bmatrix} \quad (7.38)$$

From (7.37) and (7.38) it follows:

$$\frac{1}{3}\begin{bmatrix}1 & 1 & 1\\ 1 & a & a^2\\ 1 & a^2 & a\end{bmatrix}\bar{\mathbf{I}}_{\mathbf{Y-PHASE}} = \frac{\mathbf{Y_{SEQ}}}{2}\frac{1}{3}\begin{bmatrix}1 & 1 & 1\\ 1 & a & a^2\\ 1 & a^2 & a\end{bmatrix}\begin{bmatrix}\overline{V}_{LFR-a}\\ \overline{V}_{LFR-b}\\ \overline{V}_{LFR-c}\end{bmatrix} \quad (7.39)$$

$$\bar{\mathbf{I}}_{\mathbf{Y-PHASE}} = \begin{bmatrix}1 & 1 & 1\\ 1 & a & a^2\\ 1 & a^2 & a\end{bmatrix}^{-1}\frac{\mathbf{Y_{SEQ}}}{2}\begin{bmatrix}1 & 1 & 1\\ 1 & a & a^2\\ 1 & a^2 & a\end{bmatrix}\begin{bmatrix}\overline{V}_{LFR-a}\\ \overline{V}_{LFR-b}\\ \overline{V}_{LFR-c}\end{bmatrix} \quad (7.40)$$

$$\bar{\mathbf{I}}_{\mathbf{Y-PHASE}} = \frac{1}{6}\begin{bmatrix}Y_0+2Y_+ & Y_0-Y_+ & Y_0-Y_+\\ Y_0-Y_+ & Y_0+2Y_+ & Y_0-Y_+\\ Y_0-Y_+ & Y_0-Y_+ & Y_0+2Y_+\end{bmatrix}\begin{bmatrix}\overline{V}_{LFR-a}\\ \overline{V}_{LFR-b}\\ \overline{V}_{LFR-c}\end{bmatrix} \quad (7.41)$$

Using the above equation for the healthy phase-c, Y_0 is calculated as shown in (7.42) and (7.43). Given that Y_0 is only required for asymmetrical faults, there will always be at least one healthy phase for this analysis.

$$\bar{I}_{Y-c} = \bar{I}_{Lc} + \bar{I}_{Rc} = \frac{(Y_0-Y_+)}{6}\overline{V}_{LFR-a} + \frac{(Y_0-Y_+)}{6}\overline{V}_{LFR-b} + \frac{(Y_0+2Y_+)}{6}\overline{V}_{LFR-c} \quad (7.42)$$

$$Y_0 = \frac{6(\overline{I}_{Lc}+\overline{I}_{Rc}) + Y_+(\overline{V}_{LFR-a}+\overline{V}_{LFR-b}-2\overline{V}_{LFR-c})}{\overline{V}_{LFR-a}+\overline{V}_{LFR-b}+\overline{V}_{LFR-c}} \quad (7.43)$$

7.3. Simulations and Algorithm Validation

7.3.1. The Fault Location Algorithm to be Improved

A settings-free FLA proposed by Preston et al. in [124] was used to validate the algorithm. The algorithm was chosen as it is a highly accurate settings-free algorithm for uncompensated lines, as it uses two-terminal current and voltage measurements for its calculations and does not consider the shunt admittance of the line. For the sake of clarity this algorithm will henceforth be referred to as algorithm-E3, whilst the novel algorithm discussed in this chapter will be referred to as algorithm-N3. It is important to note that algorithm-N3 was used to improve the accuracy of algorithm-E3 (and is hence used together with algorithm-E3). It was run for every simulation first without performing the shunt admittance algorithm, and then with performing the algorithm, and the errors in distance to fault are compared with one another. The FLA in consideration calculates the distance to fault based on the assumption that the positive sequence impedance of a transmission line or line section is equal to its negative sequence impedance. In its original form, the FLA neglects the shunt admittance. The final expressions for distance to fault as calculated by the algorithm for symmetrical and asymmetrical fault are shown below in (7.44) and (7.45):

$$\ell = \frac{(\underline{V}_{\mathrm{S}}^{p} - \underline{V}_{\mathrm{R}}^{p})\underline{I}_{\mathrm{R}}^{n} - (\underline{V}_{\mathrm{S}}^{n} - \underline{V}_{\mathrm{R}}^{n})\underline{I}_{\mathrm{R}}^{p}}{(\underline{V}_{\mathrm{S}}^{p} - \underline{V}_{\mathrm{R}}^{p})(\underline{I}_{\mathrm{S}}^{n} + \underline{I}_{\mathrm{R}}^{n}) - (\underline{V}_{\mathrm{S}}^{n} - \underline{V}_{\mathrm{R}}^{n})(\underline{I}_{\mathrm{S}}^{p} + \underline{I}_{\mathrm{R}}^{p})} \tag{7.44}$$

$$\ell = \sqrt{\frac{(a_1 + b_1 R_{\mathrm{F}})^2 + (a_2 + b_2 R_{\mathrm{F}})^2}{[a_1 + c_1 + (b_1 + d_1)R_{\mathrm{F}}]^2 + [a_2 + c_2 + (b_2 + d_2)R_{\mathrm{F}}]^2}} \tag{7.45}$$

The terms contained in these equations have been defined in Table 7.1 and Table 7.2.

Table 7.1: Definitions of terms in (7.44)

Term	Definition
$\underline{V}_S^p$	Positive- sequence sending end voltage
$\underline{V}_S^n$	Negative- sequence sending end voltage
$\underline{V}_R^p$	Positive- sequence receiving end voltage
$\underline{V}_R^n$	Negative- sequence receiving end voltage
$\underline{I}_S^p$	Positive- sequence sending end current
$\underline{I}_S^n$	Negative- sequence sending end current
$\underline{I}_R^p$	Positive- sequence receiving end current
$\underline{I}_R^n$	Negative- sequence receiving end current

Table 7.2: Definition of terms for (7.45)

Term	Definition	Term	Definition
a_1	$\mathrm{Re}[\frac{\underline{V}_S^p}{\underline{I}_S^p}]$	c_1	$\mathrm{Re}[\frac{\underline{V}_R^p}{\underline{I}_R^p}]$
a_2	$\mathrm{Im}[\frac{\underline{V}_S^p}{\underline{I}_S^p}]$	c_2	$\mathrm{Im}[\frac{\underline{V}_R^p}{\underline{I}_R^p}]$
b_1	$\mathrm{Re}[-\frac{\underline{I}_S^p+\underline{I}_R^p}{\underline{I}_S^p}]$	d_1	$\mathrm{Re}[-\frac{\underline{I}_S^p+\underline{I}_R^p}{\underline{I}_R^p}]$
b_2	$\mathrm{Im}[-\frac{\underline{I}_S^p+\underline{I}_R^p}{\underline{I}_S^p}]$	d_2	$\mathrm{Im}[-\frac{\underline{I}_S^p+\underline{I}_R^p}{\underline{I}_R^p}]$
p	$\frac{a_1d_1+b_1c_2-a_2d_1-b_2c_2}{b_1d_2-b_2d_1}$	q	$\frac{a_1c_2-a_2c_1}{b_1d_2-b_2d_1}$
R_F	$\frac{-p\pm\sqrt{p^2-4q}}{2}$		

7.3.2. ATP-EMTP Simulation

The ATP-EMTP software was used to model a test circuit for the purpose of simulating synchronised current and voltage samples to be used as the input data for the FLA and the algorithm for improving its accuracy (shown in Figure 7.5). It comprises of a 300km 400kV OHTL. The network parameters and transmission line parameters are provided in Table 7.3 and Table 7.4 respectively. Measurements of voltage and current were synchronously sampled here and used as input to MATLAB for processing the algorithms.

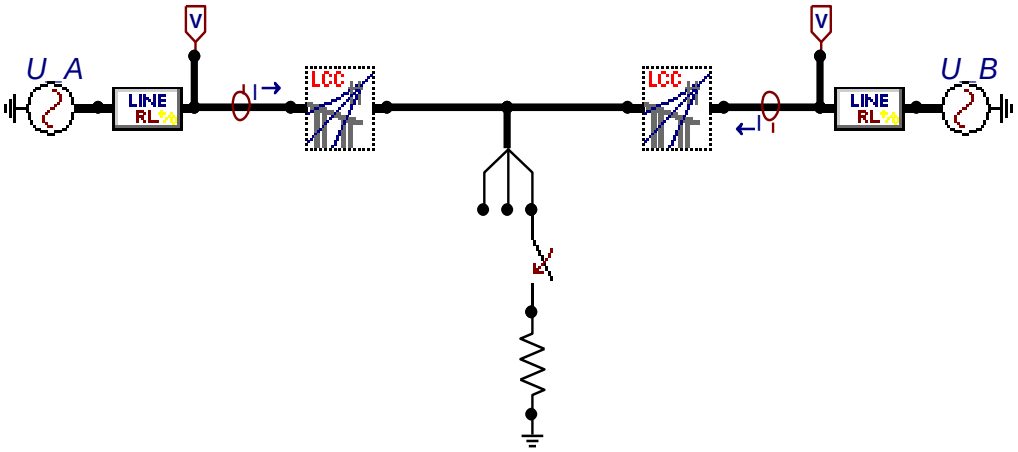

Figure 7.5: ATP-EMTP test circuit for an uncompensated line

Table 7.3: Network Parameters

Network Parameters	Local Network A	Remote Network B
Line to Line RMS Voltage (kV)	416	400
Phase Angle (^{o})	0	-20
+ve seq. Resistance (Ω)	1.019	0.637
+ve seq. Inductance (H)	0.051	0.031
$Z_1 = R_1+jX_1$	1.019+j16	0.637+j10
X_1/R_1	15.7	15.7
0 seq. Resistance (Ω)	2.037	1.273
0 seq. Inductance (H)	0.102	0.064
$Z_0 = R_0+jX_0$	2.037+j32	1.273+j20
X_0/R_0	15.7	15.7
Fault MVA	45MVA	70MVA

Table 7.4: Transmission Line Parameters

Transmission Line Parameters	Positive/Negative Sequence	Zero Sequence
resistance, Ω/km	0.065	0.195
inductance mH/km	0.955	2.864
Capacitance nF/km	10.5	5

R Ω /km	0.065	0.195
X Ω /km	0.3	0.9
B S/km	$0.329x10^{-5}$	$0.157x10^{-5}$
X/R	4.615	4.615

The algorithm for asymmetrical faults and for symmetrical faults was thoroughly tested. All fault types were considered, i.e. SLG faults, DLG, faults, DL faults and 3-phase symmetrical faults. For each such fault type, the fault distance was varied from 0-300km and the fault resistance was varied from 0-100 Ω. The errors calculated based on using the FLA alone were first recorded, after which the FLA was run in conjunction with the shunt admittance algorithm, after which the errors are recalculated. They are tabulated in Table 7.5 - Table 7.8. In each case, the fault was simulated to occur at 43 ms, and a sampling frequency of 6.4 kHz was used for synchronous sampling. The data window size for the FFT was 20 ms. An example simulation was carried out as follows. A SLG fault was simulated at 200km from the local end of the line for a fault resistance of 100Ω. The current and voltage waveforms as seen at the local and remote line-ends of the line are shown in Figure 7.6 and Figure 7.7.

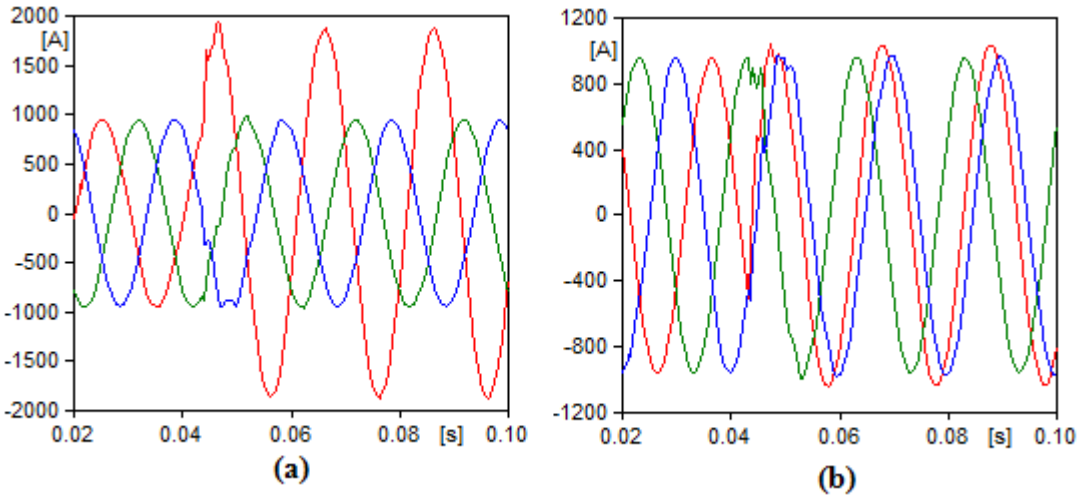

Figure 7.6: Phase currents for a SLG fault on an uncompensated line a) Local line-end currents b) Remote line-end currents

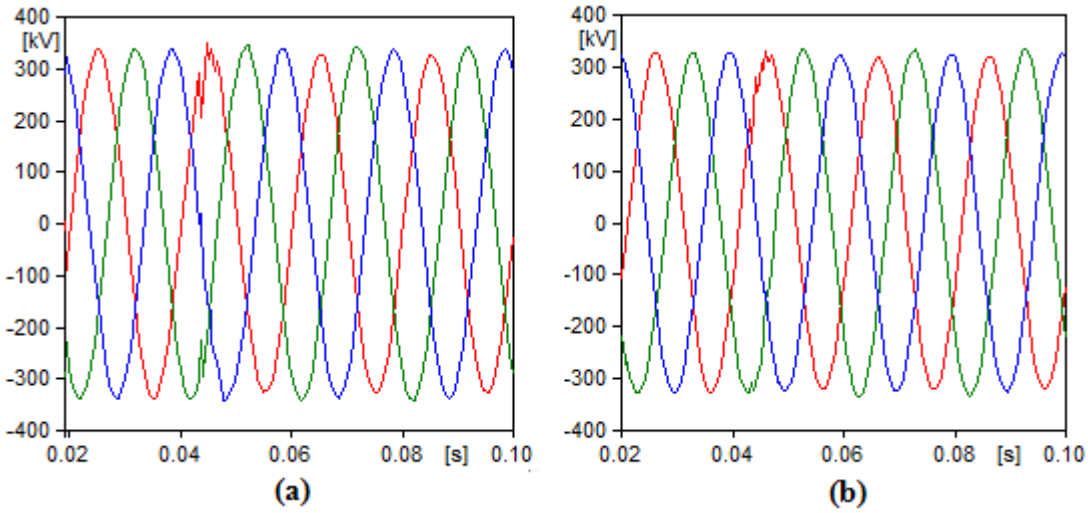

Figure 7.7: Phase voltages for a SLG fault on an uncompensated line a) Local line-end voltages b) Remote line-end voltages

The FLA to be improved is capable of locating faults in real time. Thus, the fault distance calculation for each sample was carried out and the distance to fault estimate vs. time plot has been shown in Figure 7.8. It can be seen that the FLA converges to solution shortly after the fault inception time. The FLA uses FFT without any algorithm to filter out DC components from the measured current samples. The simulation shown in Figure 7.6 and Figure 7.7, is analysed with algorithm-E3 to calculate the distance to fault. It can be seen that the accuracy is sensitive to DC components during the period from fault inception up to the end of a short convergence period, as can be seen in Figure 7.8. A second analysis is carried out again with algorithm-E3 but in conjunction with algorithm-N3. The estimates obtained are averaged over the 40-120 ms interval. The average result for this simulation was calculated to be 199.3115 km without using algorithm-N3 (only algorithm E3) and 199.6596 km using algorithm-E3 in conjunction with algorithm-N3.

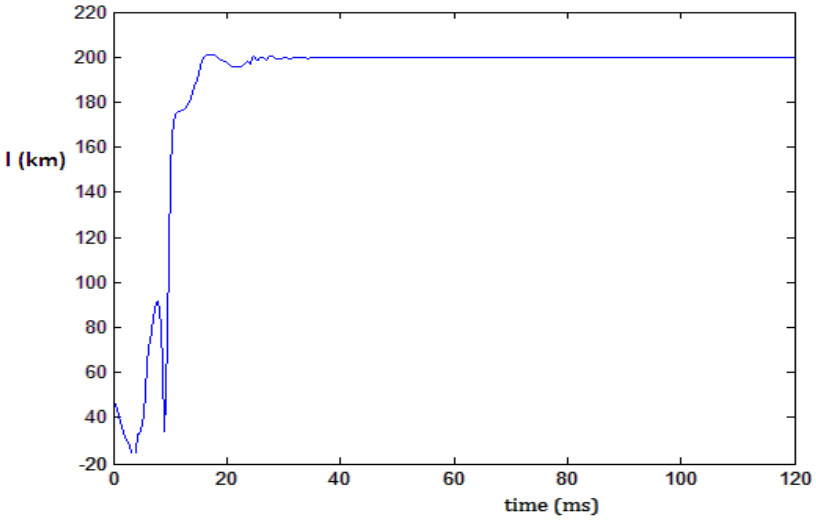

Figure 7.8: Fault distance vs. Time

7.3.3. Results and Comparison

This section tabulates the results obtained to validate the algorithm described in this chapter. The advantage of using the novel algorithm proposed in this chapter is highlighted by performing two sets of calculations for each simulation. The first of these calculations is carried out only using algorithm-E3. The second calculation is also carried out with algorithm-E3, but this time, also using algorithm-N3 to reduce the errors by taking into account the shunt admittance of the line. That is to say that the first of these calculations *does not* take into account shunt admittance by itself. The second of these calculations uses the method described in this chapter to obtain a much more accurate solution for distance to fault. The two calculated values of distance to fault are then compared against one another to evaluate the improvement brought about by the novel algorithm-N3. The improvements are expressed both as a difference in the percentage error as well as in metres.

In each case, a 300 km line is used, and the fault distance and fault resistance are varied. This set of tests is repeated for each fault type and the corresponding results are presented in Table 7.5 to Table 7.8. The first two columns in each table refer to the fault distance and

fault resistance. The third column contains the errors calculated using just algorithm-E3. The fourth column tabulates the errors using algorithm-E3 and algorithm-N3 together. The difference in the two entries indicates the improvements brought about by algorithm-N3, and the last column expresses the equivalent of this difference in metres. Adhering to IEEE standards [132], the errors presented in this section are calculated using (4.70) as described previously in Chapter 4. For each fault type, the improvements are found to be very high when the fault is simulated near the line terminals. This improvement is found to decrease as the fault is moved closer to the centre (fault location of 150 km). This is due to the mathematical principles of the existing algorithm which is being improved rather than any aspect of the addendum algorithm presented in this Chapter. The error is found to be the smallest at the middle of the line. This can be explained as being due to the fact that the accuracy of algorithm-E3 is not affected by not considering shunt admittance when the two faulted line segments are symmetrical in the sequence network. Also, this Chapter only discusses patterns observed in the improvements in accuracy rather than the errors themselves. The patterns in the errors are not due to the principles of the addendum algorithm but rather due to the original algorithm itself. A detailed analysis of results in presented in Section 7.3.4. It is important to note that while there are trends observed in the accuracies of the original algorithm, these are outside the scope of the thesis. This Chapter focuses specifically on the new addendum algorithm designed to improve the existing algorithm by accounting for the shunt admittance. Thus, the focus of this Chapter and in particular the results presented is the improvement brought about by the new addendum algorithm.

Table 7.5: Improvement in accuracy for SLG faults

Fault Location (km)	Fault Resistance	Error (%) without proposed method	Error (%) with proposed method	Improvement in Accuracy (ΔError%)	Improvement in Accuracy (m)
30	R=100	0.6023	0.1384	0.4639	1391.7
	R=10	0.6024	0.1282	0.4742	1422.6
	R=0	0.603	0.1278	0.4752	1425.6
60	R=100	0.4367	0.1724	0.2643	792.9
	R=10	0.4367	0.166	0.2707	812.1
	R=0	0.4373	0.1659	0.2714	814.2
90	R=100	0.3113	0.1576	0.1537	461.1
	R=10	0.3113	0.1532	0.1581	474.3
	R=0	0.3118	0.1532	0.1586	475.8
120	R=100	0.1254	0.0551	0.0703	210.9
	R=10	0.1254	0.0518	0.0736	220.8
	R=0	0.1258	0.0519	0.0739	221.7
150	R=100	0	0.0002	-0.0002	-0.6
	R=10	0	0.0002	-0.0002	-0.6
	R=0	0.0003	0.0003	0	0
180	R=100	-0.1185	-0.0495	0.069	207
	R=10	-0.1185	-0.0514	0.0671	201.3
	R=0	-0.1182	-0.0513	0.0669	200.7
240	R=100	-0.3606	-0.1647	0.1959	587.7
	R=10	-0.3606	-0.1663	0.1943	582.9
	R=0	-0.3604	-0.1664	0.194	582
270	R=100	-0.3876	-0.1269	0.2607	782.1
	R=10	-0.3876	-0.1287	0.2589	776.7
	R=0	-0.3874	-0.1288	0.2586	775.8

Table 7.6: Improvement in accuracy for DLG faults

Fault Location (km)	Fault Resistance	Error (%) without proposed method	Error (%) with proposed method	Improvement in Accuracy (ΔError%)	Improvement in Accuracy (m)
30	R=100	0.6024	0.1335	0.4689	1406.7
	R=10	0.6024	0.1293	0.4731	1419.3
	R=0	0.6024	0.1236	0.4788	1436.4
60	R=100	0.4367	0.1709	0.2658	797.4
	R=10	0.4367	0.168	0.2687	806.1
	R=0	0.4367	0.1658	0.2709	812.7
90	R=100	0.3113	0.1568	0.1545	463.5
	R=10	0.3113	0.1553	0.156	468
	R=0	0.3113	0.1545	0.1568	470.4
120	R=100	0.1254	0.0539	0.0715	214.5
	R=10	0.1254	0.0534	0.072	216
	R=0	0.1254	0.0533	0.0721	216.3
150	R=100	0	0.0005	-0.0005	-1.5
	R=10	0	0.0006	-0.0006	-1.8
	R=0	0	0.0006	-0.0006	-1.8
180	R=100	-0.1185	-0.0528	0.0657	197.1
	R=10	-0.1185	-0.0527	0.0658	197.4
	R=0	-0.1185	-0.0527	0.0658	197.4
210	R=100	-0.2841	-0.156	0.1281	384.3
	R=10	-0.2841	-0.1563	0.1278	383.4
	R=0	-0.2841	-0.1566	0.1275	382.5
240	R=100	-0.3606	-0.1697	0.1909	572.7
	R=10	-0.3606	-0.1704	0.1902	570.6
	R=0	-0.3606	-0.1712	0.1894	568.2
270	R=100	-0.3875	-0.1319	0.2556	766.8
	R=10	-0.3875	-0.1319	0.2556	766.8
	R=0	-0.3875	-0.1329	0.2546	763.8

Table 7.7: Improvement in accuracy for DL faults

Fault Location (km)	Fault Resistance	Error (%) without proposed method	Error (%) with proposed method	Improvement in Accuracy (ΔError%)	Improvement in Accuracy (m)
30	R=100	0.6023	0.1363	0.466	1398
	R=10	0.6023	0.1314	0.4709	1412.7
	R=0	0.6023	0.1309	0.4714	1414.2
60	R=100	0.4367	0.1734	0.2633	789.9
	R=10	0.4367	0.1698	0.2669	800.7
	R=0	0.4367	0.1694	0.2673	801.9
90	R=100	0.3113	0.1588	0.1525	457.5
	R=10	0.3113	0.1564	0.1549	464.7
	R=0	0.3113	0.1562	0.1551	465.3
120	R=100	0.1254	0.055	0.0704	211.2
	R=10	0.1254	0.0538	0.0716	214.8
	R=0	0.1254	0.0537	0.0717	215.1
150	R=100	0	0.0007	-0.0007	-2.1
	R=10	0	0.0005	-0.0005	-1.5
	R=0	0	0.0005	-0.0005	-1.5
180	R=100	-0.1185	-0.0536	0.0649	194.7
	R=10	-0.1185	-0.0529	0.0656	196.8
	R=0	-0.1185	-0.0529	0.0656	196.8
210	R=100	-0.2842	-0.1578	0.1264	379.2
	R=10	-0.2842	-0.1563	0.1279	383.7
	R=0	-0.2842	-0.1562	0.128	384
240	R=100	-0.3606	-0.1727	0.1879	563.7
	R=10	-0.3606	-0.1705	0.1901	570.3
	R=0	-0.3606	-0.1703	0.1903	570.9
270	R=100	-0.3876	-0.136	0.2516	754.8
	R=10	-0.3876	-0.1331	0.2545	763.5
	R=0	-0.3876	-0.1327	0.2549	764.7

Table 7.8: Improvement in accuracy for 3-phase faults

Fault Location (km)	Fault Resistance	Error (%) without proposed method	Error (%) with proposed method	Improvement in Accuracy (ΔError%)	Improvement in Accuracy (m)
30	R=100	-1.3203	-0.8745	0.4458	1337.4
	R=10	-1.3203	-0.8745	0.4458	1337.4
	R=0	-1.3203	-0.8745	0.4458	1337.4
60	R=100	-1.739	-0.8383	0.9007	2702.1
	R=10	-1.739	-0.8383	0.9007	2702.1
	R=0	-1.739	-0.8383	0.9007	2702.1
90	R=100	-1.8832	-0.8535	1.0297	3089.1
	R=10	-1.8832	-0.8535	1.0297	3089.1
	R=0	-1.8832	-0.8535	1.0297	3089.1
120	R=100	-1.9085	-0.9577	0.9508	2852.4
	R=10	-1.9085	-0.9577	0.9508	2852.4
	R=0	-1.9085	-0.9577	0.9508	2852.4
150	R=100	-1.7392	-1.0116	0.7276	2182.8
	R=10	-1.7392	-1.0116	0.7276	2182.8
	R=0	-1.7392	-1.0116	0.7276	2182.8
180	R=100	-1.4668	-1.0648	0.402	1206
	R=10	-1.4668	-1.0648	0.402	1206
	R=0	-1.4668	-1.0648	0.402	1206
210	R=100	-1.2141	-0.1672	1.0469	3140.7
	R=10	-1.2141	-0.1672	1.0469	3140.7
	R=0	-1.2141	-0.1672	1.0469	3140.7
240	R=100	-0.8834	-0.1796	0.7038	2111.4
	R=10	-0.8834	-0.1796	0.7038	2111.4
	R=0	-0.8834	-0.1796	0.7038	2111.4
270	R=100	-0.5714	-0.1392	0.4322	1296.6
	R=10	-0.5714	-0.1392	0.4322	1296.6
	R=0	-0.5714	-0.1392	0.4322	1296.6

7.3.4. Analysis of Results

From the results and comparison section, the algorithm may be critiqued as follows:

- The algorithm consistently improves the accuracy of the FLA, in nearly each case. In the few instances that the combined algorithm accuracy is worse than that of the

FLA alone, the errors are only marginally different to one another. This is found to occur only when the fault is simulated at the mid-point (150 km). This can be explained as being due to the fact that the accuracy of algorithm-E3 is not affected by not considering shunt admittance when the two faulted line segments are symmetrical in the sequence network. In effect, the inaccuracies from the loss of current in the shunt admittance cancel out due to this symmetry. Therefore, at the middle point (only), algorithm-N3 does not offer an improvement for asymmetrical faults, although the deterioration is seen to be negligible (<0.00021%). For symmetrical faults, (Table 7.8) the improvements are found to be much higher than for asymmetrical faults, and even at mid-point, the improvements are found to be high (>0.71%). This is since, the calculation used by algorithm-E3 is different for asymmetrical faults (see (7.44)) and symmetrical faults (see (7.45)), and the errors of algorithm-E3 are considerably higher for asymmetrical faults.

- From Table 7.5 - Table 7.8 it can be observed, that the algorithm-N3 improves the overall accuracy of algorithm-E3, for all fault types considered and various fault resistances. The four major fault types i.e. SLG, DL, DLG, 3-Phase have been considered, and fault resistance in each simulation is varied from 0Ω (solid ground), 10Ω, 100Ω (high-resistance faults). When comparing the improvements for high resistance faults to those for solid-earth faults, it is found that the algorithm-N3 performs better for solid-earth faults. The improvements are found to decrease with increasing fault resistance, although these are found to be marginal for each fault distance. This marginal decrease in improvement can be explained as being due to the simplified assumptions used to consider the shunt admittance of the line, although this simplification can be seen to be justified, given that it still performs accurately for high resistance faults. Given that the algorithm is consistently seen to reduce the errors under such various conditions of fault resistance and fault distance, it demonstrates that the method is based on sound assumptions of the line and its shunt admittance.

- The improvements are especially significant for symmetrical three phase faults, where the new estimates are closer to the actual distance to fault in some cases by

up to 3km. This difference between the results for asymmetrical faults and symmetrical faults can be explained as being due to the calculation procedure used by algorithm-E3. As discussed previously in Section 7.3.1, it uses (7.44) for asymmetrical faults and (7.45) for symmetrical faults. It can be seen from the results that the calculation method for symmetrical faults is more prone to errors due to not considering shunt admittance than that for asymmetrical faults. From (7.45) it can be seen that this calculation method used in algorithm-E3 for symmetrical faults uses the analysis of the fault resistance unlike (7.44) which does not require this. This explains the additional error in fault location introduced in the results for such fault types. Upon considering the shunt admittance using the algorithm-N3, the errors are found to be significantly reduced, in some cases by up to 3km.

- The improvements in the accuracy are especially higher at the ends of the line, i.e. closer to the fault distance being 0 km or to 300km. This is due to the fact that currents through the shunt admittances in the two line segments become significantly different to one another at these extremes. This causes inaccuracies in fault distance estimation, where shunt admittances are not considered. However, with the algorithm described in this chapter such inaccuracies can be avoided.

7.4. Chapter Summary

A novel line parameter free algorithm to improve the accuracy of FLAs for long transmission lines by accounting for shunt admittance of the line is presented in this chapter. It is able to calculate the self and mutual shunt admittance using online measurements, and therefore is able to calculate the currents through these admittances, and calculate the series currents flowing through the line. It is based on the assumption of a pi-model line, which is found to be a reasonable approximation of the electrical nature of the line [148], [4].

The chapter discussed the algorithms for symmetrical and asymmetrical faults in sufficient detail. The equations used in the algorithm were derived. Lastly, the algorithm is validated

by using it in conjunction with a settings free FLA that did not originally consider shunt admittance in its calculation. It is found to improve the accuracy of the algorithm consistently and these improvements are found to be for a long line (300km), where such shunt admittance currents become a significant influence on the accuracy of fault location. Various fault resistances, fault types and fault distances have been tested for, and the algorithm performs consistently regardless of these factors.

Chapter 8. Conclusions and Future Work

All background and original work carried out in the project are presented in the preceding chapters of this thesis. This chapter summarises the thesis, presents the conclusions of each original contribution, and discusses potential future work.

This thesis presented the original research carried out by the author towards the development of improved algorithms for fault location on series compensated lines. Algorithms designed for uncompensated traditional lines are not applicable to series compensated lines, and there are a number of challenges in accurately locating faults on such lines. Algorithms designed for uncompensated lines do not take into account factors pertaining to the electrical behaviour of the series compensated lines, such as the non-homogenous reactance of the line and the operation of the MOV during fault. The Ph.D. project which forms the focus of this thesis was aimed at addressing these challenges in an accurate and reliable manner. Therefore, the key objectives of the project were the development of accurate FLAs for series compensated transmission lines. Since series compensated transmission lines are predominantly either single-circuit lines or double-circuit lines, the project demanded that algorithms for both such lines be developed and validated using simulation studies.

The relevance of the work presented in this thesis is significant given the planned and anticipated installations of series compensation in various lines in the growing GB network. The relatively recent technological advancements have made smart grid technologies such as the use of synchronised phasor measurement units feasible, thus allowing the implementation of such complex and accurate algorithms possible. Although there are a number of existing solutions for fault location of series compensated lines, a key disadvantage of all such algorithms, is that they either require the use of line parameters or specially-tuned travelling wave filters. If fault location is to be carried out using fundamental frequency line-terminal measurements, the use of line parameters affects the accuracy of such solutions as line parameters are highly variable owing to

varying weather conditions and in cases of high loading. This disadvantage is addressed by the novel algorithms discussed in this thesis and therefore the novelty of these algorithms is that they do not require any line parameters in their calculations.

Three main research contributions of the author were presented in this thesis. The conclusions for each of these bodies of work are presented in the next section. The first of these is the novel algorithm for single-circuit series compensated transmission lines as presented in Chapter 4. The special advantage that the algorithm offers is that unlike other algorithms for such lines, it does not require the use of any line parameters. The conclusions are presented in detail in Section 8.1.1. A similar novel algorithm developed by the author for the purpose of locating faults on double-circuit lines was presented in Chapter 5. Its novelty also lies in that it is an original FLA for such lines which does not require the use of line parameters. The detailed conclusions for this body of work are presented in Section 8.1.2. Double-circuit lines and single-circuit lines are the two most common types of transmission lines; therefore it is essential that challenges for both types of lines are addressed. Although double-circuit lines are more complex, a greater number of input measurements are available to appropriately design the FLA. The two novel algorithms in Chapter 4 and Chapter 5 are thus mutually exclusive in application.

The third original algorithm was presented in this thesis in Chapter 7 which dealt with a method to improve the accuracy of existing FLAs using two-end synchronised current and voltage measurements. More specifically it carries out this improvement by accounting for the shunt admittance of long transmission lines in a line parameter free manner, and therein lies its novelty. The detailed conclusions for this body of work are presented in Section 8.1.3.

8.1. Conclusions

Conclusions for each original contribution of the author are presented as follows:

8.1.1. Novel Algorithm for Single-Circuit Series Compensated Lines

In Chapter 4, a novel algorithm for single-circuit series compensated lines for locating faults without the requirement of pre-determined line parameter settings was proposed. The fractional distance to fault is calculated in this algorithm without any knowledge of the total line length. The algorithms were derived in the phasor domain, and if sampled time domain measurements are to be used by the algorithm, an FFT must be carried out. It was assumed that these phasors from the two ends of the line would be time-synchronised with one another. Unlike other algorithms whose accuracies are significantly affected by differing weather and loading conditions, the novel algorithm remains accurate under such conditions. The algorithm also remains accurate despite synchronisation error, by means of a correction procedure carried out on the remote terminal phasors also discussed in the chapter. The algorithm is thus more robust, reliable and accurate compared to other two-ended algorithms that either use line parameters or are affected by synchronisation errors in communication of measurement data.

The key challenge solved by the algorithm is the calculation of distance to fault for series compensated single-circuit lines, whilst considering the operation of the MOV, without the use of line parameters. The algorithm was derived using analysis of phase-networks, and the voltage drop across each phase was expressed as the sum of the voltage drops across the series capacitor, the self impedance and the mutual impedances. Equations for both pre-fault and fault conditions were used. These equations were systematically reduced to a single equation of the distance to fault. In cases where there were multiple potential solutions, the set of calculated values for the six variables was analysed to see if they fall within pre-defined ranges. Only one solution was found to satisfy these conditions and therefore chosen as the correct solution.

The line parameter free algorithm was shown to perform accurately for both high resistance faults as well as low resistance faults owing to the elimination of fault resistance voltages in the derivation of the algorithm. Although the algorithms were derived neglecting the shunt admittance of the line, yet they were found to be sufficiently accurate despite this shortcoming. They were tested for simulations containing J-Marti line model

blocks where shunt admittances were modelled, and the inaccuracies of the algorithm due to these shunt admittance currents was found to be minimal. Most importantly, the algorithm was shown to be capable of accurately locating faults despite varying the degree or location of series compensation. The algorithm was also shown to be applicable to uncompensated traditional OHTLs. Other FLAs are not typically applicable to such a wide range of system topologies and fault conditions. They may even be limited to certain fault types. This makes the proposed novel algorithm comprehensive, making it ever so more favourable to be implemented on single-circuit series compensated lines. The algorithm benefits from the use of advanced synchronised two end measurement technology to achieve such applicability. Unlike FLAs using one-end measurements only, it is highly accurate when considering remote end infeed current, which is of significant magnitude for faults on transmission lines. The novel algorithm makes no assumptions regarding the value of the fault resistance, as is typically the case with single-end type algorithms.

The algorithm however, is not without its drawbacks and limitations. The algorithm calculates the fractional distance to fault (expressed as a fraction of the total length). The total line length is required to convert this value to units of distance. If there is significant line sag, an inaccurate value of the total line length will introduce further inaccuracies in this final estimate. The elongation for an ACSR 340/110mm² for example can be of the order of 0.331‰, 0.435‰ and 0.567‰ for an age of 20, 50 and 120 years respectively [152]. Although this is not significant, it is something that requires assessment. It was assumed that Rogowski coil CTs would be used in the current measurements and therefore CT saturation was not considered in the derivation or testing of the algorithm. The local and remote line-end networks were simulated using ideal blocks for impedance. The extent of the influence of these factors on the accuracy of the algorithm is required to be tested for as future work (discussed in Section 8.2). It is true however, that these factors will have a significant impact on the inaccuracy of the algorithm and must be considered and mitigated prior to implementation on a real power line.

The algorithm is limited to only lines compensated using FSCs, and would not be capable in itself for locating faults on lines compensated using variable series compensation such as with TCSCs. This is because the algorithms derivation assumed a fixed series

capacitance in parallel with the MOV. Given that TCSCs are increasingly becoming more favourable owing to the range of advantages they offer to power systems, it is important that similar algorithms be developed for TCSC compensated lines. TCSC reactance under fault is far more complex as it is influenced by its closed-loop control, MOV operation, and its complex transient behaviour. Further complexity is introduced if the TCSC is installed in series with other fixed series capacitor banks.

The algorithm was designed for fault locators rather than for real time detection and isolation of the fault. For the algorithm to be real-time capable significantly faster processing speeds are required, or appropriate simplifications are required to be made to reduce computation times. An example for such a requirement would be algorithms for the inhibition of autoreclosure. This is discussed in Section 8.2.2 as part of future work.

8.1.2. Novel Algorithm for Double-Circuit Series Compensated Lines

A novel algorithm for fault location on double-circuit lines was discussed in Chapter 5. The novelty of the algorithm is that it is an original line parameter free FLA for double-circuit series compensated lines. The second novel algorithm discussed in this thesis offers many of the advantages to double-circuit series compensated lines as the first algorithm does to single-circuit lines. It too was shown to be robust, reliable and accurate owing to its line parameter free method of calculating the distance to fault. Similarly, it was also shown to be capable of locating faults using both synchronous as well as asynchronous measurements. It was found to not be sensitive to the magnitude of the fault resistance and found to be applicable to various line topologies, locations and degrees of series compensation. It was tested for various fault types, topologies etc and for a variety of fault distances in each case, and found to be highly accurate. It was shown to suffer from a number of the shortcomings mentioned for the first novel algorithm. Its accuracy is affected by CT saturation where Rogowski coil CTs are not used, line sag, presence of variable series compensation, which have not been considered in the project and are to be tested for prior to implementation of the algorithm on a real power line.

The algorithm for double-circuit series compensated lines was derived using similar principles used for the FLA designed for single-circuit series compensated lines. The derivation expressed the voltage drops across each of the phases of the faulted circuit as a sum of the voltage drops across the series capacitor, the self impedance and mutual impedances (including the mutual impedance between circuits). These equations were then reduced to a single equation of only one variable i.e. the distance to fault. Unlike the first novel algorithm, the algorithm for double-circuit lines required knowledge of the capacitor fixed reactance. Since the reactance of the capacitor does not vary with weather and loading conditions as is the case with line parameters, this is not a significant drawback. Secondly, series capacitor reactance is accurately obtainable, unlike line parameters. The algorithm assumed that the fault only occurs at one given location on the line, and on only one of the two circuits. Thus, locating cross-country faults cannot be accurately carried out using this method. Also, cases where the healthy circuit (neighbouring circuit on double circuit line) is switched off and grounded would have an adverse effect on the accuracy of the algorithm. It is expected however that the algorithm for single-circuit lines may be applicable to this case once the effect of mutual coupling on the distance to fault calculations is considered and compensated for. The algorithm was not designed to be applicable to all types of parallel lines. It was only shown to be applicable to double-circuit lines, and where circuits run parallel to one another between the two terminals where the measurements are obtained.

The algorithm was designed primarily for fault locators, and currently is not real-time capable. However, given the relative simplicity of the expressions used for distance to fault, when compared to the expressions used for single-circuit algorithm, it is likely that appropriate simplifications can be made in future to allow for the algorithm to be real time capable.

8.1.3. Novel Algorithm to Account for Shunt Admittance

A third novel algorithm was presented in Chapter 7, which was designed to be a useful addendum to existing FLAs that use two-end synchronised measurements, but that ignore shunt admittances or require the use of pre-determined erroneous line parameters. The

algorithm was tested thoroughly for all different fault types and distances to fault, for a 300km line, when used in conjunction with the FLA proposed in [124]. It was found to improve the overall algorithm accuracy under these conditions, especially when faults were simulated to occur near the ends of the line.

Zero-sequence parameters are very difficult to obtain and are often inaccurate. This is certainly the case with shunt admittance parameters. Unlike algorithms using line parameter settings, this algorithm was shown to calculate shunt admittance parameters using online measurements of voltages and currents during fault. Moreover, since the algorithm works by recalculation of series currents, FLAs can use the algorithm without any modifications to the expressions for distance to fault, by simply using the recalculated currents.

The algorithm can only perform the shunt admittance calculations for traditional uncompensated lines. Series compensated lines would violate the assumptions which the algorithm was shown to use in its calculations of fault voltage, mutual impedance etc and would thus lead to erroneous calculations of shunt admittance currents.

The algorithm was not designed to be applicable to double circuit lines, series compensated or otherwise. Zero-sequence mutual coupling effect in such lines is required to be considered and the algorithm is needed to be modified appropriately, for calculations to be accurate. The algorithm assumed a simple lumped line model, although it was shown to be tested using simulations using the J-Marti model. The algorithm was tested using simulations containing a LCC J-Marti line model block, which considered the shunt admittance effect in a distributed manner. For the purpose of improving fault location for long lines, this simplified assumption was found to be acceptable, but there was still some error in accuracy owing to this.

The algorithm was shown to perform calculations using synchronised measurements, and large synchronisation errors will affect the shunt admittance calculations adversely. The first two novel algorithms discussed in previous sections dealt with synchronisation errors by re-synchronising phasors using the healthy phases. This method would not work for the purpose of shunt admittance calculation. This is discussed in future work.

8.2. Future Work

Future work is discussed in this section in the following three subsections:

8.2.1. Assessing the True Accuracy of the Algorithms

The algorithms developed in this project were tested based on simulation studies. A number of other tests are required to be carried out prior to implementation of these, onto real power lines. They are listed as follows:

- Influence of measurement noise requires to be assessed. The algorithms have been tested in ATP-EMTP using ideal current transformer and voltage transformer blocks. Therefore the measurements used to test the algorithm are ideal and therefore noise-free. This of course, is not the case in measurements obtained from real power lines. Therefore, this assessment is vital.

- The FLAs perform poorly for faults close to the line-ends i.e. 1% and 99%. The influence of the shunt admittance currents is too significant to be neglected unlike the cases shown for faults between 10% and 90%. It is hoped that an algorithm to accurately account for the shunt admittance of the line will be developed as part of future work. However, the significance of this drawback is required to be assessed statistically and appropriate measures are required to be taken. The algorithm may require to use shunt admittance parameters to address this issue but will still be line-parameter free with respect to the series impedances of the line.

- Lines where currents are not measured using Rogowski coil CTs are required to be considered. Influence of CT saturation must be tested for. Additional calculations may be required to be carried out prior to distance to fault calculation to deal with inaccuracies of measured currents near their peak values. Chapter 2 discussed some solutions for CT saturation. It is anticipated that either a hardware approach or the re-construction of current measurements based on periods of the cycle where the CT is not saturated will be required.

- Influence of networks outside the line (connected to the line at the local or remote end), requires to be assessed (although varying the fault levels has been tested previously), to ensure that the algorithm is not affected by high levels of subharmonic frequency oscillations.

8.2.2. Future Work Required Prior to Implementation on Real Lines

- Discussions with National Grid are currently in progress for a project extension to allow further research to be carried out for the implementation of the FLAs onto real power lines.

- Calculations of distance to fault using historically recorded fault recorder data from real-world series compensated lines require to be carried out to validate the algorithm. The UK currently does not have any series compensated lines, and therefore the appropriate fault recorder data was not available from National Grid for the purposes of validation of the proposed algorithms for such lines.

- The speed and performance on a significantly faster processor are required to be assessed, to address real-time capability if the algorithm is to be used beyond the requirements of an offline fault locator. Intermediate lab tests using Omicron generated input data and high-speed processors to test the performance of the algorithm to real signals.

- The algorithms require to be implemented first onto a prototype including communication infrastructure, stand-alone fault locator or relays.

- It is aimed in the design of the proposed FLAs to minimise the impact of temperature and loading on the accuracy of distance to fault calculations by eliminating the use of line parameters that are sensitive to these factors. However, simulation-tests must be carried out that confirm/establish that the FLAs are not sensitive to these factors. This may be carried out through the use of accurate thermal models of the transmission line, and by simulating cases where the

magnitude of line currents are close to the thermal ratings of the transmission line for the short transient period during the fault.

- Error compensation through software may be carried out if repeatable patterns are found between simulation tests and prototype tests. Although the mathematical relationships for the varying error levels for different fault conditions are not clear from the simulation tests, a repeatable pattern will still allow for error compensation based on a lookup-table type method.

8.2.3. Extending the Algorithms for Other Requirements

- The increasing popularity of TCSCs for overhead transmission lines suggests it may be beneficial to extend the algorithms to be applicable to such lines. Appendix II details the early stages of this work. Details of a work-in-progress ATP-EMTP model to be used in the testing of novel FLAs for such lines and some simulations are presented for insight.

- The algorithm to account for shunt admittance may be extended for double-circuit lines and series compensated lines. The algorithm discussed in Chapter 7 will be significantly different for such lines. The equations used to determine the fault point voltage will have to be modified to consider zero-sequence mutual coupling between circuits and series capacitor reactance respectively. The approach would be very similar to the existing algorithm, but the operation of the overvoltage protection of the capacitor during fault may present difficult challenges. Moreover, as the addendum aims to be settings-free and not just parameter free, another challenge would be to carry out this analysis without any knowledge of series capacitor reactance.

- The fault location algorithms may be extended to other fault analysis such as calculation of arc resistance, fault resistance, determination of nature of the fault etc. The fault distance would be used to calculate the arc voltage. Analysis of the electrical arc as a source of higher harmonics would be required to be included in the complete fault model and used as the starting point for the development of the

new algorithm. One such example of a "smart auto-reclosure" algorithm is included in Appendix I. This algorithm is able to perform such advanced fault analysis but for only traditional uncompensated lines. It is hoped to extend this algorithm in future for series compensated lines.

- The algorithms may be simplified so they only require single-terminal measurements at the expense of accuracy. If this accuracy and the speed of operation are sufficient, the single-terminal algorithms may be used for the purposes of protective relaying. This would however be a significant challenge as this would mean that half the measurements are no longer available. The current set of equations would no longer be valid as the number of unknowns would exceed the number of equations. How this would be simplified at the slight expense of accuracy is as of yet uncertain.

References

[1] Alternative Transients Program (ATP) Rule Book, available at http://www.emtp.org/

[2] R. Das, and D. Novosel. "Review of fault location techniques for transmission and subtransmission lines," in *proc of 54th Annual Georgia Tech Protective Relaying Conference, Atlanta*. 2000.

[3] IEEE guide for determining fault location on AC transmission and distribution lines, IEEE Standard, 2005.

[4] M.M Saha, J. Izykowski, and E.Rosolowski, *Fault Location on Power Networks, Springer*, 2010, pp. 1-367.

[5] AREVA, "Fundamentals of Protection Practice," in *Network Protection and Automation Guide – Protective Relays, Measurement & Control*, Alstom Grid, May 2011.

[6] D. Novosel, D.G. Hart and E. Udren "Unsynchronized two-terminal fault location estimation," *IEEE Transactions on Power Delivery*, Volume 11, issue 1, pp. 130–138, 1996

[7] M.M. Saha, J. Izykowski, E. Rosolowski, P. Balcerek, M. Fulczyk, "Accurate Location of Faults on Series-Compensated Lines with Use of Two-End Unsynchronised Measurements," in *proc. of IET 9th International Conference on Developments in Power System Protection, DPSP 2008*, pp.338-343, 17-20 March 2008,.

[8] G. Preston, "Faults on Overhead Transmission. Lines Using Synchronised Measurement Technology" Ph.D. thesis, School of Electrical & Electronic Engineering., University of Manchester, Manchester.

[9] L. Collatz, Numerical Treatment of Differential Equations. Springer, 1960

[10] G. Song, J. Suonan, X. Qingqiang. P. Chen and G. Yaozhong, "Parallel transmission lines fault location algorithm based on differential component net," *IEEE Transactions on Power Delivery*, Volume 20, Issue 4, pp.2396-2406, Oct. 2005

[11] A. Gopalakrishnan, M. Kezunovic, S.M. McKenna and D.M. Hamai, "Fault location using the distributed parameter transmission line model," *IEEE Transactions on Power Delivery*, Volume 15, Issue 4, pp.1169-1174, Oct. 2000

[12] M.M Saha, K. Wikstrom, J. Izykowski and E. Rosolowski, "New accurate fault location algorithm for parallel lines," in *proc. of Seventh International Conference on Developments in Power System Protection, DPSP 2001*, pp.407-410, 2001

[13] A. Wiszniewski, "Accurate fault impedance locating algorithm," in *IEE Proc - Part C (Generation, Transmission and Distribution)*, Volume 130. Issue 6. IET Digital Library, 1983.

[14] T. Takagi, Y. Yamakosi, M. Yamura et al., "Development of new type fault locator using the one–terminal voltage and current data," *IEEE Transactions on Power Apparatus and Systems*, pp. 2892-2898, 1982

[15] L. Eriksson, M.M. Saha and G.D. Rockefeller, "An accurate fault locator with compensation for apparent reactance in the fault resistance resulting from remote-end infeed," *IEEE Transactions on Power Apparatus and Systems*, Volume 104, Issue 2, pp. 424–436, 1985

[16] M.T. Sant and Y.G. Paithankar, "Online digital fault locator for overhead transmission line," in *IEE Proc - Part C (Generation, Transmission and Distribution)*, Volume 126, Issue 11, pp. 1181–1185, 1979

[17] M. Bockarjova, A. Sauhats and G. Andersson, "Statistical Algorithm for Fault Location on Power Transmission Lines". In *proc. 2005 IEEE Power Tech, Russia*, pp. 1-7, 2005.

[18] K.R. Cho, Y.C. Kang, S.S. Kim, J.K. Park, S.H. Kang and K.H. Kim "An ANN based approach to improve the speed of a differential equation based distance relaying algorithm," *IEEE transactions on Power Delivery*, Volume 14, Issue 2, pp.349-357, Apr 1999

[19] H. Khorashadi-Zadeh and M.R.A Ebrahimi, "An ANN based approach to improve the distance relaying algorithm," in *proc. 2004 IEEE Conference on Cybernetics and Intelligent Systems*, Volume.2, pp.1374-1379, Dec. 2004

[20] T. Bouthiba, “Fault Location in EHV Transmission Lines using Neural Networks”. in *proc. 2004 International Journal of Applied. Mathematics and Computer Science*, Volume.14, Issue.1, 69-78, 2004

[21] Z. Chen, D. Xinzhou and L. Chengmu. "Robustness of one-terminal fault location algorithm based on power frequency quantities." In *proc of 2002 IEEE Power Engineering Society Summer Meeting*, Volume 3. 2002

[22] M. Aurangzeb, P.A. Crossley and P. Gale, "Fault location using the high frequency travelling waves measured at a single location on a transmission line," in *Proc. 2001 IEE Seventh International Conference on Developments in Power System Protection*, pp.403-406, 2001

[23] G. Morales-Espana, J. Mora-Florez and H. Vargas-Torres, "Elimination of multiple estimation for fault location in radial power systems by using fundamental single-end measurements," in *proc of 2013 IEEE Power and Energy Society General Meeting*, pp.1, 21-25 July 2013

[24] M.M. Alamuti, H. Nouri, N. Makhol and M. Montakhab, "Developed single end low voltage fault location using distributed parameter approach," in *2009 Proceedings of the 44th International Universities Power Engineering Conference (UPEC)*, pp.1-5, 1-4 Sept. 2009

[25] T. Kawady and J. Stenzel, "A practical fault location approach for double circuit transmission lines using single end data," *IEEE Transactions on Power Delivery*, Volume.18, Issue 4, pp. 1166-1173, Oct. 2003

[26] A. Salehi-Dobakhshari and A.M. Ranjbar, "Robust fault location of transmission lines by synchronised and unsynchronised wide-area current measurements," *IET Generation, Transmission & Distribution*, Volume.8, Issue 9, pp.1561-1571, Sept. 2014

[27] A. Salehi-Dobakhshari, A.M. Ranjbar, "Application of synchronised phasor measurements to wide-area fault diagnosis and location," *IET Generation, Transmission & Distribution*, Volume 8, Issue 4, pp.716-729, April 2014

[28] L. Chih-Wen , L. Tzu-Chiao Lin, Y. Chi-Shan and Y. Jun-Zhe, "A Fault Location Technique for Two-Terminal Multisection Compound Transmission Lines Using

Synchronized Phasor Measurements," *IEEE Transactions on Smart Grid*, Volume.3, Issue 1, pp.113-121, March 2012

[29] J. Izykowski, R. Molag and E. Rosolowski, "Accurate location of faults on power transmission lines with use of two-end unsynchronized measurements," *IEEE Trans on Power Delivery*, Volume 21, Issue 2, pp. 627–633, 2006

[30] Z. Radojević and V. Terzija. "Intelligent Two-Port Numerical Algorithm for Transmission Lines disturbance Records Analysis". Springer-Verlag 2007, Published online: 16 October 2007.

[31] A. Salehi-Dobakhshari and A.M. Ranjbar, "Robust fault location of transmission lines by synchronised and unsynchronised wide-area current measurements," *IET Generation, Transmission & Distribution*, Volume 8, Issue 9, pp.1561-1571, Sept. 2014

[32] G.N. Korres and C.A. Apostolopoulos, "Precise fault location algorithm for double-circuit transmission lines using unsynchronised measurements from two anti-parallel ends," *IET Generation, Transmission & Distribution*, Volume 4, Issue 7, pp.824-835, July 2010

[33] Y. Liao and S. Elangovan, "Unsynchronised two-terminal transmission-line fault-location without using line parameters," *IET Generation, Transmission & Distribution*, Volume 153, Issue 6, pp.639-643, November 2006

[34] K. Andanapalli and B.R.K. Varma, "Travelling wave based fault location for teed circuits using unsynchronised measurements," in *Proc. 2013 International Conference on Power, Energy and Control (ICPEC)*, pp.227-232, 6-8 Feb. 2013

[35] S. Brahma and A. Girgis. "Fault Location on a Transmission Line Using Synchronized Voltage Measurements," *IEEE Transactions on Power Delivery*, Volume 19, Issue 4, pp. 1329-1332, 2004.

[36] K. Jia, D. Thomas and M. Sumner, "A New Single-Ended Fault-Location Scheme for Utilization in an Integrated Power System," *IEEE Transactions on Power Delivery*, Volume 28, Issue 1, pp.38-46, Jan. 2013

[37] T. Kawady and J. Stenzel, "A practical fault location approach for double circuit transmission lines using single end data," *IEEE Transactions on Power Delivery* , Volume 18, Issue 4, pp.1166-1173, Oct. 2003

[38] Z. Yang; Q. Xiaoan, Z. Zhenfeng and P. Hui, "HHT based single terminal traveling wave fault location for lines combined with overhead-lines and cables," in *proc of 2010 IEEE International Conference on Power System Technology (POWERCON)*. "HHT based single terminal traveling wave fault location for lines combined with overhead-lines and cables," pp.1-6, 24-28 Oct. 2010

[39] N.E. Eng and K. Ramar, "Single-ended traveling wave based fault location on two terminal transmission lines," in proc of *TENCON 2009-2009 IEEE Region 10 Conference*, pp.1-4, 23-26 Jan. 2009

[40] L.Y. Wu, Z.Y He and Q. Wu, "A New Single Ended Fault Location Technique Using Travelling Wave Natural Frequencies," in *proc of Asia-Pacific Power and Energy Engineering Conference APPEEC 2009*, pp.1-5, 27-31 March 2009

[41] S. Jamali and A. Ghezeljeh, "Fault location on transmission line using high frequency travelling waves," in *Proc of 8th Int Conf on Developments in Power System Protection –DPSP*, pp 220–223, 2004

[42] L.J. Lewis, "Travelling wave relations applicable to power system fault locators," *Transactions of the American Institute of Electrical Engineers*, Volume 70, Issue 2, pp. 1671-1680, 1951

[43] M. Aurangzeb, P.A. Crossley and P. Gale, "Fault location using the high frequency travelling waves measured at a single location on a transmission line," in *Proc. 2001 IEE Seventh International Conference on Developments in Power System Protection*, pp.403-406, 2001

[44] M. Silva, M. Oleskovicz and D.V. Coury, "A fault locator for transmission lines using travelling waves and wavelet transform theory," in *Proc of 8th Int Conf on Developments in Power System Protection – DPSP*, pp 212–215, 2004

[45] Zhen-Qiang Li and Lv Yan-ping, "A Novel Scheme of HVDC Transmission Line Voltage Traveling Wave Protection Based on Wavelet Transform," in *Proc of International Conference on High Voltage Engineering and Application*, pp.163-167, 9-12 Nov. 2008

[46] A. Cichocki and R. Unbehauen, *Neural Networks for Optimization And signal Processing*. John Wiley & Sons, Inc., New York, 1993

[47] S. Haykin, *Neural Networks: A Comprehensive Foundation*, Macmillan Collage Publishing Company Inc., New York, 1994

[48] M. Kezunovic, "A survey of neural network applications to protective relaying and fault analysis," International *Journal of Intelligent Systems for Electrical Engineering and Communication*, Volume 5, Issue 4, pp.185–192

[49] A.P.A Silva and D.M. Falcao, "Fundamentals of genetic algorithms", in Moden *Heuristic Optimization Techniques: Theory and Applications to Power Systems*. IEEE Press, Wiley-Interscience, New Jersey, 2008

[50] D.E. Goldberg, *Genetic Algorithms in Search, Optimization and Machine Learning, Addison Wesley*, Reading, 1989

[51] J. Moshtagh and R.K. Aggarwal, "A new approach to fault location in a single core underground cable system using combined fuzzy logic and wavelet analysis," in *proc of Eighth IEE International Conference on Developments in Power System Protection 2004*, pp.228-231, Volume. 1, 5-8 April 2004

[52] H. Meyar-Naimi, "A new fuzzy fault locator for series compensated transmission lines," in *proc of 2012 11th International Conference on Environment and Electrical Engineering (EEEIC)*, pp.53-58, 18-25 May 2012

[53] P. Kumar, M. Jamil and M.S. Thomas, Moinuddin, "Fuzzy approach to fault classification for transmission line protection," in *proc of IEEE Region 10 Conference TENCON 99*, Volume 2, pp.1046-1050, Dec 1999

[54] T.S. Sidhu, H. Singh and M.S. Sachdev. "Design, Implementation and Testing of An Artificial Neural Network Based Fault Direction Discriminator for Protecting Transmission Lines," *IEEE Transactions on Power Delivery*, Volume 10, No. 2, April 1995.

[55] T. Funabashi, H. Otoguro, Y. Mizuma et al. "Digital fault location for parallel double circuit multi-terminal transmission lines," *IEEE Transactions on Power Delivery*, Volume 15, Issue 2, pp.531–537, 2000

[56] J. Gracia, A. Mazon and I. Zamora "Best ANN structures for fault location in single- and double-circuit transmission lines," *IEEE Transactions on Power Delivery*, Volume 20, Issue 4. pp. 2389–2395, 2005

[57] J. Izykowski, R. Kawecki "Location of faults in partially parallel transmission networks," in *Proc of IEEE Porto Power Tech Conference*, Porto, Volume III, 2001

[58] J. Izykowski, R. Kawecki, E. Rosolowski "Accurate location of faults in parallel transmission lines under availability of measurements from one circuit only," in *Proc of Power Systems Computation Conference –PSCC'02*, Sevilla, paper 6, 2002

[59] D.A. Bradley, C.B. Gray, D. O'Kelly, "Transient compensation of current transformers," *IEEE Transactions on PAS*, Volume 97, pp. 1264–1271, 1978

[60] S.M. Brahma, "Fault location scheme for a multi-terminal transmission line using synchronized voltage measurements," *IEEE Trans on Power Delivery*, Volume 20, Issue 2, pp. 1325–1331, 2005

[61] S. Brahma and A. Girgis. "Fault Location on a Transmission Line Using Synchronized Voltage Measurements," *IEEE Transactions on Power Delivery*, Volume 19, Issue 4, pp. 1329-1332, 2004.

[62] I. Zamora, J.F. Minambres and A.J. Mazon "Fault location on two-terminal transmission lines based on voltages," in *IEE Proc – Generation Transmission and Distribution*, Volume 143, Issue 1, pp.1–6, 1996

[63] J. Izykowski, E. Rosolowski, M.M. Saha and P. Balcerek, "Accurate algorithm for locating faults in power transmission lines under saturation of current transformers," in *Proc of Power Systems Computation Conference – PSCC*, Liege, 2005

[64] M.M. Saha, J. Izykowski and E. Rosolowski, "A two-end method of fault location immune to saturation of current transformers," in *Proc of 8th Int Conf on Developments in Power System Protection – DPSP*, pp 172–175, 2004

[65] B. Kasztenny, E. Rosolowski, M. Lukowicz and J. Izykowski "Current related relaying algorithms immune to saturation of current transformers," in *Proc of 6th Int Conf on Developments in Power System Protection, – DPSP*, pp 365–369, 1997

[66] Y.H Lin, C.W Liu and C.S. Chen, "A new PMU-based fault detection/location technique for transmission lines with consideration of arcing fault discrimination-part I: theory and algorithms," *IEEE Transactions on Power Delivery*, Volume 19, no.4, pp.1587-1593, Oct. 2004

[67] Y.H. Lin, C.W. Liu; C.S. Chen, "A new PMU-based fault detection/location technique for transmission lines with consideration of arcing fault discrimination-part II: performance evaluation," *IEEE Transactions on Power Delivery*, Volume 19, no.4, pp.1594-1601, Oct. 2004

[68] C.W. Liu; T.C. Lin; C.S. Yu and J.Z. Yang, "A Fault Location Technique for Two-Terminal Multisection Compound Transmission Lines Using Synchronized Phasor Measurements," *IEEE Transactions on Smart Grid*, Volume 3, Issue 1, pp.113-121, March 2012

[69] N. Kang and Y. Liao, "Double-Circuit Transmission-Line Fault Location Utilizing Synchronized Current Phasors," *IEEE Transactions on Power Delivery*, Volume 28, Issue 2, pp.1040-1047, April 2013

[70] M. Korkali and A. Abur, "Optimal Deployment of Wide-Area Synchronized Measurements for Fault-Location Observability," *IEEE Transactions on Power Systems*, Volume 28, Issue 1, pp.482-489, Feb. 2013

[71] S.M. Brahma, "New fault-location method for a single multiterminal transmission line using synchronized phasor measurements," *IEEE Transactions on Power Delivery*, Volume 21, Issue 3, pp.1148-1153, July 2006

[72] M.H. Samimi, A. Mahari, M.A. Farahnakian and H. Mohseni, "The Rogowski Coil Principles and Applications: A Review," *IEEE Sensors Journal*, Volume 15, Issue 2, pp.651-658, Feb. 2015

[73] ABB, "Series Compensation Boosting Transmission Capacity", available at http://www02.abb.com/global/gad/gad02181.nsf/0/fba60f0238fcfd2ec1257a620031049f/$file/Series+Compensation+-+Boosting+transmission+capacity.pdf

[74] J. Berdy, "Protection of circuits with series capacitors, " in *proc of AIEE Summer General Meeting*, Denver-Colorado, June 1962

[75] J.H. Altuve, B. Joseph, and G.E. Alexander. "Advances in series-compensated line protection." in *proc. of 62nd Annual Conference for IEEE Protective Relay Engineers*, 2009

[76] D.S. Moura, F.A. Moreira, and K.M. Silva. "Effects of Subharmonic Frequencies in Phasor Estimation Algorithms for Distance Protection of Series Compensated

Transmission Lines." in *proc. of International Conference on Power System Transients*, 2013,

[77] A.T. Johns and S. Jamali, "Accurate fault location technique for power transmission lines," IEE Proceedings C Generation, Transmission and Distribution, Volume 137. Issue 6. IET, 1990

[78] A. Hammad and B. Roesle, "New Roles for Static VAR Compensators in Transmission Systems," Brown Boveri Review, Volume 73, pp. 314-320, June 1986.

[79] N. Grudinin and I. Roytelman, "Heading Off Emergencies in Large Electric Grids", *IEEE Spectrum*, Volume 34, Issue 4, pp. 43-47, April 1997

[80] C.W. Taylor, "Improving Grid Behavior", *IEEE Spectrum*, Volume 36, Issue 6, pp. 40-45, June 1999

[81] L.L. Grigsby, Power Systems, 3rd Edition, CRC Press, April 2012

[82] I.K. Kiran and A.J Laxmi, "Shunt versus series compensation in the improvement of power system performance," *International Journal of Applied Engineering Research*, Volume 2.1, pp. 28-37, 2011.

[83] J. Dixon, L. Moran, R. Rodriguez, and E. Domke, "Reactive power compensation technologies: State-of-the-art review." in *Proc of the IEEE*, Volume 93, Issue 12, 2005.

[84] C-Reyna, A. Alfredo, A. Daniel, R-Delgado, and L. O-Exclusa,. "Transient Performance for a Series-Compensation in a High Voltage Transmission System."

[85] P.M. Anderson and R.G. Farmer, Series Compensation of Power Systems, PBLSH! Inc, April 1996

[86] C. Hor, J. Finn, A. Shafiu, V. Henn, G. Kuhn and P. Crossley, "Preparing to meet the challenges of protecting series capacitor compensated lines in the UK," in *proc of 10th IET International Conference on Managing the Change, Developments in Power System Protection*, pp.1,5, March 29 2010-April 1 2010

[87] L.L. Grigsby, Power Systems, 3rd Edition, CRC Press, April 2012

[88] Y.H. Song, and A.T. Johns, Flexible ac transmission systems (FACTS), IET, 1999.

[89] M. Kowsalya, K. Garg and N. Gupta, "Series compensation for static and dynamic voltage stability enhancement," in *proc of Innovative Technologies in Intelligent Systems and Industrial Applications*, pp.402-406, 25-26 July 2009

[90] E. Clarke, S.B. Crary, "Stability Limitations of Long-Distance A-C Power-Transmission Systems," *Transactions of the American Institute of Electrical Engineers*, Volume 60, Issue 12, pp.1051-1059, Dec. 1941

[91] Maruf, N. I., et al. "Study of thyristor controlled series capacitor (TCSC) as a useful FACTS device," *International Journal of Engineering Science and Technology*, Volume 2, Issue 9, pp. 4357-4360, 2010.

[92] L. Gyugyi, C.D. Schauder, and K.K. Sen. "Static synchronous series compensator: a solid-state approach to the series compensation of transmission lines," IEEE *Transactions on Power Delivery*, Volume 12, Issue 1, pp. 406-417, 1997

[93] B. Geethalakshmi, P. Dananjayan and K. DelhiBabu, "A Combined Multipulse-Multilevel Voltage Source Inverter Configuration for STATCOM Applications," in *proc of Joint International Conference on Power System Technology and IEEE Power India Conference*, pp.1-5, 12-15 Oct. 2008

[94] ABB, "Series Capacitor Bypass Switch", available at http://www05.abb.com/global/scot/scot245.nsf/veritydisplay/ce122f6d0896b5b5c1257958003757dc/$file/1hsm%209543%2022-12en%20series%20capacitor%20by-pass%20switch.pdf, accessed Sept. 2014.

[95] L. Ebbers, et al. "New type test requirements for forced triggered spark gap in series capacitor bank applications," in *proc of 10th IET International Conference on AC and DC Power Transmission (ACDC 2012)*, pp. 1-6, 2012.

[96] IEC Publication 60143-2, Edition 2.0: Series capacitors for power systems – Part 2: Protective equipments for series capacitor banks

[97] D.L. Goldsworthy, "A Linearized Model for MOV-Protected Series Capacitors," *IEEE Transactions on Power Systems*, Volume 2, Issue 4, pp.953-957, Nov. 1987

[98] D. Novosel, A. Phadke, M.M. Saha and S. Lindahl, "Problems and solutions for microprocessor protection of series compensated lines," in *proc of Sixth International Conference on Developments in Power System Protection*, pp.18-23, 25-27 Mar 1997

[99] P. Jena and A.K. Pradhan, "A Positive-Sequence Directional Relaying Algorithm for Series-Compensated Line," *IEEE Transactions on Power Delivery*, Volume 25, Issue 4, pp.2288-2298, Oct. 2010

[100] M.E. Erezzaghi, P.A. Crossley and R. Elferes, "Design and evaluation of an adaptive distance protection scheme suitable for series compensated transmission feeders," *Eighth IEE International Conference on Developments in Power System Protection*, Volume 2, pp. 453- 456, 5-8 April 2004

[101] E. O. Schweitzer and J. B. Roberts, "Distance Relay Element Design," in *Proc of the 23rd Annual Western Protective Relay Conference*, Spokane, WA., October 15 - 17, 1996.

[102] A. Guzmán, J. B. Roberts, and D. Hou, "New Ground Directional Elements Operate Reliably for Changing System Conditions," in *proc. of 23rd Annual Western Protective Relay Conference Spokane*, October 15 - 17, 1996.

[103] J.B. Mooney and G.B. Alexander, *Applying the SEL-321 Relay on Series-Compensated Systems*, SEL Application Guide AG2000-11

[104] A. Guzman, J. Mooney, G. Benmouyal, and N. Fischer, "Transmission Line Protection for Increasing Power System Requirements," in *proc of 55th Annual Conference for Protective Relay Engineers*, Texas A&M University, 2002.

[105] M.M. Saha, B. Kasztenny, E. Rosolowski and J. Izykowski, "First zone algorithm for protection of series compensated lines," *IEEE Transactions on Power Delivery*, Volume 16, Issue 2, pp.200-207, April 2001

[106] S.R. Samantaray and P.K. Dash, "Wavelet packet-based digital relaying for advanced series compensated line," *IET Generation, Transmission & Distribution*, Volume.1, Issue 5, pp.784-792, September 2007

[107] A.I. Megahed, A.M. Moussa and A.E. Bayoumy, "Usage of wavelet transform in the protection of series-compensated transmission lines," *IEEE Transactions on Power Delivery*, Volume.21, Issue 3, pp.1213-1221, July 2006

[108] A.K. Pradhan, A. Routray, S. Pati and D.K. Pradhan, "Wavelet fuzzy combined approach for fault classification of a series-compensated transmission line," *IEEE Transactions on Power Delivery*, Volume 19, Issue 4, pp. 1612- 1618, Oct. 2004

[109] C. Aguilera, E. Orduna and G. Ratta, "Fault detection, classification and faulted phase selection approach based on high-frequency voltage signals applied to a series-compensated line," in *IEE Proceedings-Generation, Transmission and Distribution*, Volume 153, Issue 4, pp. 469- 475, 13 July 2006

[110] V.J. Pandya and S.A. Kanitkar, "A novel unit protection scheme for protection of series compensated transmission line using wavelet transform," in *proc. of Power Engineering Conference*, Australasian Universities, pp.1-5, 9-12 Dec. 2007

[111] S.M. Atif Saleem and A.M. Sharaf, "A Novel Travelling Wave Based Relaying Scheme Using Wavelet Transforms for Arcing Faults Detection on Series Compensated Transmission Lines," in *proc. of Canadian Conference on Electrical and Computer Engineering*, pp.575-578, 22-26 April 2007

[112] U.B. Parikh, B. Das and P. Maheshwari, "Combined Wavelet-SVM Technique for Fault Zone Detection in a Series Compensated Transmission Line," *IEEE Transactions on Power Delivery*, Volume 23, Issue 4, pp.1789-1794, Oct. 2008

[113] B. Bachmann, D. Novosel, D. Hart, Y. Hu and M.M. Saha, "Application of artificial neural networks for series compensated line protection," in proc. of *International Conference on Intelligent Systems Applications to Power Systems, ISAP '96.*, pp.68-73, 28 Jan-2 Feb 1996

[114] Q.Y. Xuan, R. Morgan, D. Williams, Y.H. Song and A.T. Johns, "Adaptive protection for series compensated EHV transmission systems using neural networks," in *proc. of International Conference on Control*, Volume 1, pp.728-732 21-24 March 1994

[115] D. Novosel, B. Bachmann, Hart, D. Hart, Y. Hu and M.M. Saha, "Algorithms for Locating Faults on Series Compensated Lines Using Neural Network and Deterministic Methods," IEEE *Power Engineering Review*, Volume 17, Issue 13, pp.47-48, Oct. 1996

[116] J.A.S.B Jayasinghe,.R.K. Aggarwal, A.T. Johns and Z.Q. Bo, "A novel non-unit protection for series compensated EHV transmission lines based on fault generated high frequency voltage signals," *IEEE Transactions on Power Delivery*, Volume 13, Issue 2, pp.405-413, Apr 1998

[117] I. Kamwa, R. Grondin, V.K. Sood, C. Gagnon, V.T. Nguyen and J. Mereb, "Recurrent neural networks for phasor detection and adaptive identification in power system control and protection," *IEEE Transactions on Instrumentation and Measurement*, Volume 45, Issue 2, pp.657-664, Apr 1996

[118] R.K. Aggarwal, A.T. Johns and D.S. Tripp, "The Development and Application of Directional Comparison Protection for Series Compensated Transmission Systems," *IEEE Power Engineering Review*, Volume PER-7, Issue 10, pp.40, Oct. 1987

[119] P.K. Dash; S.R. Samantaray and G. Panda, "Fault Classification and Section Identification of an Advanced Series-Compensated Transmission Line Using Support Vector Machine," *IEEE Transactions on Power Delivery*, Volume 22, Issue 1, pp.67-73, Jan. 2007

[120] H.E. Prado-Felix, V.H. Sema-Reyna, M.V. Mynam M. Donolo and A. Guzman, "Improve Transmission Fault Location and Distance Protection Using Accurate Line Parameters", in proc *of International Conference on Power System Transients 2009*, Kyoto, pp. 1-5, 2009.

[121] Schweitzer Engineering Laboratories, "Improve Transmission Fault Location and Distance Protection Using Accurate Line Parameters", available at https://www.cavs.msstate.edu/iPCGRID_Registration/presentations/2014/TZIOUVARAS_i-PCGRID_2014_Improving_Transmission_Fault_Location_and_Distance_Protection.pdf , accessed July 3013

[122] Dr. E.O. Schweitzer, "A Review of Impedance-Based Fault Locating Experience", a presentation at the Nebraska Power System Protection Seminar, 1990

[123] J. Myeong-ryeal, O. Sei-ill, L. Hee and S. Chang-gyun, "Analysis of Measured Transmission Line Constants", pacworld magazine winter 2008, 2008

[124] G. Preston, Z.M. Radojević, C.H. Kim and V. Terzija, "New settings-free fault location algorithm based on synchronised sampling," IET Generation, Transmission & Distribution, Volume. 5, Issue 3, pp.376-383, March 2011.

[125] S. Padmanabhan and V. Terzija, "New parameter-free fault location algorithm for transmission lines in phasor domain," in *proc of 2012 IEEE Power and Energy Society General Meeting*, IEEE, 2012.

[126] C.A. Apostolopoulos and G.N. Korres. "A novel algorithm for locating faults on transposed/untransposed transmission lines without utilizing line parameters." *IEEE Transactions on Power Delivery*, Volume 25, Issue 4, pp. 2328-2338, 2004

[127] D.A.G. Vieira, D.B. Oliveira, and A.C. Lisboa "A Closed-Form Solution for Transmission-Line Fault Location Without the Need of Terminal Synchronization or Line Parameters," *IEEE transactions on power delivery*, Volume 28, Issue 2, pp. 1238-1239, 2013

[128] C.A. Apostolopoulos and G.N. Korres. "A novel fault-location algorithm for double-circuit transmission lines without utilizing line parameters," *IEEE Transactions on Power Delivery*, Volume 26, Issue 3, pp.1467-1478, 2011

[129] G. Preston, Z. Radojević and V. Terzija. "Novel parameter-free fault location algorithm for transmission lines with series compensation," in *proc. of 10th IET International Conference on Developments in Power System Protection (DPSP 2010)*, pp.54-54, 2010

[130] S.A. Soman, S.A. Khaparde, and S. Pandit, Computational methods for large sparse power systems analysis: an object oriented approach, Springer, 2002.

[131] Y. Cho, C.K. Lee; G. Jang and H..J. Lee, "An Innovative Decaying DC Component Estimation Algorithm for Digital Relaying," *IEEE Transactions on Power Delivery*, Volume 24, Issue 1, pp.73-78, Jan. 2009

[132] IEEE Std C37.114-2004: 'IEEE Guide for Determining Fault Location on AC Transmission and Distribution Lines'. pp. 0–36, 2005

[133] Tony Seegers, "AC Transmission Line Model Parameter", A report to the Line Protection Subcommittee of the Power System Relay Committee of the IEEE Power & Energy Society, Sept 2014

[134] C.S. Yu; C.W. Liu; S.L. Yu; J.A. Jiang, "A new PMU-based fault location algorithm for series compensated lines," *IEEE Transactions on Power Delivery*, Volume 17, Issue 1, pp.33-46, Jan 2002

[135] N. Kang, J. Chen and Y. Liao, "A Fault-Location Algorithm for Series-Compensated Double-Circuit Transmission Lines Using the Distributed Parameter Line Model," *IEEE Transactions on Power Delivery*, early access, pp.1-8, 2014

[136] National Grid, "Appendix-B System Data", Ëlectricity Ten Year Statement 2013", available at - http://www2.nationalgrid.com/UK/Industry-information/Future-of-Energy/Electricity-ten-year-statement/Current-statement/, accessed July 2013

[137] N. Peter, U. Kaintzyk, and J.F. Nolasco, Overhead power lines: planning, design, construction. Springer, 2003.

[138] P. M. Anderson, Analysis of Faulted Power Systems, Wiley-IEEE, New York, 1995

[139] Electricity Network Strategy Group, "Our Electricity Transmission Network: A Vision for 2020," Jul. 2009.

[140] ABB Application Manual - REL 501 Line Distance Protection Terminal, available at http://www08.abb.com/global/scot/scot354.nsf/veritydisplay/09b2a06b6171ab62c12578570041e42b/$file/1MRK506114-UEN_en_Application_manual_REL_501-C1_2.3.pdf

[141] ABB Application Manual - REL 511 Line Distance Protection Terminal, available at http://www08.abb.com/global/scot/scot354.nsf/veritydisplay/144e168546ea112cc12578570041e45c/$file/1MRK506097-UEN_en_Technical_reference_manual_REL_511-C1_2.3.pdf

[142] ABB Application Manual - REL 521 Line Distance Protection Terminal, available at http://www08.abb.com/global/scot/scot354.nsf/veritydisplay/e561550478c08871c12578570041e43f/$file/1MRK506111-UEN_en_Application_manual_REL_521_2.3.pdf

[143] SIEMENS Numerical Distance Protection Relay - SIPROTEC 7SA510 Instruction Manual, available at www.siemens.com/download?DLA10_49

[144] SIEMENS Numerical Distance Protection Relay - SIPROTEC 7SA511 Instruction Manual, available at www.siemens.com/download?DLA10_171

[145] SIEMENS Numerical Distance Protection Relay - SIPROTEC 7SA513 Instruction Manual, available at www.siemens.com/download?DLA10_121

[146] M.M. Mansour, G.W. Swift, "A Multi-Microprocessor Based Travelling Wave Relay - Theory and Realization," *IEEE Transactions on Power Delivery*, Volume 1, Issue 1, pp.272-279, Jan. 1986

[147] Schweitzer Engineering Laboratories - Protective Relay Traveling Wave Fault Location, available at: https://www.selinc.com/WorkArea/DownloadAsset.aspx?id=101114

[148] Glover JD, Sarma M, Power System Analysis and Design, PWS Publishing Company, 1994

[149] Bogdan Kasztenny, "Distance Protection of Series Compensated Lines–Problems and Solutions", in proc. of *28th Annual western protective relay conference*, pp 1-34, October, 2001

[150] Y. Liao, N. Kang, "Fault-Location Algorithms Without Utilizing Line Parameters Based on the Distributed Parameter Line Model," *IEEE Transactions on Power Delivery*, Volume 24, Issue .2, pp.579-584, April 2009

[151] A.H. Al-Mohammed, M.A. Abido, "A Fully Adaptive PMU-Based Fault Location Algorithm for Series-Compensated Lines," *IEEE Transactions on Power Systems*, Volume 29, Issue 5, pp. 2129-2137, Sept. 2014

[152] M. Muhr, S. Pack, R. Schwarz, S. Jaufer, "Calculation of overhead line sags", *51st Internationales Wissenschaftliches Kolloquium Technische Universitat Ilmenau*. Sep. 11-15, 2006.

[153] J. Izykowski, E. Rosolowski, P. Balcerek, M. Fulczyk, M.M. Saha, "Fault Location on Double-Circuit Series-Compensated Lines Using Two-End Unsynchronized Measurements," , IEEE Transactions on Power Delivery, Volume 26, Issue 4, pp.2072-2080, Oct. 2011.

[154] J.V.H. Sanderson, *The analysis and protection of systems containing series compensated power lines*. Thesis submitted to the University of Nottingham for the degree of Doctor of Philosophy, University of Nottingham, 1973.

[155] C.J. Kim, B. Don Russell. "Harmonic behavior during arcing faults on power distribution feeders." *Electric power systems research*, Volume 14, Issue 3, pp. 219-225, 1988.

[156] P.S. Georgilakis, and P.G. Vernados. "Flexible AC transmission system controllers: An evaluation," *Materials Science Forum*, Volume. 670, 2011.

[157] Zheng Xiao-Dong; Tai Neng-Ling; J.S. Thorp, Yang Guang-Liang, "A Transient Harmonic Current Protection Scheme for HVDC Transmission Line," *IEEE Transactions on Power Delivery*, Volume 27, Issue 4, pp. 2278-2285, Oct. 2012

Appendix I. List of Publications

Journal Publications

1. Z. Radojevic, V. Terzija, G. Preston, S. Padmanabhan, D. Novosel, "Smart Overhead Lines Autoreclosure Algorithm Based on Detailed Fault Analysis", *IEEE Transactions on Smart Grid*, vol.4, pp.1829-1838, Dec. 2013.

2. S. Padmanabhan, V.Terzija, "Line parameter Free Novel Fault Location Algorithm for Series Compensated and Traditional Lines" (Re-submitted after first revision based on reviewers' feedback).

Conference Publications

1. S. Padmanabhan, V. Terzija, "Line parameter-free fault location algorithm for series compensated transmission lines", *2013 IEEE Power and Energy Society General Meeting*, pp.1-6, 21-25 July 2013

2. S. Padmanabhan, V. Terzija, "Settings-free method to account for shunt admittance in fault location", *2012 3rd IEEE PES International Conference and Exhibition on Innovative Smart Grid Technologies (ISGT Europe)*, pp.1-7, 14-17 Oct. 2012

3. S. Padmanabhan, V. Terzija, "New parameter-free fault location algorithm for transmission lines in phasor domain", *2012 IEEE Power and Energy Society General Meeting*, pp.1-6, 22-26 July 2012

Appendix II – Thyristor Controlled Series Compensator Model

TCSCs as previously discussed are a variable form of series compensation. They offer numerous advantages over fixed series compensation. These include improved transmission capability, controlling line power flow, subsynchronous resonance mitigation and inter area oscillation damping. FLAs developed over the course of this Ph.D. project are focused on lines compensated using FSCs as they are the most common type of series compensation. However, TCSCs are increasingly becoming the preferred means of the series compensation, given the array of advantages offered as discussed above. Moreover, with respect to the GB network, the first TCSC installed in the UK is planned to be installed at Hutton substation. For these reasons, it is important to develop models of TCSCs in ATP-EMTP, so that similar FLAs can be developed for such lines.

This Appendix discusses the work-in-progress model of a TCSC developed thus far for the purposes of fault location. It should be noted that the model is in its early stages and is only provided in this thesis to provide some insight into the work that is being carried out as an extension of the project. The model is capable of operating in its various modes namely; blocked thyristor mode, bypassed thyristor mode, capacitive boost mode, and inductive boost mode. For the last two of these modes, the firing angle of the TCSC can be controlled to achieve the appropriate inductive or capacitive net reactance.

Flexible Alternating Current Transmission Systems (FACTS) are defined by the IEEE as "AC transmission systems incorporating power electronics-based and other static controllers to enhance controllability and increase power transfer capability" 311[156]. FACTS devices have been well discussed and greatly implemented since the early 90s. They provide a means to improve power transmission capability, system stability, power quality and to minimise transmission losses. Of these FACTS devices, TCSCs have shown the best results as far as improving performance and flexibility are concerned. They may be used (primarily) for one or more of the many advantages offered: scheduling of power flow, decreasing unsymmetrical components, reducing net losses, providing voltage

support, limiting short-circuit currents, mitigation of sub-synchronous resonance, damping inter-area oscillations and enhancing transient stability. TCSCs are different from FSCs in that they can be controlled to achieve the desired operation mode and net reactance. This offers not only controllability but can also provide a very high level of series compensation using a capacitor bank of relatively small reactance. The model discussed in the subsequent sections is a work-in-progress model designed only to be controlled using the firing of thyristors. Other aspects of the model will be carried out as part of future work.

AII.1. Fundamental Operating Principle

The diagram of a TCSC is shown in Figure 2.1. It comprises of series capacitor in parallel with an inductor branch containing thyristors to allow control of the effective reactance of the unit as a whole. The firing of the thyristors is based on the input firing angle α. This is defined as the angle corresponding to the first instance of firing of a thyristor in the reactor branch, after the negative peak of the voltage (using this peak as the 0^c phase reference point). The conduction angle σ is the period during which the thyristor conducts current. The working of the TCSC during normal operation can be described as follows. The corresponding waveforms for the capacitor voltage, capacitor current and thyristor branch current are shown subsequently in Figure 2.1. The firing angle α and the conduction angle σ are also denoted here.

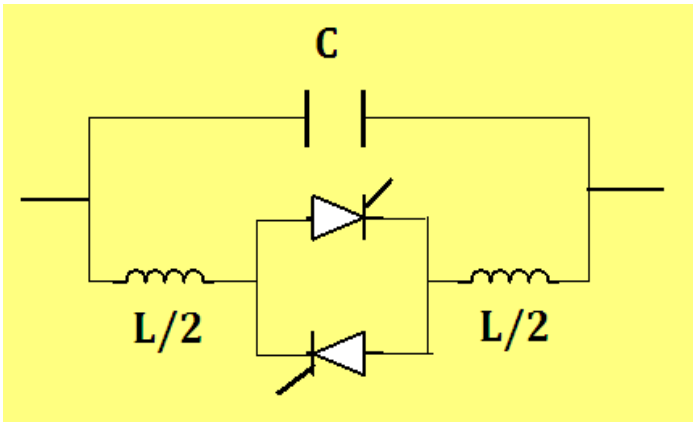

Figure AII.1: Block diagram of a TCSC

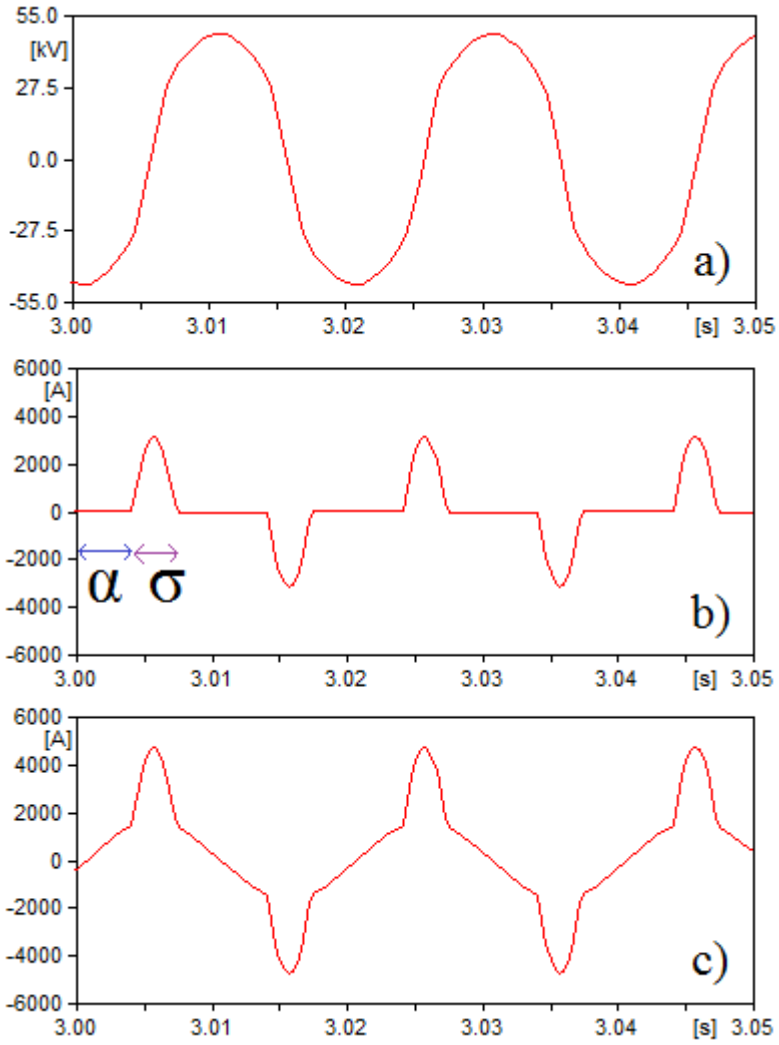

Figure AII.2: a) Capcitor voltage b) Inductor branch current c) Capacitor current

1. The capacitor voltage is initially at the negative peak. At this point neither of the thyristors is conducting, and the inductor branch is effectively an open switch. At this point the line current flowing through the capacitor is discharging the capacitor.

2. Once the phase of the capacitor voltage coincides with the firing angle α (using the negative peak as the 0^o reference), the top thyristor fires and inductor branch begins to conduct. This inductor branch current adds an additional discharging component to the capacitor current as can be seen in Figure AII.2, giving it a non-sinusoidal

shape. It conducts for a period corresponding to the conduction angle σ which can be expressed in terms of α as π-2α

3. The inductor branch stops conducting current when the voltage phase angle is α+σ at which point it is effectively an open circuit. At this point the capacitor voltage is in its positive half cycle, and the line current charges the capacitor until it reaches its positive peak.

Stages 4, 5 and 6 are analogous to stages 1, 2 and 3 respectively for the second half of the power system cycle except that now the lower thyristor is fired instead, to appropriately control to TCSC. The voltage and current waveforms are seen to be non-sinusoidal. The line current however still maintains a sinusoidal shape as shown in Figure AII.3

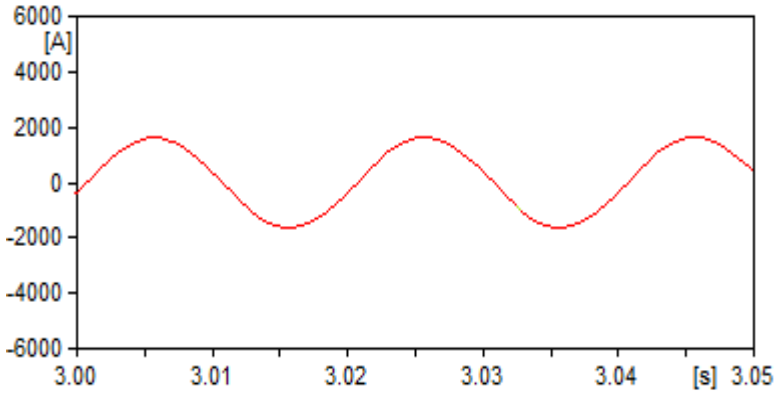

Figure AII.3: Line Current in a TCSC compensated line

Shown below is the equation for the capacitive reactance of the TCSC as a function of the firing angle (AII.1). As a result, as the firing angle α increases beyond $\pi/4^c$, the TCR is in on for a lesser duration and the impedance of the TCSC thus decreases to that of the series capacitor (at $\pi/2^c$). On the other hand as the angle α increases beyond 0^c towards $\pi/4^c$ it exhibits inductive behaviour and the inductive reactance increases.

$$X_{TCSC}(\alpha) = \frac{X_C X_L(\alpha)}{X_C - X_L(\alpha)} \qquad \text{(AII.1)}$$

where,

$$X_L(\alpha) = X_L \frac{\pi}{\pi - 2\alpha - \sin(\pi - 2\alpha)} \quad \text{(AII.2)}$$

The effective capacitive reactance of the TCSC can thus be controlled by adjusting the firing angle.

AII.2. Operation Modes of a TCSC

The TCSC can operate in one of the four following modes:

- Blocked Thyristor mode: In this mode the valves are switched off when they encounter a zero crossing current through them. This way the TCR is effectively blocked and all the current flows through only the series capacitor. The TCSC in effect, becomes a fixed series capacitor. DC offset control is required to discharge any dc offset voltages that may be present in order to avoid harm to the transmission system.

- Thyristor bypassed mode: In this mode the reactor is always conducting. The firing angle is set to 0^c. The moment the voltage across the thyristors exceeds zero (positive), gate pulses are applied. This results in a continuous current through the thyristor valves. There is thus a net inductive current flow through the module as a whole. This mode is not to be confused with the breaker bypass mode, where the circuit breaker in parallel with the TCSC is closed to bypass the entire module. The bypass breaker is provided to protect the system in the event of transient over-voltages across the TCSC, or when the TCSC is manually required to be taken out of service, while leaving the rest of system in service.

Partially Conducting Thyristor Modes: In these modes the TCSC operates as a continuously controllable capacitor or inductor. This is the normal operation mode of a TCSC. It must be noted that it is not possible to smoothly transition between the inductive and capacitive modes, due to the presence of a resonant region (in the vicinity of $\pi/4^c$ firing angle) between the two modes where the TCSC is not stable:

• Inductive Boost Mode: In this mode the firing angle of the thyristors is varied in the range of 0 to $\pi/4^c$. The effective capacitive reactance can be varied to up to 5-6 times the inductor branch reactance.

• Capacitive Boost Mode: In this mode the firing angle of the thyristors is varied in the range of $\pi/4^c$ to $\pi/2^c$. This is the conventional operating mode of the TCSC. The effective capacitive reactance can be varied to up to 3 times the fixed series capacitor reactance.

AII.3. ATP-EMTP Single-Phase Model of a TCSC

The Electromagnetic Transient Program (EMTP) was used to model the TCSC and the simulation framework. EMTP is a very useful program for not only its accuracy, speed and availability of major power system components but also for the features that allow for modelling of logical and mathematical function blocks that may be used for control or assessment purposes. These are carried out using "MODEL" [1] and "TACS" [1] components of EMTP [1]. In particular TACS is a very useful EMTP feature that is used in this project in the modelling of the TCSC since the measurement, signal processing and control systems within the interface circuit required the use of special function blocks available in the TACS feature. TACS comprises of several useful components such as integrators, comparators, logic operators, multipliers etc. A combination of several of these can be used to create the desired circuits.

The purpose of this TCSC model is for the testing of future FLAs similar to the ones discussed in the main chapters of this thesis, but for lines compensated using TCSCs. Thus, the primary focus was to create a model capable of simulating the transient processes during an electrical fault. The TCSC is a complex device comprising of the HV circuit and its interface circuit. The model of the HV circuit as shown in Figure AII.4 comprises of a series capacitor in parallel with an MOV, and also in parallel with a reactor branch and its snubber circuit. The reactor branch comprises of inductors and thyristors which are integral to the alterability of the reactance of the overall system. The thyristors have been modelled here in the form of diodes in series with signal controlled switches. The switches are

controlled by the interface circuit depending on the phase of the measured current. The snubber circuit is required to minimise the magnitude of the voltage transient peak, which can be seen in the form of spikes in the voltage waveform.

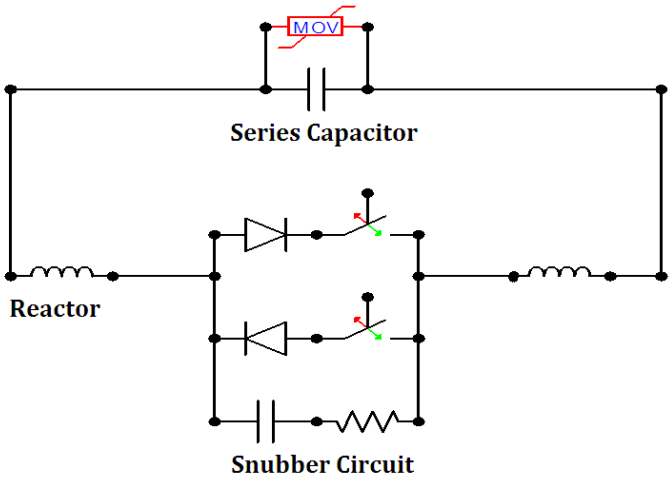

Figure AII.4: HV circuit of the ATP-EMTP TCSC model

The interface circuit is used to appropriately control the reactance and operation of the TCSC based on the firing angle input. It comprises of subsystems for measurement, filtering, synchronisation, and firing of the thyristors. The phase of the voltage difference across the capacitor is used to determine the firing signal for the thyristors. The measurement of the voltage difference is carried out in TACS using the 'coupling to circuit' component and an "x-y" (signal difference) component. A key requirement of the measurement subsystem is to allow the interface to "see" the waveform and thereby perform the required functions to determine the phase of the signal. This is shown in Figure AII.5.

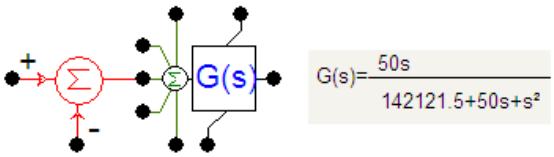

Figure AII.5: Measuring and filtering components

Initially, attempts were made in EMTP to determine the phase in a simple manner using the voltage signal directly. Due to the thyristor firing action the high harmonic distortion of the signal was significant and detection of zero crossing was not always precise. This leads to incorrect firing and further contributes to the problem leading to a increasingly distorted voltage signal (Figure AII.6).

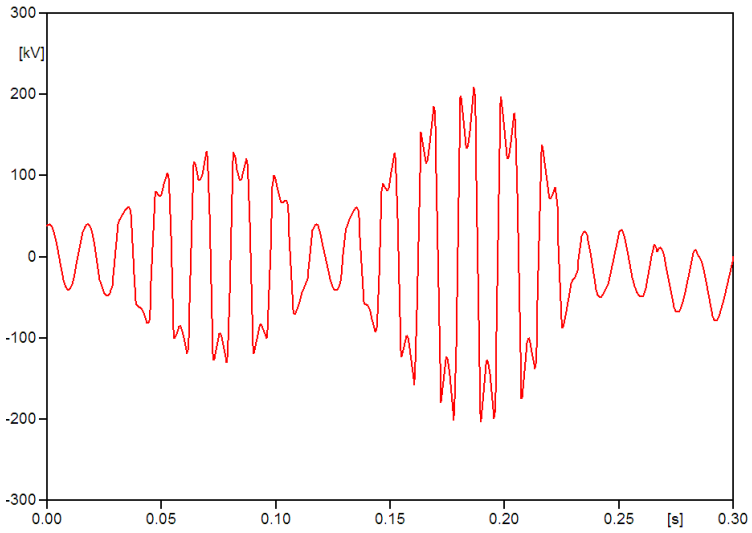

Figure AII.6: Distorted voltage signal as a result of poor synchronisation

This made it very difficult to keep the system synchronised with respect to the phase of the voltage. In order for the synchronisation subsystems to correctly be able to determine the phase of the signal, the signal had to be a perfect sinusoid. Thus a band pass filter was introduced into the circuit to allow only the signals at system frequency (assumed 50 Hz) and a bandwidth of +8 Hz. The equation for a typical bandpass filter is given below. Substituting the corresponding values:

$$\frac{(\omega_n / Q)s}{s^2 + (\omega_n / Q)s + \omega_n{}^2} = \frac{40s}{s^2 + 40s + 98696} \qquad \text{(AII.3)}$$

where,

$$\omega_n = 2\pi(50) \qquad \text{(AII.4)}$$

$$\Delta B = 8 \tag{AII.5}$$

The method of phase detection is often based on finding the recurrence of vital points on the system such as a zero crossing or peak. As mentioned previously the filtering circuit was introduced to aid the phase detection process. Although the waveform is perfectly sinusoidal prior to any thyristor firing action, it soon gets highly distorted, and continues to get worse due to incorrect firing signals sent to the thyristors. While this is only a transient phenomenon, if the phase is detected incorrectly, the system loses accuracy of its firing and never reaches its new steady state. Filtering of the signal for the fundamental frequency component made it possible to maintain a sinusoidal input and thus maintain synchronisation of firing in the system.

The synchronisation subsystem comprises of the 'negative-to-positive-zero-crossing detection' circuit and the ramp generating circuit. The function of the former is to detect the zero-crossing corresponding to the signal transitioning from the negative half cycle to the positive half cycle. The subsystem works by creating a ramp that integrates time and resets when this zero crossing is encountered. Thus, it is a linear measurement of time period between two such zero crossings for a complete cycle. This measurement of time is then amplified accordingly to provide the phase angle of the waveform at any given instant.

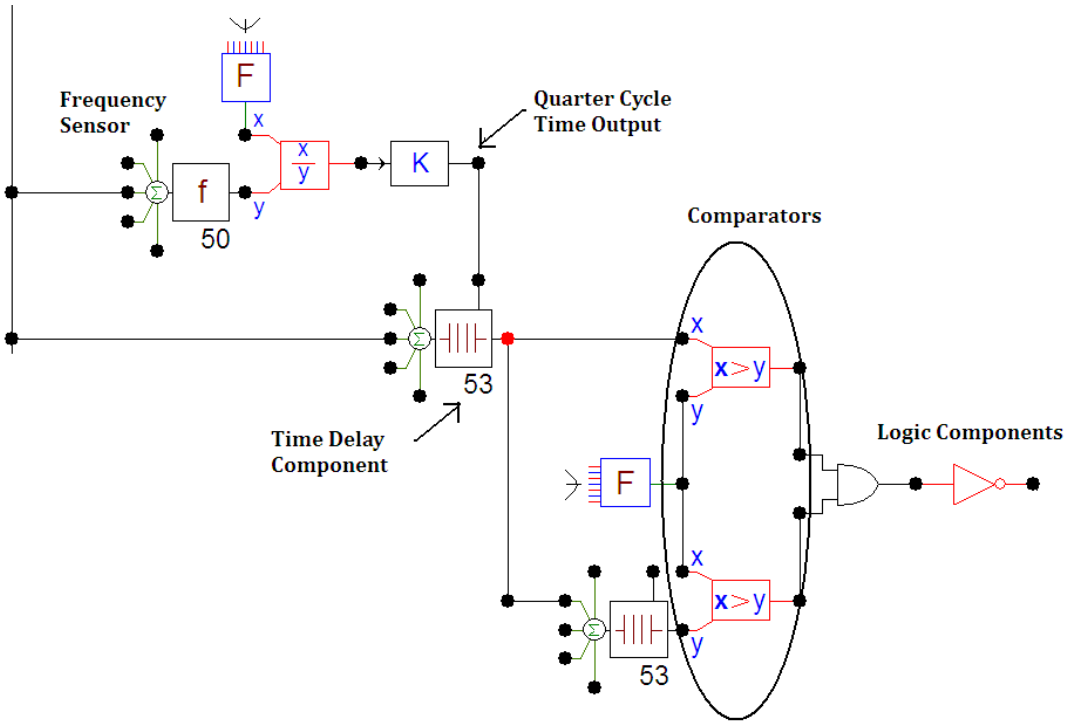

Figure AII.7: Negative to positive zero crossing detector circuit

Using the "Frequency Sensor" component [1] of TACS the frequency of the filtered waveform was accurately measured and mathematically inverted to give the time period of the signal. This time period was input to a 'Transport Delay' component [1] and used to appropriately delay the voltage signal by $\pi/2^c$ (the original signal is still available). Using the delayed and the original signal, the moment when the signal crosses zero as it goes from negative half cycle to the positive half cycle is detected and using the appropriate logic components it is used to reset the ramp generator back to zero. The ramp generator [1] thus measures the time between two such zero crossings. It is implemented in EMTP using the 'Controlled Integrator' component [1]. Its output is multiplied by the 2π/time period which was measured at an earlier stage, such that its output linearly increases from 0 to 2π during the course of one cycle. Thus the synchronisation circuit successfully measures the phase of the signal. This circuit is shown in Figure AII.8

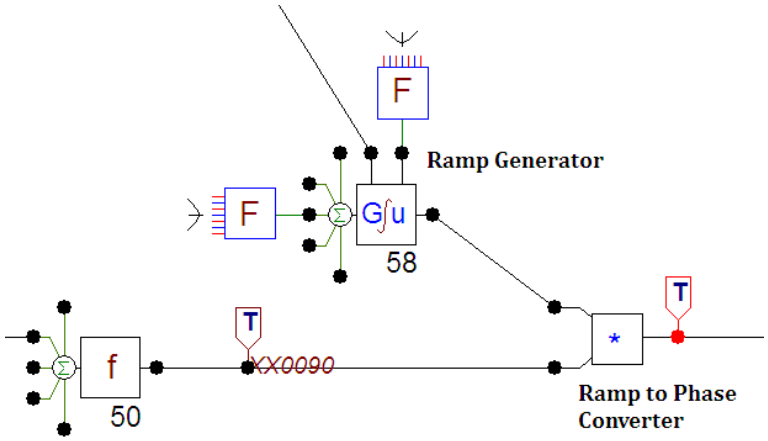

Figure AII.8: Phase determination circuit

The firing mechanism was implemented in EMTP as shown in Figure AII.9. The phase measurement from the ramp generator is used and transformed by $\pi/2^c$ to change the reference from zero crossing to negative peak. The phase angle is then checked against the required angles based on the firing angle input as shown in Figure AII.9 using logic operators to determine the duration of the on and off states of the corresponding thyristors. The signal controlled switch corresponding to the top thyristor is switched on between the when the phase angle is equal to the firing angle and when the phase angle is equal to π^c. For the remainder of the power system cycle it is switched off. On the other hand, the switch corresponding to the bottom thyristor is switched on for the period exactly π^c radians after the switching of the top thyristor.

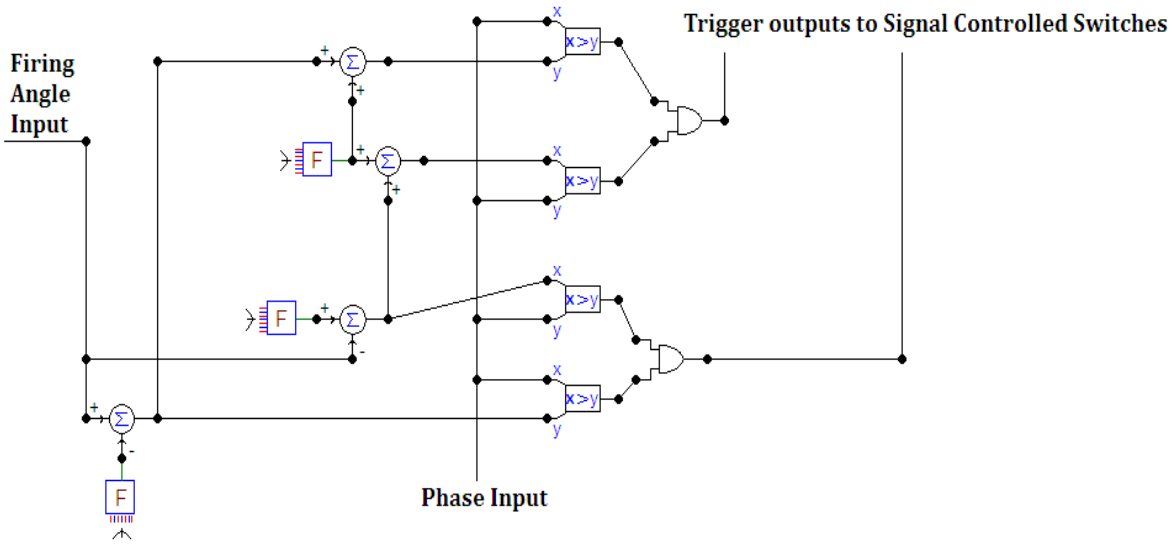

Figure AII.9: Firing Mechanism

AII.4. ATP-EMTP 3-Phase Model of a line compensated using a TCSC

Figure AII.10 shows the 3-phase ATP-EMTP circuit for the TCSC compensated line. It comprises of voltage sources and source impedances as used previously in Chapter 4. The parameters used are identical to those in Table 4.4. LCC J-Marti line blocks are used for the transmission line. A 'splitter' ATP-EMTP component [1] can be seen on either side of the TCSC. This is an ATP-EMTP component that can be used to model each of the phases individually in a system otherwise comprising of 3-phase components. The component with a circled 'T' symbol is known as 'TACS coupling to circuit' [1], and is used to pass voltage of points on the HV circuit for analysis using TACS components. One TCSC unit can be seen for each of the phases comprising of the HV circuit elements discussed previously in Section AII.3. The interface circuit comprising of the elements discussed previously in Section AII.3 is compressed into an encapsulated black-box module shown here in red. It requires three inputs, namely the firing angle and the voltages on each side of the TCSC. The MOV is excluded in this 3-phase model as it is currently only capable of simulating the steady state operation. The future model will include the operation of the MOV and closed loop control to accurately simulate the behaviour of the TCSC during fault.

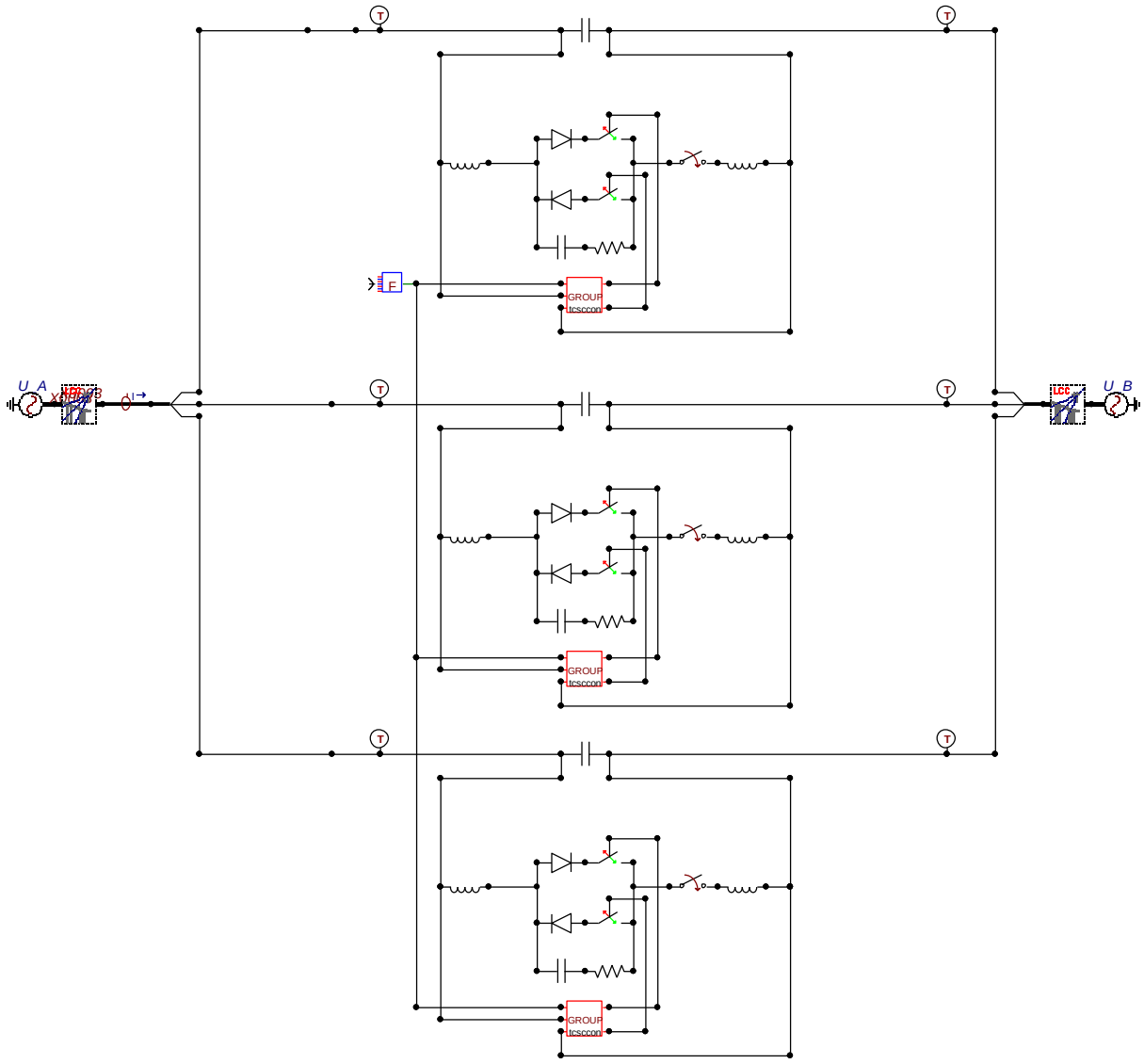

Figure AII.10: 3-Phase TCSC Model

3.7.4. Simulations

The current functionality of the work-in-progress model is that it is capable of simulating the variation in the reactance based on the input firing angle. It is thus capable of operating under the various modes of the TCSC discussed previously in Section AII.2. It is important to highlight that these are only the initial results obtained from the premature model of the TCSC. A more detailed model of the TCSC will be created as part of future work. This

section is aimed at presenting the preliminary results of the model. The various modes are simulated by adjusting the firing angle of the TCSCs. They are shown as follows:

1. Inductive Boost Mode: In this mode the firing angle of the thyristors is varied in the range of 0^c to $\pi/4^c$. The details for this particular instance of the inductive boost mode shown in the simulation are as follows:

   - Firing Angle = $\pi/16^c$
   - C= 177μF, L = 10mH
   - $X_C = \frac{1}{2\pi fC} = 17.98\Omega$
   - $X_L = 2\pi fL = 3.14\Omega$
   - $X_L(\alpha) = X_L \frac{\pi}{\pi - 2\alpha - \sin(\pi - 2\alpha)} = 4.1711\Omega$
   - Effective TCSC reactance (theoretical) $X_{TCSC}(\alpha) = \frac{X_C X_L(\alpha)}{X_C - X_L(\alpha)} = 4.8606\Omega$
   - Calculated value of reactance based on measurements = 5.4306Ω

   The Simulations for the TCSC voltage, line current, reactor branch current and capacitor current are shown in Figure AII.11, Figure AII.12, Figure AII.13, and Figure AII.14 respectively. The TCSC voltages can be seen to have a highly distorted non-sinusoidal waveform. This is the expected waveform shape for this mode of operation of the TCSC. The reactor branch currents show periods of thyristor conduction and periods of the thyristor blocking. The inductor current is also distorted, but this is the expected waveform shape for this operation mode. It can be seen that the line current still maintains a sinusoidal shape. It must be noted that the inductive reactance of the TCSC unit as a whole is significantly higher than that of the inductance in the reactor branch. This is what is referred to as the

inductive boost mode, as inductive reactance can be increased significantly beyond the reactor branch reactance by the appropriate firing of the thyristors.

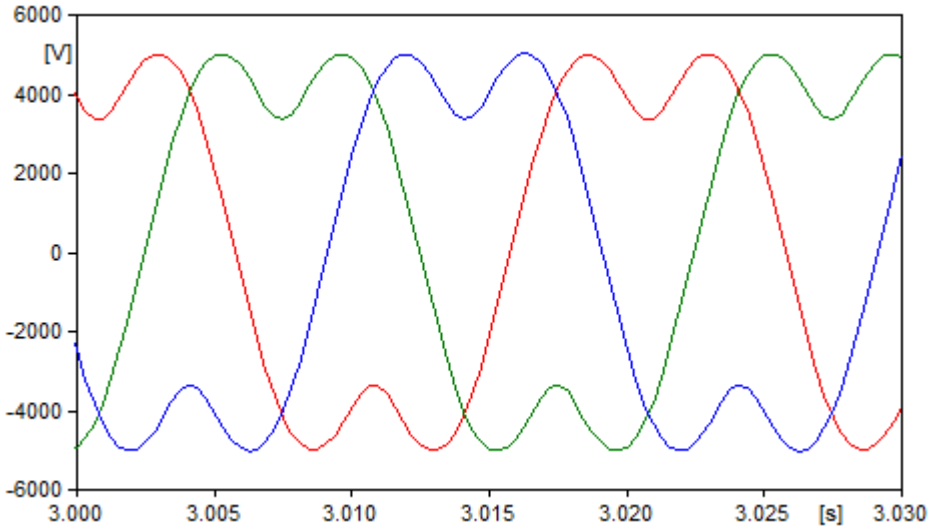

Figure AII.11: TCSC phase voltages – Inductive boost mode

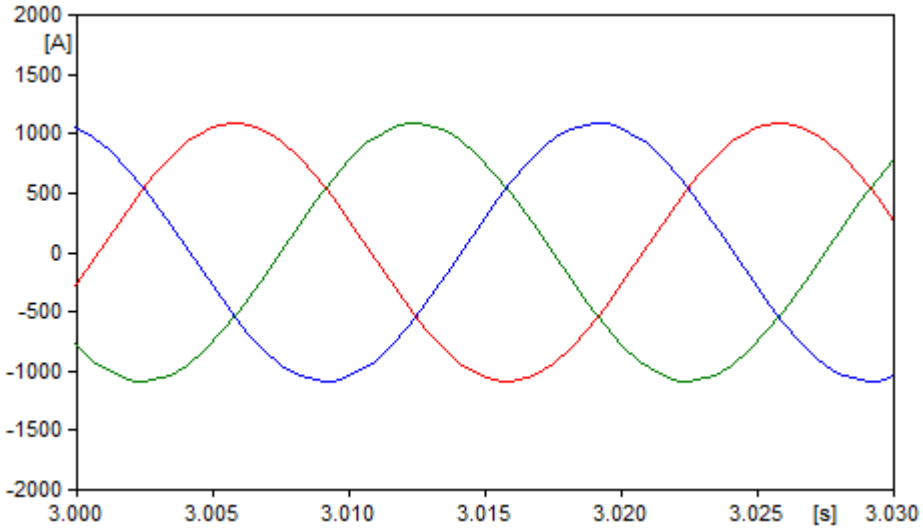

Figure AII.12: Phase line Currents – Inductive boost mode

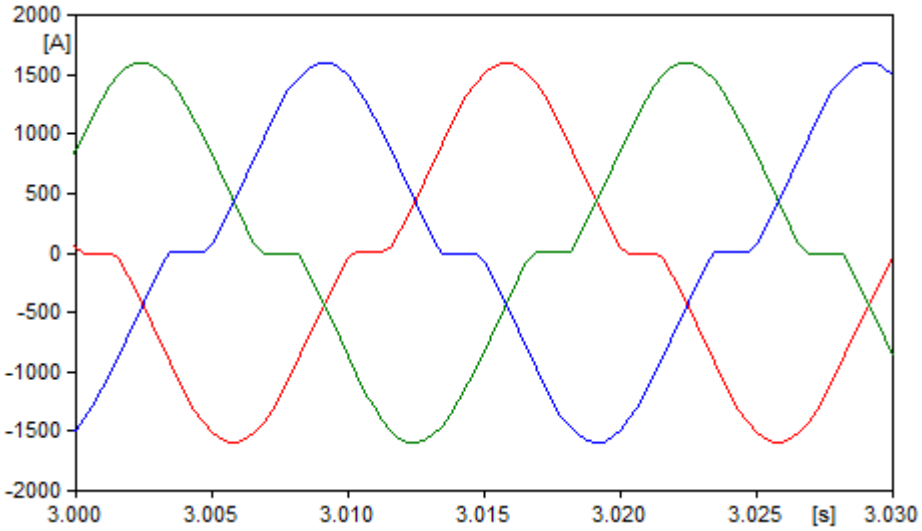

Figure AII.13: Reactor branch phase currents – Inductive boost mode

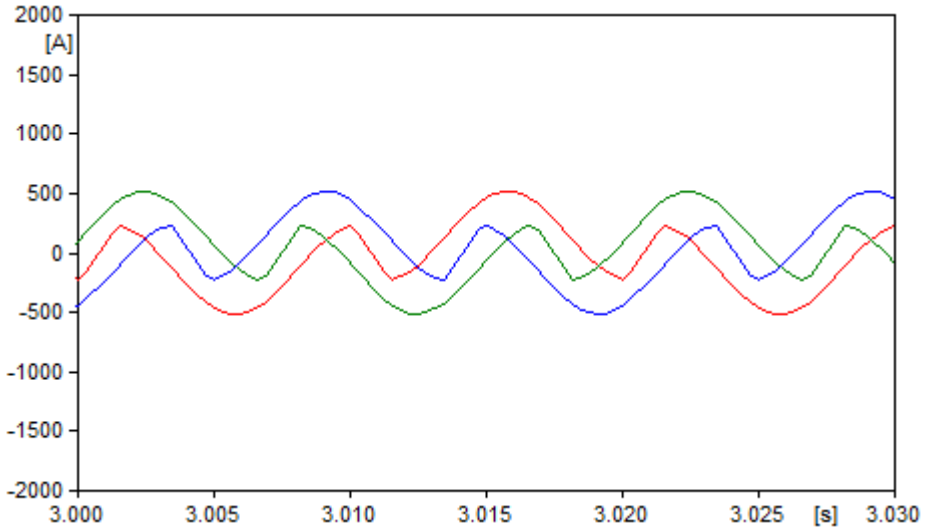

Figure AII.14: Capacitor phase currents – Inductive boost mode

2. Capacitive Boost Mode: In this mode the firing angle of the thyristors is varied in the range of $\pi/4^c$ to $\pi/2^c$. The details for this particular instance of the capacitive boost mode shown in the simulation are as follows:

- Firing Angle = $6\pi/16$ [c]
- C= 177μF, L = 10mH
- $X_C = \frac{1}{2\pi fC} = 17.98\Omega$
- $X_L = 2\pi fL = 3.14\Omega$
- $X_L(\alpha) = X_L \frac{\pi}{\pi - 2\alpha - \sin(\pi - 2\alpha)} = 126.06\Omega$
- Effective TCSC reactance (theoretical) $X_{TCSC}(\alpha) = \frac{X_C X_L(\alpha)}{X_C - X_L(\alpha)} = -20.98\Omega$
- Calculated value of reactance = -21.59Ω

The theoretical calculation is only an approximation and this explains the discrepancy with respect to the actual impedance. However, this must be investigated as a part of future work through validation against existing models and using data obtained from TCSC compensated lines. The simulations for the TCSC voltage, line current, reactor branch current and capacitor current are shown in Figure AII.15, Figure AII.16, Figure AII.17, and Figure AII.18 respectively. The capacitor voltages and currents can be again be seen to have a distorted non-sinusoidal waveform. These are the expected waveform shape for this mode of operation of the TCSC.

It must be noted that the capacitive reactance of the TCSC unit as a whole is higher than that of the capacitor. This is what is referred to as the capacitive boost mode, as the capacitive reactance of the unit can be increased significantly beyond the capacitor reactance by the appropriate firing of the thyristors.

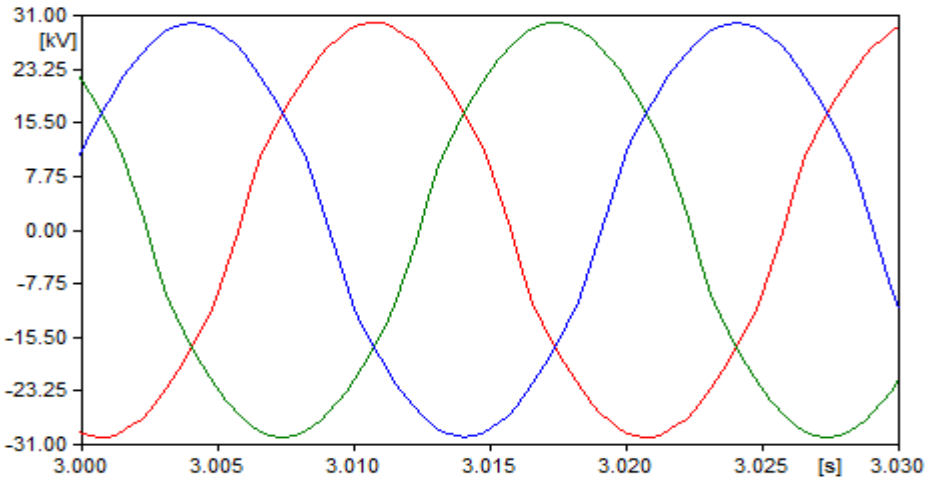

Figure AII.15: TCSC phase voltages – Capacitive boost mode

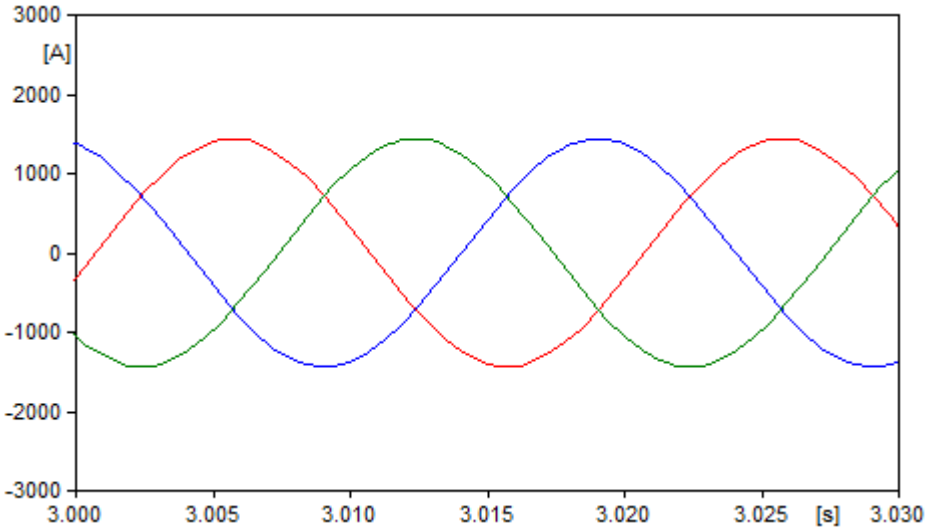

Figure AII.16: Phase line Currents – Resonant condition

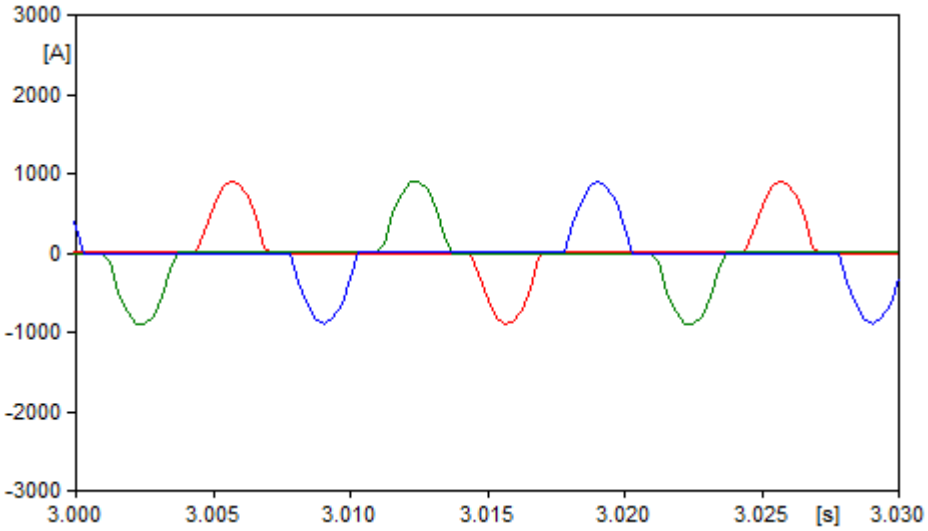

Figure AII.17: Reactor branch phase currents – Capacitive boost mode

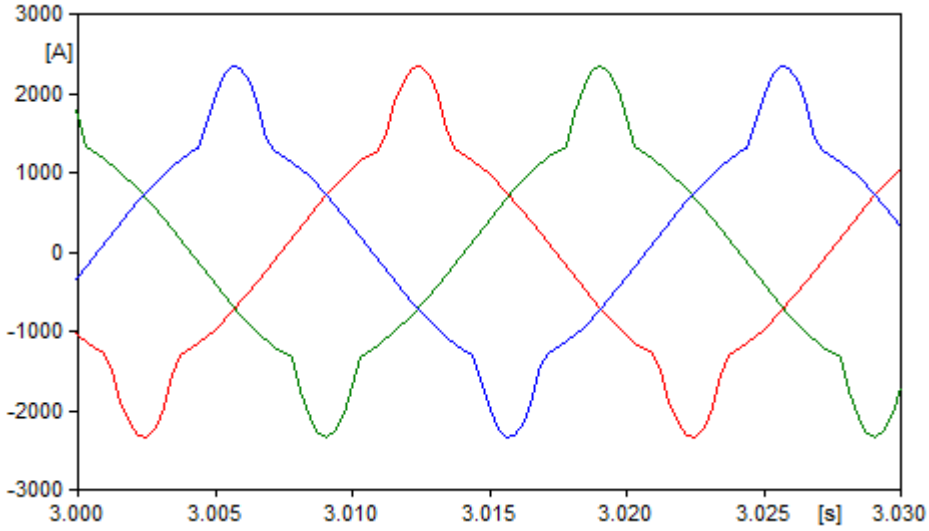

Figure AII.18: Capacitor phase currents – Inductive boost mode

3. The resonant region: The resonant region refers to angle close to $\pi/4^c$ where the TCSC operation is inhibited. Therefore, this is not an operation mode of the TCSC. However simulations for the TCSC voltage and line current are shown for a period of 4 seconds, to demonstrate the behaviour of the TCSC in this resonant region.

The firing angle here is $\pi/4^c$. It can be seen that the magnitudes of the voltage and current increase to very large values. This is obviously not a stable mode of operation and is therefore inhibited.

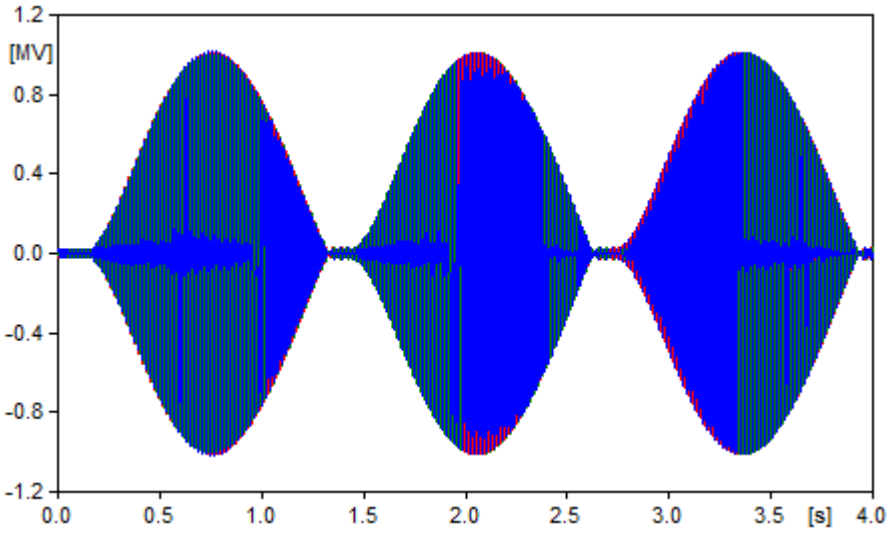

Figure AII.19: TCSC phase voltages – resonant region

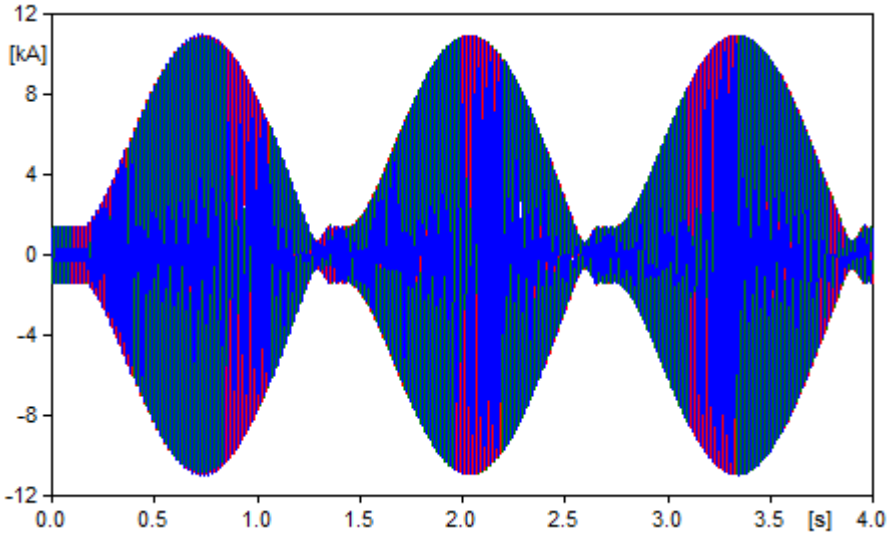

Figure AII.20: TCSC phase currents – resonant region

4. Bypassed thyristor mode: This mode is achieved by setting the firing angle input to 0^c. In this mode both the capacitor branch and the reactor branch conduct current during the full power system cycle. The details for this mode shown in the simulation are as follows:

   - Firing Angle = 0^c
   - C= 177μF, L = 10mH
   - $X_C = \frac{1}{2\pi fC} = 17.98\Omega$
   - $X_L = 2\pi fL = 3.14\Omega$
   - $X_L(\alpha) = X_L \frac{\pi}{\pi - 2\alpha - \sin(\pi - 2\alpha)} = 3.14\Omega$
   - Effective TCSC reactance (theoretical) $X_{TCSC}(\alpha) = \frac{X_C X_L(\alpha)}{X_C - X_L(\alpha)} = 3.8\Omega$
   - Calculated value of reactance based on measurements = $j3.8\Omega$

   The TCSC voltages, line currents, capacitor currents, and the reactor branch currents are shown in Figure AII.21, Figure AII.22, Figure AII.23 and Figure AII.24 respectively. The waveforms for each case are sinusoidal, and in line with what can be expected for an inductor in parallel with a capacitor.

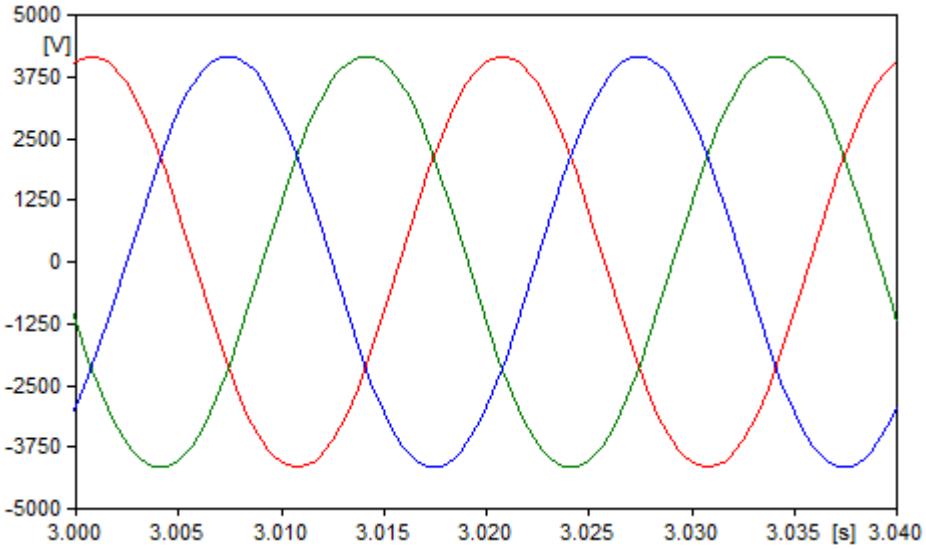

Figure AII.21: TCSC phase voltages – Bypassed thyristor mode

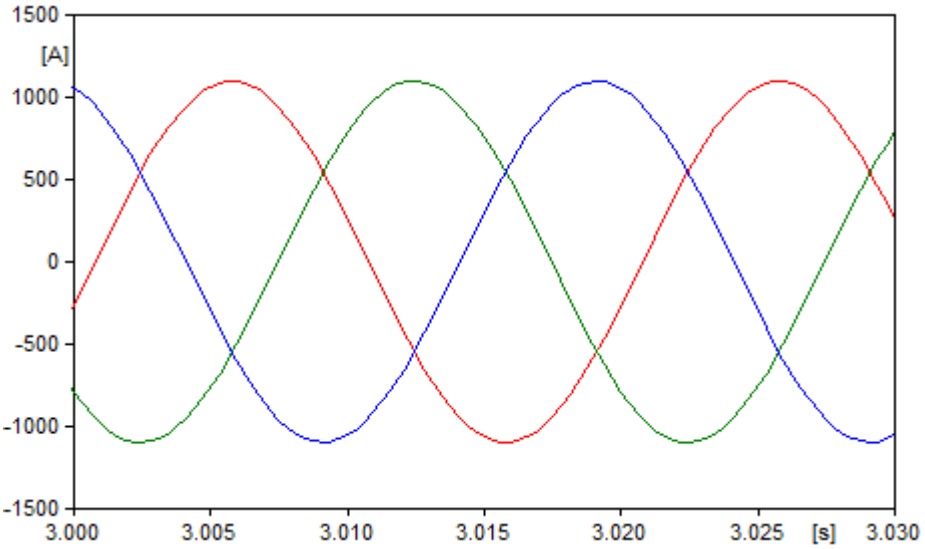

Figure AII.22: Phase line currents – Bypassed thyristor mode

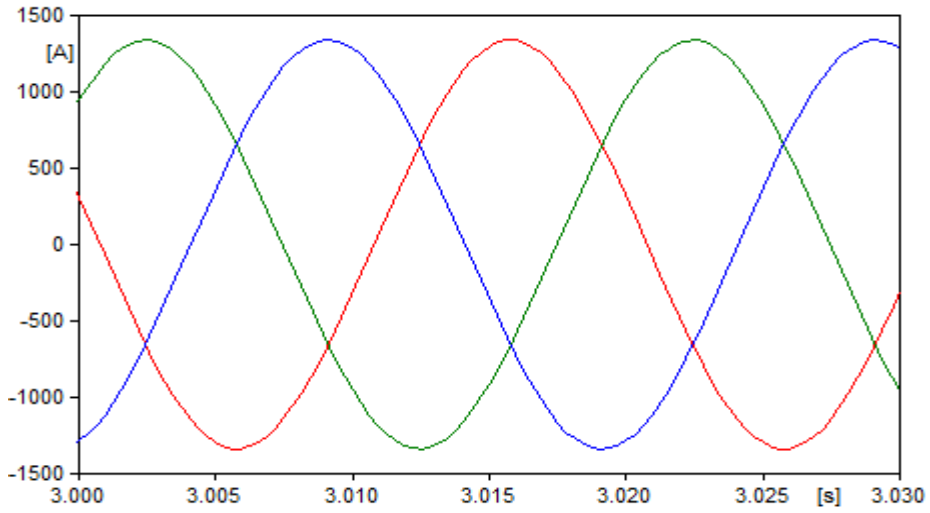

Figure AII.23: Reactor branch phase currents – Bypassed thyristor mode

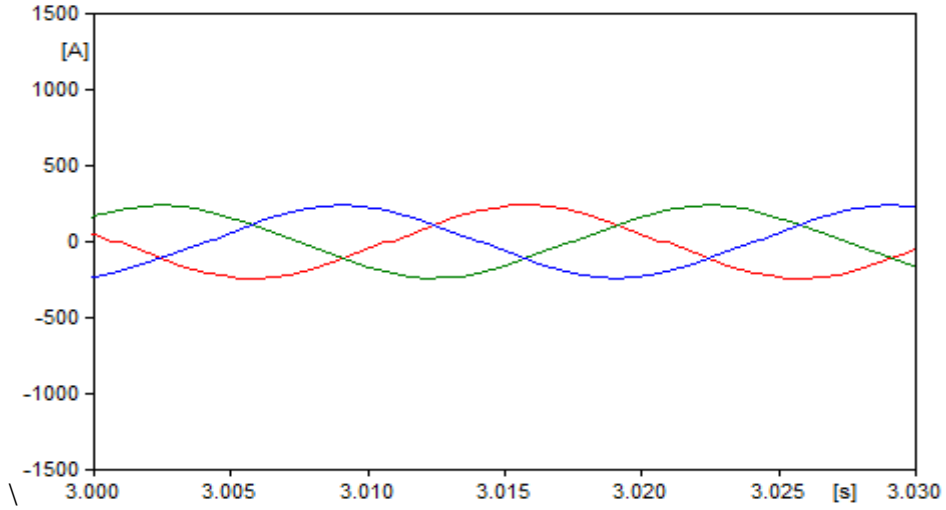

Figure AII.24: Capacitor phase currents – Bypassed thyristor mode

5. Blocked Thyristor mode: The blocked thyristor mode allows the inductor branch to be taken out of circuit such that the TCSC behaves as a FSC. This mode is achieved by opening the switch in series with the inductors in the reactor branch, thereby

effectively achieving a FSC behaviour. The waveforms for TCSC voltages and line currents are shown in Figure AII.25 and Figure AII.26 respectively.

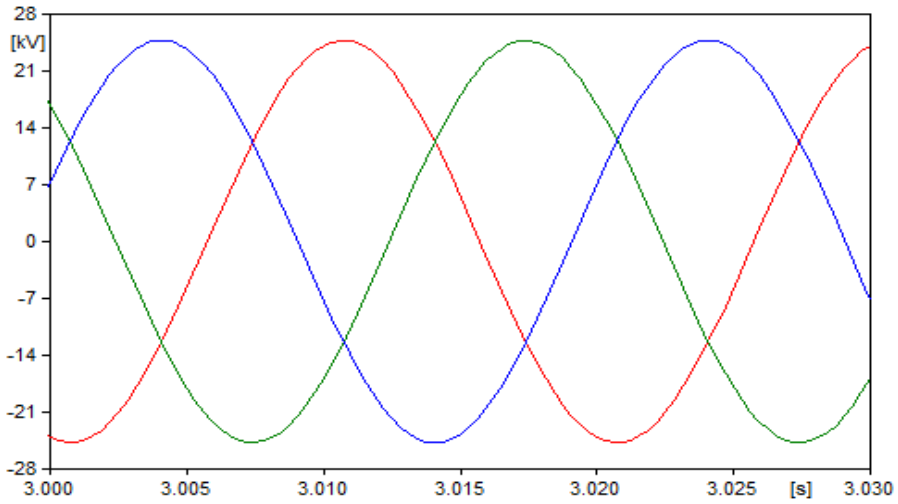

Figure AII.25: TCSC phase voltages – Blocked thyristor mode

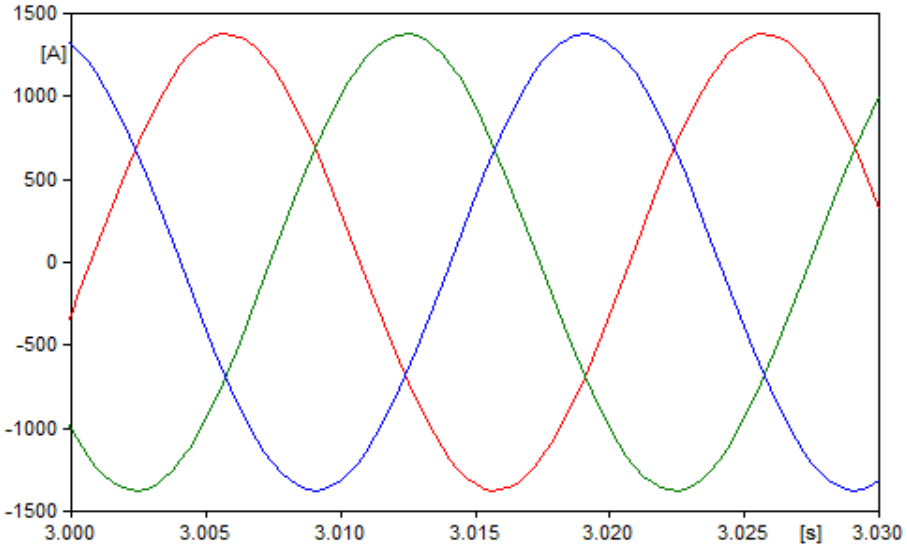

Figure AII.26: Phase line currents – Bypassed thyristor mode

AII.5. Appendix Summary

This Appendix presented a work-in-progress ATP-EMTP model of a TCSC, presented the background information and the preliminary results obtained thus far. The TCSC model is currently only capable of simulating the steady-state behaviour of the TCSC and does not model the closed loop control typically implemented. The principle of the operation of the TCSC in terms of the variability of the reactance by means of appropriate thyristor firing was explained. The four operation modes of the TCSC were also discussed. The HV circuit of the TCSC comprises of the series capacitor, MOV, the snubber circuit and the reactor branch consisting of the inductors and thyristors. The interface circuit of the TCSC comprises of the functions that are used to control the firing of the thyristors, so that the required behaviour can be achieved. The current model of the TCSC was discussed with respect to these circuits. The modelling of the sub-functions within the interface circuit was also discussed i.e. the measurement, filtering, negative-to-positive zero sequence detection, ramp generation and the firing of the thyristors.

Lastly, simulations for each of the four operation modes of the TCSC were presented which were simulated by varying the firing angle of the TCSC. The future model of the TCSC requires the inclusion of the MOV modelled with the appropriate characteristics, closed-loop control, and a mechanism required for receiving the desired impedance as input and calculating the appropriate firing angle to be used in the control of the thyristors. The current model has been modelled using the basic the theoretical information on the operation and behaviour of TCSCs. A significantly more detailed model is expected to be created using manufacturer data as part of future work.